# MICROFLUIDIC TANGENTIAL FLOW FILTER AND CONTINUOUS-FLOW REACTOR FOR BIOPROCESS DEVELOPMENT

James Peter Lawrence

Department of Biochemical Engineering

University College London

Torrington Place

London

WC1E 7JE

A thesis submitted for the degree of

*Doctor of Philosophy*

2015

# Declaration

I confirm that the work presented in this thesis is my own unless indicated otherwise. The work presented was carried out under the supervision of Dr Nicolas Szita at the Department of Biochemical Engineering, University College London, between October 2008 and May 2013. This thesis has not been submitted, either in whole or in part, for another degree or another qualification at any other university.

James P. Lawrence

London, May 2015

# Acknowledgements

I would like to express my gratitude to:

The Biotechnology and Biological Sciences Research Council, for funding the project and making this possible.

My supervisor, Prof. Nicolas Szita, for his guidance, advice and patience throughout the course of my research, and particularly for his support in the weeks that I was unwell.

Marcel and Tim, who showed me the ropes in the microfluidics lab, and Leo and Pat, for generously sharing their expertise in biocatalysis. My thanks also to Dr. Brian O'Sullivan, for helping me to reframe the challenges I faced in my research and for his guidance in writing publications.

My friends and family, who have all listened to me talk about my research for far too long now, and to whom I am deeply thankful for their forbearance and wholehearted support while I finished my thesis.

My future wife, Anna, who has seen me through the entirety of the project and has lived through the writing of my thesis with me. I cannot thank you enough for your constant love and support, particularly in the difficult times. I couldn't have done it without you.

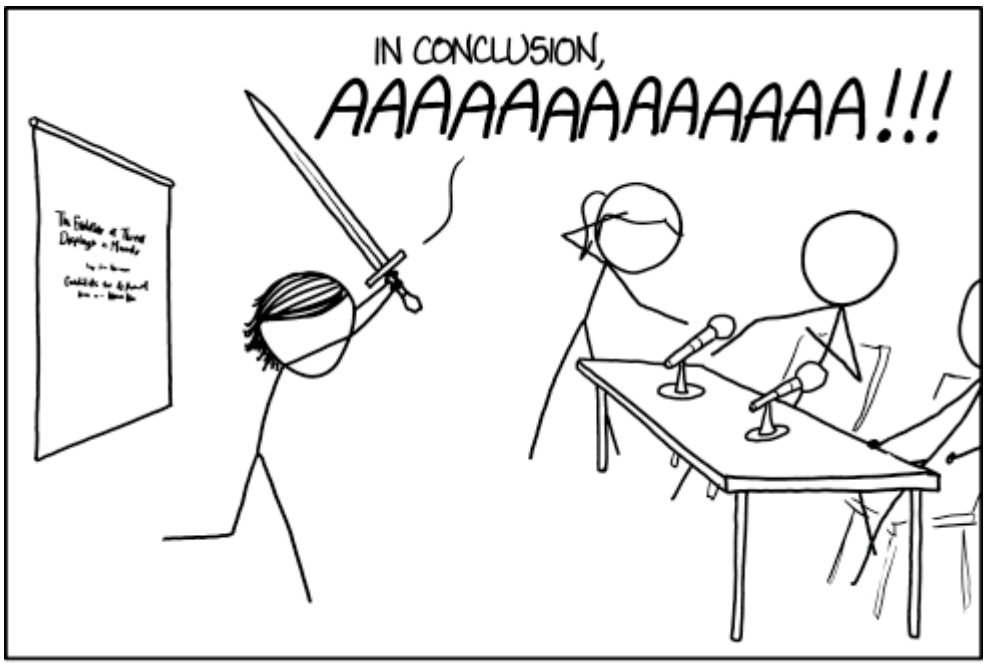


THE BEST THESIS DEFENSE IS A GOOD THESIS OFFENSE.



xkcd.com/1403/

# Abstract

The development of new biocatalytic processes is hindered by the number of factors that must be investigated and optimised in order to create a robust and reproducible process, particularly where a novel enzyme is involved. It is therefore advantageous to perform process development experiments at micro scale, in order to reduce the material requirement for experimentation and increase experimental throughput by parallelisation.

The initial focus of the thesis is on the design of a microfluidic tangential flow filter to test downstream processing conditions. The device was designed for reversible clamp sealing, allowing the simple integration of different filtration membranes, and the seal achieved with the device was shown to be robust up to internal pressures of 100 psi. The filtration device was applied to the recovery of L-erythrulose (ERY) from a synthesis reaction performed using transketolase (TK), where it was demonstrated that the enzyme could be fully retained using a commercially-available membrane, while ERY was able to permeate the membrane freely. The filtration device was joined in-line to the output of a T-junction reactor with a staggered herringbone mixer, used to perform the synthesis reaction. The filter was capable of continuously separating the ERY from the lysate mixture exiting the reactor over the course of several hours, producing 3.6 mg $h^{-1}$ of pure ERY.

A novel multi-input reactor (MIR) is also demonstrated for the purpose of intensifying ERY output, designed to overcome the effect of substrate inhibition on the TK enzyme by mimicking a fed-batch reactor. Feeding strategies were designed for the conversion of various concentrations of the less inhibiting substrate hydroxypyruvate (HPA) and tested in the MIR. A 4.5-fold increase in output concentration and a 5-fold increase in throughput were achieved compared with the single input reactor used in previous experiments. However, conversion in the MIR was reduced at higher concentrations, suggesting that the reaction in the MIR was being inhibited by the evolution of carbon dioxide.

# Glossary

The descriptions of acronyms and shortenings that are frequently used in this thesis can be found below.

| | |
|---|---|
| ERY | Erythrulose |
| FBS | Fetal bovine serum |
| GA | Glycolaldehyde |
| GFP | Green fluorescent protein |
| HPA | Lithium-hydroxypyruvate |
| HPLC | High-pressure liquid chromatography |
| MEF | Murine embryonic fibroblast |
| mES | Murine embryonic stem cell |
| MIR | Multi-input reactor |
| MWCO | Molecular weight cut-off |
| PBS | Phosphate-buffered saline |
| PC | Polycarbonate |
| PDMS | Poly(dimethyl)siloxane |
| PMMA | Poly(methyl)methacrylate |
| PVDF | Polyvinylidene fluoride |
| SHM | Staggered herringbone mixer |
| TFA | Trifluoroacetic acid |
| TK | Transketolase |
| TMP | Transmembrane pressure |
| Tris | Trisaminomethane |
| VI | Virtual instrument (LabVIEW subroutine) |

# Table of Contents

# Table of Figures and Tables

# 1

# Introduction

# 1.1 Bioprocessing

## 1.1.1 Challenges in Bioprocess Development

Bioprocessing refers to the use of cells or cellular components in the manufacture of a desired product (Doran, 2004). Bioprocessing has its origins in the production of beer through yeast fermentation, a process that is more than two thousand years old, but the advent of DNA sequencing, proteomics and genetic engineering techniques has vastly increased the number of potential applications. Where early bioprocessing involved the exploitation of a naturally-occurring pathway to produce a useful chemical, for example in the use of plant extract to synthesise (R)-mandelonitrile, modern bioprocesses use cells or enzymes that have been manipulated specifically to produce a desired product (Bornscheuer et al., 2012). With this understanding it has become possible to use cells and enzymes to produce not only useful small molecules, but also larger macromolecular products including therapeutic proteins such as insulin, creating a huge range of opportunities for novel therapies (Ladisch and Kohlmann, 1992).

Bioprocessing now encompasses a wide range of products including biopharmaceuticals (therapeutic proteins, antibiotics and vaccines), industrial chemicals (food and agricultural products, fuels, fibres and sustainable chemicals) and waste management tools (including sewage processing and waste clean-up; Ladisch et al. 1992). In the last decade, bioprocessing of human cells for regenerative medical treatments has also become a concern, (Yang et al., 2010), marking a change from the use of cells for the manufacture of products to the manufacture of cells as a product in of themselves (Placzek et al., 2009).

Aside from their use to produce novel products, bioprocesses also have advantages over equivalent chemical processes in terms of sustainability. In the synthesis of small molecules in particular, the use of enzymes rather than chemical catalysts allows reactions to be performed at lower temperatures and pressures, and the high selectivity and specificity of

enzymes can reduce the number of side reactions, reducing waste (see section 1.2 on Biocatalysis).

The primary disadvantage of bioprocesses is the amount of time and resources that must expended on up-front development in order to characterise the process. The added complexity of biological systems in the process makes it difficult to predict how the system as a whole will behave and adds to the number of process conditions that must be investigated to determine the optimum conditions for the best quality of product. The conditions chosen for each stage of the process will also have a knock-on effect on other stages of the process, adding to the complexity of the whole and the amount of experimental work that must be done in order to characterise each stage.

This is a particular issue where the target product is a pharmaceutical, where the design and operational tolerances of the process must be fixed before clinical trials begin. In this case the whole process of development, from drug discovery through the clinical trials process to marketing, is put under time pressure by the length of the patent on the drug – usually 20 years – which limits the amount of time available to recoup the investment in the product. In addition, the large number of potential pharmaceutical products which fail to pass through the regulatory procedures adds an additional burden of cost, with products that fail later in the regulatory process incurring higher costs. Given that around one in 10,000 potential drugs make it from the drug discovery phase through the regulatory process and onto the market, it becomes increasingly important to minimise the cost and time involved in process development, to reduce the losses from the drugs which fail to make it to market.

### 1.1.2 Scale-Down Bioprocess Development

The use of small-scale processing technologies as analogues to industrial-scale processes offers a way to increase the speed of bioprocess development and reduce the upfront cost involved. These technologies historically aimed to mimic different large-scale unit operations such as fermentation, centrifugation, filtration and chromatography at the bench-top scale,

using volumes in the range of millilitres to litres. Using such small-scale devices allows experiments to be parallelised so that multiple condition sets can be evaluated simultaneously, for example by running several fermentations of *E. coli* in parallel and testing the effect of different media compositions on the rate of cell growth. This increases the throughput of experimentation and reduces the time required to characterise unit operations. Furthermore, the reduction in scale decreases the materials requirement for each experiment, cutting the overall cost of the development. Once a process has been characterised with bench-scale equipment and key scaling parameters have been established (such as the oxygen mass transfer coefficient, $k_La$, in the case of fermentations), the process can be scaled up as required.

In recent years, the size of scale-down tools has been reduced further by the introduction of microwell plate technology. These are of increasing importance for bioprocess development because of the very small volumes that they operate with, typically in the range of microliters to millilitres (Micheletti and Lye, 2006). The reduced volume means that between 6 and 3456 wells can be incorporated onto a single plate with a footprint of 110 cm², allowing the simultaneous testing of as many different condition sets in one plate. Using such plates, screening of up to $10^5 – 10^6$ condition sets per day has been reported in pharmaceutical process development (Lye et al., 2003; Zhao and Ran, 2007). Again, the reduction in operating volume and multiplexing of experiments means that the materials and time required for process development can be significantly reduced.

The plates themselves are available in a range of materials and can be adapted to mimic different unit operations by the use of inserts, including membranes, specialist coatings and miniature impellers and baffles (Puskeiler et al., 2005; Weuster-Botz et al., 2005). In addition, a range of tools has been developed to automate numerous aspects of fluid handling, preparation and data acquisition. A single automated platform might now include robotics for fluid handling, a centrifuge, a plate reader for spectrographic analysis of individual wells and a chromatography unit. These platforms can further increase the speed of process development

and optimisation, as well as increasing the range of industrial-scale unit operations that can be mimicked at the microliter scale using microwells.

Using automation tools, the optimisation of a biotransformation and subsequent extraction of the synthesised product has been performed, with the fermentation of the cells, biotransformation, liquid extraction and analysis of the final product concentration all being performed on an Tecan robotic platform (Baboo, 2012). The fermentation data has also been shown to be comparable to that collected in a pilot-scale unit. The same platform has also been used to rapidly screen conditions for denaturation and refolding of lysozyme inclusion bodies, performing wash, mixing and incubation steps as well as enzymatic activity assays automatically (Ordidge et al., 2012).

The drawback of microwell plate systems is that they are suitable only for the evaluation of batch process; they cannot be used as analogues for continuous-flow processes which are common in bioprocessing and which are becoming increasingly popular for chemical and biochemical synthesis in particular. Microfluidic systems, however, can be used as small-scale analogues as they are almost exclusively run with continuous fluid flow.

### 1.1.3 Microfluidics for Bioprocess Development

Microfluidics has been generally defined as the study of fluids and particles within artificially created systems of micron-sized channels (Tabeling, 2006). It has originated from research into multiple fields, with roots in microanalytical technologies, biodefense (particularly the detection of chemical and biological warfare agents) and microelectronics (Whitesides, 2006). Microfluidic devices typically use fluid volumes in the range of millilitres to nanolitres and, more recently, picolitres.

Flow in microfluidic channels is characterised by the lack of convective mixing that is seen at larger scales. This is caused by the small scale of the channels, in which the viscous forces of the fluid become more influential than the inertial forces (Squires and Quake, 2005). In this type of fluid flow regime, known as laminar flow, two streams of fluid can be flowed

together without any intermingling aside from diffusion, and a number of different types of devices have been developed that exploit this effect to perform operations that would not be possible at larger scales. An example of this the is ability to generate stable gradients of a solubilised molecule, by co-flowing two streams with different concentrations of the molecule for long enough that a concentration gradient can form by diffusion. These gradients have a number of applications, but are of particular significance because of their use to create gradients of chemical signalling molecules for the purposes of pharmacokinetic studies or the mimicking of *in vivo* conditions for investigation of cancer metastasis and stem cell biology (Pihl et al., 2005; Kim et al., 2010).

The small scale of microfluidic devices offers advantages in terms of reagent usage and precise control of the microenvironment on the chip, with devices being reported for the investigation of individual cells and their response to chemical stimuli (Umehara et al., 2003; Mahoney et al., 2005). The integration of online sensing, in particular through optics, is also a reported advantage. The materials commonly used in microfluidic devices are optically transparent, allowing fluids to be interrogated by optical fibres for the purpose of measuring cell optical density, UV absorbance and, through the use of sensor patches or particles, pH and oxygen concentration (Chang-Yen and Gale, 2003; Kuswandi et al., 2007; Funfak et al., 2008). Where observation of whole cell cultures is useful, chips can be fixed under a microscope and monitored in real-time, with automated image analysis providing cell counting and confluency measurement for adherent cultures (Jaccard et al., 2014). Measurements of relevant chemical concentrations, such as concentrations of glucose and lactate, can also be made with the use of specialised microelectrodes (Kurita et al., 2002). Online sensing allows the response of systems to environmental changes to be monitored in real-time, meaning that the response to multiple condition sets can be evaluated in a shorter time frame than offline methods, increasing the throughput of data for development.

Parallelisation has also been reported in microfluidic devices as a way of increasing data throughput. Several devices have been reported for the purpose of performing multiple cell

culture or biotransformation experiments simultaneously, using compartmentalised reactors with common fluidic connections, all fabricated into a single device (Barbulovic-Nad et al., 2010; Wu et al., 2010). Advances in droplet microfluidics, where individual fluid droplets containing nanolitres or picolitres of fluid are created to perform thousands to millions or individual experiments on a single device, offer the potential for massive parallelisation, though these devices rely on the addition of a reporter molecule or cell to each droplet and it can be difficult to quantify data from the droplets (Theberge et al., 2010).

Furthermore, there are now examples of automated microfluidic systems being used to perform experimentation and analysis without human supervision, resulting in further time saving and a reduction in the manpower required (Gómez-Sjöberg et al., 2007). One such example uses microstructures built onto CD-based platforms to create 'micro-laboratories' with multiple functions. A custom built workstation with a robotic pipetting system is used to add reagents and samples to the CDs before they are spun, as well as performing analysis afterwards (Ducrée et al., 2007).

A combination of these approaches to microfluidic devices could provide very powerful tools for bioprocess development. This thesis will therefore focus on development of new tools for investigation and intensification of bioprocesses, as applied to cell processing for cell therapy products and biocatalysis for small molecular products. The following sections of the chapter will discuss bioprocessing with mammalian cells and biocatalysis, their applications and examples of microfluidic technology that has been reported to aid process development and intensification.

## 1.2 Biocatalysis

### 1.2.1 Features of Biocatalysis

Biocatalysis is the use of a biological catalyst, i.e. an enzyme, to catalyse a synthetic reaction. The enzyme may be used by itself, having been separated from the cell it was produced by, or *in situ* inside the cell. The latter may be useful where multiple enzymatic

pathways are required, or where the enzyme requires a co-factor that can also be produced by the cell. However, using a biocatalyst in place inside a cell can add complications to the production process, especially in terms of mass transfer and ensuring that the cells remain viable, though it can be beneficial in terms of the stability of the enzyme and the replenishment of cofactors.

Both enzymatic and cellular catalysts can be used in free solution or immobilised to aid retention, reuse and stability. Immobilisation can simplify the downstream purification requirements of a process by reducing the amount of crude purification that would be needed to remove a solution-phase biocatalyst. However, it adds to the cost and complexity of the upstream process of producing the biocatalyst itself and, in the case of enzymatic catalysts, can reduce the activity through steric inhibition; however the beneficial effect on stability and reuse can outweigh these considerations.

Biocatalysis is gaining popularity as a method of producing small molecular products or intermediates, and increasingly for large molecular weight polymers. An estimated 150 large scale (over 100 kg product per annum) biocatalytic processes have been implemented in the chemical synthesis industry, the majority of which are pharmaceuticals or fine chemicals (Straathof, 2006). A number of technological advances in DNA sequencing, bioinformatics and genetic engineering have contributed to the viability of biocatalysis for industrial synthesis. The discovery of restriction enzymes and their subsequent use to produce recombinant plasmids by S. Cohen and H. Boyer in 1973 allowed enzymes with specific functions to be introduced into rapidly-growing microorganisms such as *E. coli* (Bornscheuer and Buchholz, 2005).

Recombinant technologies also allow enzymes to be modified to act on non-natural substrates, tolerate a different range of temperature or pH extremes, or remain active for longer periods of time. Advances in sequencing, analysis and bioinformatics have been particularly

advantageous in this regard, allowing insights into the relationship between genomics and proteomics, and therefore likely candidates for mutagenesis.

More recently, directed evolution techniques have been used to modify the properties of enzymes, using random mutagenesis and high throughput evaluation of their activity to select mutants that are more effective in terms of substrate specificity, activity in organic solvents or stability at extremes of temperature (Bornscheuer and Pohl, 2001). You and Arnold used error-prone PCR to increase the activity of 13M subtilisin E 16-fold over the previous mutant 10M, and 470-fold in 60% DMF over the wild-type enzyme (You and Arnold, 1996). A similar technique was used to improve the specificity of Cytochrome *c* peroxidase from *S. cerevisiae* towards guaiacol, a non-natural substrate, by 300 times over the wild-type enzyme (Iffland et al., 2000).

### 1.2.2 Biocatalysis for Chemical Synthesis

Biocatalysis has a number of advantages by comparison with more common chemical catalysis methods. Biocatalysts typically do not require the high temperatures and pressures that chemical catalysts do, usually being able to operate a little above room temperature and at atmospheric pressure (Woodley, 2008). Biocatalysts also tend to have high specificity for particular substrates arising from the particular configuration of their active sites, as well as selectivity in terms of the product formed (Saibi et al., 2012). This limits the number of side reactions that occur, improving molecular efficiency and avoiding the need for numerous protection and deprotection steps that might be required when using a chemical catalyst, and may even render production using a chemical catalyst impossible, or at least impractical (Wohlgemuth, 2010).

Furthermore most biocatalysts exhibit stereoselectivity, favouring conversion to a single stereoisomer of a product while some enzymes – dehydrogenases or lyases in particular – can catalyse asymmetrical reactions, creating new chiral centres with a single stereoisomer. This is of particular benefit to the synthesis of pharmaceutical products, where enantiomeric purity

is required and would be quite costly to achieve by using multiple chemical protection and deprotection steps or purification alone (Pollard and Woodley, 2007). A number of enzymes have been identified that are capable of asymmetrical reactions that would useful to the synthesis of high-value chemicals, including hydroxylation, transamination and Baeyer-Villiger oxidation. Use of these enzymes at an industrial scale tends to be limited by their supply, though Merck and Co. Inc. have established a process using alcohol dehydrogenase from *Rhodococcus erythropolis* to perform an asymmetric ketone reduction to form an intermediate for the product of NK-1 receptor antagonists (Pollard et al., 2006; Woodley, 2008).

Aside from molecular efficiency, biocatalysts also have advantages in terms of the sustainability of synthesis. Biocatalysts conventionally operate in aqueous solution, avoiding the use of organic solvents that are commonly required for chemical synthesis. They also have the potential to avoid the use of toxic substrates. For example it has been demonstrated that the production of ketones, an essential active pharmaceutical ingredient (API), can be performed in aqueous solution with alcohol dehydrogenase from *Rhodococcus erythropolis* using non-toxic co-factors (Pollard et al., 2006).

Naturally-occurring biocatalysts can also be adapted to perform industrially useful operations, most commonly by modifying them to accept non-natural substrates or tolerate different conditions of pH or temperature. For example, the L-arabinose isomerase enzyme is a potentially useful catalyst for the industrial production of D-tagatose, but has a high optimal operating pH and temperature, which accelerate the formation side products when the reaction is run at an industrial scale (Rhimi et al., 2009). However, mutation of the enzyme to introduce a sequence associated with a greater tolerance of acidic conditions, and combination with an existing mutant that was stable at lower temperatures, resulted in a mutant enzyme with a relatively lower optimum pH of 6.5 and temperature of 65°C. Directed evolution methodologies are also particularly useful for the purpose of adapting enzymes, allowing large

libraries of mutant recombinant enzymes to be screened for the desired trait, with the best-performing mutants selected for further rounds of recombination and selection.

### 1.2.3 Biocatalysis in Microfluidics

A number of applications have arisen that utilise the strengths of biocatalysts and of microfluidic platforms. One of the advantages of using microfluidics is the reduction in the use of reagent and biocatalyst required to perform reactions, from the millilitre scale used in typical bench-top technologies down to micro- or nanolitre volumes (Wang, 2002). This is particularly beneficial when attempting to evaluate the properties of a biocatalyst as it is often expensive and time-consuming to produce large volumes of purified enzyme, but it is useful to be able to study its sensitivity to a range of conditions such as pH, temperature, substrate concentration and inhibitory factors. In such cases, use of microfluidic platforms can reduce the amount of enzyme and consumables required by a hundred to a million-fold.

Devices have been developed which take advantage of this feature to determine the kinetic parameters of enzymes such as β-galactosidase and acetylcholinesterase (Hadd et al., 1997, 1999). In both instances the chip design relied on electrokinetics to perform the fluid transport and mixing, combining enzyme and substrate. In the case of β-galactosidase catalysed reaction, a fluorescent product was formed which allowed the direct online measurement of the product concentration by laser-induced fluorescence. The thiocholine product catalysed by acetylcholinesterase was not itself fluorescent, but the chip design in this instance featured an additional junction which allowed the derivitisation of the product with coumarinylphenylmaleimide and subsequent detection in a similar fashion.

Both chips were used to determine the substrate dissociation constant ($K_M$) and turnover number ($k_{cat}$) of the respective enzymes, which were comparable to those determined by standard experimental methods. However, the enzyme and reagent consumed by the chips was much reduced, down to 120 pg of enzyme and 7.5 ng of substrate per assay in case of galactosidase. Furthermore, in this case the chip could be operated in continuous-flow mode

and the concentration of the substrate introduced to the enzyme could be stepped up or down by changing the relative flow rates. By stepping the concentration of substrate up and measuring the resultant change in fluorescence continuously a complete kinetic profile could be generated in a single 30-minute assay, from which the kinetic parameters of the enzyme could be determined. This was also applied to varying concentrations of the inhibitor phenylethyl β-D-thiogalactosidein order to determine the $K_I$ value (Hadd et al., 1997).

The scale of microfluidic devices offers further advantages beyond reduction of reagent usage. The scale of the channels used in reactor devices means that the flow regimes within them are predominantly laminar, so mixing of fluids occurs by diffusion only. The behaviour of fluids and dissolved species within the channels are therefore more simple to predict, allowing precise control of heat and mass transfer in reactions (Miyazaki and Maeda, 2006; Wiles and Watts, 2008; Fernandes, 2010). The scale of the channels also provides high surface area to volume ratios for heat exchange with the external environment and the laminar flow behaviour can be used to create large interfacial areas for exchange of soluble species where multiple fluid phases are used (Miyazaki et al., 2008; Fernandes, 2010).

Microreactors designed to exploit these properties have become increasingly popular in the chemical synthesis industry. Here additional advantages are offered in terms of temperature control, where the efficiency of heat-exchange means that isothermal operation is easier to achieve, preventing runaway reactions and the formation of side products (Jähnisch et al., 2004; Roberge et al., 2008 a). The size of the reactors also limits the hazard created by use of high pressures, temperatures or toxic reagents (Murphy et al., 2007; Roberge et al., 2008 b). Furthermore, the continuous flow operation of microfluidic reactors can serve to reduce reaction time and increase throughput, increasing volumetric efficiency and offering a way to avoid the use of large batch reactors (Anderson, 2001). Continuous flow can also be used to overcome problems with unstable or hazardous reaction intermediates by ensuring they are consumed in the next reaction step as soon as they have been synthesised (Zhang et al., 2004).

For these reasons the adoption of microreactors is steadily increasing in the chemical synthesis industry, either by scaling up or scaling out the reactor designs that have been established at the bench scale. Examples of this approach range from the production of ethylacetoacetate at a throughput of 150 g $d^{-1}$, using 30 reaction channels operated in parallel, to the use of a single scaled-up microreactor to produce 2 tons of a lithiated product over the course of a year, to the use of 100 parallel microreactors to produce 100 kilotonnes of monoammonium phosphate per year (Chambers et al., 2005; Chen et al., 2011 a; Kockmann et al., 2011).

There is increasing interest in biocatalytic microreactors for chemical synthesis, given that they can provide shorter synthesis routes and can be used to perform asymmetrical synthesis of chiral metabolites (see Section 1.2.1). Relevant examples of reactions performed include the production of pharmaceutical compounds such as L-DOPA as well as synthesis of optically-pure cyanohydrins, important precursors for the synthesis of fine chemicals and pharmaceuticals (Koch et al., 2008; Tišma et al., 2009). Biocatalytic reactors have been developed to use biocatalysts in various forms; in free solution, in the form of cell lysates or purified catalyst, or immobilised, entrapped or covalently bound within microchannels. Where the water solubility of the desired substrate is problematic, reactors have also been developed for multi-phasic systems, primarily using solubilised free enzyme in the aqueous phase (Fernandes, 2010; Marques and Fernandes, 2011).

Biocatalytic microreactors can offer similar advantages to synthesis reactions as those noted for chemical microreactors above. However, they have not yet been shown to be capable of the high throughputs of chemical microreactors, not is their adoption as wide-spread in industry. Chemical microreactors have also been demonstrated for perform multi-step synthesis reactions to work up to complex molecules, something that is lacking for biocatalytic processes to date, despite the potential advantages in terms of the products that could be synthesised (Bolivar et al., 2011). Furthermore, there has been a lot of focus on the upstream

reaction, but little on downstream steps such as purification that would help to bring about multi-step synthesis in a compartmentalised manner (Marques and Fernandes, 2011).

## 1.3 Microfluidic Downstream Processing

Numerous applications of microfluidic devices have been developed for the analysis of multi-component fluids, including a variety of different chemical species, biological samples such as DNA and proteins and analysis of cell concentration and population. Generally these components must be individually extracted in order to effect an efficient analysis of their properties, or the samples need to be prepared in some way (such as concentration or removal of particular components), which has led to the development of a number of different 'on-chip' separation techniques suitable for the processing of biological samples (Pamme, 2007 b). These techniques rely on microscale fluid phenomena, in particular laminar flow, as well as the enhanced effects of electrical, thermal and magnetic fields in order to differentiate particles and molecules based upon size, charge:size ratio, polarizability, magnetisation, density and, in the case of peptides or polypeptides, isoelectric point (see Table 1). This section will discuss these techniques and their applicability to downstream processing of biological material.

| Technique | Separation by | Separation of | Flow rate | Reference |
|---|---|---|---|---|
| **Acoustophoresis** | Size, density, compressibility | Polyamide spheres, red blood cells | 0.1 – 0.4 ml $min^{-1}$ | (Nilsson et al., 2004; Petersson et al., 2005) |
| **Obstacle-based (including membranes)** | Size | Polystyrene beads (0.6 – 1.0 µm), DNA (100 bp – 158 kbp), blood components | 10 – 100 pg $h^{-1}$ (DNA) 5 – 12 µl $min^{-1}$ (blood) | (Duke and Austin, 1998; Huang et al., 2004; Sethu et al., 2006) |
| **Obstacles and electric field** | Size | DNA (50 bp – 209 kbp) | 10 pg $h^{-1}$ – 10 ng $h^{-1}$ | (Huang et al., 2002; Fu et al., 2007) |

| Technique | Separation by | Separation of | Flow rate | Reference |
|---|---|---|---|---|
| **Hydrophoretic separation** | Size | Polystyrene beads (8 – 20 µm), white from red blood cells | Not specified | (Choi and Park, 2007; Bernate et al., 2013) |
| **Free-flow isoelectric focusing** | Isoelectric point | Proteins | 42 nl $s^{-1}$ | (Macounová et al., 2001; Xu et al., 2003) |
| **Dielectrophoresis** | Size, polarisability | Yeast (viable from non-viable), *E. coli* (labelled from unlabelled) | 40 – 300 µl $h^{-1}$ | (Doh and Cho, 2005; Hu et al., 2005; Li et al., 2007) |
| **Optical lattice** | Size, refractive index | Protein microcapsules (2 – 4 µm) | 1,200 particles $s^{-1}$ | (MacDonald et al., 2003) |
| **Free-flow magnetophoresis** | Size, magnetic labelling, inherent magnetic properties | Magnetic particles, *E. coli*, HeLa cells, red/white blood cells | 5 – 40 µl $h^{-1}$ | (Han and Frazier, 2006; Pamme and Wilhelm, 2006; Xia et al., 2006) |
| **Thermal fluid-flow fractionation** | Size, thermal capacity | Small molecules, polystyrene beads (nm) | 0.01 – 7 ml $h^{-1}$ | (Edwards et al., 2002) |
| **Sedimentation** | Size, density | Polystyrene beads (1 – 20 µm) | 1 ml $h^{-1}$ | (Huh et al., 2007) |

**Table 1: Types of microfluidic separation techniques and applications to biological materials.**

### 1.3.1 Diffusion Based Separation

The simplest device allowing the separation of species based on diffusion is the H-filter or 'membraneless' filter (Squires and Quake, 2005). This design makes use of the lack of convective mixing at micro-scale to combine two streams of fluid in a single channel. The relationship between mass transfer due to advection and transfer due to diffusion is represented by the Péclet number, which is the product of the Reynolds number (Re) and the Schmidt number (Sc), defined as:

$$Pe = Re \cdot Sc \quad (1)$$

$$Pe = \frac{\rho u L}{\mu} \cdot \frac{\mu}{\rho D} \quad (2)$$

$$Pe = \frac{uL}{D} \quad (3)$$

Where $\rho$ and $\mu$ are the density and viscosity of the fluid, $u$ is the velocity of the fluid, $L$ is the characteristic length of the surrounding channel (perpendicular to the flow of fluid) and $D$ is the diffusivity of the molecule concerned. A high Pé value indicates the dominance of mass transfer by advection within system, whilst a low Pé value indicates the dominance of diffusive transfer. The Péclet number is typically very low in microfluidic channels, so mixing between two solutions is poor and mass transfer occurs only by diffusion.

In an H-filter two fluid streams are able to flow in parallel without mixing, but particles are able to diffuse across the liquid-liquid boundary. Smaller particles with lower Péclet numbers (i.e. higher diffusivity) can diffuse across the boundary into the clear stream more quickly, and were separated out when the two streams were split at the other end of the device (see Figure 1). By selecting appropriate channel lengths and fluid velocities a variety of particles with different diffusivities could be separated (Brody et al., 1996). This device was limited in its separation resolution and selectivity, but more sophisticated designs have been presented utilising multiple H-filters or so called 'flat' filters (where the streams are brought together in the vertical plane) to improve both of these properties (Yager and Brody, 2004). This device was proposed for use as a tool for extracting urea from blood and was theoretically capable of reducing the level of urea to 0.01% of its original level in 1.1 hours.

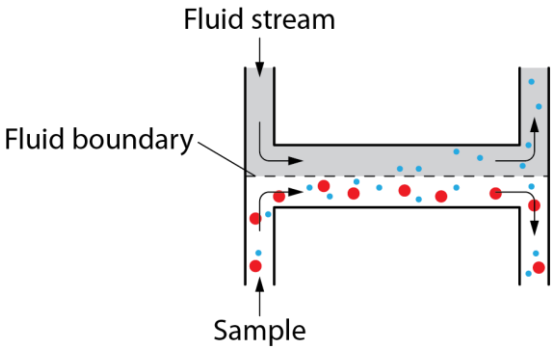


**Figure 1: Illustration of an H-filter device.**
**Smaller particles with lower Péclet numbers (blue) are able to diffuse more quickly and cross the fluid boundary, whilst larger particles (red) cannot.**

Microscale diffusional separation methods are governed by the characteristic diffusional length, *l*:

$$l = \sqrt{Dt} \tag{4}$$

Where *D* is the diffusion coefficient of a spherical particle and *t* is the time over which diffusion takes place. *D* is given by:

$$D = \frac{k_B T}{6\pi\eta r} \tag{5}$$

Where $k_B$ is the Boltzmann constant, *T* is temperature, $\eta$ is viscosity and *r* is the particle radius. Assuming a particle radius of 8μm, the diffusion coefficient of a stem cell in water at room temperature would be 6.13×10-14 $m^2s^{-1}$, which in turn gives a characteristic diffusion time of 1630 seconds for a distance of 10 μm. This may be useful for separating stem cells from proteins, which generally have diffusion times a factor of 10 smaller over the same distance. Having said this, the maximal separation efficiency that could be achieved from a single H-filter would be 0.5, as the concentrations of proteins in the two streams would eventually equilibrate. Multiple H-filters arranged in series would be required to achieve higher efficiencies, making the design more complex.

### 1.3.2 Flow Based Separation

Pinched flow fractionation also allows the sized-based separation of particles, but does not rely on their relative diffusivities. Two streams are brought together, one containing particulates and moving at a lower flow rate, the other clear and moving at a higher flow rate, which are then focused through a narrow aperture (47-82μm) into a wider channel. This focusing causes the path of the particles to deflect when they enter the wide channel, with smaller particles being deflected to a greater degree than larger particles. The focussing causes the smaller particles to become trapped in the slower moving fluid due to their closer proximity to the channel wall, while larger particles are accelerated due to their greater exposure to the faster flow (see Figure 2A). The particulate mixtures can be fractionated by dividing the wider channel into a series of parallel channels of smaller width, such that particular sizes are deflected into specific outlets. This method has been used to separate polystyrene beads based on size and red blood cells from serum (Yamada et al., 2004; Takagi et al., 2005).

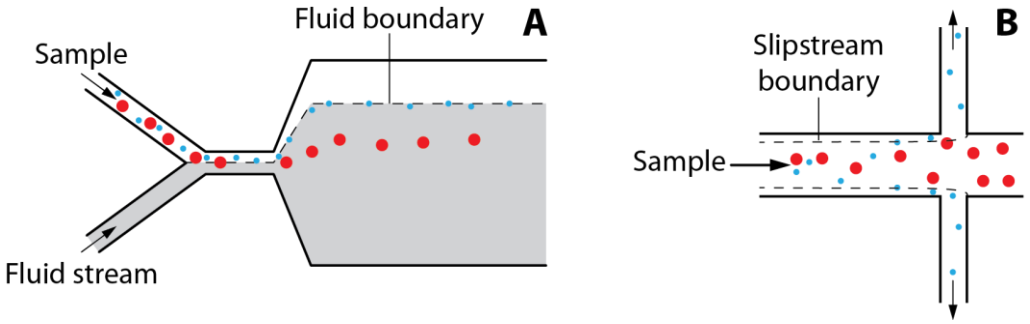


**Figure 2: Illustration of pinched-flow fractionation (A) and hydrodynamic filtration (B) devices.**

Hydrodynamic filtration utilises a similar effect to purify and concentrate streams of particulates. A main central channel is used with sets of smaller channels branching off at right angles. The flow rate is set so that fluid exits from both the main channel and the branched channels, creating a 'slipstream' of fluid that runs along the walls of the main channel and is drawn into the branches. When particles flow through the main channel, the slipstream draws them towards the wall of the main channel and, if the particles are small enough, they will be drawn out of the main channel altogether (see Figure 2B). This effect can be used to purify particles by size or to concentrate a suspension (Yamada and Seki, 2005).

This has been applied specifically in the extraction of plasma from whole blood, adjusting the branch channel such that red blood cells remain in the centre of fluid flow and allowing high throughputs of near-pure plasma to be achieved (Jaggi et al., 2007). A more recent design has used a gradually decreasing branch channel length to incrementally reduce the hydraulic resistance of each successive channel, allowing the gradually fractionation of smaller particulates. This was used to separate fungal spore populations from larger cellular debris (Inglis and Herman, 2013).

A system with a very similar design was used to separate white blood cells from red blood cells, but a buffer solution was perfused through the side channels and across the main channel, perpendicular to the main flow of fluid. This secondary fluid flow pushed the red blood cells into the side channels and out of the device whilst retaining white blood cells, which were too large to fit through the narrow (~3µm) apertures and were driven along the main channel (VanDelinder and Groisman, 2007).

Hydrophoretic separation employs a similar phenomenon to hydrodynamic filtration, but in this case the boundary flow effect is used to differentiate particulate sizes within a single channel rather than using additional side channels. Angled grooves are fabricated into the floor of a wide channel, sized such that the smaller particles to be separated will be able to fit into them wholly but the larger particles will not. The grooves create stagnant zones where fluid flow slowed and aligned towards the direction of the groove. Two or more fluid streams are used to focus the mixed population of particles to one side of the channel. Larger particles, unable to fit completely into the grooves, will be driven over them by main fluid flow and will not deviate across the channel from the point at which they were entered it. Smaller particles, slowed by the boundary flow at the channel floor, will be able to drop into the stagnant zones and will be drawn towards the opposite side of the channel. This principle has been demonstrated for the separation of polystyrene beads by size as well as for the separation of red and white blood cells, where the discoid shape of the former allowed them to be drawn into the grooves more easily (Choi and Park, 2007; Bernate et al., 2013).

### 1.3.3 Obstacle Based Separation

Devices that operate in a manner analogous to filters have been developed from scratch, as demonstrated by Chen et al. Their device was designed to allow the integrated isolation, lysis and DNA purification of white blood cells from whole blood. The separation system consisted of a tortuous channel lined with 20µm pillars, which were spaced out to leave 6.5µm gaps. This allowed red blood cells and other contaminants to move into the two waste streams alongside the main channel, whilst retaining the white blood cells (Chen et al., 2007 b). Having the fluid flow perpendicular to the mass transfer across the bordering pillars in this way prevented the device from becoming clogged.

Other, more conventional, filtration systems have also been developed. PDMS lends itself to the incorporation of membrane materials such as polysulphone due to its compressibilty and the relative ease with which it can be sealed (Duffy et al., 1998). A polyvinylidene fluoride (PVDF) membrane was sandwiched into a PDMS system and pre-treated with BSA to enantioselectively separate a racemic mixture of L- and D-tryptophan (Wang et al., 2002). Another device developed by Ismagliov et al. incorporated two polycarbonate membranes into two sets PDMS channels aligned perpendicularly to one another, forming a grid of microreactors. Gradients of chemical inputs could be applied along the two sets of channels, allowing reactions to be performed under a variety of input conditions simultaneously (Ismagilov et al., 2001). Although not strictly a separation technology, it demonstrates the ability to incorporate prefabricated membranes into microfluidic devices.

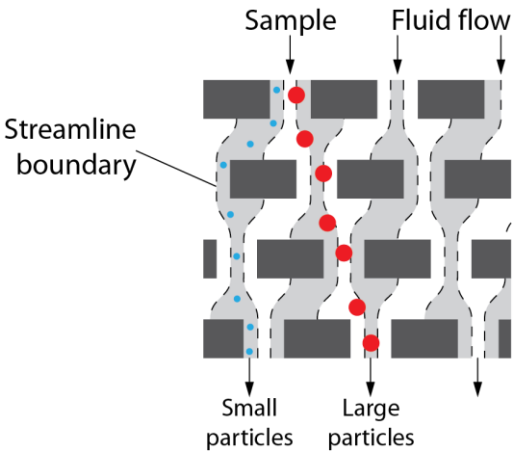


**Figure 3: Illustration of a lateral displacement device.**
**Smaller particles (blue) are able to remain with a single streamline and follow the most direct route through the obstacles. Large particles (red) cannot remain within the streamlines and are displaced towards the side of the device.**

Several methods of sized-based particle separation have been developed to work without the need for physical retention. One such method, lateral displacement, uses a wide channel containing rows of micron-sized posts, each row being slightly out of line with the other. When fluid is passed through the channel from one corner to the opposing corner it creates streamlines which follow the most direct path through the posts (see Figure 3). Smaller particles are able to remain within these streamlines and pass through the device quickly, whilst larger particles are displaced towards the side of the channel (Duke and Austin, 1998). This technique has been applied to separate DNA by size and individual components of whole blood (Huang et al., 2004; Sethu et al., 2006). Importantly, the effectiveness of the separation depends more on the lateral displacement between the successive rows of posts than it does on the gap between individual posts. This means that particles can be effectively separated without the risk of them becoming trapped within the device, unlike more conventional physical trapping techniques which rely on the particles or molecules being directly retained by the obstacles (Pamme, 2007 a).

### 1.3.4 Homogenous Electrical Field Separation

Homogenous electrical field separations use a combination of flow-driven and electrophoretically-driven movement to separate molecular mixtures. Typically, the solution

is passed through a shallow chamber with an electrical field applied across is, perpendicular to the direction of flow. The molecules are deflected from their flow path by the field depending on their charge and can be collected in separate outlets (see Figure 4).

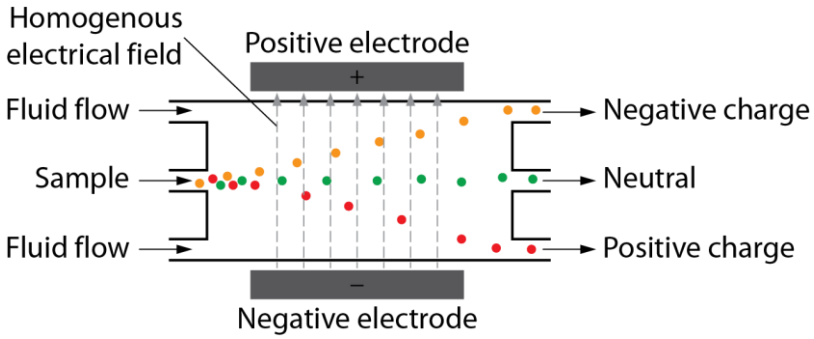


**Figure 4: Illustration of a device using free-flow electrophoresis.**
**A particle mixture is passed through a homogenous electrical field; particles with a positive charge (red) move towards the negative electrode, whilst particles with a negative charge (orange) move towards the positive electrode. Particles with no net charge (green) do not move towards either electrode.**

One of the first examples of homogenous electrical field separation was free-flow electrophoresis (FFE), originally developed at larger scale to carry out rapid separations in chemistry and biochemistry. Devices designed to perform such separations at micro-scale were found to have distinct advantages over their larger-scale counterparts as their greater surface area:volume ratio allowed better heat dissipation. This meant that stronger fields could be used without the adverse effect of heating and thermal convection currents on separation performance (Krivánková and Bocek, 1998; Pamme, 2007 a).

There are numerous examples of free-flow electrophoresis available, based around molecular separations of molecules with different charge:size ratios. One particular example allowed the very rapid, high-resolution separation of amino acid mixtures, where the average residence time of a molecule on the chip was only two seconds (Krivánková and Bocek, 1998; Zhang and Manz, 2003; Pamme, 2007 a).

A large proportion of the systems developed attempt to address the problem posed by generating high voltage fields without exposing the solution being separated to the electrodes. The original devices fabricated from silicon without electrodes which directly contacted the

solution were only able to generate fields up to 100 V $cm^{-1}$ whilst later revisions in other materials such as PDMS and glass were able to reach 200-300 V $cm^{-1}$ (Raymond et al., 1994). This was better than the devices with electrodes which directly contacted the solution, where field strengths could only reach a few tens of V $cm^{-1}$ (Macounová et al., 2001). More elaborate solutions have since been developed by exploiting the laminar flow conditions at microscale to introduce trenches of fast-flowing fluid between the electrodes and the sample solution, allowing the field strengths of up to 580 V $cm^{-1}$ (Fonslow et al., 2006).

A slight enhancement of this separation method has been made to efficiently separated proteins or polypeptides according to their isoelectric point (pI), known as free-flow isoelectric focusing. The device design is essentially the same as those described above, but a pH gradient is created across the width of the channel by flowing an acidic and an alkali solution through troughs at either side. When the sample of polypeptides is passed through the channel, they migrate according to their charge towards the area of channel where the pH is equivalent to their pI. At this point their overall charge becomes zero and migration ceases. A device of this kind was developed by Kohlheyer et al. which was capable of generating a pH gradient from 3 to 10, as well as efficiently transmitting the majority of the electric potential to the separation channel (Kohlheyer et al., 2006). Devices have been used to separate mixtures of amino acids, peptides and whole proteins by their pI, in some cases resolving the individual components is sub-second residence times (Macounová et al., 2001; Xu et al., 2003).

Electrophoresis has also been combined with obstacle-based separations to resolve DNA chains based on their length. The devices consist of several channels joined by weirs which are a significantly shallower than the channels themselves. By flowing a sample of mixed lengths of DNA into one of the channels and applying an electric field, the different lengths of DNA could be separated into separate channels, with shorter chains being able to travel through the weirs more easily and therefore travelling further across the chip from the starting point (Huang et al., 2002; Fu et al., 2007).

### 1.3.5 Inhomogeneous Electrical Field Separation

Inhomogeneous electrical field separation (also known as dielectrophoresis or DEP) utilises a non-uniform electric field to generate dipoles on particles within a solution and has an advantage over FFE methods since the particles do not need to have an inherent charge to be separated. Instead, the field exerts a force on the particles, the strength of which is dependent on the polarizability of the particles. More polarisable particles move towards the highest field strength area, whilst less polarisable particles move towards the field minimum (see Figure 5). DEP is a widely adopted separation technique at microfluidic scale, but is difficult to scale up as the force generated by the electrical field decays exponentially from the electrode surface (Hughes, 2002).

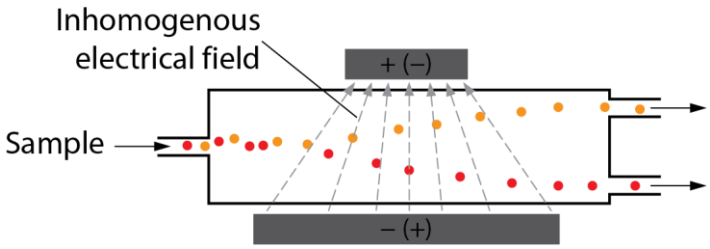


**Figure 5: Illustration of a device using dielectrophoresis.**
**A particle mixture is passed through an inhomogenous electrical field; particles with greater polarizability than the surrounding fluid (orange) move towards the area of stronger electrical field, whilst particles with a lesser polarizability than the surrounding fluid (red) move towards the area of weaker electrical field.**

Inhomogeneous electrical fields can be generated by applying a fixed voltage across a microfluidic channel containing obstacles. A uniform voltage can be applied across the entire length of the channel, generating non-uniform fields where the depth of the channel changes. This can be used to effect a separation in a number of ways, depending upon the channel design. Barrett et al. designed a chip which was able to separate *Bacillus subtilis* cells from polystyrene beads by placing ridges at either side of a central channel. When an electrical field was applied to the chip, the shallow areas over the ridges became charged, preventing the cells from passing into side channels but leaving the polystyrene beads unaffected (Barrett et al., 2005).

A more complex system was designed by Fu et al. to separate DNA molecules, consisting of a series of trenches separated by arrays of alternating pillars and shallows. Two electrical fields were applied, one parallel to the trenches and another perpendicular to them. The parallel field drove the negatively charged DNA molecules along the length of the channel, whilst the perpendicular field drove the molecules to cross from one channel to the next. The molecules could be separated in three different ways, depending upon the electrical fields applied and the ionic properties of the fluid, either on the basis of size (favouring small or large molecules) or of charge (Fu et al., 2007).

DEP may prove to be particularly useful for label-free cell separations. The current methods for separating and counting stem cells from populations of differentiated cells revolve around antibody labelling either with fluorescent particles (for FACS) or magnetic particles (for MACS). Antibody labelling has previously been used to modify the polarizability of cells with specific surface markers (Hu et al., 2005), but a newer method allows separation on the basis of the surface markers themselves, without the need for antibodies. This was used to separate populations of yeast into live and dead cells (Li et al. 2007). The resolution was relatively low, as was the efficiency (around 25% of the cells were trapped in the chip), but with further development this method could potentially be used to separate stem cells on the basis of pluripotency markers, without antibody labelling.

### 1.3.6 Other Flow Fractionation Techniques

A multi-functional rotating platform known as Bio-Disk has been developed which can be used to carry out centrifugal separations at the microfluidic scale. By equipping a Bio-Disk with an appropriate channel design, the rotary force generated by a CD player (or the proprietary Bio-Disk rotor) can be used to carry out single or multi-step separations on the basis of density. A simple single channel design has been used to separate hematocrit from pure blood to determine its concentration, whilst a more complex design featuring two separation chambers connected by a channel was used to isolate pure plasma. A battery-

powered DEP device was also integrated to allow two-dimensional separation by density and polarizability, used to separate dead from viable cells (Ducrée et al., 2007).

A high-throughput technique for clarifying particulate suspensions, the 'microfluidic equivalent of centrifugation,' was developed using high-frequency acoustic standing waves to isolate the particles from the fluid. A piezoelectric transducer was used to generate the standing waves within a silicon cavity which the fluid was then passed through. The particles were drawn to and held in the pressure node created by the standing waves, allowing clear fluid to be drawn out (Harris et al., 2003).

### 1.3.7 Separation Technique to be Investigated

There are a number of criteria to be fulfilled in the selection of a suitable microfluidic downstream processing platform. The platform must of course be capable of performing the separations required without causing damage to the desired product. It must also be scalable if the platform is to be used to evaluate conditions for potential large-scale processes. The flexibility to test different separation conditions is also important. The ease of design, fabrication and use are not as critical to the selection, but must still be considered.

A simple dead-end filtration chip is likely to be the best option for an initial design. Filter membranes can be bonded into PDMS, one of the more popular material choices for microfluidic chips, relatively easily (Ng et al., 2002). Also, the fabrication of a membrane filtration chip would potentially be much easier and quicker to perform than that of other chip designs, such as the more complicated hydrodynamic filtration chip developed by Yamada and Seki or the lateral displacement channel described by Duke and Austin, due to the lack of small feature sizes. Additionally, the simpler membrane filtration chip would have fewer internal surfaces which could entrap cellular material, an effect noted in hydrodynamic filtration chips with large internal surface areas (Carlson et al., 1997).

Whilst a dead-end membrane filtration chip could be used to concentrate cell suspensions or to remove reagents, a more complex chip designed for tangential or 'cross-flow' filtration

might have more versatility. The tangential flow regime is advantageous as it tends to prevent an excessive build-up of solid material on the membrane, a problem which would be observed in the dead-end flow configuration. This fouling effect would reduce the efficiency of the dead-end filter and may also damage the cells.

A tangential flow filter could allow a greater degree of control over the separation process by the fine tuning of the feed flow rate, cross flow rate and transmembrane pressure (TMP) to alter the rate of diffusion across the membrane. Such a device might be used to exchange growth media where necessary (e.g. during directed differentiation processes) and would allow the cells to be recirculated more easily.

## 1.4 Membrane Filtration in Bioprocessing

Membrane filtration has historically played a major role in bioprocessing, including some of the earliest examples of modern bioprocesses, and is still commonly used for a variety of purposes due to its versatility and the range of filtration technologies, membrane types and pore sizes available (Ladisch and Kohlmann, 1992; van Reis and Zydney, 2007). Filtration processes are susceptible to fouling, accumulation of particles on the surface or inside the pores of the membrane, reducing its permeability. This in turn reduces its capacity, the amount of material that the membrane can be used to process before it must be cleaned or replaced, adding to the cost of the process. Determining the best conditions for product yield and membrane lifetime is therefore a high priority for the development of a bioprocess involving membrane filtration.

This section will discuss the types of membrane available, applications to bioprocessing, the equations that have been developed to describe the behaviour of membrane separations (particularly with regards to fouling) and finally the developments that have been made in microfluidic filtration.

### 1.4.1 Filtration Technology, Membrane Types and Applications

Types of membrane filtration operation can be broadly categorised by the size of particle or molecule that is retained by the membrane, with the membranes being classified by their average pore size or molecular weight cut-off (the largest size of molecule that is able to pass through the membrane). Different membrane filtration operations can be used at various stages in a bioprocess, though the operations typically directly involved are microfiltration, ultrafiltration and virus filtration. Nanofiltration and reverse osmosis are also used, but usually in preparative steps such as water purification, rather than the process itself.

Microfiltration uses pore sizes in the region of 0.1 – 10 μm and is therefore used for the purpose of retaining cells, particularly for performing initial separations of cells from smaller solutes or for removing excess liquid. Virus filtration uses smaller pore sizes on the order of hundreds of nanometers to retain virus particles, a function which is particularly important in bioprocessing for ensuring the sterility of thermolabile products such as proteins, which could not be sterilised by heat treatment. Ultrafiltration has pore sizes on the order of tens of nanometers, which are typically defined by a MWCO in Daltons (Da, equivalent to one twelfth of the weight of a carbon atom), and is typically used at the latter stages of the process where retention of macromolecular components is required. It is commonly used in diafiltration operations, used to exchange buffer solutions between different chromatography steps (Kalyanpur, 2002).

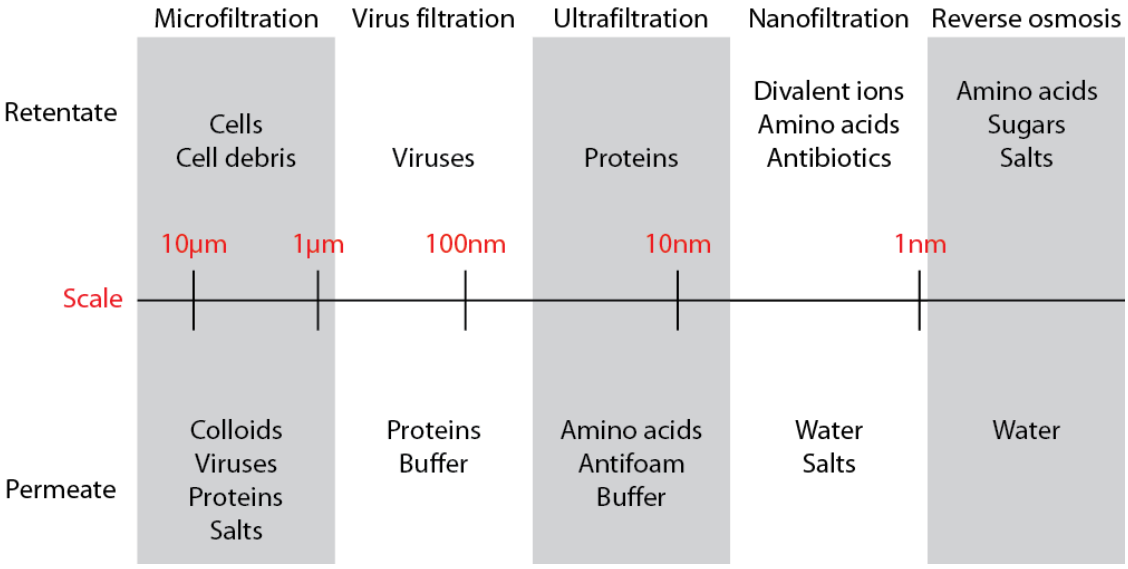


**Figure 6: Typical separations in different membrane technologies (adapted from van Reis and Zydney, 2007).**

Membrane filtration is operated in one of two flow modes; normal flow, where the feed solution is applied perpendicularly to the membrane surface, and tangential flow, where the feed solution is applied in parallel to the surface (see Figure 7). In the case of tangential flow a fluid stream may also be applied in parallel to the permeate side of the membrane, either in the same direction as the feed solution (co-current) or in the opposite direction (counter-current).

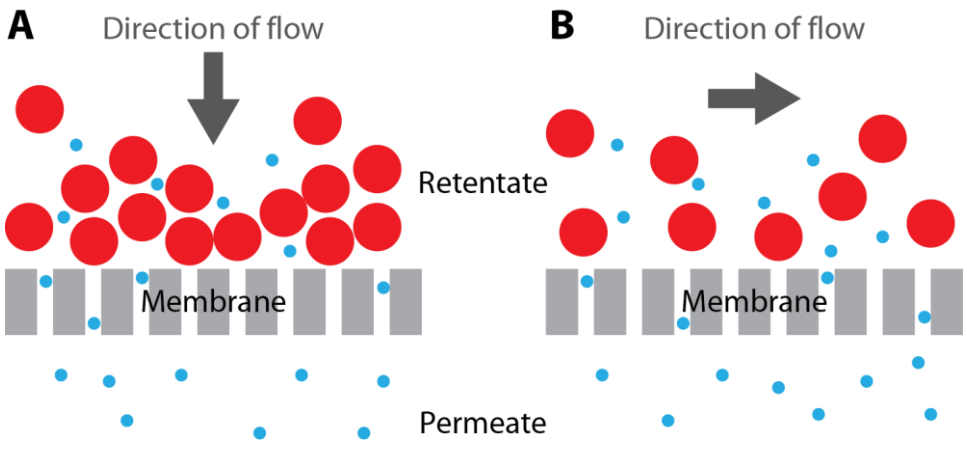


**Figure 7: Illustration of two main modes of filtration; normal flow (A) and tangential flow (B).**

Normal flow filtration is typically only used with microfiltration membranes in situations where the feed solution contains a low concentration of particulates, as rapid fouling can occur otherwise. In particular, normal-flow microfiltration has been used in place of centrifugation

for the industrial-scale harvesting of mammalian cells immediately following their growth, in order to avoid exposing the cells to the high shear forces generated by centrifuges at this scale. Higher cell concentrations can also be recovered using tangential flow microfiltration in order to overcome the fouling effects observed in normal flow mode (van Reis et al., 1991; Kalyanpur, 2002).

Ultrafiltration membranes are used almost exclusively in tangential flow mode and usually utilised in the later stages of downstream processing. Ultrafiltration unit operations tend to involve the concentration of protein solutions or the exchange of solutes with much smaller molecular weights (at least 5 – 10 times smaller) than the protein being retained. In the case of concentration operations the filter would be operated without any permeate fluid stream, just recycling the retentate stream until the proteins were at the desired concentration. Where exchange of solutes is required, a permeate stream could be run in counter-current mode, creating a constant concentration gradient across the length membrane.

### 1.4.2 Governing Equations

In membrane filtration the key metric of filtration performance is the membrane flux, the volumetric flow rate of fluid through the membrane normalised to the membrane area, with units of $L{\cdot}m^{-2}{\cdot}s^{-1}$. The pressure applied to the retentate ($P$) and the flux through the membrane ($J$) can be related by Darcy's law:

$$J = \frac{P}{R\mu} \tag{6}$$

Where $\mu$ is the viscosity of the solution and $R$ is the resistance of the membrane to fluid flow, a property which increases as the filtration process proceeds and the membrane becomes fouled by particulates.

There are several models of pore blocking in membrane filtration which can be used to relate the changing resistance of the membrane to the volume of fluid that has been processed or the length of time that the process has been running for. The standard model describes the

membrane as a series of cylindrical pores with a defined initial radius that decreases as particulates build up on the inner surface (Bolton et al., 2006). In this case, the changing resistance caused by fouling ($R$) can be related to the initial resistance of the membrane itself ($R_0$) as a function of the volume of liquid processed by the following equation:

$$R = R_0 \sqrt{1 - \frac{K_S V}{2}} \tag{7}$$

Where $K_S$ is the standard blocking constant, which can be determined experimentally for particular combinations of membrane and liquid by measuring the change in flux as the volume of liquid processed increases and fitting the model to the data.

Fouling can also be modelled as the complete blockage of pores by particulates, reducing the overall area of membrane available for fluid to flow through rather than increasing the resistance of the membrane. The ratio of available membrane area ($A$) to the initial area ($A_0$) can be related to the volume of liquid processed by the following equation:

$$\frac{A}{A_0} = 1 - \frac{K_b}{J_0} V \tag{8}$$

Where $J_0$ is the initial flux of fluid through the unfouled membrane and $K_b$ is the pore blocking constant, which again can be determined for a particular combination of membrane and process fluid by fitting the model to experimental data.

Finally, fouling can be modelled as the build up of a cake layer on the surface of the membrane, causing additional resistance to fluid flow on top of the resistance of the membrane itself. This increase in resistance is related to the volume of fluid processed by:

$$\frac{R}{R_0} = (1 + K_c J_0 V) \tag{9}$$

Where $K_c$ is the cake filtration constant, determined as above for $K_i$ and $K_b$. In reality the fouling of a filtration membrane will involve a combination of the above models, such as cake

formation and standard fouling models. Where the pressure or volumetric flow rate is kept constant throughout the process, the combined effect of the different models on the change in flux can be related through Darcy's law, essentially becoming a summation of the different resistances. For example, relating the cake formation and standard fouling model for a constant pressure filtration operation, Darcy's law becomes:

$$J_0 R_0 \mu = P = JR \tag{10}$$

$$\frac{J}{J_0} = \frac{R_0}{R} = \frac{1}{\sqrt{1 - \frac{K_S V}{2}} + (1 + K_c J_0 V)} \tag{11}$$

The equation can then be integrated to determine the change in flux as a function of time and, with $K_s$ and $K_c$ determined experimentally, can be used to predict the rate of flux decline and determine the point at which the membrane would need to be changed. Other models of fouling can be combined in same manner (Bolton et al., 2006).

### 1.4.3 Microfluidic Devices for Membrane Filtration

The number of reported microfluidic devices featuring integrated filtration membranes has increased significantly over the past decade, primarily for the purposes of on-chip sample preparation (de Jong et al., 2006). A large number of microfluidic chips have been developed for investigation of complex biological samples, particularly for the purposes of medical diagnostic tests, where the size of the devices and the ability to incorporate multiple sample preparation and analysis steps onto a single chip is especially attractive for point-of-care diagnostics (Rivet et al., 2011). Where membranes have been integrated into these chips, they have been used to remove unwanted components from test samples, for example isolating plasma or white blood cells from whole blood, or to isolate bacterial cells or spores for the purposes of detection (Crowley and Pizziconi, 2005; Floriano et al., 2005; VanDelinder and Groisman, 2006, 2007).

Microfluidic chip designs have also been reported for the non-invasive analysis of fouling of membranes when used for the filtration of particulate streams, including biological samples,

which may be of particular interest for bioprocessing applications. These devices tend to consist of a membrane fabricated or sealed in place into a set of channels, with a clear window over a part of the membrane to allow the cake formation to be observed under a microscope (see Figure 8A). Other methods such as laser triangulometry or refractometry have also been used to observe the rate of cake formation (see Figure 8B), where respectively the distance that an angled laser beam is deflected by the surface of the cake or the degree of refraction of the laser through the cake layer was used to estimate the cake thickness (Chen et al., 2004).

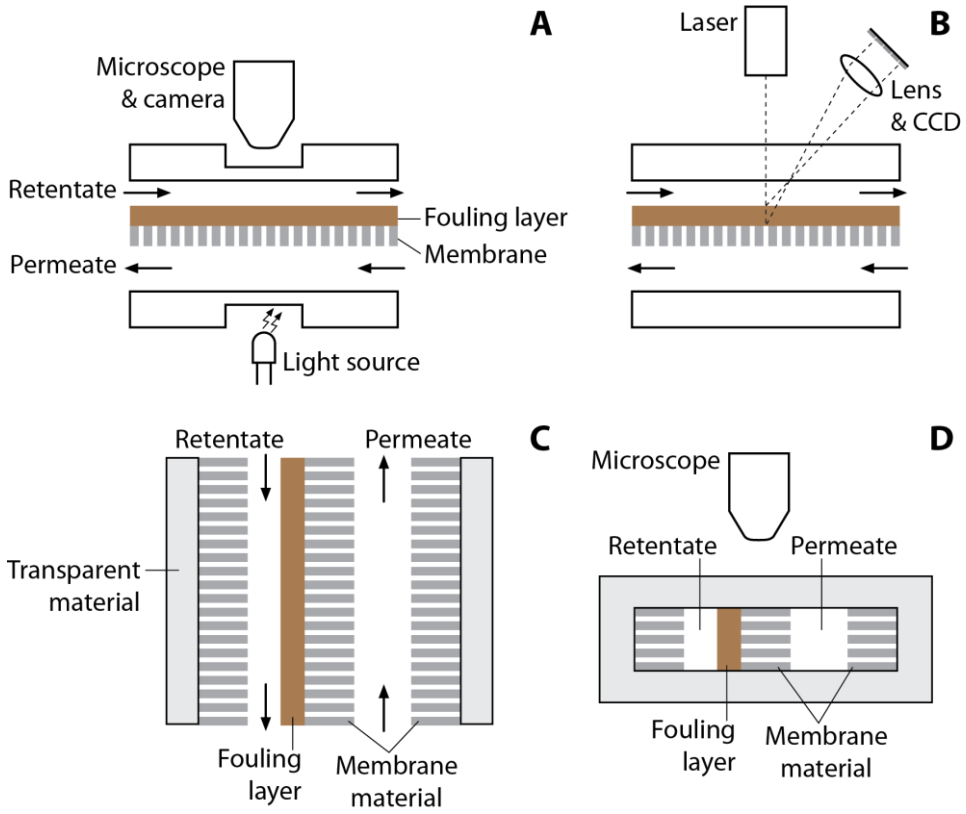


**Figure 8: Illustration of devices reported in literature for in-situ analysis of fouling in membrane filtration. (A) and (B) respectively show measurement of the fouling by transmission of light through the fouling layer and by laser refractometry. (C) and (D) show a top view and side view of a device designed to allow the direct observation of fouling layer formation during filtration.**

Mores and Davis demonstrated the direct observation of membrane fouling in the microfiltration of yeast, carried out using cellulose acetate and anodised alumina membranes sealed into an acrylic support with glass plates on either side providing transparent windows for the observation the membrane. This setup was used to evaluate the rate of cake formation and the distribution of yeast cell deposits in the two membrane types by continuously

recording the build-up of dyed cells on the surface. Significantly, from a bioprocess evaluation perspective, it was also used to determine the effect of different lengths of back-washing steps on the removal of the deposited cells from the membrane surface, using the images generated to estimate the clearance of the surface (Mores and Davis, 2001).

The main disadvantage of this system was that the thickness of the cake layer could not be determined *in situ*, but had to be measured after the filtration experiment had been completed by SEM. Ngene *et al.* reported the use of a microfluidic chip that overcame this problem, which consisted of two parallel channels fabricated in membrane material (polyetherimide/polyvinylpyrrolidone/N-methylpyrrolidone), separated by a small strip of membrane and sealed on one side with a glass slide (see Figure 8C & D). A solution of 6 µm polystyrene particles in water was flowed through one channel, the retentate, and were retained, while the water was able to flow through the divide and into the permeate channel. By continuously observing the process under a light microscope, the build-up of particulates on the membrane surface could be recorded, allowing the change in cake thickness to be measured in real time (Ngene et al., 2010). This demonstrates the potential power of microfluidic membrane devices for bioprocess evaluation, although relatively few devices have been reported specifically for this purpose, nor for the purpose of evaluating whole bioprocesses at the microfluidic scale.

## 1.5 Aims of the Thesis

The overall aim of this thesis is to demonstrate the use of microfluidics for scale-down studies of bioprocessing, in particular for the investigation of upstream and downstream steps and their interaction when combined, an aspect that has not been extensively explored in the literature to date. An additional aim is to investigate how microfluidics might be used to intensify the output of established scale-down bioprocesses. There are examples in literature of the intensification and subsequent scale-up of chemical synthesis reactions and it may be beneficial to investigate whether the same might be possible for biocatalytic synthesis reactions.

Chapter 3 of this thesis shows the development and initial characterisation of a device for the investigation of filtration processes at the microfluidic scale. Chapter 4 demonstrates how the filtration device could be combined with a biocatalytic reaction performed in a continuous-flow microfluidic reactor and, in particular, how the operation of the two devices could be investigated separately before they were brought together into a single network.

Chapter 5 presents the development of a novel microfluidic reactor for the intensification of the biocatalytic reaction performed in Chapter 4, creating an analogue of a fed-batch operation in a continuous-flow device. Finally, Chapter 6 outlines a conclusion of the presented work and suggests what further work might be performed to make the devices more suitable for bioprocess development and for intensive production of chiral metabolites at microfluidic scale.

# 2

# Materials and Methods

## 2.1 Fabrication

### 2.1.1 Micromachining

Rigid parts of the filter and SHM reactor were designed with 3D modelling software Solidworks (Dassault Systèmes, Vélizy-Villacoublay, France) and translated into G-code instructions using Mastercam (CNC Software Inc, Tolland, USA). Parts were fabricated in poly(methylmethacrylate) (PMMA) or polycarbonate (PC; RS Components Ltd, Corby, UK) with a CNC milling machine (Folken IND, Glendale, USA), using various gauges of micromill tools from 0.1 to 2 mm (Kyocera, Kyoto, Japan). Areas were cut in a spiral pattern with a 70% overlap and maximum depth cut of 0.5 mm.

### 2.1.2 Laser Ablation

The parts of the multi-input reactor were designed in Adobe Illustrator (Adobe, San Jose, USA) and fabricated in 1.5 mm PMMA using a $CO_2$ laser marking head (Laserlines, Banbury, UK) with a maximum power of 25 W. The features were ablated with a power of 50% and a mark speed (laser tracking speed) of 200 mm $s^{-1}$ and 10 mm $s^{-1}$ for channels and cut-outs, respectively.

### 2.1.3 Polymer Casting

Gaskets for the filtration devices were made from poly(dimethylsiloxane) (PDMS, Sylgard 184, Dow Corning, Midland, USA). The liquid polymer was prepared in a ratio of 10:1 monomer to curing agent, degassed and then cast in PMMA moulds which had been fabricated on a milling machine (as described above). The PDMS was degassed in the mould and then cured at 90°C for 2 hours.

### 2.1.4 Assembly of Filter by Clamping

Membranes for the filtration unit were cut to size from commercially available regenerated cellulose or polysulphone sheets (Durapore, Millipore, Cork, Ireland) using a $CO_2$ laser marking head (Synrad Inc., Mukilteo, WA, USA). Polyvinyldifluoride (PVDF) membranes (Durapore) were cut to size with a scalpel.

Interconnect ports were milled from 5 mm PMMA, with two holes tapped with an M3 thread for attachment to the device, and an M6 threaded hole to allow standard connection fittings to be used (P-221, Upchurch Scientific, Oak Harbor, USA).

The interconnect ports were attached to each half of the device, before the PDMS gasket and appropriate filter membrane were placed into the retentate side of the device. The two halves of the device were aligned and clamped together using screws, applying a specific torsion to each using a torque driver in order to generate an even seal around the membrane.

### 2.1.5 Assembly of Microreactors by Thermal Bonding

Microreactor PMMA components were thoroughly cleaned after milling or ablation and then sealed by thermal bonding (1.5 h, 105°C). Interconnect ports (made as described above) were attached with screws to allow the connection of tubing.

## 2.2 Cell Filtration for Trypsin Removal

### 2.2.1 Reagents and Analysis

Unless otherwise stated, all chemicals and reagents (Invitrogen, Paisley, UK) involved in the cell filtration experiments were used without further purification.

A colourimetric assay was used to determine the concentration of trypsin present in the output and compare to concentration of the original solution. 100 μL of output sample was added to 100 μL of 1 mM of L-BAPNA in 2.5% v/v dimethylformamide in 20 mM $CaCl_2$ and 40 mM Tris (Sigma-Aldrich, Gillingham, UK). The change in absorbance at 405nm was recorded every 20 seconds for 25 cycles, a total of 10 minutes.

A ViCell™ XR (Beckman Coulter, High Wycombe, UK) automated counting device was used to acquire viability and cell count data, using Trypan Blue as a stain for non-viable cells.

### 2.2.2 Cell Culture

Oct4-GFP mouse embryonic stem cells (mESCs) were grown in T25 adherent culture flasks (Nunc, Langenselbold, Germany) pre-treated with 0.1% v/v gelatine in water. The culture media used was Knock-Out Dulbecco Modified Eagle Medium (KO-DMEM), supplemented with 50 mL fetal calf serum, 5 mL l-glutamine, 5ml non-essential amino acid solution, 3.5 μL β-mercaptoethanol and 200 μL leukaemia inhibitory factor.

The cells were passaged every three days. They were removed from the culture surface by incubation with 0.5 mL of 0.025% v/v trypsin in chick serum for three minutes, which was then inactivated with a further 0.5 mL of media. The cell colonies were broken up into a suspension of single cells by repeated aspiration with a Pasteur pipette before being diluted and seeded into ten separate T25 flasks.

### 2.2.3 Cell Exposure to Trypsin

To determine the effect that longer trypsin exposure might have on cell viability, four 6-well plates were seeded with Oct4-GfP cells at a density of $3\times10^5$ cells $cm^{-2}$ and left to grow for 3 days. They were then exposed to ES trypsin for 5, 10, 20 and 30 minutes before being quenched with media as per the standard passaging protocol.

### 2.2.4 Cell Exposure to Filtration Device

The filtration rig was assembled with a PVDF membrane (0.45μm pore size) which had been wetted in a solution of 1x D-PBS. The clamp screws were tightened to a torsion of 15cN-m and the inlet and outlet ports on one size of the device were sealed.

Single T25 flasks of Oct4-GFP mESCs were incubated with 0.025% v/v trypsin in chick serum to detach the cells (as per the standard passage method described above). After three minutes the trypsin was quenched with 2 mL culture media. 0.5 mL of the cell suspension was drawn off for prefiltration cell counts. The remaining 2 mL of suspension was drawn up into a 5ml syringe, which was connected to the device via a leur-lock fitting and placed on a syringe pump (KD Scientific, Holliston, USA). The cells were passed through the device at a flow

rate of 0.5 mL $min^{-1}$ and collected from the outlet port in an Eppendorf tube. 0.5 mL of this suspension was taken for postfiltration cell counts.

### 2.2.5 Crystal Violet Stain

After passing the cells through the device as per the method described above, the PVDF membrane was removed from the device and placed into a Petri dish. A layer of methanol was added to the dish to fix any retained cells onto the membrane surface. The methanol was removed and replaced with 1 mL crystal violet. After incubating briefly, the crystal violet was removed and the membrane was rinsed thoroughly with 1x D-PBS before being placed on a microscope slide for imaging with an inverted microscope (Nikon, Kingston upon Thames, UK).

### 2.2.6 Centrifugation/Filtration Exposure

T25 flasks of Oct4-GFP mES cells were incubated with trypsin as per the standard passaging protocol. As in the filtration protocol, the trypsin was quenched with 2ml culture media and 0.5ml of suspension was withdrawn for cell number and viability analysis. The remaining suspension was transferred to a Falcon tube and centrifuged at 1200 rpm for 3 minutes. The supernatant was removed and the cell pellet was resuspended in a further 2 mL of culture media. 0.5 mL of this suspension was taken for a post-centrifugation cell count. As before, all cell counts were conducted with a ViCell™ cell viability analyser. The count data was compared to that of the filtration exposure results.

### 2.2.7 Trypsin Filtration

The filtration rig was assembled with a PDVF membrane (0.45 μm pore size) as described above. A milliGAT™ pump was used to circulate 1xD-PBS (Sigma-Aldrich) along one side of the membrane. A 5 mL leur-lock syringe was loaded with a 0.025% v/v solution of trypsin in chick serum, connected to the opposing side of the membrane and placed in a syringe pump (KD Scientific). The two pumps were then operated at a variety of flow rates and the output trypsin solution was collected.

A set of standard solutions were made up to form a calibration curve. A solution of 0.025% v/v trypsin in chick serum was diluted to 1 in 2, 5, 10, 20, 50, 100, 200 and 500 and the absorbance rates were measured as above.

## 2.3 Biocatalytic Synthesis and Filtration

### 2.3.1 Reagents and Analysis

Unless otherwise stated, all chemicals and reagents (Sigma-Aldrich) for the biocatalytic synthesis and filtration experiments were used without further purification. Pure L-erythrulose (ERY) for HPLC standards was produced by flash silica chromatography of commercially-available ERY as per the method of Smith *et al* (Smith et al., 2008).

Protein concentrations were measured by SDS-PAGE electrophoresis with 12% Tris-glycine resolving gel, using purified transketolase (TK) standards. 20 μg of total protein was applied to each lane and the samples were stained with Comassie Blue R-250.

HPLC analysis of products from TK-catalysed reactions was performed on an Aminex (Biorad, Hemel Hempstead, UK) ion-exchange column (HPX-87H, 300 × 7.8 mm), mobile phase: 0.1% v/v aqueous trifluoroacetic acid (TFA) at 0.6 mL $min^{-1}$. HPA and ERY were detected by UV absorption at 210 nm.

Enantiomeric excess data for the formation of ERY were calculated from chiral HPLC analysis of the derivatised ketodiols compared to racemic standards (Smith et al., 2008, 2009). The enantiomeric excess for (3S)-l,3-dihydroxypentan-2-one was obtained by chiral HPLC (Cázares et al., 2010).

### 2.3.2 Preparation of Transketolase Lysate

Transketolase lysates were prepared according to the method of Matosevic *et al.* (Matosevic et al., 2008). For the wild type TK, overnight cultures of *E. coli* BL21gold(DE3) (with transketolase-producing plasmid pQR791) were grown in 200 mL shake-flasks from

inoculation of 20 mL Lysogeny Broth (LB)-glycerol with a single colony obtained by streaking out cells from glycerol stocks (25% v/v glycerol stored at -80 °C) on (LB)-agar plates. This was incubated for 12-16 hours at 37°C. The resulting cell suspension was transferred to a conical flask with 200 mL LB-glycerol medium, which was incubated at 37 °C until the bacterial growth had reached stationary phase, as confirmed by optical density measurements. The contents of the flask were transferred to 50 mL falcon tubes and centrifuged at 5000 rpm for 10 min. The supernatant was discarded and the cell paste was frozen at -80 °C until needed for lysis and purification.

For lysis, the cell paste was resuspended in 5 mL 50 mM tris buffer, cooled on ice and sonicated (10 cycles of 10 seconds on, 10 seconds off) with a sonication probe (Soniprep 150, Sanyo, Japan). The suspension was then centrifuged and filtered with a 0.2 μm filter, and stored at -80°C until required.

For the mutant D469T TK, the same procedure was followed except the pQR791 plasmid had been specifically mutated according to the methods of Hibbert *et al.* (Hibbert et al., 2007, 2008).

### 2.3.3 Batch Transketolase Reaction

For the reaction of HPA with glycolaldehyde (GA), 30 μL wild type TK lysate (4.47 mg $mL^{-1}$) was incubated with 170 μL cofactor solution (23.1 mM $MgCl_2$, 5.7 mM thiamine diphosphate in 50 mM Tris-HCl buffer, pH 7) for 20 minutes at room temperature. 150 μL of this solution was added to 150 μL substrate solution (100 mM HPA, 100 mM GA in 50 mM Tris-HCl buffer, pH 7) in a 96-well plate to initiate the reaction (final concentrations: 50 mM HPA, 50mM GA, 0.34 mg $mL^{-1}$ wild type TK, 2.4 mM ThDP, 9.8 mM $MgCl_2$). Aliquots (20 μL) were removed at the required time intervals, quenched with 180 μL 0.1% v/v aqueous TFA, centrifuged (5000 rpm, 5 minutes) and the supernatant analysed by HPLC.

### 2.3.4 Continuous Flow Microfluidic Transketolase Reaction

TK lysate solutions and substrate solutions were prepared at the concentrations described above. Using a twin syringe drive, the solutions were pumped into separate inlets of the microfluidic reactor at the same flow rate for at least 1.5 times the residence time before collecting the output in pre-weighed sample vials containing 360 μL 0.1% TFA. The quenched reaction mixture was centrifuged and analysed by HPLC as above. Residence times were calculated by dividing the reactor volume (60 μL) by the flow rate.

### 2.3.5 Filtration Back Pressure Measurements

Constricting capillaries (internal diameter 50, 75, 100 and 200 μm) were attached to the retentate outlet of the filtration device in cross-flow mode (Figure 2D). The resulting back pressure was measured with an inline pressure sensor (40PC100, Honeywell, Morristown, USA), and the data was logged with a LabVIEW instrument (National Instruments, Austin, USA).

### 2.3.6 Filtration of Model Reactor Output and Integration

The filtration unit was charged with Tris buffer (50 mM, pH 7). A model stock solution of TK (0.34 mg $mL^{-1}$) and ERY (50 mM) in Tris buffer (50 mM, pH 7) was pumped through the retentate inlet with a syringe drive, while tris buffer was pumped through the permeate inlet. Samples were collected at the retentate and permeate outlets for analysis by HPLC and SDS-PAGE.

For the integration of the microfluidic reactor and the filtration unit, a HPA/GA solution (both 100 mM) and a TK/cofactors solution (0.68 mg $mL^{-1}$ TK) were combined and flowed through a microfluidic reactor at 10 μL $min^{-1}$. The output was connected to a filtration unit via a length of tubing to give the desired residence time. A 50 μm i.d. capillary was fitted to the retentate outlet of the filtration unit. The reaction was run for a total of 10 hours. Samples taken from the retentate and permeate outlets were analysed by HPLC.

## 2.4 Biocatalytic Synthesis in Microfluidic Multi-Input Reactor

### 2.4.1 Reagents and Analysis

Unless otherwise stated, all chemicals and reagents (Sigma-Aldrich) were used without further purification. Concentrations of TK, HPA and GA we determined as described in Section 2.3.1.

### 2.4.2 Continuous Flow Microfluidic Reaction of HPA to ERY (with multiple GA Inputs)

Two separate solutions were used to perform the reaction. The main reaction mixture (solution A) consisted of 0.069 mg $mL^{-1}$ clarified transketolase lysate, different HPA concentrations (211/316/421/526 mM HPA, depending on experiment), 2.53 mM thiamine diphosphate (ThDP) and 10.3 mM $MgCl_2$ in 50 mM Tris-HCl buffer, pH 7. The concentrations of the solutes were chosen such that they would be diluted to the following concentrations once combined with the first GA input: 0.066 mg/mL clarified transketolase lysate, 200/300/400/500 mM HPA, 2.4 mM thiamine diphosphate (TDP) and 9.8 mM $MgCl_2$. The supplementary GA solution (solution B) consisted of 1 M GA in 50 mM Tris-HCl buffer, pH 7.

The MIR was primed with Tris-HCl buffer (50 mM, pH 7). Solution A was pumped into the first primary input of the reactor with a single-drive syringe pump. Solution B was pumped into the second primary input, along with a number of auxiliary inputs, using a dual-drive syringe pump adapted to fit ten 1 mL syringes. The flow rates and the number of auxiliary inputs used were dependent upon the desired residence time and input HPA concentration (see Table 5, Section 5.3).

The reactor was allowed to equilibrate for 2.5 residence times before sampling began. Samples were collected in pre-weighed vials containing 270 μL 0.1% (v/v) aqueous trifluoroacetic acid (TFA). The quenched samples were weighed, centrifuged and the supernatant was diluted 1:1 with 0.1% TFA before being analysed by HPLC as described in section 2.1.

### 2.4.3 Fed-Batch Reactions in Microwell Plates

Fed-batch reactions were performed in 96-microwell plates. 200 µL of solution A was made up in each well. 10 µL of solution B was manually added to each well to start the reactions. Further 10 µL doses of solution B were then manually added to the reaction mixtures at specific time points, corresponding with the feeding strategy used in the continuous-flow reactions. Endpoint samples were taken after the reactions had run for the equivalent residence times, diluting 30 µL of reaction mixture in 270 µL 0.1% TFA. Samples were centrifuged before being analysed by HPLC.

### 2.4.4 12-Hour Continuous Production of ERY

The experiment was run at the conditions of the 500 mM HPA conversion (Table 5), using the same solutions and reactor setup as described in section 2.4.2. The output tubing from the MIR was connected to a RotAXYS auto-sampling system (cetoni GmbH, Korbussen, Germany), programmed to take 30 µL samples every hour from the start of the reaction. 12 wells of a 96-microwell plate were each filled with 270 µL of 0.1% TFA to quench the samples. Samples were centrifuged before being analysed by HPLC.

## 2.5 Confocal Imaging of Mixing in Microreactors

### 2.5.1 Confocal Imaging of Mixing in SHM Microreactor

Two solutions (phosphate buffered saline and fluorescein-conjugated bovine serum albumin in phosphate buffered saline, pH 7) were flowed through separate inlet ports of the microreactor. Confocal microscopy images were taken before and after the SHM structures (at 1 cm and 6 cm from the T-junction, respectively) with a Leica TCS SP2 (Leica Microsystems UK Ltd, Milton Keynes, UK). A 10× objective was used with 12% laser power, taking 5 µm sections from the top to the bottom of the channels. The sections were compiled into composite images using with Leica Confocal Imaging software (Leica Microsystems UK Ltd).

### 2.5.2 Confocal Imaging of Mixing in MIR

Confocal imaging was used to analyse the rate of diffusion of substrate fed at the auxiliary inputs into the main reaction mixture. A microfluidic chip was designed specifically for this purpose, mimicking the structure of a single auxiliary input and channel section in the MIR, with some modification to accommodate confocal imaging (Figure 9). The chip was fabricated from two layers of PMMA using laser ablation, with an adhesive-free microwell plate sealing film used to seal the channels of the top layer. The cross section of the channels was identical to those of the MIR i.e. 1 x 0.5 mm (w x d). The two PMMA layers were bonded together as described in Section 2.1.5, with the sealing film being attached and smoothed to remove trapped air pockets after the PMMA had cooled.

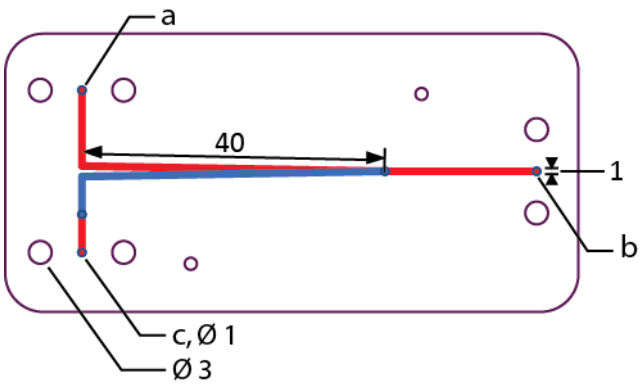


**Figure 9: Design of chip used to mimic MIR auxiliary input for confocal imaging. Areas filled in red represent channels cut into the bottom layer and areas filled in blue represent channels in the top layer. Blue lines indicate through cuts in the top layer only, while purple lines indicate through cuts in both layers.**

Water and 0.1 mg $ml^{-1}$ fluorescein in water were flowed through the primary and auxiliary inputs respectively (labelled a and b in Figure 9). Confocal microscopy images were taken 1 and 2 cm downstream from the channel join with a Leica TCS SP2 confocal microscope (Leica Microsystems UK Ltd). A 10× objective was used with a 488 nm argon laser at 30% power and a FITC filter. The channel was imaged from the top to the floor in horizontal sections 5 microns apart. The flow rates and location of the imaging were adjusted to visualise the diffusion at different residence times, between 1.4 and 60 seconds. The ratio of the water to fluorescein solution flow rates were maintained at 20:1, regardless of the residence time

investigated. The sections were compiled into composite images using with Leica Confocal Imaging software to create vertical cross-sections of the channel.

### 2.5.3 Confocal Imaging of Backflow at MIR Inputs

The rate of diffusion along the auxiliary channel itself was also evaluated in order to ensure there was no backflow of reaction mixture out of the auxiliary ports. In this case the fluorescein solution was flowed through the primary input (a in Figure 9) and water was flowed into the auxiliary input (b in Figure 9). The join between the channels was imaged across both layers in horizontal sections 10 microns apart, using the same settings as above. Fluorescein solution and water were flowed into the chip in a 20:1 ratio, at 3.3µl $min^{-1}$ and 0.17 µl $min^{-1}$ respectively. A control image was taken with static fluorescein solution in the main channel and the auxiliary input.

# 3

# Development of Microfluidic Tangential Flow Filter for Harvesting of Mammalian Cells

This chapter illustrates the development of a microfluidic filtration device for bioprocessing, with the aim that it could be used to test filtration conditions for a range of potential applications. The application initially used as a model for development was the capture of mammalian cells after removal from a culture plate using the enzyme trypsin. The chapter shows the proof of concept experiments performed using a bench scale filter and the subsequent development of a modular tangential filtration device that could be used with commercially available membranes.

The results in this chapter have been presented in part in several conference proceedings and the design and burst pressure characterisation of the final device have been published in the Journal of Molecular Catalysis B: Enzymatic in a contribution entitled '*Modular Microfluidic Reactor and Inline Filtration System for the Biocatalytic Synthesis of Chiral Metabolites*' (see Appendix C).

Some of the data in this chapter was produced as part of a Bachelor's degree in collaboration with Mélissa Nafir. The data in Figure 28, Figure 29, Figure 30 and Figure 31 was produced by Mélissa Nafir using the filtration device detailed in section 3.4.1.

## 3.1 Introduction

Filtration is a widely-used and established technology in bioprocessing, owing to the fact that it can be applied to separations in variety of bioprocesses as well as at several stages within individual bioprocesses. It is commonly used in initial clarification and cell harvest steps as well as later purification and preparation steps such as protein concentration and buffer exchange (van Reis and Zydney, 2007). This versatility arises from the range of pore sizes and membrane materials available, allowing the fractionation of different components across many orders of magnitude in size (see Figure 6 in Section 1.4.1), therefore making it an attractive choice for the creation of a microfluidic downstream separation device that is industrially-relevant when compared with other examples discussed in Section 1.3.

Filtration processes usually take the form either of normal flow (or dead-end) filtration, where the fluid flow and pressure are applied perpendicularly to the membrane, or tangential flow (or cross-flow) filtration, where the fluid flow runs in parallel to the surface of the membrane but the pressure is applied perpendicularly (see Figure 7 in section 1.4.1). Whilst normal flow filtration is more simple to implement, the driving of fluid flow directly into the membrane results in the adsorption of both soluble and suspended components, causing rapid fouling of the membrane (Belfort et al., 1994).

In tangential flow filtration, however, inertial lift and shear-induced diffusion effects cause back-flow of particulates away from the membrane surface, reducing the rate at which debris can build up on the membrane. Furthermore, tangential flow filtration units possess a 'critical flux', a level of flux below which fouling is negligible, or at least minimal, and there is little or no measurable decline in flux over the course of operation (Field et al., 1995; Pollice et al., 2005). This makes tangential flow filtration particularly useful in bioprocessing, where the typically high concentration of biological debris can cause very high fouling rates if not mitigated. The widespread use of tangential flow filtration in industry and its range of applications therefore makes it the most relevant choice for a scale down device.

The foremost requirement for the proposed device was that it should be able to test a variety of conditions for possible separations processes, be it cell harvesting, protein recovery or others. The primary conditions that would need to be varied to be relevant to industrial scale bioprocessing were identified as the membrane material, pore size and filtration pressure. In order to achieve this it should ideally be possible to integrate any one of the range of commercial membranes available into the device for testing, and the device and the connections to it would also need to be robust to typical filtration pressures, in the range of 10 – 60 psi (Zeman and Zydney, 1996; van Reis and Zydney, 2007).

A key requirement of the device design was that it should be possible to produce the device without resorting to complex or costly fabrication techniques, which can be time-consuming and costly (Han and Frazier, 2005). Alternatively, if such fabrication techniques were unavoidable, the device should be readily reusable. Designs which relied on the use of micro-patterned features were therefore excluded, as these generally required complex fabrication processes and were not compatible with the integration of pre-made membranes (Pamme 2007).

## 3.2 Proof of Principle Experiments

The test case initially chosen for the development of the microfluidic filter was the separation of mammalian cells, in particular mouse embryonic stem (mES) cells grown in adherent culture from the trypsin enzyme used to remove them. The standard method for separating the cells from the trypsin is centrifugation, but both mES and human embryonic cells have been shown to be sensitive to excessive shear forces, which can bring about differentiation. The long-term aim was to be able to use the filtration device to exchange soluble media components within cell suspensions, retaining the cells themselves so that they could be cultured further and reducing the amount of shear they were exposed to. The aim of the test case was therefore to establish whether mammalian cells could be retained by the filter without suffering any adverse effects, whilst the trypsin enzyme was completely removed. This was tested first in a bench-scale system using commercially-available hollow fibre membranes, to determine whether separation could be achieved before starting the design and fabrication of a microfluidic filter. Oct4-GFP mES cells were selected as the test cell culture as they produce green fluorescent protein while they remain undifferentiated.

### 3.2.1 Feasibility of Stem Cell Recovery Using Filtration

A bench scale filter was fabricated for the purpose of running proof-of-concept experiments with mES cells, to determine whether the recovery of the cells using a filtration system was feasible.

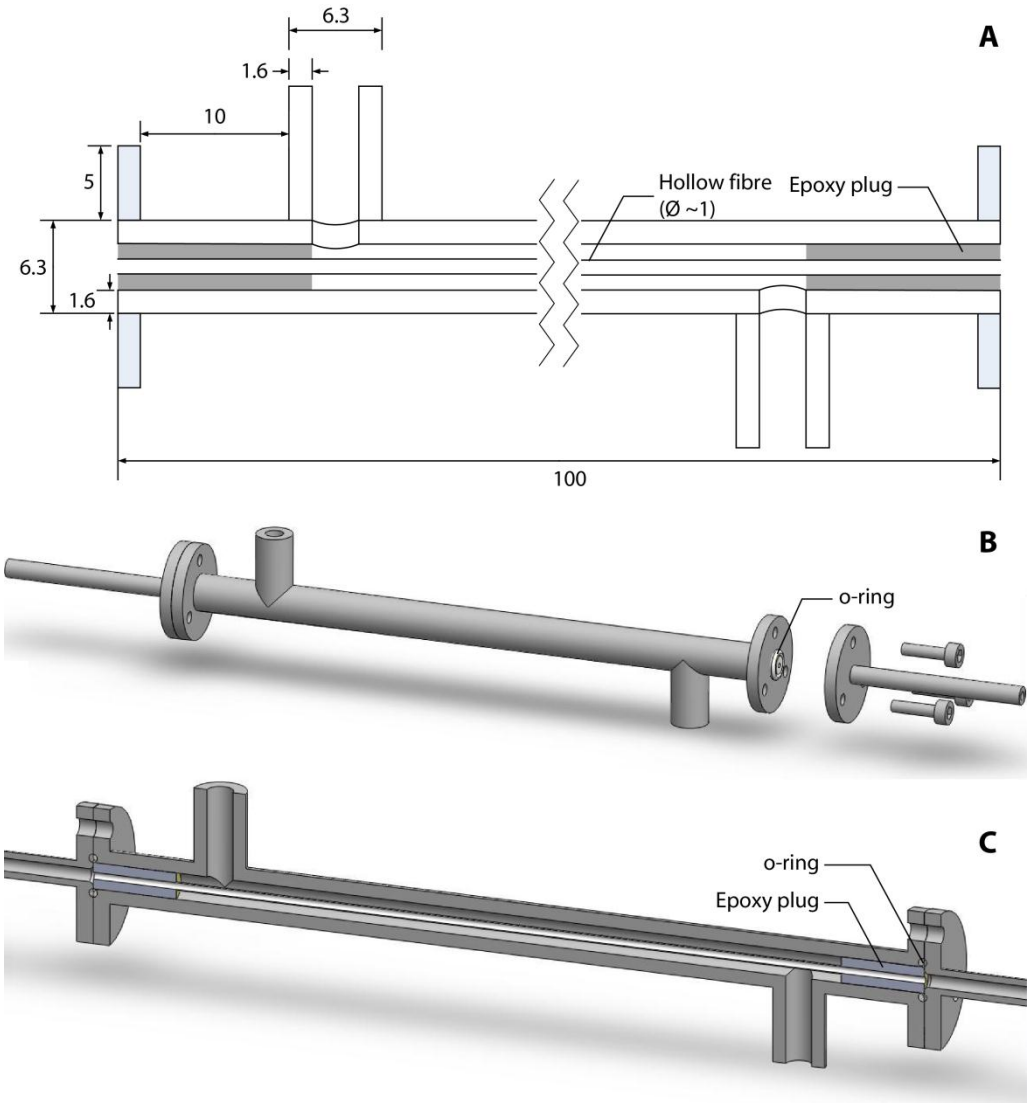


**Figure 10: Design of bench scale hollow fibre filtration unit for proof of concept experiments. (A) Dimensions of filtration unit (units in mm); (B) partially exploded view of unit showing sealing of hollow fibre connection with epoxy plug and o-ring; (C) longitudinal cross section through unit.**

The body of the filter unit was designed to accommodate a single polysulphone hollow fibre with a diameter of 1 mm and length of 100 mm, leaving a clearance of 1.6 mm between the fibre and the inner wall of the body (Figure 10A). The hollow fibre was cut to size and fitted with epoxy 'plugs' at either end, then threaded into the filter body. A seal was made around either end of the fibre by fitting o-rings around the plugs and clamping two flanged sections of pipe, which provided connections for tubing (Figure 10B). Two further inputs on either side of the filter unit provided connections for tangential flow in co-current or counter-current mode (Figure 10C).

To determine the effect of filtration on the viability of the mES cells (including any toxicity caused by parts such as the epoxy plugs), several suspensions of Oct4-GFP cells were passed through the bench scale device. The cells were detached from the culture flasks as per the standard passage protocol, removing the cells from the culture surface with a solution of trypsin enzyme and inactivating with FBS after detachment to eliminate any adverse effect on the cells from exposure to the active enzyme. The cells were passed through the hollow fibre at a rate of 5 ml $min^{-1}$, with a counter-current of 5 ml $min^{-1}$ media in the space around the fibre.

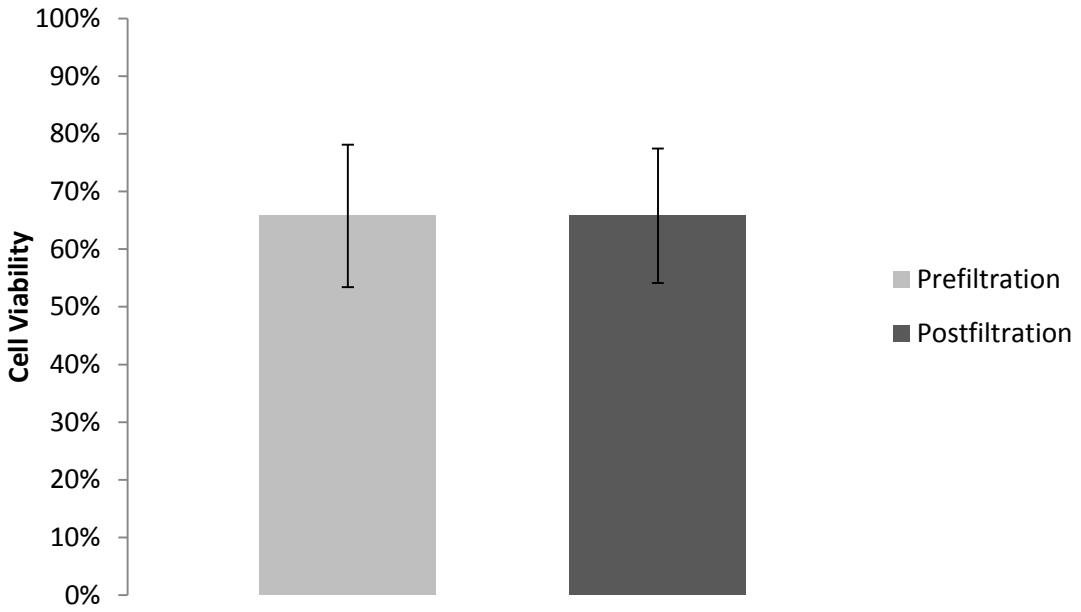


**Figure 11: Viability of Oct4-GFP cells before and after filtration with bench-scale device (n = 8, error bars show standard deviation)**

The cell suspension recovered from the filtration device was more dilute than the input, suggesting either that cells were becoming entrained on the membrane surface or that the net flux was into the cell suspension, or a combination of these effects. However, the main purpose of the experiment was to determine whether filtration could be a viable method for recovering the cells and not, at this stage, what might determine the efficiency of the recovery. Cell counts performed with trypan blue on samples collected after filtration showed no significant difference in percentage viability compared with samples taken before filtration, confirming that the process had no short-term effects on cell viability (see Figure 11).

### 3.2.1 Effect of Trypsin Exposure on Cell Viability

The standard method of removing trypsin during passage involves quenching the enzyme with an excess of FBS-containing media then centrifuging the cell suspension to separate the cells from the media. Under these conditions the cells are exposed to the trypsin for around five minutes after the trypsin is inactivated. Separating the cells using filtration would likely require exposing them to active trypsin for longer periods of time; hence it was necessary to determine whether this would have a detrimental effect on cell viability. Four 6-well plates of mES Oct4-GFP cells were trypsinized and quenched with FBS-containing media after 5, 10, 20 and 30 minutes respectively, before the cell viability was analysed (Figure 12).

The cell counts after exposure to trypsin showed an average overall cell viability of 95%, with the length of exposure to active trypsin having no significant effect on the viability of the cell suspension. This suggested that filtration could be a feasible method of clearing trypsin from suspensions of stem cells. Longer and repeated exposure to proteolytic enzymes has the potential to reduce the pluripotency and proliferation potential of stem cells, though this effect was not investigated at this point (Majd et al., 2009).

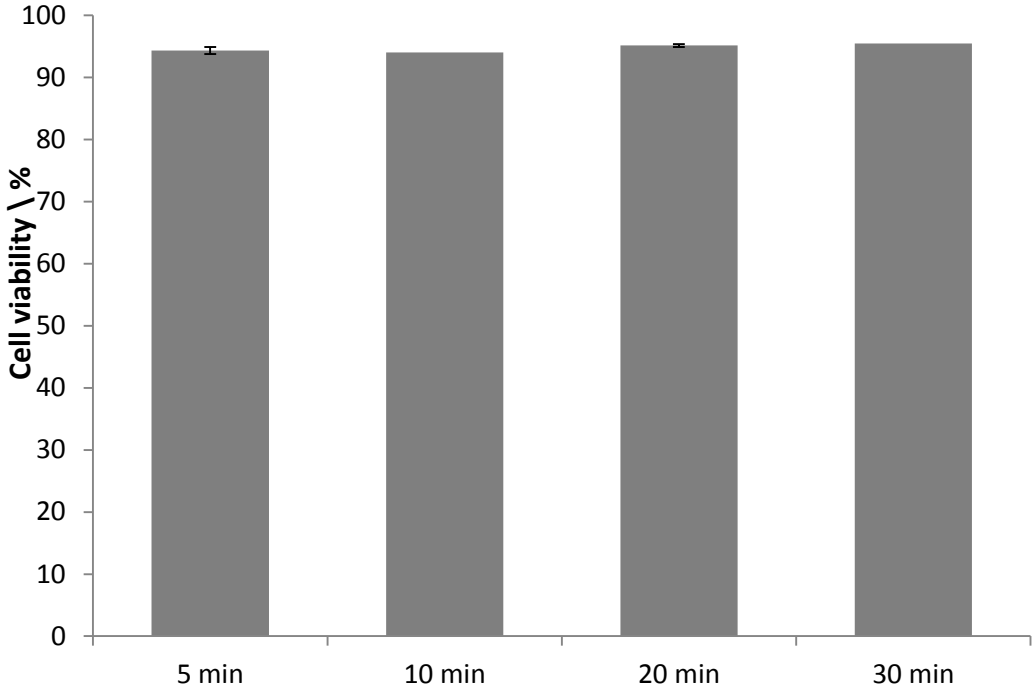


**Figure 12: Viability of mES Oct4-GFP cells after exposure to active trypsin for different lengths of time (n = 6).**

### 3.2.3 Detection of Trypsin with Colourimetric Assay

Detection of trypsin was achieved by a colourimetric assay with L-BAPNA, a chromogenic substrate for proteolytic enzymes which releases p-nitroaniline when hydrolysed. Several concentrations of trypsin were combined with the substrate and incubated while the change in absorbance was measured. An initial rate was taken to determine the concentration of active enzyme in each sample (see Figure 13).

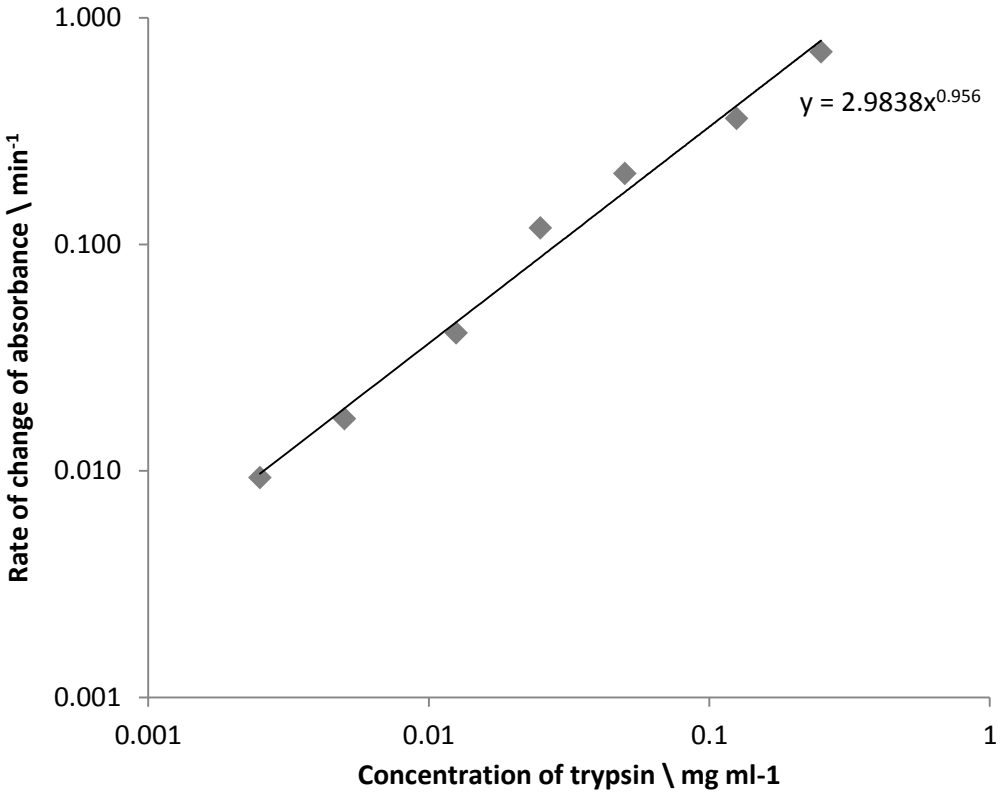


**Figure 13: Calibration curve for the determination of trypsin concentration using L-BAPNA colourimetric assay**

The assay was capable of providing an accurate measure of trypsin concentration between concentrations of 0.025 and 0.25 mg $ml^{-1}$, equivalent to a 1 – 100x dilution of the enzyme when used in cell culture. This was suitable for determining whether the removal of trypsin had taken place.

## 3.2.4 Separation of Trypsin from Cell Media using Bench-Scale Filter

The bench scale filtration rig (shown in Section 3.2.1) was used to perform a series of preliminary experiments to test whether it was possible to remove of trypsin from mES cell culture media and, if so, what conditions were necessary to remove the enzyme. FBS-free media containing trypsin was passed through the hollow fibre of the filtration rig, with back pressure applied by a tubing clamp on the outlet and monitored by an in-line pressure meter. Trypsin- and FBS-free media was passed through the void space around the fibre in counter-current mode. The amount of active trypsin present in the retentate and permeate was then

measured using the colorimetric assay described in Section 3.2.3 The percentage of trypsin removed for each condition set is shown in Figure 14.

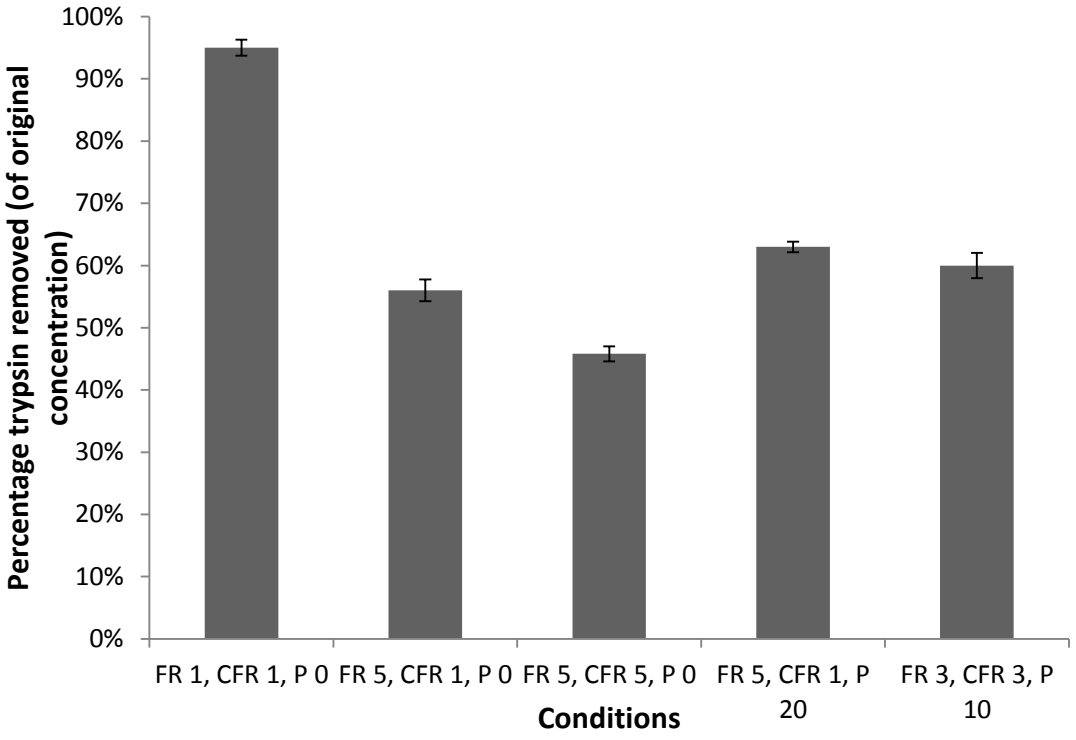


**Figure 14: Clearance of trypsin using bench scale filter (n = 3, error bars indicate standard deviation). FR is flow rate through hollow fibre, CFR is counter flow rate through outer housing, P is back pressure applied to outlet from hollow fibre.**

The initial tests suggest that the contact time of the two fluids was more important for the removal of trypsin than the back pressure on the hollow fibre. The highest clearance of trypsin occurred while using flow rates of 1 ml $min^{-1}$ for the retentate and permeate streams, meaning that the trypsin-containing media was in contact with trypsin-free media for approximately 15 seconds.

### 3.2.5 Feasibility of Microfluidic Filter Fabrication

The design of a dead-end microfluidic filter was attempted in the first instance to test the principle of filtration at the microfluidic scale. The filter was fabricated in PMMA and PDMS, with a polysulphone membrane. The PMMA enclosure acted as a rigid frame for the PDMS assembly, providing support and fluidic connections to tubing, and was intended to be

reusable, whilst the PDMS and membrane assembly were intended to be disposable (see Figure 15). The design was adapted from that of Ismagilov, who sealed polycarbonate membranes into their PDMS chips by manually wetting the areas of membranes that they wanted to seal with liquid PDMS prepolymer before curing at 65°C, preventing any leakage from the chip or exchange of fluids between channels (Ismagilov et al., 2001). Ismagilov's method was chosen because it presented the simplest way to integrate a range of different membranes into PDMS, avoiding the complication of having to identifying functionalising methods for each membrane type.

The PDMS and polysulphone membrane made up the main structure of the filter. Both PDMS layers were 60 x 25 x 2 mm (l x w x d) with 5 x 5 x 1 mm cavities in their centre and 7.5 x 1 x 1 channels to connect the cavities to the ports. These were inverted to make one continuous fluid path from one end of the chip to the other. The filter membrane was sealed into the PDMS layer by treating the edge with liquid polymer, then clamping and curing it in place. The PDMS/membrane chip was clamped into the PMMA enclosure, and commercially available interconnects (N-333, Upchurch Scientific, Oak Harbor, USA) were bonded onto the surface of the enclosure to allow the connection of tubing.

The seal achieved by this method was reasonably reproducible provided that the placement of the liquid PDMS was done carefully, with a failure rate of around 1 in 5 PDMS/membrane chips which did not form a complete seal around the edge of the membrane (as observed by testing with water blue solution). However, the liquid PDMS was observed to spread laterally through the pores of the membrane and in some chips this reached the main cavity such that, when cured, the area available for filtration was reduced.

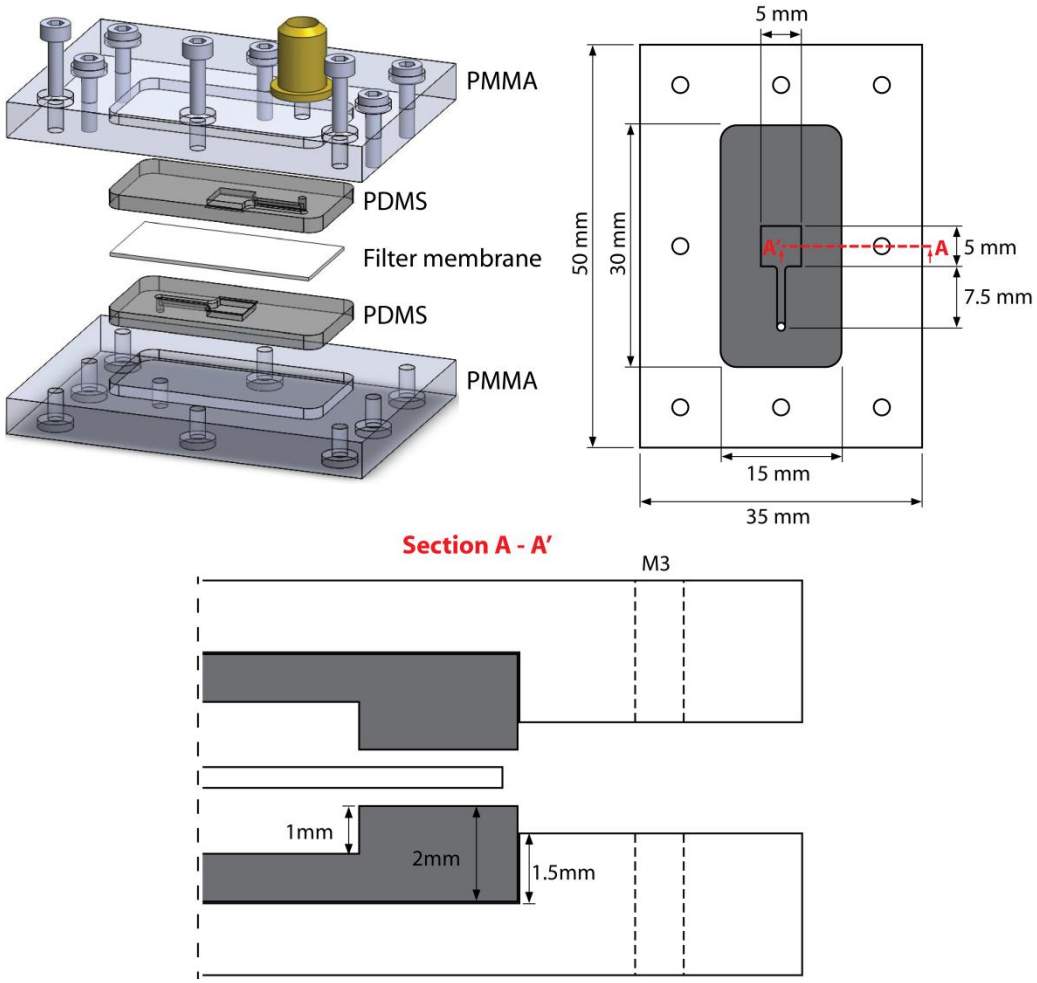


**Figure 15: Design of first generation dead-end filtration chip (not to scale)**

The filtration device was tested for the recovery of mES cells from a suspension after passage using standard passage protocol. The suspension, containing active trypsin, was passed though the device at 0.5 ml $min^{-1}$. The permeate was collected from the output of the device. FBS-free media was then passed through the device in the opposite direction to recover the cells; this was the retentate.

Analysis of the concentration of trypsin remaining in the permeate and retentate showed that the filter was capable of separating the cells from the trypsin, which was able to permeate through the membrane (see Figure 16). However the recovery of the cells from the device was difficult, presumably because of impaction on the membrane, and the retentate cell concentration was reduced by two orders of magnitude from the prefiltration concentration. The resulting cell suspension was too dilute to be replated without further concentration,

having an average viable cell count of $4.2 \times 10^4$ cells $ml^{-1}$ with a standard deviation of $2.4 \times 10^4$ cells $ml^{-1}$ (see Figure 17), where a concentration of around $1.0 \times 10^6$ cells $ml^{-1}$ would be necessary for the cells to grow to confluency.

Cells were also observed in the suspension collected from the permeate at a concentration of $1.3 \times 10^4$ cells $ml^{-1}$, around a quarter of the total number of cells recovered from the filtration process, implying that leakage occurred through or around the membrane. The cell population was around 40% viable, suggesting that the route taken through the filter was traumatic to the cells. This, combined with the low overall yield of cells from the filter and the low concentration at which they were recovered, indicated that normal-flow filtration would not be a viable method for recovery.

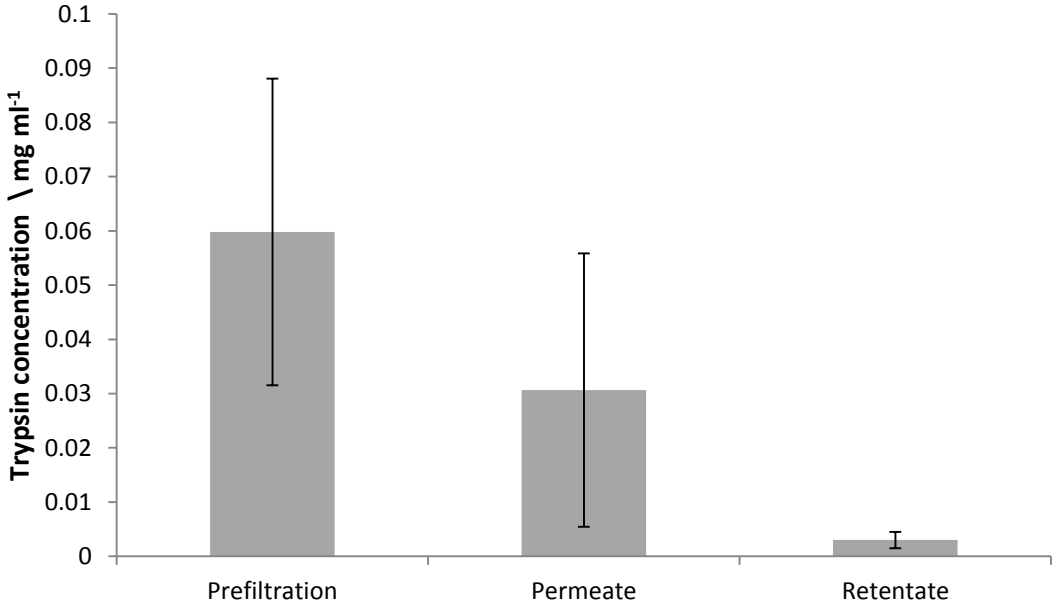


**Figure 16: Concentration of cell suspension before and after recovery using microfluidic normal flow filtration device (n = 3, error bars indicate standard deviation).**

Normal flow has the additional disadvantages that it is very susceptible to fouling by biological materials and is relatively inflexible in the range of unit operations that it can be applied to (it cannot, for example, be used to exchange solutes).

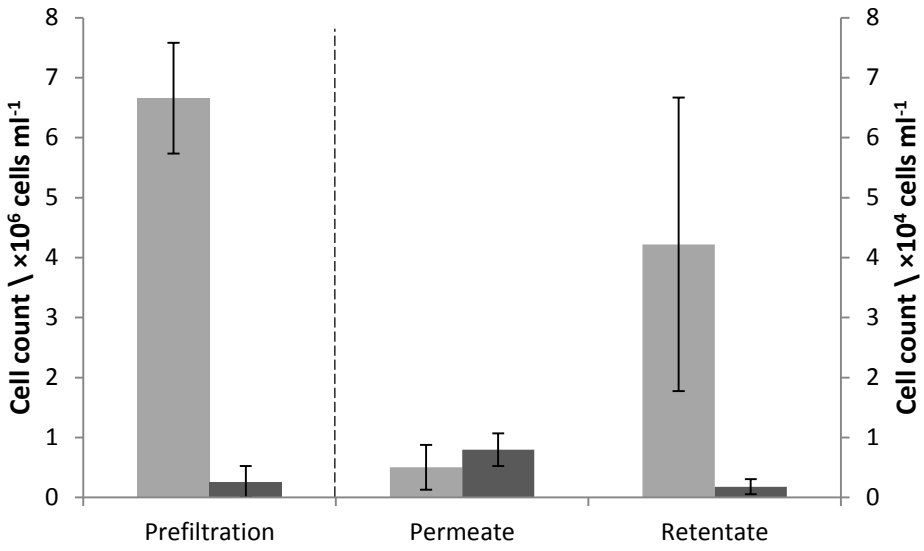


**Figure 17: Cell number and viability after recovery using microfluidic normal flow filtration device (n = 3, error bars indicate standard deviation).**
**Light grey indicates viable cell count; dark grey indicates non-viable cell count. Refer to the left axis for prefiltration cell counts (units are $\times 10^6$ cells $ml^{-1}$). Refer to the right axis for the permeate and retentate cell counts (units are $\times 10^4$ cells $ml^{-1}$).**

The initial proof of principle experiments showed that separation of the cells from the trypsin enzyme was possible, but several challenges had been presented. The key challenge was the reproducible integration of the filtration membrane, without leakage and without obstructing the area for fluid transmission. Secondary to this was the poor recovery observed in the normal flow filtration device, resulting from impaction of the cells on the membrane. This would likely prove problematic for processing of other biological materials, so the choice was made to continue development with a tangential flow design instead.

An additional challenge identified was that mammalian cell suspensions were not the most suitable test system for filtration, given the amount of ancillary work required to maintain them and prepare samples for experimentation. For this reason the filtration of cells was made a lower priority, with research focussing on the technical challenges that had been identified. Further cell filtration experiments were carried out once these had been overcome, the results of which are shown in Section 3.5.

## 3.3 Development of Tangential Flow Filtration Device

A number of designs were evaluated in the process of developing the final design from the initial proof of concept device shown in Figure 15. This section will consider the rationale for the device's final design in the context of these. The final design of the tangential flow filtration device had several key features, developed over the course of a number of iterations of prototyping and testing. These were:

- Straight channel with cross-sectional area of 1 x 1 mm and filter area of 45.8 mm²
- Clamp sealing
- Rigid hard polymer chip, robust to pressures of up to 100 psi
- PDMS gasket to enclose membrane
- Modularity of parts and standard interconnect fittings

### 3.3.1 Straight Channel Design

The initial normal-flow filter design featured a large cavity in the centre of the PDMS chip which formed the filtration area. Its relatively large geometry was chosen for ease of fabrication and to minimise the likelihood of clogging of the channels; however, this caused problems with priming, frequently resulting in large bubbles which reduced the effective filtration area (Figure 18).

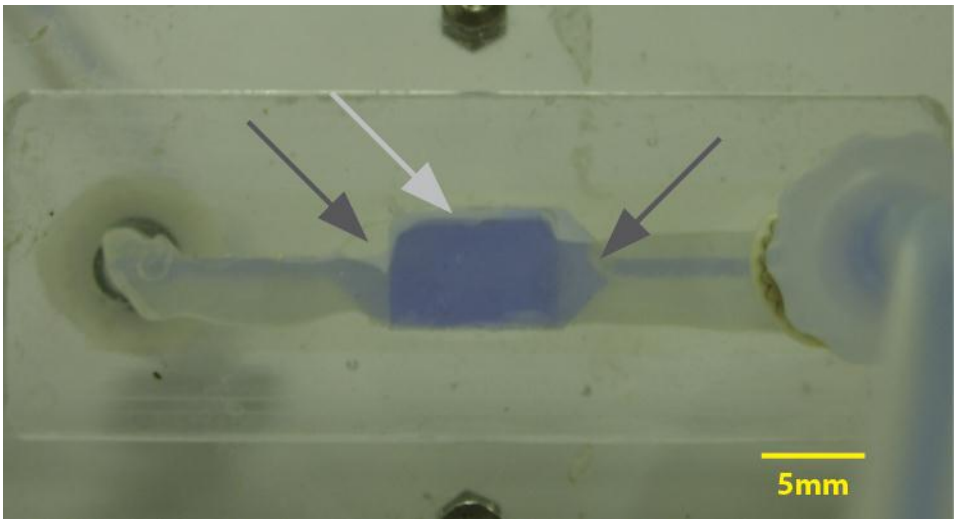


**Figure 18: Water blue test of normal flow microfluidic filter design.**

**Grey arrows indicate bubble formation; white arrow indicates area of membrane inadvertently sealed with prepolymer.**

The next design iteration therefore aimed to improve priming by using a narrower channel with a 1 x 1 mm cross-section as the filtration area. This was fabricated as a meander in order to give the same overall filtration area as the normal-flow filtration device, 25 mm² (Figure 19), with a fluidic connection at either end of the chip so that it could be used as a tangential flow filter. Use of a meander structure was intended to provide a torsional flow pattern secondary to the direction of flow, which might have helped to reduce the rate of membrane fouling. However, the meander made alignment of the two parts of the chip more crucial, as any slight misalignment could reduce the available filtration area. In addition, when the design moved to clamp sealing (see next section) it quickly became apparent that a meander would significantly increase the complexity of the design, as an even sealing pressure would be needed over the length of the channel. The meander was therefore abandoned in the final design, but the channel was lengthened to 50 mm in order to provide a larger filtration area. If a larger area were required it may be possible to widen the channel, using a flow distributor such as those evaluated by Vangelooven *et al.* (Schoenmakers et al., 2010; Vangelooven et al., 2010).

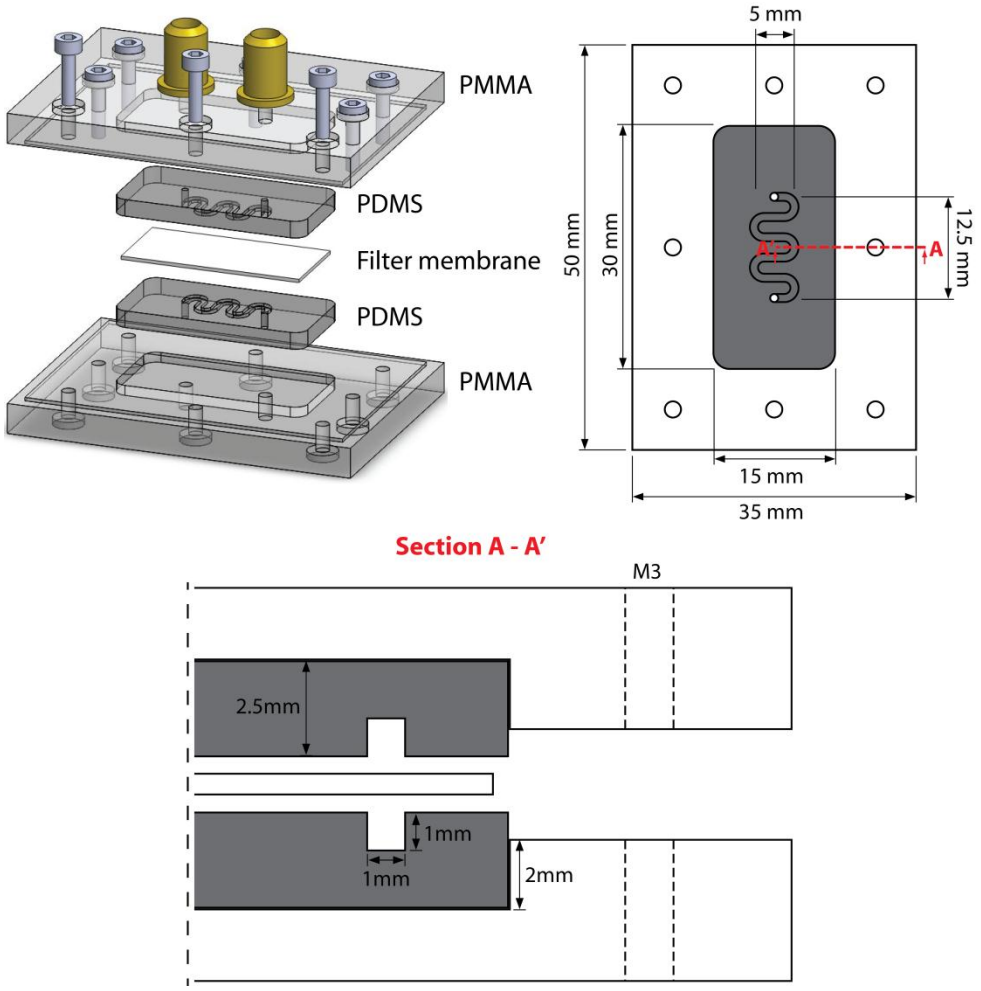


**Figure 19: Design of first generation tangential flow filtration chip (not to scale)**

## 3.3.2 Clamp Sealing of Filtration Membrane

The normal-flow filter design and subsequent early tangential flow designs relied upon the bonding of the membrane into PDMS structures with liquid prepolymer in order to seal the filter. As mentioned before, the spread of the prepolymer could cause inadvertent blocking of parts of the membrane in the filtration chamber. In the proof of concept design this problem did not completely block the filtration area, although it did reduce the reproducibility of the design. When using smaller channel geometries however, the PDMS could spread to cover the majority of the filtration area if too much prepolymer was applied. Changing the filter design to seal the membrane in place by clamping was therefore chosen as a way to make the filter work more reproducibly.

Using clamp sealing also meant that the fabrication could be simplified. Sealing the membrane in place inside a PDMS chip added another step to the fabrication process which needed to be repeated in preparation for each filtration test, since the PDMS components could not easily be reused. Use of clamp sealing meant that these components were no longer required and the main body of the filtration device could be designed to be reusable, with only the membrane being disposed of between experiments, saving time and resources.

### 3.3.3 Rigid Hard Polymer Chip

In order to maintain a robust seal, the clamp sealing filtration device had to have minimal flex. Where earlier designs had used thinner (3mm) hard polymer PMMA and PC components as enclosures to facilitate fluidic connections to the PDMS and membrane component (see Figure 15 and Figure 19), the hard polymer components in the clamp sealed device served as the fluidic connection and channel. They were therefore fabricated in thicker 5 mm PMMA or PC to give the structure of the filtration device greater rigidity and help to ensure a robust seal.

The use of hard polymer for the channels and fluidic interconnects meant that they could be joined by screws and that there was no soft/hard polymer interface to consider. This was a significant design advantage, as non-permanent interfaces between soft and hard polymers often require a significant amount of development to ensure a robust seal at high pressures (Reichen, 2011). The use of PC rather than PMMA also meant that the device could be used in applications where sterility is necessary, such as cell handling, where sterilisation is typically achieved by autoclaving at 121°C. The glass transition temperature of PMMA is 105°C, meaning that any parts would likely suffer deformation during the autoclaving process. PC has a glass transition temperature of 147°C, reducing the risk of deformation of parts during autoclaving.

### 3.3.4 PDMS Gasket to Enclose Membrane

Earlier filter designs used roughly-cut membranes, relying on sealing by treatment with liquid PDMS or pressure to prevent fluid from entering parts of the membrane outside of the filtration area. As discussed above, the former resulted in inadvertent sealing of parts of the membrane in the filtration area. A design was therefore tested which aimed to cut off the lateral flow through the membrane by sealing with a combination of a PC boss fabricated in the permeate side of the device and a recessed PDMS gasket fabricated in the retentate side of the device. The two sides were clamped together around the membrane with screws, using a specific torque. The height of the PDMS gasket recessed in the retentate side could also be changed to tune the quality of the seal (see Figure 20).

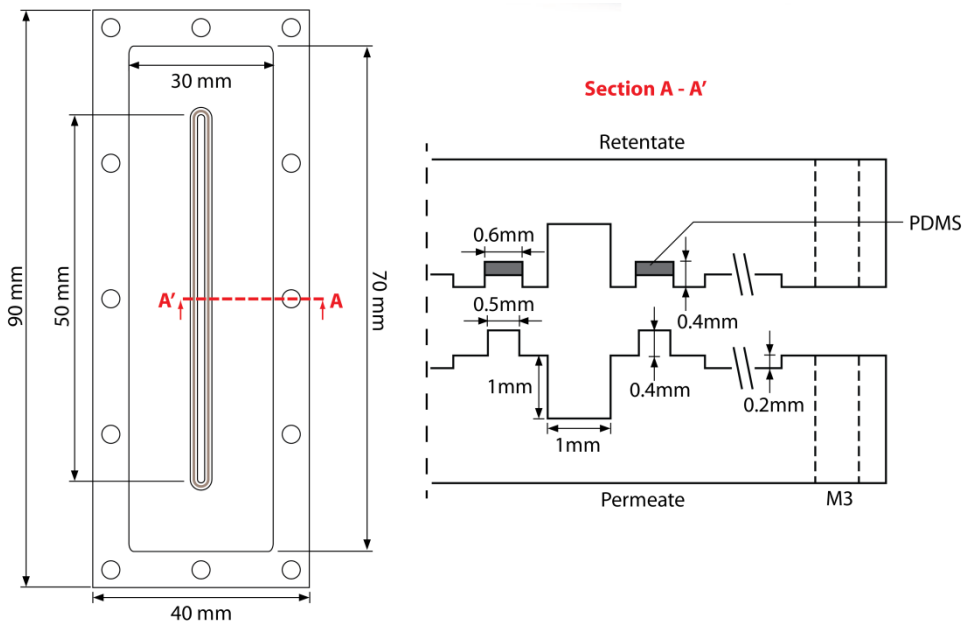


**Figure 20: Design of tangential flow filtration chip with interlocking PC and PDMS seal mechanism.**

The quality of the seal was evaluated by flowing a defined weight of water blue through the retentate side of the device whilst the fluidic connections of the permeate side were sealed. The difference between the weight of water blue flowed through the device and the amount collected was recorded first under varying assembly screw torsions, then with different PDMS gasket heights (using the screw torsion that caused the least leakage of water blue).

The use of a PDMS gasket did reduce the amount of leakage, as did the use the of a screw torsion of 15 cN-m; however the combination of the two was not enough to prevent leakage

altogether (see Figure 21A and B), as lateral diffusion of fluid through the membrane was still possible. Use of a gasket height above 0.4 mm or screw torsion above 25 cN-m also caused shearing in the channel wall (Figure 21C).

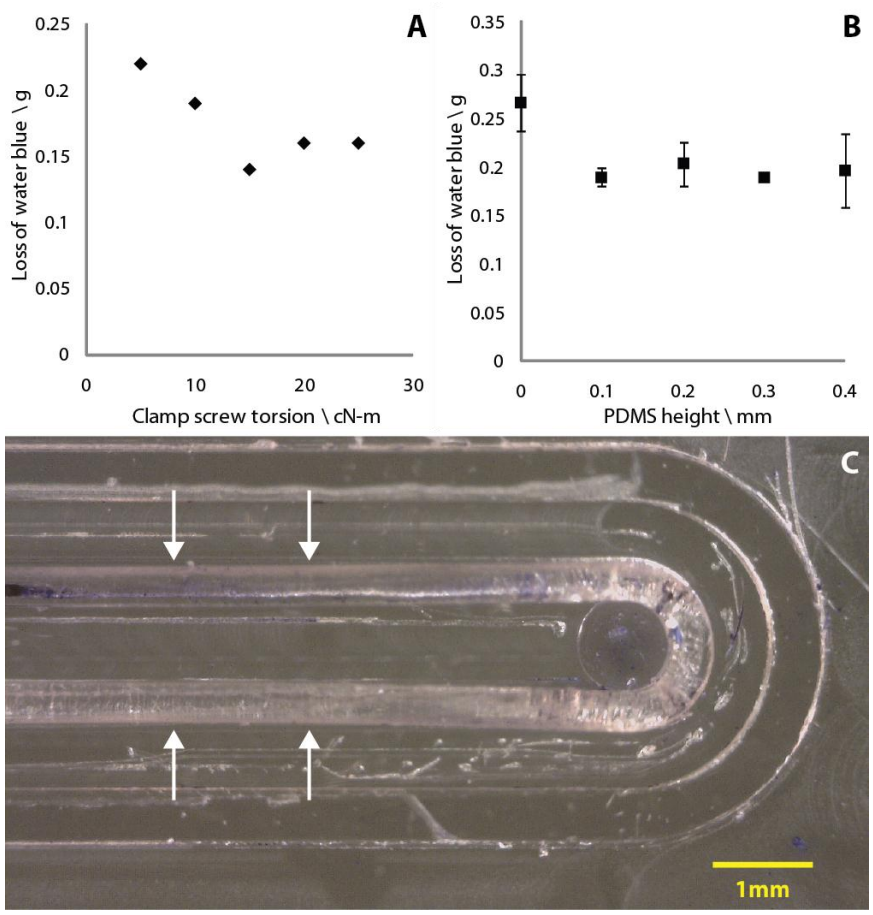


**Figure 21: Effect of clamp screw torsion and PDMS gasket height on integrity of membrane seal. (A) Effect of clamp screw torsion on loss of water blue from device; (B) effect of PDMS boss height on loss of water blue; (C) shearing of the retentate channel wall by expansion of 0.4 mm PDMS gasket under sealing pressure.**

The final design therefore aimed to completely seal the membrane within the filtration area, rather than clamp over a part of the membrane. This made the preparation of the membranes slightly more complicated, although they could be cut to fit the device quite accurately using laser ablation. The combination of a hard polymer lip and recessed PDMS gasket was also abandoned in favour of a raised PDMS gasket, which aimed to put less stress on the channel walls when the two halves of the device were clamped together. The offset

between the channel structure and the recess in which the gasket sat was also increased for the same purpose.

### 3.3.5 Modularity of Design

The use of clamp sealing in the filter design meant that the individual parts could be exchanged or replaced as required, facilitating the reuse of the device. The interconnects were also designed for use with standard M6 fittings, meaning that the device could be integrated into a larger network of devices if desired (see Chapter 4).

## 3.4 Clamp-Sealed Microfluidic Tangential Flow Filtration Device

### 3.4.1 Final Design

The final design was fabricated in 5 mm PC, with a PDMS gasket. The retentate and permeate sides each had a 1 x 1 x 46 mm channel milled into the centre (45.8 mm² filtration area), with a 1 mm diameter through-hole at either end for fluid connection. The recess for the gasket was offset from the channel wall by 1 mm and was 0.85 mm deep. The gasket itself was fabricated in a mould and was 1 mm deep, leaving a 650 µm prominence over the surface of the permeate plate to accommodate the membrane, and which deformed on clamping to seal the membrane in position. The two sides were clamped together with M3 screws placed at regular intervals along the length of the device. Interconnect ports were also attached with M3 screws; these had M6 threads for compatibility with standard fittings (Figure 22).

The interconnects were adapted from a design by Reichen *et al.* and were changed to attach to the side of the device without interfering with the main assembly screws (Reichen et al., 2010). The choice to use these rather than the commercially available interconnects, used in earlier phases of the development and more widely across other reported designs, was made because of the difficulty encountered in attaching the commercially available ports in a robust way, particularly when the devices were exposed to filtration pressures. Such problems are common across microfluidic device designs and could affect their reproducibly and utility,

although commercial solutions such as chip holders have become available more recently from specialist manufacturers of microfluidic devices (Nittis et al., 2001; Mair et al., 2006). These products allow the rapid connection of multiple fluidic inputs through clamping, and could potentially have made the assembly of the filtration device easier and the clamping more reproducible. However, the cost of the holders is quite prohibitive and they can be quite restrictive in terms of the size and port layout of the chip that can be used.

Use of clamping meant that a reversible seal could potentially be created around any commercial membrane that was cut to size. This made for a very simple fabrication process and meant that the device could be used to test a variety of process applications and conditions without needing to change any part of the device itself. It also meant that the device could be quickly repurposed to test different conditions, such as material and pore size, and that the device itself could be reused. This is preferable to previously demonstrated tangential flow filtration devices where the membrane surface was fabricated into the devices themselves, where changing the membrane properties would mean refabricating the entire device (VanDelinder and Groisman, 2007; Chen et al., 2008).

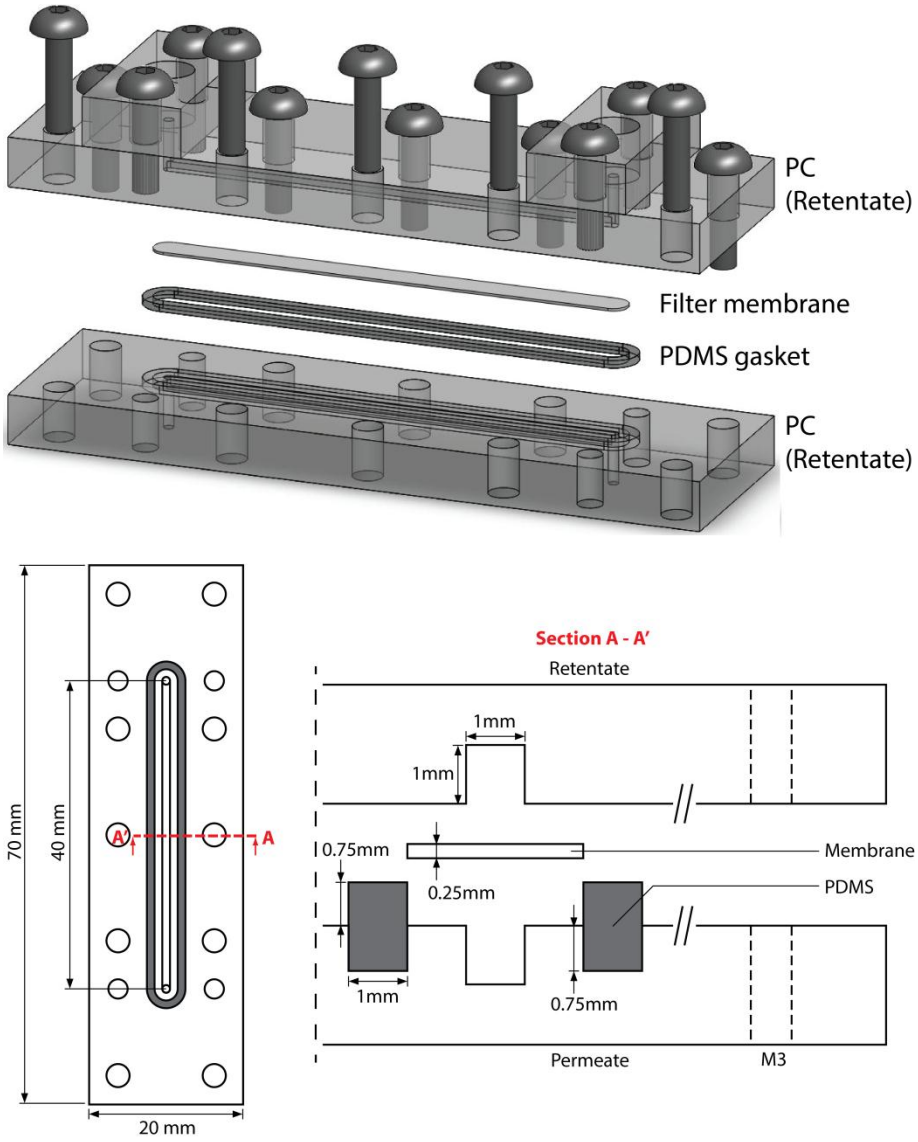


**Figure 22: Final design of clamp-sealed tangential flow filtration chip (not to scale).**

## 3.4.2 Burst Pressure Characterisation

The seal achieved in the device was dependent upon the clamping pressure applied with the screws. A torque driver was used to apply a specific torque to each screw in order to maintain an even pressure over the length of the device. The effect of the clamping pressure on the seal quality was characterised by measuring the burst pressure in the device under different assembly and interconnect port screw torsions. A pressure transducer was attached to the outlet of the retentate and air was flowed into the inlet with a syringe drive; the permeate connections were sealed (Figure 23A).

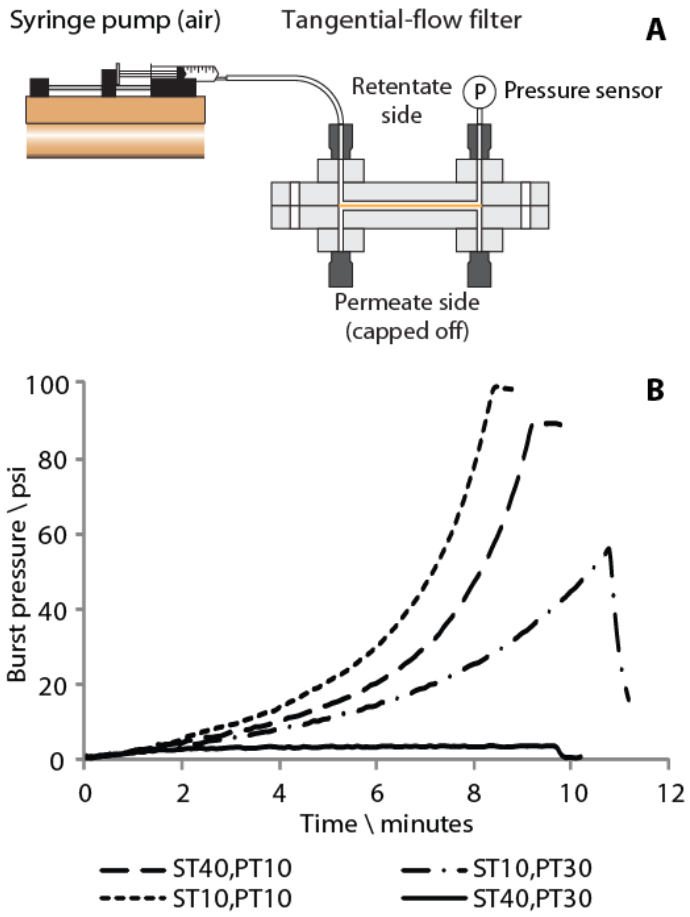


**Figure 23: Burst pressure characterisation.**

**(A) Diagram of setup used to measure burst pressure in microfluidic filtration device; (B) representative pressurisation profiles recorded after device was sealed with various assembly screw torques. ST refers to torque on screws of main assembly, PT to torque on screws used to attach interconnect ports. Torque units are cN-m.**

Evaluation of the burst pressure data suggests that the use of a 10 cN-m torsion for both sets of screws (ST and PT) creates a more effective seal than any of the other assembly conditions tested (Figure 23B). Using this torsion for both the main assembly screws and the interconnect port screws created a seal that did not burst at pressures up to 100 psi, the measurement limit of the pressure transducer used (40PC100, Honeywell), although a slow leak was observed after the maximum pressure had been reached.

Higher torsions resulted in a lower-quality seal; a screw torsion of 10 cN-m on the main assembly screws and 30 cN-m on the interconnect screws caused the seal to burst at around 55 psi, while a screw torsion of 40 cN-m on the main screws and 30 cN-m on the interconnect

screws prevented the device from being pressurised at all. This is presumably due to deformation of the plates and resulting poor contact between the PDMS gasket and the permeate side of the device.

The data also suggested that the torsion applied to the interconnect screws was a greater factor in determining the quality of the seal than that applied to the main assembly screws. Increasing the interconnect screw torsion from 10 to 30 cN-m resulted in a much greater drop in burst pressure (40 psi) than a corresponding increase from 10 to 40 cN-m (10 psi; see Figure 23B).

## 3.5 Mammalian Cell Recovery in Microfluidic Tangential Flow Filter

### 3.5.1 Separation of Trypsin from Cell Media using Microfluidic Tangential Flow Filter

To validate the results of the bench scale test and to further investigate the conditions required for trypsin removal in the microfluidic tangential flow filter, further tests of trypsin clearance were performed using the filter design described in Section 3.4. FBS-free media solution containing trypsin enzyme at 0.25 mg $ml^{-1}$ was passed through the retentate side of the filter whilst FBS- and trypsin-free media was passed through the permeate side of the filter. A polysulphone membrane with 0.45 µm pore size was used for the experiments, equivalent to that used in the proof of concept tests in the bench scale device. Flow rates were controlled with a syringe drive and MilliGAT pump (see Figure 24).

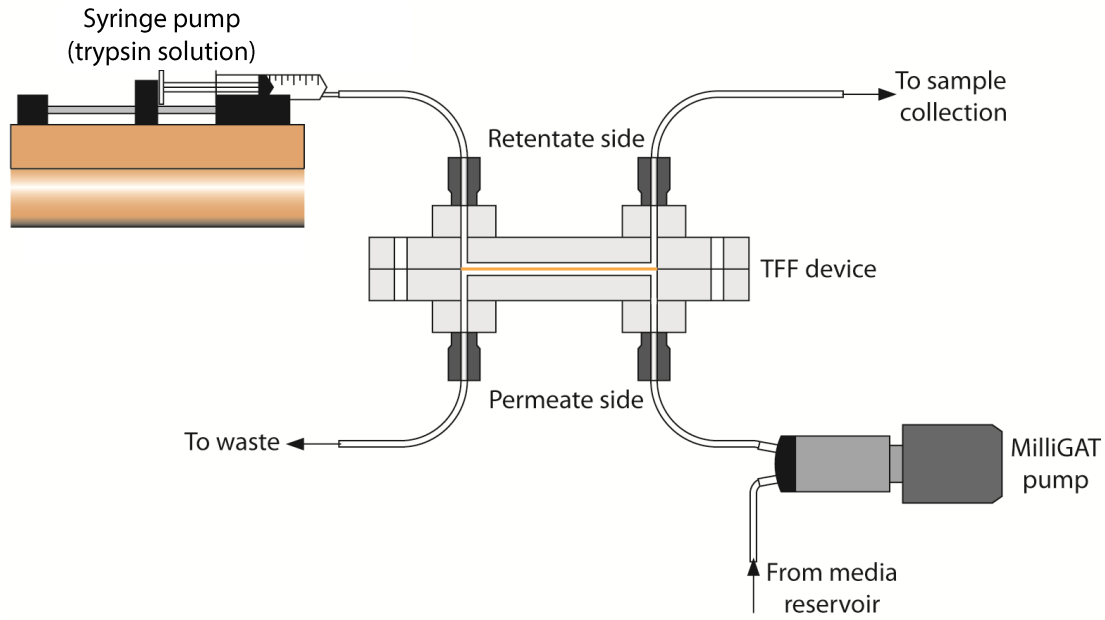


**Figure 24: Illustration of setup used to test clearance of trypsin from solutions of FBS-free media.**

The measurement of trypsin remaining after filtration using various retentate and permeate flow rates suggest that a lower flow rates result in a greater trypsin clearance, particularly where a lower retentate flow rate and higher permeate flow rate are used (see Figure 25). The greatest clearance of trypsin was achieved when using permeate and retentate flow rates of 0.1 and 0.01 ml $min^{-1}$ respectively, resulting in a 50% reduction in trypsin concentration compared with the original media solution. This is a better clearance than was observed where flow rates of 0.01 ml $min^{-1}$ were used on both sides of the membrane, suggesting that the mechanism of clearance is a combination of diffusion of trypsin from the retentate to the permeate side, along with dilution by the trypsin-free media flowing through the permeate side.

Whilst this result demonstrated that it was possible to remove a substantial amount of trypsin with the microfluidic filter, it was not sufficient for the purpose of using the device for media exchange in cell culture, where complete removal of all undesired media components would be necessary. Further optimisation of the filtration conditions was therefore undertaken, using a combination of flow rate control and flow restriction with capillaries to affect the contact time of the media with the membrane and the transmembrane pressure (TMP).

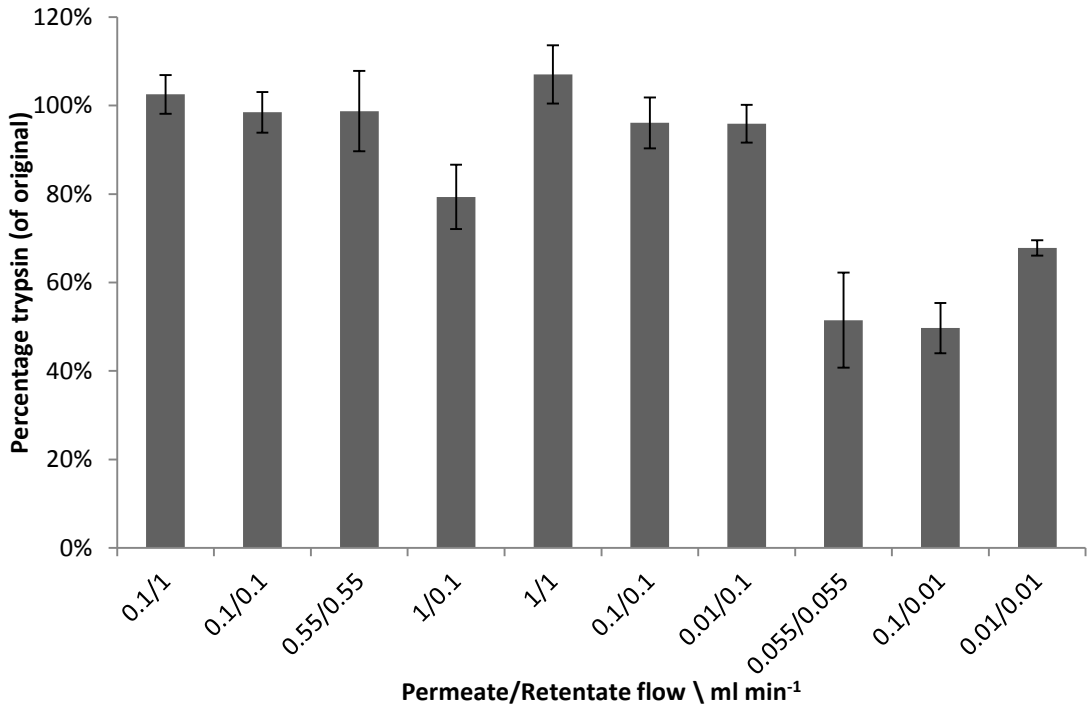


**Figure 25: Effect of retentate/permeate flow rate on trypsin clearance from cell suspensions (n = 3, error bars indicate standard deviation).**

### 3.5.2 Control of TMP with Flow Restricting Capillaries

Initial investigation into the filtration conditions required to remove trypsin suggested that control over transmembrane pressure (TMP) would be necessary to make the process feasible. To this end, glass capillaries with defined diameters were used in combination with the input flow rate to control the pressure on the retentate and permeate sides, and hence the TMP. The selection of capillaries was made by calculating the theoretical pressure that each would supply at defined flow rates and hence the TMP in the filter. The calculations were based upon the Hagen-Poiseulle equation, using the diameter and length of the capillaries, the tubing connecting them to the microfluidic filter and the channels of the filter itself. The selection of flow rates and capillary diameters and the TMP they were used to supply is shown in Table 8. The spreadsheet used to calculate the pressures that each capillary would supply and select the condition set for the desired TMP is shown in Appendix A.

| TMP (bar/psi) | Capillary length, mm | Capillary diameter, mm | Flow rate, mm min$^{-1}$ |
|---|---|---|---|

| | Retentate | Permeate | Retentate | Permeate | Retentate | Permeate |
|---|---|---|---|---|---|---|
| **0.696/10.09** | 100 | 100 | 0.32 | 0.32 | 0.1 | 1.0 |
| **1.344/19.49** | 200 | 100 | 0.32 | 0.32 | 0.1 | 1.0 |
| **2.078/30.14** | 100 | 200 | 0.5 | 0.32 | 1.0 | 5.0 |

**Table 2: Condition sets used to achieve specific TMP in cell filtration experiments.**

### 3.5.3 Separation of MEF Cells from Trypsin using Microfluidic Tangential Flow Filter

Having established that trypsin could be at least partially removed by filtration, and that TMP could be controlled using glass capillaries of defined size, the recovery of mammalian cells was tested with the tangential flow microfluidic filter. Murine embryonic fibroblast (MEF) cells were used as a stand-in for mES cells due to the relative ease with which they could be cultured. The cells were detached from the surface of culture flasks using 0.25 mg $ml^{-1}$ trypsin and the resulting suspensions were made up to 3 ml with FBS-free media.

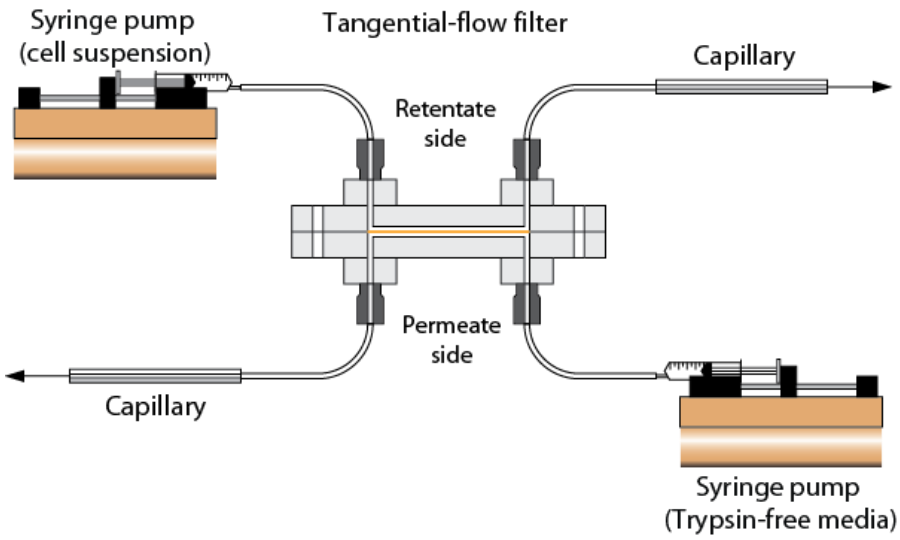


**Figure 26: Illustration of setup used to test the separation of MEF cells from trypsin during passage.**

The suspension of dissociated cells was then divided into three samples; one to determine the initial concentration of trypsin and cell count, one to be passed through the filter, and a final sample to be centrifuged and resuspended as per the stand passage protocol. The filtration experiments were carried out using the condition sets defined in Table 8, with the cell

suspension being passed through the retentate side of the filter and FBS- and trypsin-free media being passed through the permeate side (see Figure 26). The performance of the filtration step was evaluated in terms of the amount of trypsin removed, the number of cells recovered and the effect on cell viability before and after filtration.

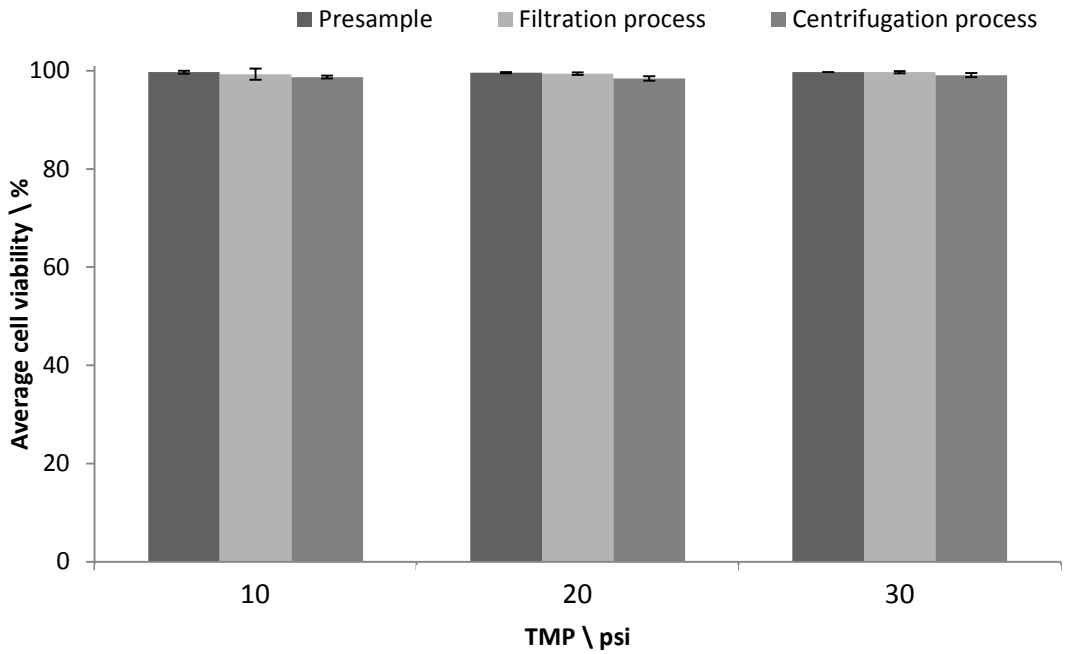


**Figure 27: Cell viability after filtration with tangential flow filter and centrifugation (n = 6, error bars indicate standard deviation)**

The effect of filtration on cell viability was determined to be negligible, regardless of the TMP used (see Figure 27). Cell suspensions were found to have 99-100% viability before and after filtration with no variation at TMPs of 10, 20 and 30 psi. Cell suspensions processed by the standard passage method had viabilities in the range of 98-99%, but the difference between this and the filtration samples was not significant. This indicated that the filtration process, in particular the shear that the cells would likely have been exposed to in the capillaries used for pressure control, was not damaging to the cells.

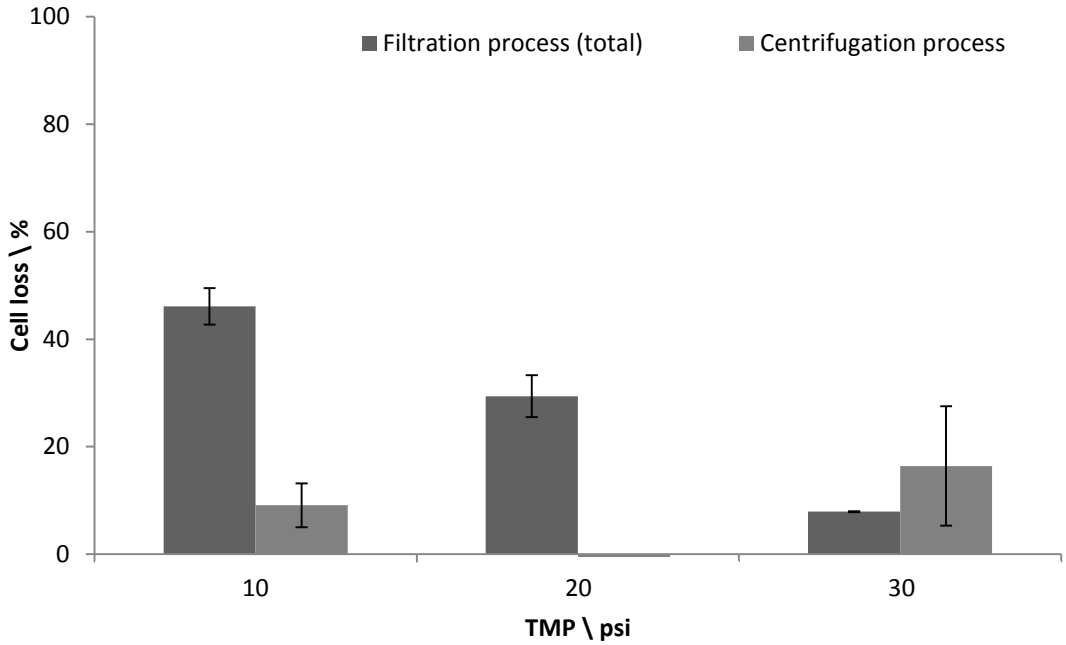


**Figure 28: Percentage cell loss after filtration and centrifugation (n = 6, error bars are standard deviation)**

The cell loss, as a percentage of the number of cells in the initial samples, was in most cases significantly higher for filtration than it was for centrifugation (see Figure 28). At 10 psi almost 50% of the cells fed into the filter were not recovered, with around 30% lost at 20 psi. However at the highest operating TMP, 30 psi, only 8% of the cells entering the filter were lost.

The loss of these cells could be attributed to their accumulation on the surface of the filtration membrane as the fluid passed through to the permeate side. Investigation of the membranes by staining with crystal violet after filtration showed large numbers of cells on the surface which would seem to confirm this (see Figure 29). This being the case, it might be expected that a higher TMP would correlate with a greater loss of cells through accumulation on the membrane surface, in which case the lowest cell loss encountered at 30 psi would seem to be counter-intuitive. However, to achieve a TMP of 30 psi the retentate had to be passed through the filter at a higher flow rate of 5 ml $min^{-1}$ (see Table 8, Appendix A), which would generate a greater shear force at the membrane surface and reduce the accumulation of cells, thus reducing the overall cell loss. This illustrates the main drawback of using capillaries to

control fluid pressure; since a limited range of capillary diameters were available, higher flow rates had to be used to reach pressures above 20 psi, but in doing so additional variability was created between the condition sets, which made them less comparable.

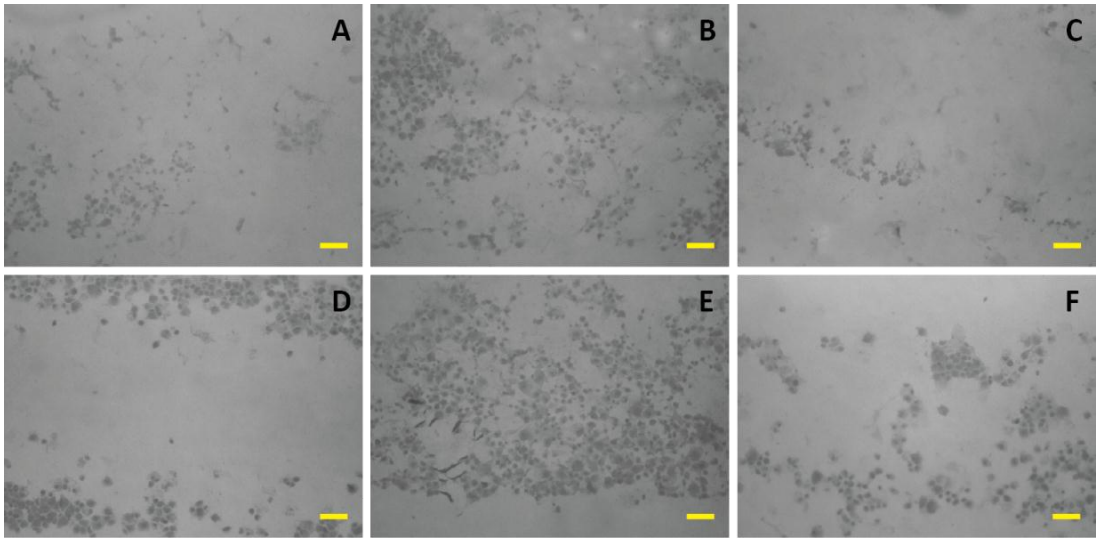


**Figure 29: Analysis of the surface of two membranes after filtration of cell suspensions at 20 psi TMP. A, B and C and D, E and F are collections of three images taken from two different membranes. A and D show the area of the membrane immediately under the filter input, B and E show the area in the centre of the membrane and C and F show the area under the filter output. Scale bars are 100 µm in length.**

The amount of trypsin remaining in the samples was measured using the colourimetric method shown in Section C.1.3. Analysis of the cell suspension exiting the filter showed that the maximum clearance of trypsin was a 45% reduction from the original mass, achieved at a TMP of 10 psi (see Figure 30). At the highest TMP of 30 psi, where the transmission of trypsin would be expected to be highest, 85% of the original mass remained in the retentate. Again, this is likely due to the fact that the retentate flow rate had to be increased in order to reach a TMP of 30 psi, reducing the residence time of the cell suspension within the filter and therefore also reducing the efficiency of the transmission.

The ability of the filtration unit to remove trypsin was very poor when compared to the standard centrifugation protocol; samples which had been centrifuged contained a maximum of 7% of the original amount of trypsin used to dissociate the cells, and in some cases the trypsin concentration was reduced below detectable levels.

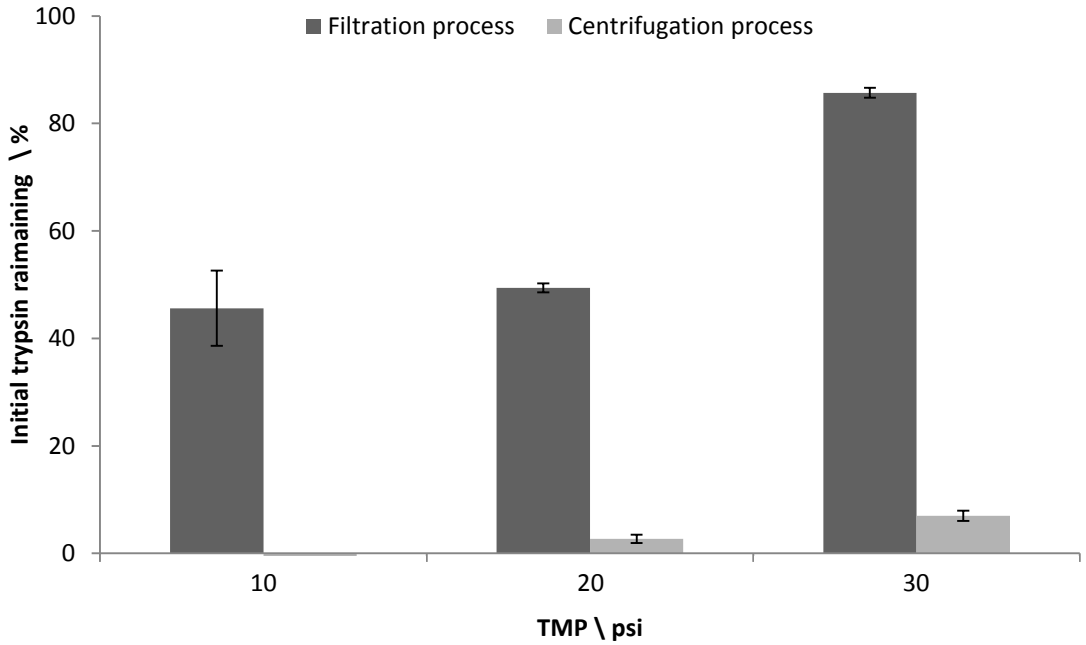


**Figure 30: Percentage of initial trypsin remaining after filtration and centrifugation (n = 6, error bars are standard deviation)**

## 3.5.4 Replating of MEF Cells after Filtration

Although the filtration process tested in Section 3.5.3 was shown to have no significant effect on the viability of the cells, other effects such as contamination and phenotypic changes induced by shear stress could not be determined immediately after the recovery of the cell suspensions. Such effects only become apparent over several days, or weeks, through repeated passages. The filtered cell suspensions were therefore replated in fresh culture flasks to determine whether any of these effects became apparent.

Suspensions of cells filtered at 20 psi were chosen to be replated, as these had relatively low concentrations of trypsin of the three condition sets tested and had high enough populations remaining after filtration to make confluency feasible. Two cell suspensions were at 20 psi as detailed in C.2.2, the retentate was collected, diluted with media containing FBS and then left in new culture flasks to reattach (see Figure 31C and D). These were compared with suspensions processed by the standard centrifugation protocol (see Figure 31A and B).

Cultures passaged using filtration had visibly lower concentrations of cells, and failed to reach confluency after 6 days of incubation with daily media exchange. The cultures did not show any signs of contamination, indicating that the PC components and the membrane itself were properly sterilised. However, the cultures could not be sustained over more than one passage due to the very low cell concentration, meaning that any longer-term phenotypic effects of the filtration process could not be investigated.

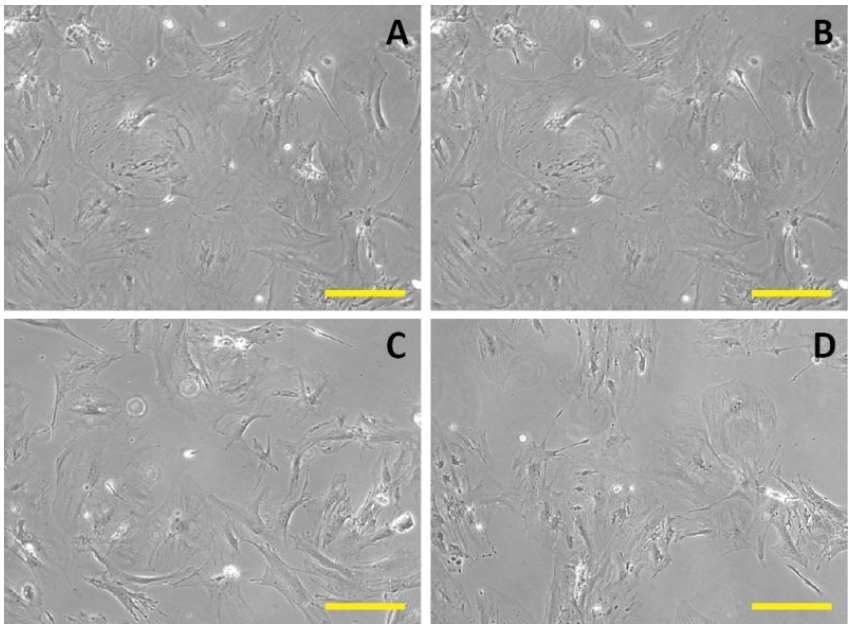


**Figure 31: Culturing of cells recovered after centrifugation (A and B) and filtration (C and D). Cells recovered after filtration were unable to reach confluency after 5-6 days of culture. Scale bars are 20 µm in length.**

## 3.6 Summary of Findings

This chapter has demonstrated the design of a microfluidic tangential flow filtration device. A microfluidic normal flow filter was developed as proof of concept device, to establish whether a membrane could reliably be sealed into PDMS. This design was abandoned after testing with the normal flow filter showed that the device became inoperable very quickly as a result of membrane fouling. Testing of the normal flow device for the recovery of mES cells from suspension after passage showed that the cells could be separated from the trypsin used to detach them, but not without significant cell loss due to impaction on the filter membrane and subsequent dilution when recovering the retentate. Tangential flow filtration was therefore chosen instead because of its improved resistance to fouling, as well as the additional flexibility it offered.

The final device design was fabricated primarily in PC with a PDMS gasket, allowing filter membranes to be sealed into the device by clamping. This design was chosen over soft polymer designs due to the challenges involved in sealing membranes into PDMS by thermal compression bonding and the complexity of chemical bonding methods. The fabrication of the filter enclosure in 5 mm rigid polymer reduced the degree of deformity that occurred and facilitated clamp sealing. The seal was shown to be robust to bursting up to 100 psi for defined clamping screw torsions of 10 cN-m, with increasing torque causing deformation and reducing the ‘burst pressure’ of the device.

The device was designed to be wholly reusable, with only the membrane being disposed of between applications. The use of polycarbonate as the hard polymer meant that it could be autoclaved for use in sterile applications if desired. It was also designed to be modular and intercompatible with other devices, such that single parts could be quickly redesigned or so that it could be integrated into a series of cascaded devices (see the application to biocatalytic synthesis in Chapter 4).

The membranes used were cut to size to fit within the PDMS gasket in order to achieve a good fluidic seal. This added a small amount of extra complexity to the setup of the filter, but was shown to be necessary after the failure of several filter devices which were designed to clamp over a larger piece of filter membrane. In these cases the lateral spread of fluid through the membrane allowed leakage out of the devices.

Finally, the use of clamp sealing meant that the device could be used in conjunction with different membrane types, allowing its application to different downstream bioprocessing scenarios. The use of the device as part of a larger process could therefore be evaluated, working towards the investigation of a bioprocess at the microfluidic scale.

The recovery of mammalian cells from a suspension containing the enzyme trypsin was investigated as an application of the filtration device. Although initial experiments indicated that trypsin could potentially be removed from cell suspensions by filtration as opposed to centrifugation, further investigation indicated that it would not be practical, at least not by the methods described in this chapter. Though filtration was shown to have no effect on the viability of the mES and MEF cells filtered, the loss of cells as a result of accumulation on the filtration membranes was generally very high, with up to half of the cells unrecovered. The concentrations of trypsin remaining in recovered cell suspensions were also too high, possibly as a result of the short residence time of the cell suspensions in the filter.

Cell suspensions recovered from filtration at a TMP 20 psi were replated in an attempt to determine any adverse effects of the process on the cells that were not detectable immediately after sampling. Although this did show that the cells were not contaminated, the cell concentrations were too low for the cultures to be able to reach confluency, preventing them from being passaged more than once. Investigation into the use of the tangential flow filter for filtration of mammalian cell cultures was therefore abandoned.

Work towards an alternative application of the filter is shown in Chapter 4, looking at the recovery of a small molecular product from a biocatalyst. However, since the device is clamp

sealed and is robust to high pressures, the use of a wider range of membranes and testing conditions is possible, meaning that it could be used to investigate other bioprocesses where membrane separation is a candidate for downstream processing. Candidate membranes would need to be cut to fit within the device however, and the device itself might require modification to accommodate different thicknesses of membrane and further burst pressure testing to validate the seal if higher pressures were required.

# 4

# Biocatalytic Synthesis Using Inline Microfluidic Filtration Device

This chapter explores how the tangential filtration device developed in Chapter 3 could be used with an upstream biocatalytic reactor to produce and purify a chiral metabolite. The metabolite chosen as a test case for the work was L-erythrulose (ERY), a product of the reaction between glycolaldehyde (GA) and hydroxypyruvate (HPA) and catalysed by transketolase (TK) from *E. coli* cell lysate.

Some of the results in this chapter were produced in collaboration with Homan Al-Bahrani and Dr Brian O'Sullivan. The data in Figure 32 and Figure 33 was produced in collaboration with Brian O'Sullivan and Homan Al-Bahrani. The reactor design (presented in Figure 34) was developed by Homam Al-Bahrani, based on a design by Stroock *et al.*; the data in Figure 36 was produced in collaboration with Homam Al-Bahrani.

The data in this chapter has been published in part in "*Modular microfluidic reactor and inline filtration system for the biocatalytic synthesis of chiral metabolites*", by O'Sullivan *et al.* (2012).

## 4.1 Introduction

There are many advantages associated with biocatalytic synthesis of chemical products, in particular the lower requirements in terms of temperature and pressure, and fewer protection or deprotection steps and side reactions as a result of the greater selectivity and specificity of biocatalysts. For these reasons biocatalysis is viewed as a more sustainable alternative to chemical catalysis, with many current and potential industrial applications, particularly in the production of metabolites and active pharmaceutical ingredients (Woodley, 2008; Wohlgemuth, 2010; Clouthier and Pelletier, 2012; Meyer et al., 2013).

The properties of microfluidic systems have a number of useful benefits to biocatalytic synthesis, and especially for process development. These include improved heat and mass transfer for control of reaction conditions, as well as real-time monitoring and parallelisation for rapid optimisation of yield (Miyazaki and Maeda, 2006; Wiles and Watts, 2008; Mak et al., 2009). As a result, a number of microfluidic reactors have been reported for use with biocatalysts, including use of cellular and enzymatic catalysts; however relatively few have focussed on the need for downstream purification of the desired product, and particularly not on scalable methods of separation.

When developing any biocatalysed synthesis process it is necessary to consider the purification of the product, especially the retention of the catalyst itself. In many reported cases the biocatalyst is immobilised inside the reactor, either by adherence to the channel walls or to another surface that is trapped inside the reactor (e.g. membrane, beads or monolith). While this eliminates the requirement for downstream separation (assuming that no leaching of the catalyst occurs), immobilisation can significantly reduce the activity of the biocatalyst through diffusional limitation or steric inhibition. It also increases the complexity of development, usually requiring that the biocatalyst be adapted for immobilisation, and can reduce the flexibility of reactors if the channel walls are used as the immobilisation surface. Solubilised enzymes can therefore provide more flexibility and simpler development of

reactor design, as well as an increased yield of active biocatalyst, though this comes at the cost of long-term stability.

Solubilised enzymes require separation from the reaction product downstream of the reactor. Given the size difference between the biocatalyst (a cell or large molecular weight protein) and product (generally a small molecular weight chemical), membrane separation is feasible and commonly used in industry. The flexibility of the microfluidic filter design previously described in Chapter 3 means that it could be used in combination with a membrane with a suitable molecular weight cut-off, in order to retain the biocatalyst downstream of the reactor. In addition, the tangential flow design of the filter should reduce the rate of fouling of the membrane, a particular problem when dealing with solutions containing cells or cell debris. This could also allow the recovered biocatalyst to be recycled for further use in the reactor, depending on its stability.

Similar microfluidic devices for biocatalysed reactions and membrane recovery of the product have been reported previously. Once such device was used for the separation of pectin hydrolases from pectin lyase. A microfluidic enzyme reactor was integrated with a regenerated cellulose membrane to create an *in situ* product recovery system, which was used to separate low molecular weight pectin hydrolysate product from higher molecular weight pectin fragments and the lyase enzyme (Alam et al., 2011). The configuration was suitable for this particular application as a relatively low residence time was required for the hydrolysis of the pectin, and because the unreacted substrate could be retained by the same membrane that was used to prevent the pectin lyase enzyme from leaching.

Further devices have been developed which use membranes to immobilise enzymes in place either by chemical immobilisation on the membrane surface or physical trapping between two membranes with specific hydrophobicities to allow the enzyme to be retained without fouling (Zhang et al., 2010; Machsun et al., 2011). However, these devices either failed to achieve complete conversion of substrate to product or relied on relatively rapid

reaction rates which allowed complete conversion with a short residence time. This would not necessarily be applicable to biotransformations requiring longer residence times to go to completion or which used low molecular weight substrates, as unreacted substrate could potentially exit the reactor before being converted, therefore requiring further separation downstream. It may be possible to take the output from such a reactor and recycle it in order to achieve complete conversion; however this would likely require a further separation step to isolate the unreacted substrate from the product (Pohar et al., 2012).

It would be therefore be advantageous to have a modular continuous reaction and filtration system that could be adapted to different reaction setups, allowing the reactions to go to completion before the catalyst is removed and thereby eliminating the need for further purification steps or substrate recycling. Such a system would also allow the separate testing and optimisation of upstream and downstream processing conditions before the two units were combined.

This chapter will show the development and characterisation of such a system for the biocatalytic synthesis of ERY from hydroxypyruvate HPA and glycolaldehyde GA using a solubilized transketolase TK enzyme. This particular reaction was selected as it is a well-characterised biotransformation which yields a single product and is driven to completion by the evolution of carbon dioxide as a by-product. Transketolases are attractive biocatalysts for asymmetric synthesis due to their wide substrate tolerance, ability to form carbon-carbon bonds with high enantioselectivity and high specificities (Hibbert et al., 2007, 2008; Charmantray et al., 2009; Liese et al., 2009; Cázares et al., 2010).

## 4.2 Synthesis of ERY in Microfluidic Reactor using Transketolase

### 4.2.1 Determination of HPA and ERY concentrations by HPLC

HPA and ERY were analysed by HPLC using an ion-exchange column and 0.1% TFA mobile phase. Measurement of UV absorbance at 210 nm under these conditions returned single peaks for HPA and ERY at 9-10 minutes and 11-12 minutes respectively. Calibration curves were established for the two species using pure standards (see Figure 32 and Figure 33). The response factors for HPA and ERY were determined to be 526 mM $Au^{-2}$ ($R^2$ = 0.9935) and 667 mM $Au^{-2}$ ($R^2$ = 0.9797) respectively. The maximum concentration that could be accurately measured was 20 mM for both species.

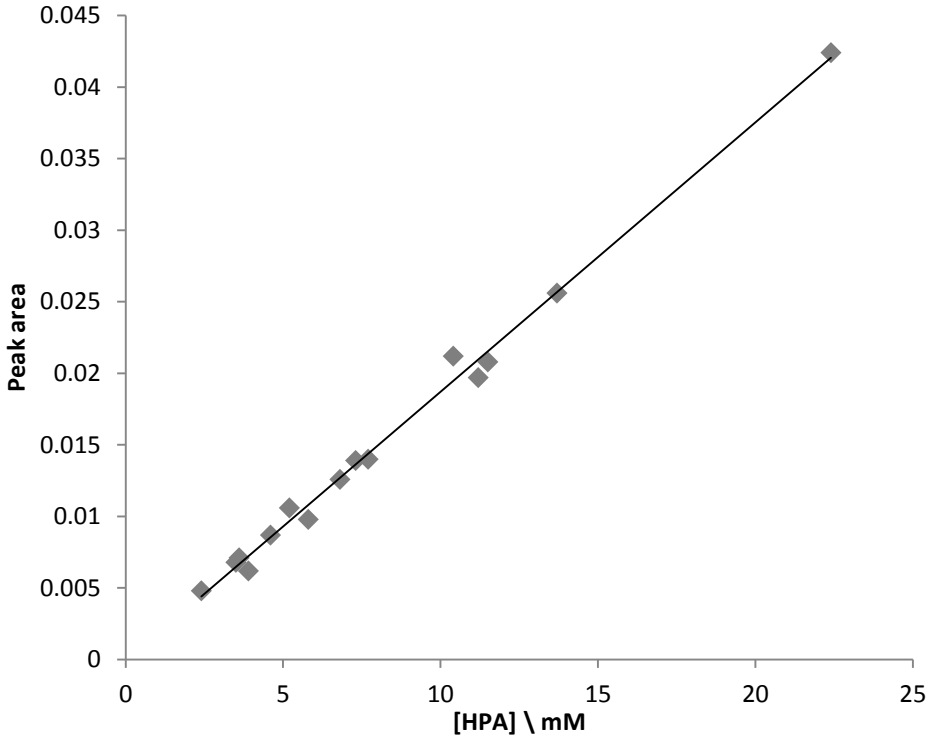


**Figure 32: Calibration curve for HPA standards**

GA could not be detected with this method but, as the substrates were being used at equimolar concentrations, it was assumed that the concentration would be equivalent to that of HPA.

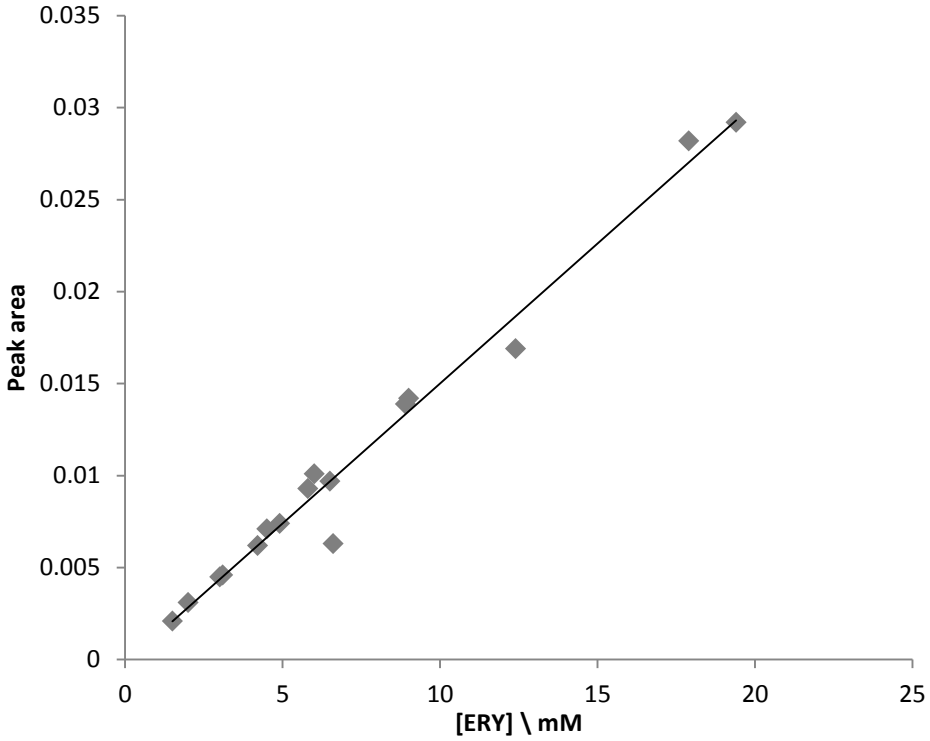


**Figure 33: Calibration curve for ERY standards**

## 4.2.2 Design and Characterisation of SHM reactor

The microfluidic reactor used to perform the TK-catalysed reactions was a modified version of Stroock's staggered herringbone mixer (SHM), chosen to facilitate passive mixing of the enzyme and substrates entering the reactor through separate inlets (Stroock et al., 2002; Ansari and Kim, 2007). The structures were required to ensure rapid homogenisation of the enzyme and reactants in the absence of turbulent flow and thereby create a defined point at which the solution could be said to be well-mixed, for the purposes of accurately measuring the reaction residence time. This was necessary in order for the reactions performed in the SHM reactor to be comparable to those performed in the 96-well plates that are commonly used in batch mode for bioprocess evaluation, which are generally stirred to ensure homogenisation of the reaction mixtures.

The channels of the reactor were arranged into a T-junction, each channel having a cross-section of 500 x 250 µm (w x d), with a channel length of 89.5 mm between the junction to

the outlet (see Figure 34). The choice of a relatively large channel size was made to allow soluble enzymes to be used in the reactor without causing clogging that might occur in smaller geometries. The use of larger structures also meant that the reactor could be fabricated in with the same technology as the filter device, facilitating the potential later integration of the two devices. The SHM structure, consisting of 7 groups of 10 grooves with an alternating bias, was milled directly into the floor of the channel, starting one centimetre from the channel join. The sizes of the structures are shown in the inset of Figure 34.

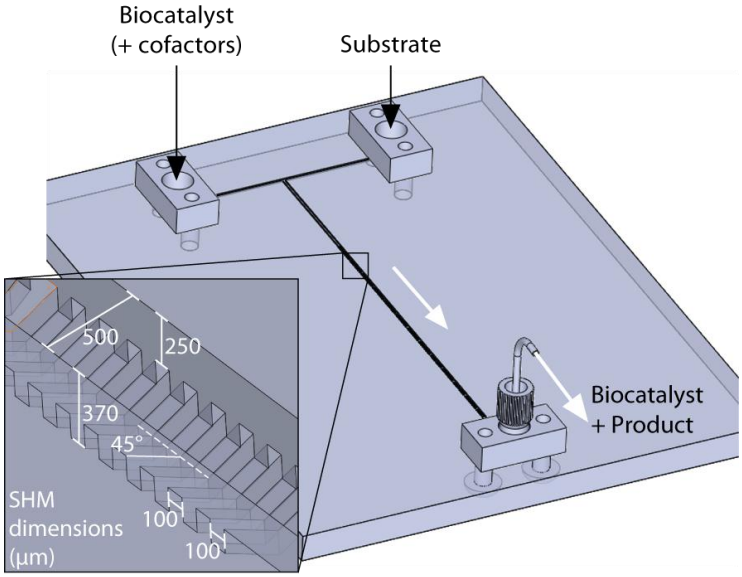


**Figure 34: Design of staggered herringbone mixer (SHM) reactor.**

Given the size of the enzyme used (72 kDa), it was necessary to ensure that the SHM structures in the reactor were capable of homogenising a solution of small molecular weight substrates and large molecular weight proteins. To demonstrate the efficiency of the structures for this purpose, two T-channel reactors of identical size were fabricated, with and without the SHM structures. Two solutions were run through the inlets at various flow rates: reverse osmosis purified water and a 0.3 mg $ml^{-1}$ solution of fluorescein-conjugated bovine serum albumin (BSA, 65 kDa). Confocal images were taken at 6 cm from the T-junction (downstream from the SHM structures, see Figure 35A) and a composite of the images was built to give a cross-section view of the intermingling of two solutions.

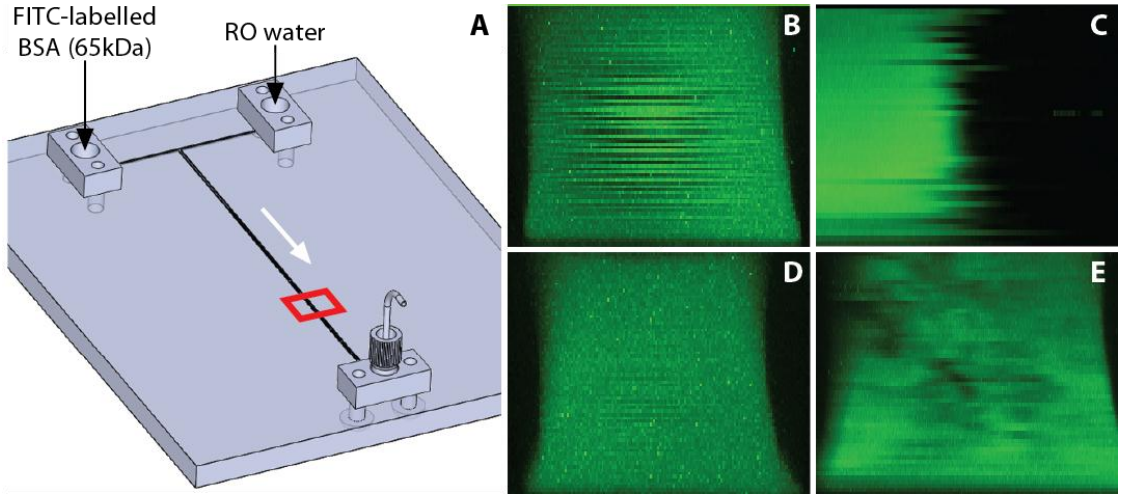


**Figure 35: Imaging of mixing conditions in SHM using confocal microscopy.**
**Setup of reactor for confocal imaging (A), vertical sections of channels (B - E). Sections taken in reactor with SHM (B and C) and without (D and E), at flow rates of 0.03 ml min$^{-1}$ (B and D) and 3 ml min$^{-1}$ (C and E).**

At higher flow rates (3 ml min$^{-1}$, Figure 35C and E), distinct separation of the labelled and non-labelled fluid streams was observed in the non-SHM channel, while the streams in the SHM channel appeared to be well mixed. At lower flow rates (0.03 ml min$^{-1}$, Figure 35B and D) the two streams appeared to be well mixed in both reactors, regardless of the presence or absence of SHM structures, presumably since the residence times at this point in the channel are long enough to allow diffusion of the protein across the channel width. At this flow rate and with a mass diffusion coefficient of $6.8 \times 10^{-7}$ cm$^2$ s$^{-1}$ (equivalent to that of BSA in aqueous solution; Wojcieszyn et al. 1981), the Péclet number is 294,000 (see below). This value is typical for the small channel dimensions used in microfluidic reactors.

$$Pe = \frac{uL}{D} = \frac{0.4cm \cdot s^{-1} \times 0.05cm}{6.8 \times 10^{-7} cm^2 \cdot s^{-1}} = 29{,}400 \qquad (12)$$

These results suggested that the SHM structures were unnecessary where low flow rates were used, as diffusion was the predominant method of transport and appeared to occur at a sufficient rate to allow the enzyme to spread across the width of the reactor. However, ensuring that the input streams were well mixed regardless of the flow rate was essential in order that the reactor could be used for a range of residence times, for evaluation of reaction kinetics and for compatibility with more rapid reactions. It was also necessary to be able to define where

the streams would be homogenous, regardless of the flow rate used, in order to be able to accurately control the concentrations of each component and define the starting point of the reaction for the purpose of measuring the residence time of the reaction.

### 4.2.3 Kinetics of Transketolase-Catalysed Synthesis of ERY

The kinetics of the transketolase-catalysed conversion of HPA and GA to ERY were investigated in the SHM reactor and compared to batch reactions carried out in 96-well plates. The residence time of reactions performed in the SHM reactor were controlled by adjusting the flow rate, where the residence volume was defined by the combined volume of the reactor channel and the outlet tubing. The reaction endpoint was defined by the collecting samples from the outlet tubing in a vial containing 0.1% TFA, which inactivated the enzyme. Placing the end of the outlet tubing into the TFA solution ensured that the reaction was quenched immediately after exiting the tubing, so that the residence time could be precisely defined. Batch reactions were controlled in a similar manner, by diluting samples of the reaction mixture in defined volumes of TFA at the specified end point. Reaction residence times in the range of 1 to 180 minutes were evaluated and were controlled in the SHM by adjusting the flow rate in the range of 0.07 – 12 µl $min^{-1}$.

The reaction kinetics showed that complete conversion of 50 mM HPA and GA to ERY, in both the SHM reactor and 96-well plate, occurred in 120 minutes (see Figure 36). This is in agreement with previous work by Matosevic *et al.* (Matosevic et al., 2010). The evolution of $CO_2$ as a by-product allows the reaction to go to completion, although no gas bubbles were observed in the reactor, possibly because the concentration (and therefore partial pressure) was too low for evaporation to occur in the sealed channels.

The reaction profiles in both the batch-mode 96-well plate and the continuous-flow SHM reactor were reproducible and comparable, showing similar concentrations of HPA and ERY at each time point. The enantiomeric excess (e.e.) values of the ERY produced were also similar, measured at 90% and 87% L-ERY for the batch and SHM reactors respectively. This

might be expected given that the chemical interaction is the same in both systems, though it was necessary to rule out any variability in the reaction profiles brought about by clogging of the SHM reactor, which could have increased the apparent reaction rate by increasing the reaction residence time beyond its intended value.

The use of clarified lysate containing biocatalyst, rather than immobilised enzymes, can be problematic in the small channel geometries that are common to microfluidics. However, the larger cross-sectional area channels used in the reactor were able to accommodate the lysate without clogging. The reactor could therefore be used for early process evaluation where testing with a number of different enzymes is necessary and therefore the requirement to immobilise would be a disadvantage.

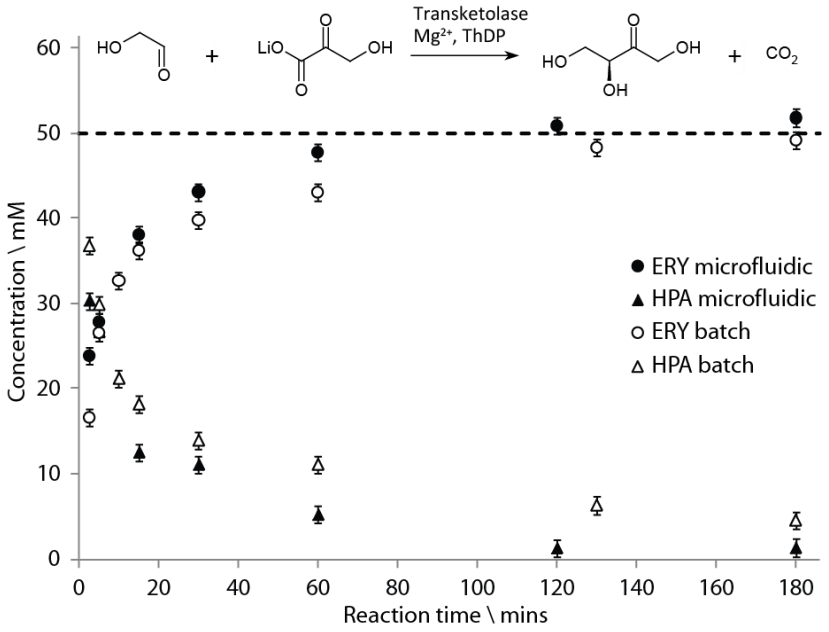


**Figure 36: Kinetics of transketolase-catalysed synthesis of ERY, performed in microwell plates and SHM reactor (n = 6, error bars indicate standard deviation).**

As the reaction data was comparable, it is worthwhile examining whether the reactor could be considered as a viable alternative to 96-well plates, for the purpose of evaluating synthesis processes using biocatalysts. Multi-well plates have the advantage of being able to perform a large number of different reaction conditions simultaneously, something that is not possible in a single SHM reactor. Increased experimental throughput could of course be achieved by

'numbering up,' though running an equivalent number of reactions in parallel in SHM reactors would likely be impractical at this scale. Being a continuous flow reactor however, it may be more suitable for use in scale-down evaluations of continuous synthesis bioprocesses, as this is increasingly the preferred option in industry due to the advantages that continuous processes offer in terms of improved process efficiency and the conversion of unstable intermediates using multi-step synthesis processes (Yoshida et al., 2013).

The continuous flow reactor provides the additional possibility of a step towards small-scale industrial production. At the conditions required for 100% conversion (i.e. with a 120 minute residence time) the reactor produced 50 mM ERY at a rate of 10 µl $min^{-1}$, or 3.6 mg $h^{-1}$. This may be too low for an industrial process, but could be relatively easily increased by scaling or numbering up the reactor, or a combination of the two. Given the size of the channel geometry it may even be possible to include several parallel channels on a single chip. This possibility has already been explored by for industrial chemical synthesis of monoammonium phosphate, where 100 microreactors were combined into a single parallel reaction system with a process capacity of 100 kilotonnes per annum (Chen et al., 2011 b). Assuming continuous production, this equates to the production of 114g of monoammonium phosphate per reactor, per hour. This is several orders of magnitude greater than the output both of the SHM reactor shown above and the majority of biocatalytic reactors in current literature. Given the advantages of microfluidic systems for chemical reaction control, it is feasible that such systems could also be applied to biochemical synthesis; however the limitations on reactor output, imposed primarily by enzymatic inhibition at high substrate and product concentrations, would need to be addressed.

## 4.3 Filtration of SHM Reactor Output

The filtration device described in Chapter 3 offers a number of possibilities for the investigation of downstream processing conditions. The purification of the output of the reactor described in the previous section, in order to separate the synthesised ERY from the

crude lysate containing TK, was chosen as a test case for the filtration device, to determine whether it could be used to establish a set of operating conditions for the purification.

One of the advantages of continuous flow synthesis is that it offers the possibility of performing several reaction steps in a single network of reactors, linking the output from one reaction to the input of the next, such as those that have been exploited for chemical synthesis applications (Sahoo et al., 2007). It also makes possible the use of unstable intermediates, which can be synthesised continuously and converted to more stable products before degradation occurs, something that is more difficult to achieve in batch processes (Yoshida et al., 2013). However, if we wish to connect reactor modules in series for a multi-step reaction, it is desirable to have a purification step for the product of the first reactor before it enters the next one, such that the reactors can operate independently of one another at their own optimal conditions. This provides a further potential use for the filtration device.

### 4.3.1 Control of Back Pressure using Capillaries

Control of back pressure on the retentate output of the microfluidic filter was required to regulate the flux of fluid across the filtration membrane and separate the ERY synthesised in the reactor from the TK lysate catalyst. This was achieved by the attachment of capillaries of specific length and diameter to the retentate outlet of the tangential-flow filter (see Figure 37A).

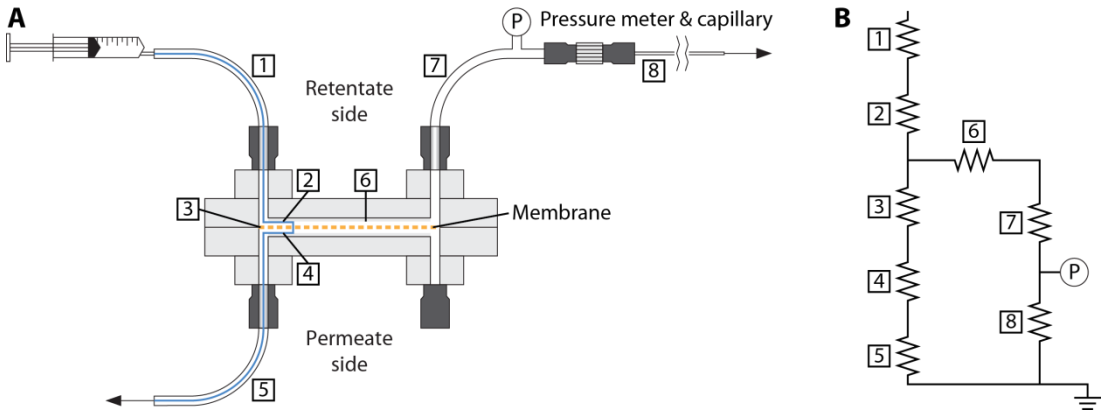


**Figure 37: Schematic of setup of microfluidic tangential flow filter for back pressure measurement (A) and equivalent hydraulic resistive network (B).**

In the schematic illustrated above, the blue line in Figure 37A indicates the hypothetical path of fluid through filtration device. The numbered sections correspond to the following resistances:

[1] the resistance of inlet tubing and port,

[2] the resistance of retentate channel up to point at which fluid crosses membrane,

[3] the resistance of membrane itself,

[4] the resistance of permeate channel from point at which fluid crosses membrane to permeate outlet,

[5] the resistance of permeate outlet port and tubing,

[6] the resistance of the retentate channel from point at which fluid crosses membrane to the retentate outlet,

[7] the resistance of the retentate outlet port and tubing,

[8] the resistance of the capillary used to apply pressure to retentate channel.

In this context, 'back pressure' indicates the resistance to flow created by the capillary at point 8. The resistance at this point and at point 3, where the fluid crosses the membrane, will be the most dominant over flow through the device. As long as the resistance caused by the capillary at point 8 remains higher than that of the membrane at point 3, fluid will cross the membrane into the permeate. However, as filtration progresses, the resistance at point 3 will increase due to the build-up of material on the membrane.

The Hagen-Poiseuille equation was used to identify the length and diameter of capillaries that would be required to generate back pressures in the range of 5 – 30 psi in the retentate channel at the operating flow rate of the SHM reactor. Capillaries with lengths of 30 cm and internal diameters of 50, 75, 100 and 200 μm (Upchurch) were identified as being able to generate the desired range of back pressures. These were connected to the output of the retentate channel and purified water was run through both the retentate and permeate channels at various flow rates. The back pressure on the retentate flow was measured using a pressure transducer (Honeywell, NJ, USA) with a LabVIEW virtual instrument (National Instruments,

TX, USA) that recorded the voltage output from the transducer and converted it into a pressure value (Figure 38A). The virtual instrument code is shown in Appendix A.

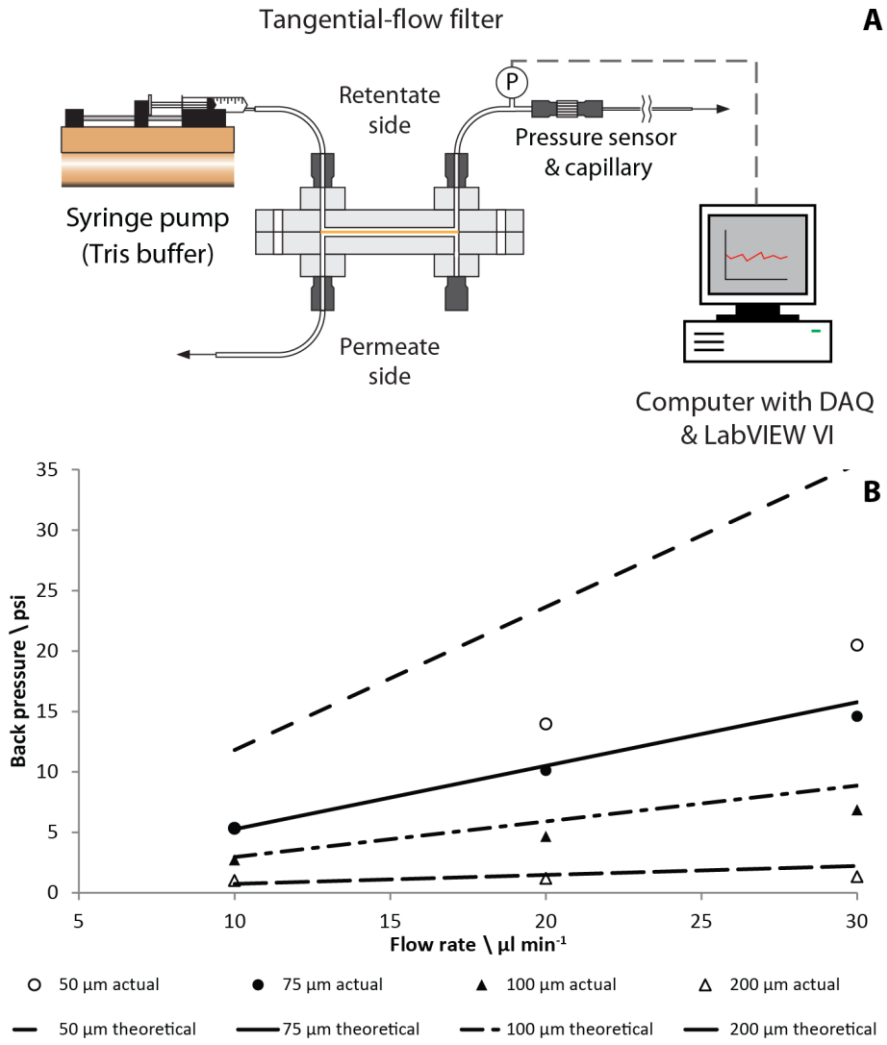


**Figure 38: Control of back pressure in filter with capillaries of fixed diameter.**
**(A) Illustration of setup used to measure back pressure on retentate side of filter; (B) effect of capillary diameter and flow rate on recorded back pressure.**

The flow rates tested were in the range of 10 - 30 µl $min^{-1}$, at the higher end of the range of flow rates used in the SHM reactor. Using the above capillary diameters the pressures generated were in the range of 1 - 15 psi (Figure 38B), lower than those predicted by the Hagen-Poiseuille equation. The calculation did not take account of capillary forces, which may have reduced the pressure drop across the capillaries tested.

The path of least resistance will initially be closest to retenate inlet; however this will only remain so whilst membrane is unfouled. As filtration progresses and that area of membrane

becomes fouled, the path of least resistance will move along membrane to unfouled areas until the entire membrane is fouled and the resistance exceeds that of the capillary. To balance flow across membrane at all points would require an increase in the overall resistance to flow at closest point of membrane to the retentate inlet a reduction at furthest point from the inlet. This could be achieved by modification of permeate side channel to constrict the channel dimensions and increase resistance to flow closest to retentate inlet. A slope could be introduced to the floor of permeate side channel, with the narrowest point nearest the retentate inlet and the widest point near to the retentate outlet, as well as moving the permeate outlet to the opposite end of the channel. This would serve top increases the overall resistance to flow across the membrane at one end and reduce it at the other, evening out the total resistance and therefore the flux across membrane at all points.

Overall, control of back pressure with capillaries was found to be more reproducible than with commercially available micro-metering valves, with the added advantages of being considerably cheaper, and having no moving parts, but at the expense of being able to adjust the back pressure to maintain a constant flux throughout the filtration process.

### 4.3.2 Filtration Experiments with Model Reactor Output

The ability of the tangential flow filter to purify a solution of enzyme and product was investigated using solutions containing ERY and lysate at the same concentrations as the expected output from the reactor. These solutions were flowed through the retentate of the filter under different flow rates and with different diameters of capillary attached to the retentate outlet.

SDS-PAGE studies from a representative selection of flow conditions confirmed that a regenerated cellulose membrane with 10 kDa molecular weight cut-off was sufficient to ensure the full retention of transketolase along with all other protein in the lysate (Figure 39). Similar concentrations of ERY were found in the permeate and retentate solutions (as

measured by HPLC), indicating that the compound was able to permeate the membrane freely, without adsorption or other interactions.

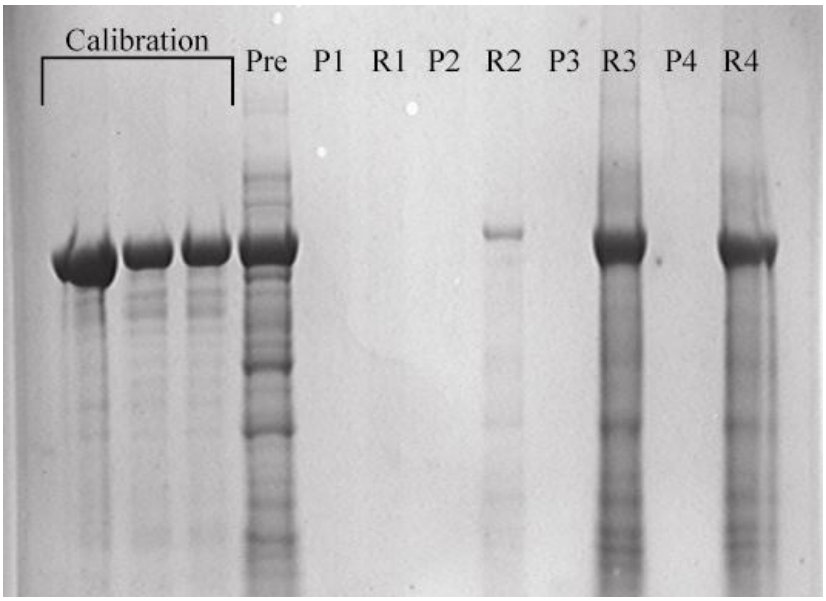


**Figure 39: SDS-PAGE showing protein present in reaction mixture before filtration (Pre), and in the retentate (R) and permeate (P) after filtration**

The ultimate aim of the filtration step was to maximise the fluid flux across the membrane, and therefore the amount of ERY recovered. To investigate this, 30 cm capillaries with internal diameters of 100 μm, 75 μm and 50 μm were connected to the retentate outlet, allowing the evaluation of recovery under different back pressures, and the permeate and retentate volume outputs were measured under various flow conditions (Table 3).

| Flow rate \ μl min$^{-1}$ | | | 10 | 20 | 30 |
|---|---|---|---|---|---|
| Capillary diameter \ μm | 50 | *% Permeate* (Pressure \ psi) | *89* (5.3) | *56* (14) | *67* (20) |
| | 75 | *% Permeate* (Pressure \ psi) | *85* (5.3) | *41* (10) | *36* (15) |
| | 100 | *% Permeate* (Pressure \ psi) | *31* (2.7) | *24* (4.6) | *25* (6.9) |

**Table 3: Comparison of permeate volumetric output as a percentage of the total filter output, and the back pressures generated, under various conditions of capillary diameter and flow rate.**
**Figures in italics represent the amount of fluid recovered in the permeate as a percentage of the output from both outlets. Figures in brackets are the back pressures measured at the retentate outlet for each flow condition (n = 6).**

As expected, the yield was increased as the internal diameter of the capillaries used was decreased. However, increasing the flow rate from 10 to 30 µl $min^{-1}$ tended to decrease the permeate yield for any given capillary, despite the corresponding increase in back pressure. Of the condition sets investigated, the best conditions for maximum product recovery were found to be a capillary diameter of 50 µm and an operating flow rate of 10 µl $min^{-1}$, resulting in a back pressure of 5.3 psi (Table 3), which gave a permeate yield of 89%. This also meant that the tangential flow filter could be connected directly to the output of the SHM reactor, as the flow rate at the outlet of the reactor was 10 µl $min^{-1}$.

With regards to the effect of increasing flow rate on the permeate yield, it is possible that, by further increasing the flow rate and hence the pressure on the retentate, the system was being pushed past the critical flux. Beyond this point the effects of inertial lift caused by the tangential flow would be cancelled out by the increasing concentration polarization of protein and cellular debris towards the membrane (Field et al., 1995). This would lead to more rapid fouling of the membrane and a therefore a reduced fluid flux, despite the increased pressure. However, further investigation of the operational space around the established optimum would be required in order to characterise the change in the rate of flux that would accompany the passing of the critical flux point.

### 4.3.3 Integration of SHM Reactor with Microfluidic Tangential Flow Filter

In order to demonstrate that the two devices could be used for continuous synthesis and purification of ERY, the output of the SHM reactor was connected in series with the filtration unit and run for 10 hours (Figure 40A). Conditions had been optimised for the complete conversion to ERY, with GA and HPA concentrations of 50 mM, 0.34 mg $mL^{-1}$ TK and a residence time of 120 minutes. The conditions were also optimised for the best recovery of ERY from the reactor output, using a 10 µl $min^{-1}$ flow rate and a 50 µm diameter capillary fitted to the retentate outlet to maximise the permeate yield (see Section 4.3.2). A 236 cm

length of tubing was used to connect the two devices in order to extend the residence time of the reaction to 120 minutes while operating at the higher flow rate.

HPLC analysis showed that complete conversion of the GA and HPA to ERY occurred throughout the experiment – there was no loss of activity of the TK over the ten hours that the reactor was running. The yield of ERY recovery was therefore entirely dependent on the partition of fluid between the permeate and retentate. It was found that the permeate output was stable at almost 100% for two hours (once the remaining tris required for the priming of the system had been flushed out), after which it declined sharply, presumably due to build-up of cell debris on surface of membrane, reducing the permeability and therefore the flux (Figure 40B). After 7 hours, the filtration unit was back-washed with purified water in an attempt to remove this material, and the permeate yield was temporarily restored to 70-80%.

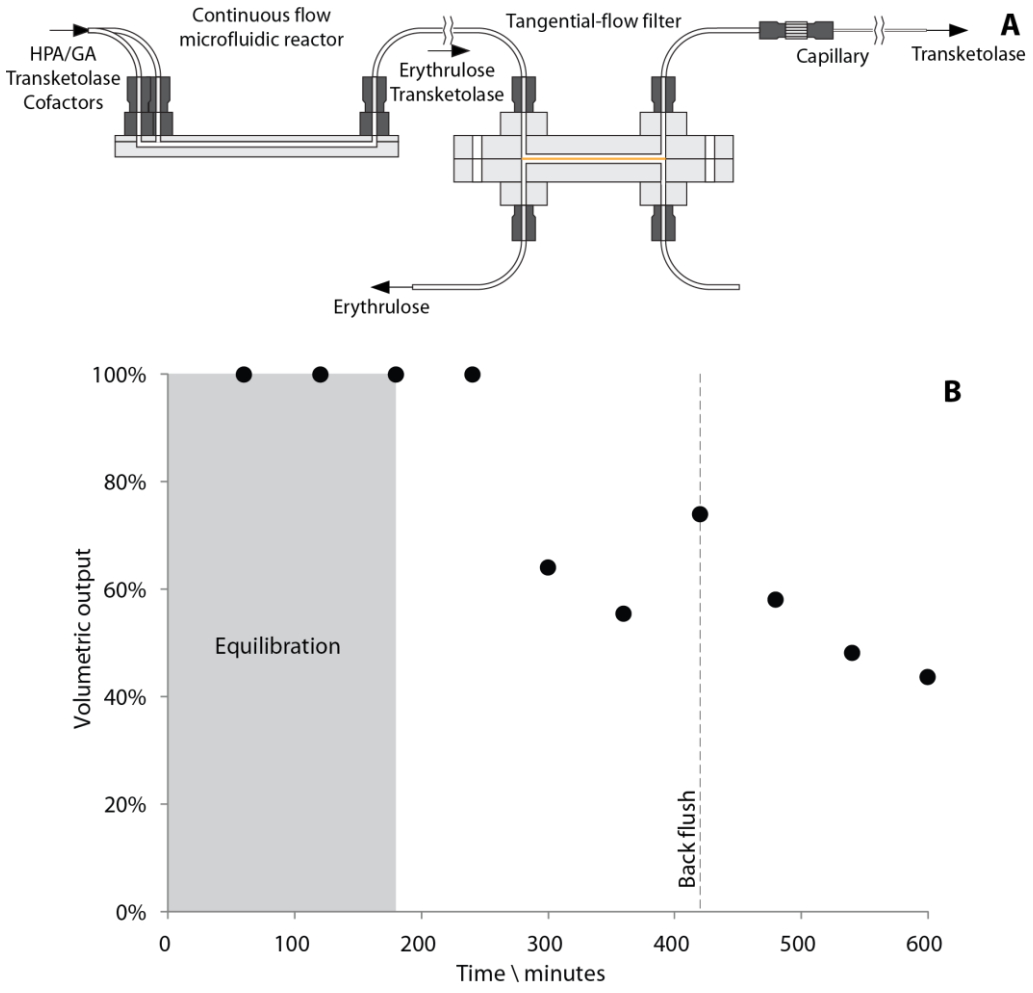


**Figure 40: Showing the setup (A) and results from (B) the continuous flow TK-catalysed reaction with filter separation.**

The long-term performance of the filter could be improved in several ways. Modifying the reaction conditions to reduce the residence time (for example, by increasing TK concentration) would also reduce the amount of time required to prime (and equilibrate) the system, thereby reducing the material lost during this stage of the process. Further investigation of the optimum filtration flow rate and back pressure to reduce the rate of fouling would also allow the filter to operate for longer, though possibly at the cost of the rate of product transmission.

The filter itself could also be modified to improve the surface area available for product transmission, for example by widening the filtration channel and incorporating flow splitter structures to ensure that the fluid is spread evenly over the surface area (Schoenmakers et al., 2010; Vangelooven et al., 2010). Finally, the back-washing process could be incorporated into the system and automated with the help of electronically-actuated valves and pumps to reduce the build-up of cellular debris on the membrane surface.

## 4.4 Summary of Findings

This chapter has demonstrated the use of a modular microfluidic reactor in combination with the developed microfluidic tangential flow filtration unit for the transketolase-catalysed synthesis of ERY and subsequent separation of the biocatalyst from the product. The two devices were initially used separately to identify the optimal conditions for conversion and separation, which were a 120 minute residence time and filtration back pressure of 5.3 psi (achieved with a flow rate of 10 μL $min^{-1}$ and a 50 μm capillary attached to the retentate outlet). Under these conditions, complete conversion of HPA and GA to ERY was achieved in the reactor and a maximum yield of ERY of 89% was achieved in the filtration unit.

The reaction profiles generated in the continuous flow reactor were found to be comparable to those performed in batch 96-well plates, indicating that it could be used for the investigation and development of other continuous flow biocatalytic processes at the microfluidic scale. A commercially-available 10 kDa MWCO was used in the filtration unit

and was able to fully retain the crude lysate used to catalyse the reaction, whilst allowing the product to permeate freely. The successful integration and testing of different filtration conditions with this membrane suggests that the unit could be used in the scale-down testing other membranes as part of the evaluation of other bioprocesses.

The two devices were integrated for the continuous synthesis and purification of ERY over a ten-hour period, achieving complete conversion of GA and HPA to ERY and full retention of the crude lysate biocatalyst throughout the operation. An average product yield of approximately 63% was achieved from the permeate outlet over this period, with a maximal yield of 100% for the first hour after equilibration.

The successful integration of an initial downstream separation step into continuous flow synthesis at the microfluidic scale could also provide opportunities for the cascading of additional purification or reaction steps to generate more complex, high-value products. In the latter case, the ability to generate a pure stream of product from one reactor is particularly important to prevent any undesirable side reactions and to allow each reaction step to operate at with its own ideal condition set (Wohlgemuth, 2009). The additional devices could also include online analysis tools, to facilitate more rapid feedback on changes to operating conditions and therefore accelerate the optimisation of bioprocesses (DeMello, 2006; Whitesides, 2006), the ultimate aim being a system of devices that can be brought together for the rapid development of whole biocatalysed processes at the micro scale.

# 5

# Microfluidic Multi-Input Reactor for Biocatalytic Synthesis

This chapter shows the development of a microfluidic multi-input reactor (MIR), designed to mimic fed-batch processes in a continuous flow reactor, in order to improve yields from a substrate inhibited biocatalytic reaction. The reaction chosen to as a test case for the work was the synthesis of L-erythrulose (ERY) from hydroxypyruvate (HPA) and glycolaldehyde (GA), using *E. coli* cell lysates containing a transketolase (TK) enzyme.

The data in this chapter has been published in part in "*Microfluidic multi-input reactor for biocatalytic synthesis using transketolase*", by Lawrence *et al.* (Lawrence et al., 2013).

## 5.1 Introduction

Chemical synthesis using biocatalysts in microreactors has a number of advantages, as discussed in Section 1.2 and Chapter 4. However, unlike their chemical counterparts, microreactors using biocatalysts have for the most part been used to produce only very low concentrations of product, in the range of nM – mM. Whilst this may be suitable for the investigation of reaction kinetics, it would be advantageous to be able to produce higher concentrations of product for the purposes of chemical synthesis.

In a typical microreactor consisting of a microchannel with two (or more) inputs at one end of the channel, the substrate concentration is defined at a single point (the input) and cannot be supplemented further. In such reactor designs, a higher concentration of product is obtained by increasing the concentration of substrate at the input. This poses a fundamental challenge for flow-based biocatalytic synthesis, as the effects of increased substrate concentrations, such as substrate inhibition and enzyme denaturation, set limits on the amount of substrate that can be added at a single point and therefore the concentration of product that can be synthesised.

Fed-batch reactors are a well-established solution to this problem, having been used to gradually feed substrate in order to maintain reaction rate and achieve a higher yield of product without exposing the biocatalyst to concentrations that are inhibitive. Miniaturised versions of fed-batch reactors have been demonstrated for this purpose (Weuster-Botz et al., 2005; Funke et al., 2010) though there has been no example of a similar principle operated in continuous-flow mode.

Microreactor systems that allow the injection of substrates at multiple points have been demonstrated for the purpose of controlling chemical reactions. These systems were designed for the continuous synthesis of allylcarbinol and of organometallic compounds, using multi-point feeding to control the formation of impurities and the generation of heat respectively

(Barthe et al., 2008; Roberge et al., 2008 a; Cervera-Padrell et al., 2012). However, such systems have not been applied to the problem of substrate inhibition in biocatalytic reactions.

Continuous-flow microreactors, designed to allow the recycling of unconverted substrates, have previously been demonstrated for biocatalytic synthesis (Alam et al., 2011; Tudorache et al., 2011). It is possible to use these reactors to gradually feed substrate and avoid inhibitory effects; however the continuous injection of substrate into the recycling loop at a single point means that complete conversion to pure product is fundamentally difficult to achieve. These reactors also use *in situ* removal to recover the product, requiring that the biocatalyst is either immobilised or removed by an in-line separation system, with the latter option necessitating a more complex reactor design.

In the case of the TK-catalysed synthesis of ERY, an increase in reaction rate and yield with increased HPA and GA input has been observed up to concentrations of 300 mM GA; however it has previously been shown that GA concentrations of 500 mM GA cause a significant reduction in the activity half-life of TK, to 200 minutes as compared with 400 minutes for a concentration of 250 mM (Chen et al., 2007 a). In addition, from observations when performing microfluidic reactions with GA concentrations of 500 mM, visual inspection of the reactor has shown that denaturation occurs at the boundary layer where the enzyme and substrate meet, causing a build-up of solid material and clogging the reactor channel. This is in spite of the use of relatively large channel geometries (w x h, 500 x 250 µm). This severely impaired the functionality of the reactor, halting the flow before it had time to equilibrate.

This chapter explores whether feeding strategies such as those used in fed-batch processes could be mimicked in the design of a continuous-flow microfluidic reactor. The concept is illustrated in Figure 41. A prospective microfluidic reactor for this purpose would need a primary input (or inputs) for the reaction mixture containing the enzyme and non-inhibiting substrate, plus small amount of inhibiting substrate to start reaction (at $t = 0$ in Figure 41). In equivalent fed-batch system the non-inhibiting substrate and enzyme would be present in the

reactor already, and a small amount of inhibiting substrate would be added through a separate input to initiate the reaction. As the reaction proceeded, the amount of inhibiting substrate present would decrease as it was consumed (*t = 1, 2*), until it needed to be replenished to maintain the reaction rate at a reasonable level. In a fed-batch system this would involve dosing more of the substrate into the reactor through the same input, but in the microfluidic reactor this would require an entirely separate 'auxiliary' input, connected to the main channel, to feed a continuous supply of the substrate into the reaction mixture at the desired residence time (*t = 3*). By including multiple auxiliary inputs in the microfluidic reactor it should be possible to perform further gradual addition of inhibiting substrate to the reaction mixture over time, sustaining the reaction without allowing the concentration to reach a detrimental level, in the same way as a fed-batch process (*t = 4, 5, 6*).

This chapter will show the development of the concept described into a microfluidic multi-input reactor and its application to the transketolase-catalysed reaction described in chapter 4, in an attempt to overcome the limitations of substrate inhibition at high substrate concentrations and intensify the production of ERY at the microfluidic scale.

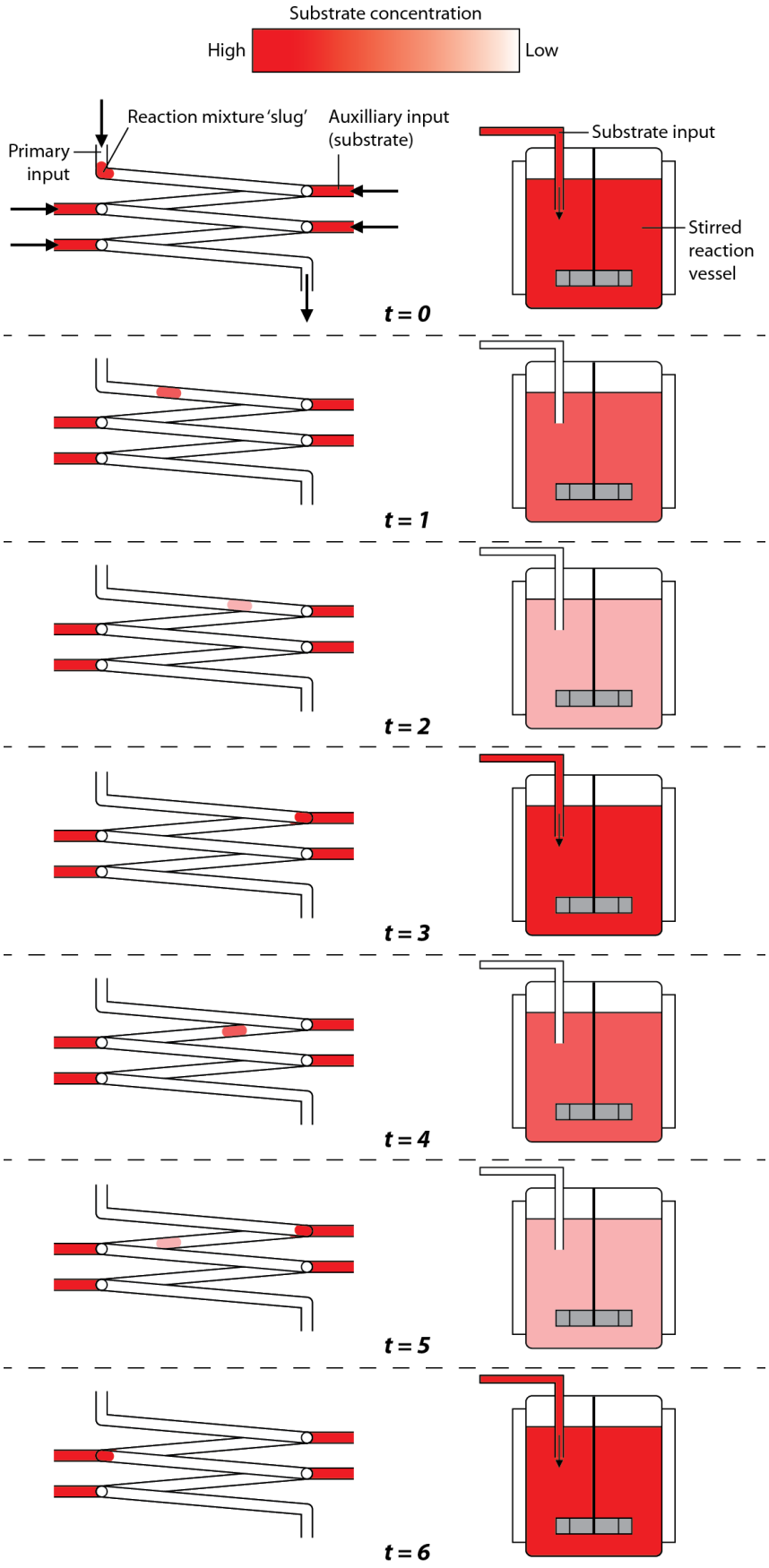


**Figure 41: Illustration of the conceptual design of a continuous-flow microreactor (left) to mimic a fed-batch process (right).**

## 5.2 Reactor Design and Characterisation

### 5.2.1 Reactor Design

The motivation behind the design of the multi-input reactor was the desire for a device that could be easily reconfigured to suit different feeding strategies for biocatalytic reactions requiring multiple substrate inputs to avoid inhibitory effects. The design therefore needed to provide a large enough channel volume that long residence times could be tested, multiple ports that could be sealed off when not required, as well as a cross-sectional area that was suitable to avoid clogging by dissolved cell lysate. The design also needed to be able to operate leak-free over long periods of time, and ideally could be fabricated quickly.

The chosen reactor design was a single channel with a Y-junction at the top and multiple side-feeding ports along its length, such that substrate could be fed into the reaction mixture at several points as it progressed down the channel. The design consisted of one main channel with a total volume of 1650 µL, fabricated in PMMA, with two primary inputs at the front end of the channel where the biocatalyst and substrate could be combined to start the reaction (Figure 42A). Ten further auxiliary inputs were spaced evenly along the channel, for the feeding of additional substrate, along with a priming port that was located 3 cm from the Y-junction. The inputs and priming port were designed for standard M6 fittings, facilitating the easy reconfiguration of the reactor as well as the potential to integrate it into the devices shown in Chapters 3 and 4.

To allow the substrate inputs to be reconfigured for the testing of different reaction conditions, PDMS plugs were also designed that could be inserted into the ends of standard interconnect plugs, allowing any unused inputs to be reliably and reversibly sealed by screwing the plugs into place. In this way the reactor could easily be configured to test a range of different feeding strategies, sealing off certain inputs where required.

The reactor was designed with a relatively large total volume to allow the use of long residence times, such that conversion of large amounts of substrate would be possible. At the

same time, to allow it to be fabricated quickly on the available laser ablation system and make it more widely usable with other laser cutting systems, the maximum outer dimensions of the reactor were constrained at 85 x 85 mm. The reactor was therefore divided over three layers of PMMA, with the main reaction channel and inlets being divided over the base and middle layers and the top layer serving to seal the reactor and provide fluidic connections. The main channel was comprised of 55 individual sections, each 60 mm long with a cross section of 1 x 0.5 mm. These sections were arranged in an alternating 'zig-zag' from one side of the reactor to the other, reducing the overall footprint of the reactor to 85 x 84 mm. A priming port was added to the first section of channel, 20 mm downstream from the Y-junction, which had the same standard fitting as the other ports and could be sealed with the use of a PDMS plug described above.

The sections of channel in middle layer (labelled in yellow in Figure 42) were aligned 1° degree from the horizontal and channels on the base layer (labelled in red) were aligned 179° degrees from the horizontal. These angles were chosen such that the spacing between alternating ends of the channel sections were 2 mm, leaving a 1 mm radius of intact PMMA around each section to form a seal with the layer above it during bonding. Through-holes were ablated into either end of the channels in the middle layer such that, when the layers were bonded together, they aligned to join individual channels on the different layers into a single continuous channel. The alignment of the three layers for bonding was therefore very important, and was ensured by placing steel dowel pins into 1.6 mm though-holes fabricated into each layer (Figure 42B).

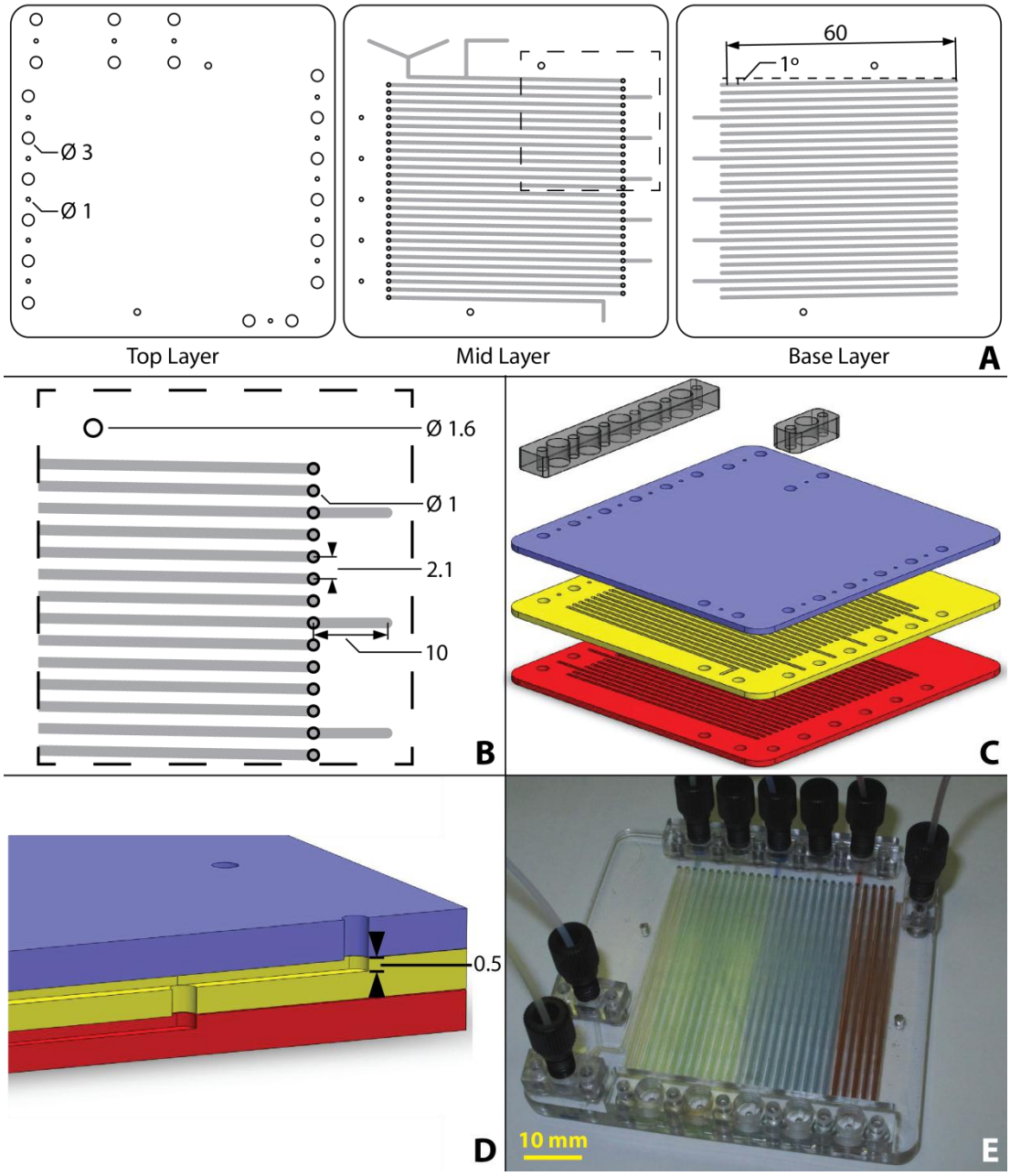


**Figure 42: Design of multi-input reactor.**

(A**) Design of individual layers showing size of large features (grey areas indicate ablated channels, black lines indicate cuts through the substrate); (B) zoomed view of mid layer showing distance between channels; (C) exploded view of layers of reactor; (D) zoomed view of intersection between main channel and auxiliary input; (E) photograph of assembled reactor with multiple dye colours. All units in mm.**

For simplicity of design, the fluidic connections for the auxiliary input ports were joined to the main channel laterally, with the two streams coming into contact at the point that the fluid ascends or descends between the layers of the reactor (Figure 42D). The interconnects were offset from the main channel by 7 mm to allow the physical connection of the interconnect blocks whilst minimising the dead volume to be cleared when equilibrating the

reactor, as well as the overall footprint. The offset also means that the structure of the main channel could be changed, for example to adjust the residence volume between individual ports, without the need to modify the port layout.

Laser ablation was chosen to fabricate because of the rapidity with which it can be used to create features in PMMA. Using the laser, it was possible to fabricate the features of the middle layer in less than 6 minutes and to complete all three layers of the reactor in around 15 minutes. Given the number of channels and other features involved, fabricating the same design using a micro milling machine, another commonly used tool for rapid fabrication, would have taken a few days. Profilometry of the surface of the channel showed the mean roughness $R_Z$ to be 6.8µm, a similar value to that shown in previously-published work describing the roughness of channels fabricated in PMMA by laser ablation (Klank et al., 2002).

The rapidity of fabrication combined with the low cost of PMMA made the reactors quite inexpensive to produce, meaning that it could easily be disposed of and replaced at the end of their useful life. Furthermore, the increasing availability of laser ablation technology and, in particular, the range of sizes of systems, means that the reactor could be reproduced easily and could be scaled up by simple modifications to the design and by use of a larger laser ablation system. This would then allow bench-top or even pilot scale production using fed-batch methodology in continuous-flow mode, which is of interest to the chemical and biochemical industries due to the opportunities for process intensification and the use of valuable but unstable intermediates (Roberge et al., 2008 b; Yoshida et al., 2013).

### 5.2.2 Distribution of Substrate from Auxiliary Inputs

Confocal imaging was used to analyse the rate of diffusion of substrate fed at the auxiliary inputs into the main reaction mixture. A microfluidic chip was designed specifically for this purpose, mimicking the structure of a single auxiliary input and channel section in the MIR, with some modification to accommodate confocal imaging (Section 2.5.2, Figure 9). The chip

was fabricated primarily in PMMA except for the top plate which was an adhesive-free microwell plate sealing film, used to facilitate the transmission of light from the interior of the channel. Fluorescein was used as an analogue for GA to allow the dispersion to be imaged.

The flow regime within the main reactor channel was determined to be laminar, with a Reynolds number of $2.2 \times 10^{-4}$ at a flow rate of 10 µl $min^{-1}$ (calculated using the viscosity and density of water). This was confirmed experimentally by confocal imaging using the setup described above, determining the diffusion of fluorescein into water downstream of a junction between an auxiliary input and the main channel, where the dye fed though the auxiliary was shown to form a lamina over the bulk fluid in the channel (see Figure 43).

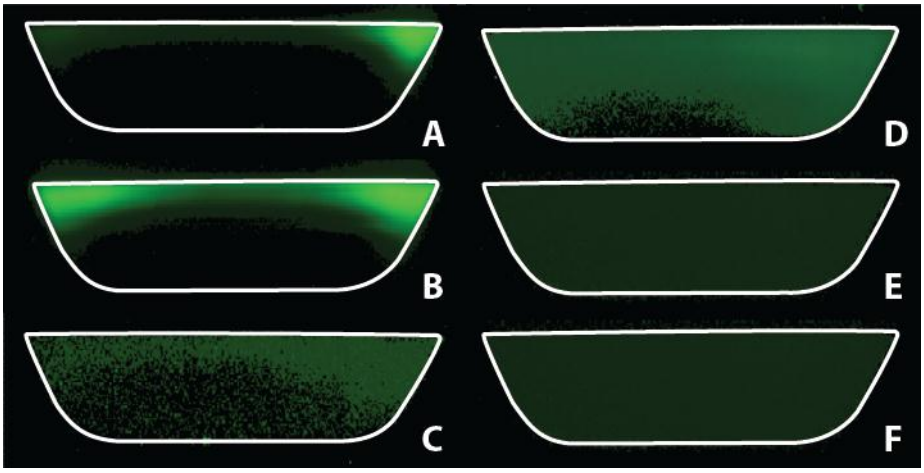


**Figure 43: Cross-sectional images of diffusion in MIR channels taken with confocal microscopy. Images of diffusion of fluorescein dye in channels taken at a range of residence times: (A) 1.4; (B) 2.8; (C) 14.8; (D) 29.6; (E) 45.0 and (F) 60.0 seconds.**

The confocal images show that the solution fed into the auxiliary input was initially deflected to the outer edges of the main channel by the faster-flowing fluid from the primary inputs (Figure 43A and B). However, despite the laminar regime and the absence of mixing structures, the dye in the auxiliary solution began to diffuse into the bulk fluid quite rapidly, and the two solutions appeared to be homogenous within 45 seconds of being combined at the channel join (Figure 43C to F). This is in agreement with the calculation of the diffusional length of the tracer in the channel, which predicts that it will have propagated 0.39 mm across

the channel depth in one minute, where the diffusion coefficient of fluorescein in water is 0.64 $\times 10^{-9}$ $m^2$ $s^{-1}$ (Galambos and Forster, 1998).

The maximum flow rate used in any of the synthesis experiments performed with the MIR (see Table 5, Section 5.3) is 14.4 µl $min^{-1}$, which is the combined flow rate of the primary and auxiliary inputs used for the conversion of 200 mM HPA. Even at this flow rate, 45 seconds corresponds to less than half of the residence time of a single section of the main reactor channel. Given that the molecular weight of fluorescein is five times as large as that of GA (332 g $mol^{-1}$ and 60.1 g $mol^{-1}$ respectively), it is expected that the GA fed will be well-distributed into the reaction mixture within a similar amount of time.

The distribution of substrate from the auxiliary inputs across the main channel could be improved by the inclusion of herringbone or similar structures on the channel floor, as in the microreactor shown in Chapter 4. Laser ablation would not be a suitable fabrication method in this case as the size of the herringbone structures would be below minimum achievable feature size; however hot embossing could be used instead. A positive of the existing channel structure with additional grooves in the base of the channels near the auxiliary inputs could be micromilled and used to create the channel structures in PMMA. Although the machining of the positives for each layer would be quite time-consuming, once they had been produced the time required to fabricate each device would probably not be much different to that of the existing laser ablation process. Herringbone grooves could also be embossed on to the undersides of the layers above each channel, creating a parallel set of herringbone grooves adjacent to each auxiliary input. This would create more lamination between the two fluids and reduce the time required to distribute the substrate across the channel even further.

### 5.2.3 Flow of Substrate at Auxiliary Inputs

To minimise the dilution of the product, the setup for the synthesis of ERY required that GA be fed into the reactor at high concentration but at a much lower flow rate compared to that of the reaction mixture. The feeding of substrate along the auxiliary channel itself was

therefore also evaluated with confocal microscopy in order to ensure there was no backflow of reaction mixture or GA out of the auxiliary ports. In this case the fluorescein solution was flowed through the primary input and water was flowed into the auxiliary input of the chip described in the previous section. The join between the channels was imaged across both layers while fluorescein solution and water were flowed into the chip in a 20:1 ratio, at 3.3 µl $min^{-1}$ and 0.17 µl $min^{-1}$ respectively. A control image was taken with static fluorescein solution in the main channel and the auxiliary input.

The control images (Figure 44A and C) clearly show the structure of the channel join. A column of fluid is visible on the right side of the images which links the channels on the top and base layers. The auxiliary input channel is shown on the left side of the images. Under flow conditions (Figure 44B and D), no fluorescein is visible in the input channel, indicating that there was no backflow from the main channel. Given that the images were taken whilst operating at around half of the minimum flow rate used in the synthesis experiments, it can be assumed that there was no backflow through the auxiliary input channels during synthesis either.

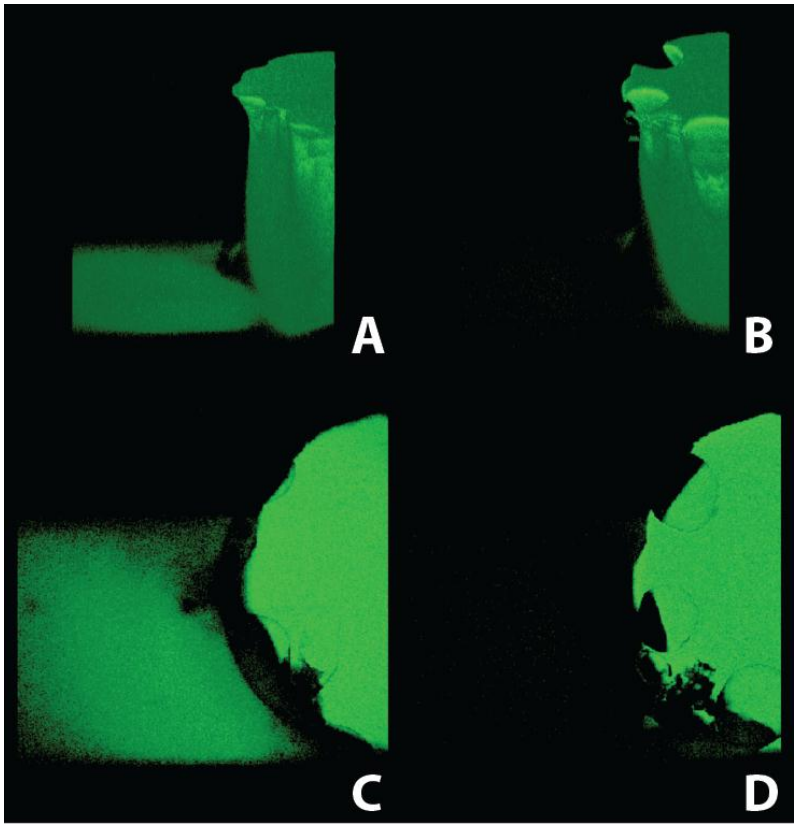


**Figure 44: Confocal imaging of input channel and join.**

**Images captured to show absence of backflow from main to input channel. (A) and (B) show view of composites at 45° from normal, (C) and (D) show view from top. (A) and (C) show control images of static fluorescein, (B) and (D) show images taken while flowing fluorescein dye and water at rates of 3.3 µl $min^{-1}$ and 0.17 µl $min^{-1}$ respectively.**

## 5.3 Determining of Substrate Feeding Schedules Using Activity Models

Michaelis-Menten kinetics were used to estimate when GA would need to be fed into the reaction mixture in order to complete the conversion of HPA to ERY without exposing TK to GA concentrations higher than 50 mM. A previously-published equation describing the kinetics of the TK-catalysed condensation of HPA and GA was used, along with reported kinetic and inhibitory constants (Gyamerah et al., 1997). The kinetic parameters are shown in Table 4.

$$V = \frac{k_{cat} E_i [A][B]}{K_B[A]\left(1 + \frac{[A]}{K_{iA}}\right) + K_A[B]\left(1 + \frac{[B]}{K_{iB}}\right) + [A][B] + \left(\frac{K_A}{K_{iP}}\right)[B][Q] + \left(\frac{K_A K_{iB}}{K_{iP}}\right)[Q]} \quad (13)$$

| Kinetic parameter | Value |
|---|---|
| Rate constant: $k_{cat}$ | 5076 $min^{-1}$ |
| Michaelis constant for HPA: $K_A$ | 13.2 mM |
| Michaelis constant for GA: $K_B$ | 16.1 mM |
| Inhibition constant for HPA: $K_{iA}$ | 42.2 mM |
| Inhibition constant for GA: $K_{iB}$ | 597.6 mM |
| Inhibition constant for ERY: $K_{iP}$ | 565.8 mM |

**Table 4: Table of kinetic parameters determined by Gyamerah and Willetts (1997).**

The equation was used in an Excel spreadsheet model to make an estimation of the reaction's progress over time in order to estimate where GA feeding points would be required (see Appendix A for the full spreadsheet). The model effectively treated the reactor was as a series of discrete sections of constant volume, and the reaction rate and substrate and product concentrations were calculated for each section in sequence. In the first section the reaction rate was calculated using the initial concentrations of TK, HPA and GA; this was assumed to remain constant over the length of the section. The consumption of HPA and GA and the production of ERY were then calculated, and this data was used as the input to determine the reaction rate for the next section.

The feeding concentration of GA (i.e. the concentration in the reaction mixture after the GA input was dispersed) was set at 50 mM. To minimise the dilution of the product in reactions where numerous GA inputs would be required, whilst keeping the flow rate above the minimum that a syringe drive could reliably deliver, the GA input flow rate was limited to 5% of the primary flow rate. From this, the dilution of the other chemical species in the reaction mixture upon the addition of a further GA input could be calculated.

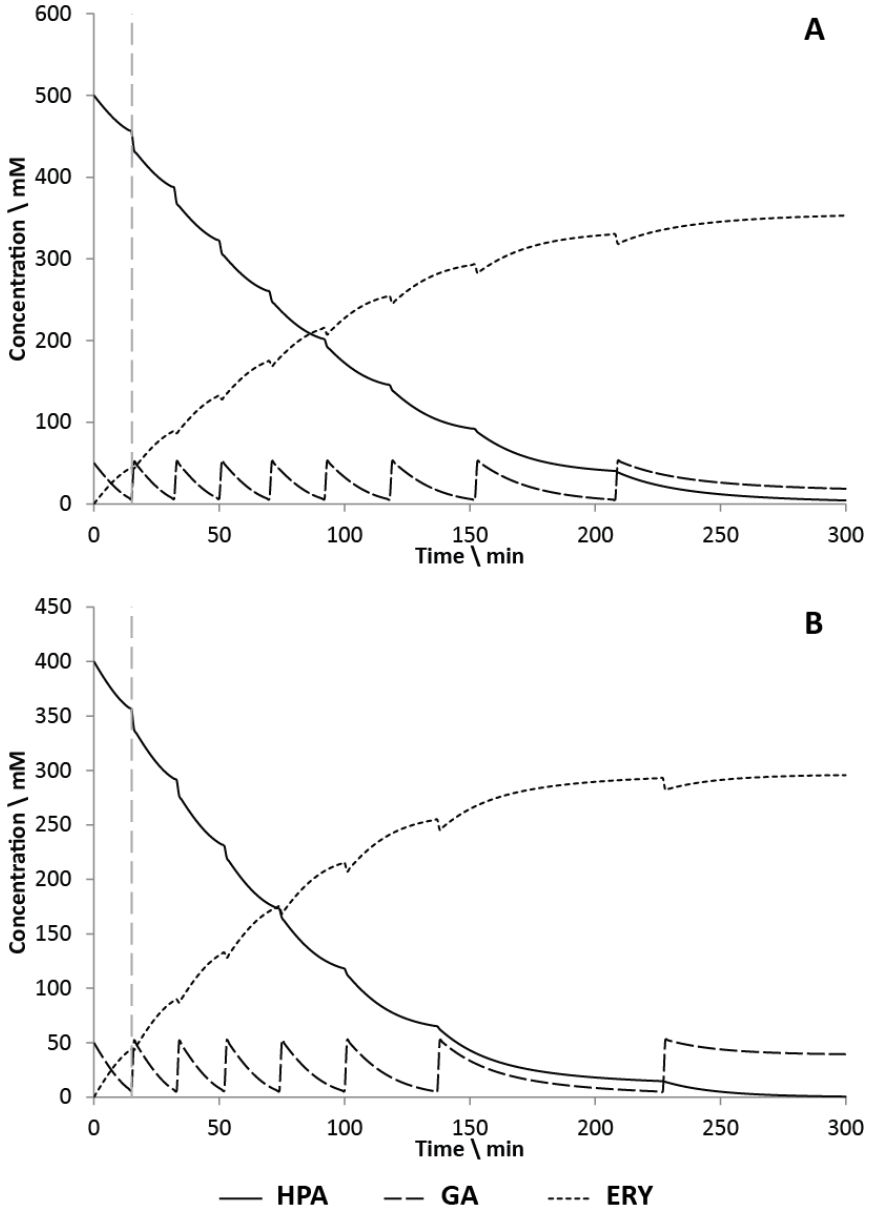


**Figure 45: Calculated concentration profiles of HPA, GA and ERY over course of reaction in MIR for input concentrations of 500 mM HPA (A) and 400 mM HPA (B).**
**The grey dotted line indicates a point at which GA feeding is simulated.**

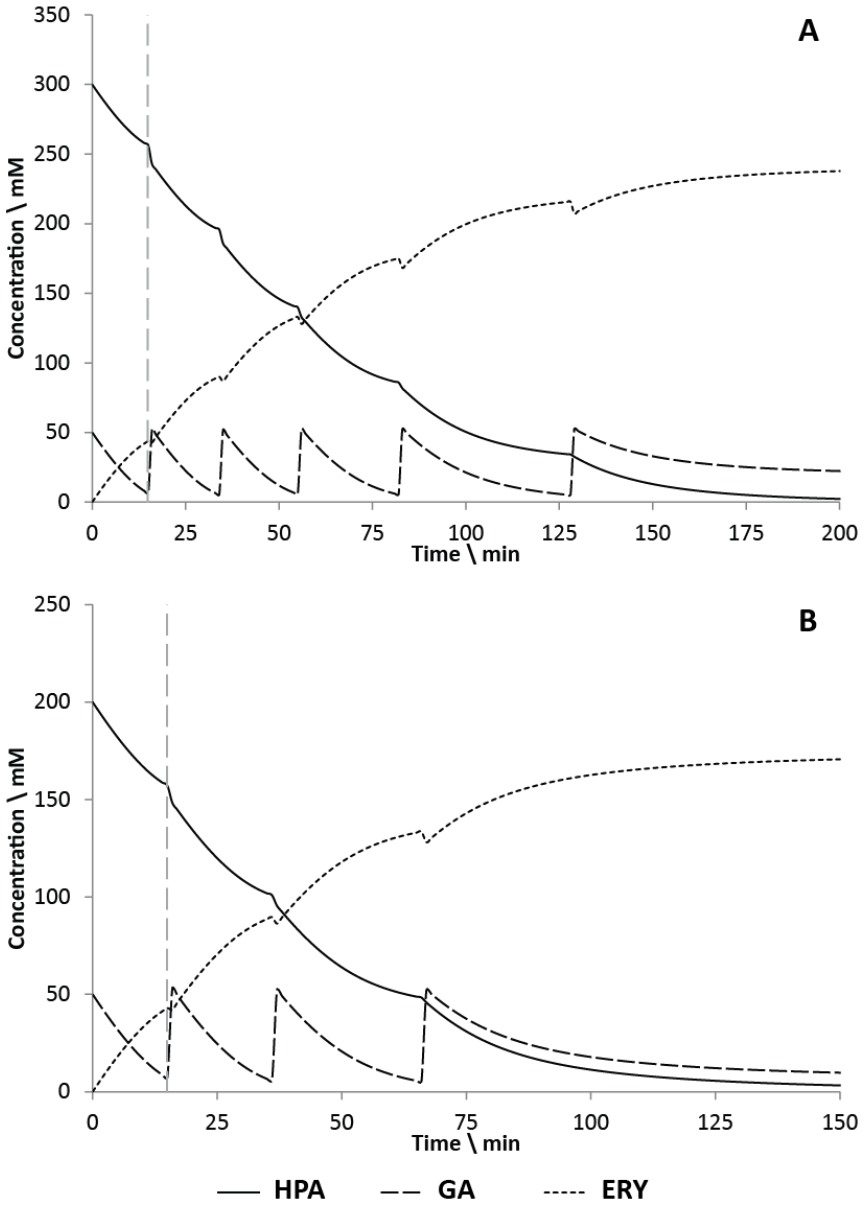


**Figure 46: Calculated concentration profiles of HPA, GA and ERY over course of reaction in MIR for input concentrations of 300 mM HPA (A) and 200 mM HPA (B).**
**The grey dotted line indicates a point at which GA feeding is simulated.**

The lower limit of GA concentration in the reaction mixture was set at 5 mM. If the model calculated that the GA concentration would drop below this threshold in a particular section, the addition of a further GA input would be simulated instead. The GA concentration would therefore be increased by 50 mM, while all other components in the reaction mixture would be diluted by 5%. For the purposes of calculating the reaction rate over the section in which the GA was fed, and subsequent sections, it was assumed that the GA and reaction mixture

streams would combine instantaneously, so there would be no diffusion limitation of the reaction rate.

By simulating the feeding of GA every time the concentration dropped below the 5 mM limit, it was possible to estimate the number and timing of GA inputs that would be required to achieve complete conversion to ERY. The conversion of 200, 300, 400 and 500 mM input HPA was evaluated using this model. The reaction profiles generated by the model are shown in Figure 45 and Figure 46.

From the estimated reaction profile generated for each input concentration of HPA tested, a mean residence time (of the reaction mixture) was established based upon the estimated time required to achieve a minimum of 97.5% theoretical conversion to ERY. A mean flow rate was then established to allow the calculated GA feeding time points to be assigned to physical input positions on the reactor, chosen to be closest to the required points estimated by the model. Finally, the actual flow rates were calculated using the overall residence time, the number of GA inputs required and the ratio of the primary flow rate to auxiliary flow rates (1:20). This was calculated using the following formula:

$$t = \sum_{i=0}^{i=n} \frac{V_i}{u_i} \tag{14}$$

$$t = \sum_{i=0}^{i=n} \frac{V_i}{u_{primary}(1 + 0.05i)} \tag{15}$$

$$\frac{1}{t} = u_{primary} \sum_{i=0}^{i=n} \frac{(1 + 0.05i)}{V_i} \tag{16}$$

$$\therefore u_{primary} = \frac{1}{t \times \sum_{i=0}^{i=n} \frac{V_i}{(1 + 0.05i)}} \tag{17}$$

Where $u_{primary}$ is the primary flow rate, $t$ is the total residence time, $i$ denotes sections of the MIR for which the flow rate is constant (starting at $i = 0$ where the flow is determined by

the primary rate only), and $V_i$ is the volume of a section $i$ for which the flow rate is constant at $u_i$.

The feeding strategies generated from the estimation of the reaction's progress at various input HPA concentrations, including the GA input positions and flow rates, is shown in Table 5.

| | | HPA input concentration (mM) | | | |
|---|---|---|---|---|---|
| | | 200 | 300 | 400 | 500 |
| **Residence time (mins)** | | 120 | 165 | 264 | 286 |
| **Position** | Primary 1 | TK/HPA | TK/HPA | TK/HPA | TK/HPA |
| | Primary 2 | GA | GA | GA | GA |
| | Aux 1 | GA | GA | GA | GA |
| | Aux 2 | - | - | GA | GA |
| | Aux 3 | - | - | GA | GA |
| | Aux 4 | GA | GA | GA | GA |
| | Aux 5 | - | GA | GA | GA |
| | Aux 6 | GA | - | GA | GA |
| | Aux 7 | - | - | - | GA |
| | Aux 8 | - | GA | - | GA |
| | Aux 9 | - | - | GA | - |
| | Aux 10 | - | - | - | - |
| **Total GA inputs** | | 4 | 6 | 8 | 9 |
| **Flow rate (µl min$^{-1}$)** | Primary 1 | 11.90 | 8.24 | 4.94 | 4.49 |
| | Primary 2 & Aux | 0.63 | 0.43 | 0.26 | 0.24 |

**Table 5: Input configuration and flow rates used in the feeding strategies developed for each input HPA concentration.**

The estimated end-point concentrations calculated for different input HPA concentrations using the model are shown in Table 6.

| **HPA input concentration (mM)** | | **200** | **300** | **400** | **500** |
|---|---|---|---|---|---|
| Residence time (mins) | | 120 | 165 | 264 | 286 |
| Estimated end-point concentrations (mM) | HPA | 4.5 | 3.7 | 0.7 | 3.9 |
| | ERY | 173 | 240 | 296 | 353 |

**Table 6: End-point concentrations estimated by the reactor model.**

## 5.4 Continuous Multi-Input Synthesis of ERY

### 5.4.1 Effect of Tris on Transketolase Activity

The evolution of $CO_2$ posed a potential problem in the synthesis of ERY in the MIR as the reaction was taking place in a sealed channel. In previous experiments (see Chapter 4) the target concentration of ERY, and therefore the concentration of $CO_2$ evolved, was 50 mM, not high enough for any adverse effects. However, the maximum target concentration of ERY in the proposed feeding strategy was over seven times this amount. It was thought that the concomitant evolution of a higher concentration of $CO_2$ could lower the pH of the reaction to a level outside of the operating pH range of the wild type TK enzyme used, pH 6.0 – 8.0, limiting the yield of the reaction where higher input HPA concentrations were used (Torres, 2008).

50 mM Tris buffer has been used in the ERY synthesis experiments performed so far. The concentration could have been increased to compensate for the evolution of additional $CO_2$, but Tris buffer has also been shown to have an inhibitory effect on TK. Multi-variate experiments were therefore performed to attempt to establish whether the TK concentration could be increased from 50 mM without having a detrimental effect on TK activity.

The conversion of 100 mM of HPA and GA was evaluated over the course of 120 minutes at Tris concentrations of 81, 143, 205, 267 and 329 mM (see Figure 47 and Figure 48). The results indicated a sharp decline in the amount of ERY produced in 120 minutes, from near-complete conversion at 81 mM Tris concentrations to yields of around 50% at Tris concentrations of 267 mM. The drop in yield appeared to plateau at this point. The consumption of HPA reflected a similar trend.

The longer-term effects of Tris concentration on storage of the enzyme were also evaluated. In each synthesis experiment, the crude lysate containing TK was taken from a frozen stock, pre-prepared from *E. coli* cells lysed in batches and stored in aliquots at -20°C

until required. These lysates were prepared and stored in 50 mM Tris, and it was these same lysates that were used in the range-finding experiments described above.

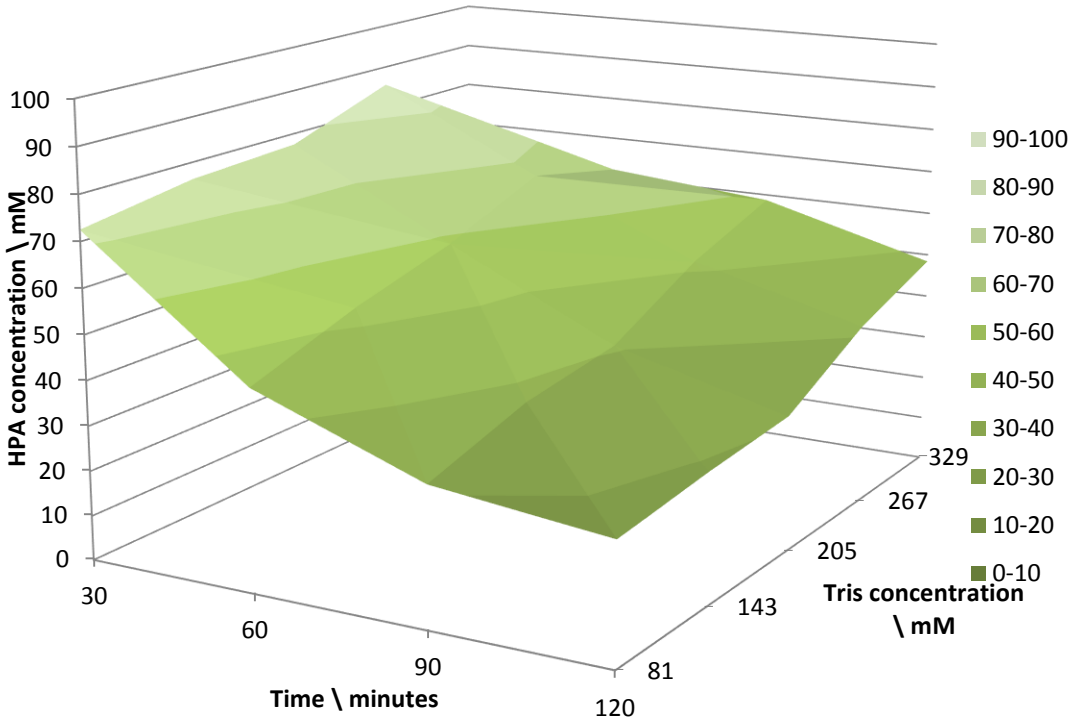


**Figure 47: Effect of Tris concentration on rate of HPA consumption.**

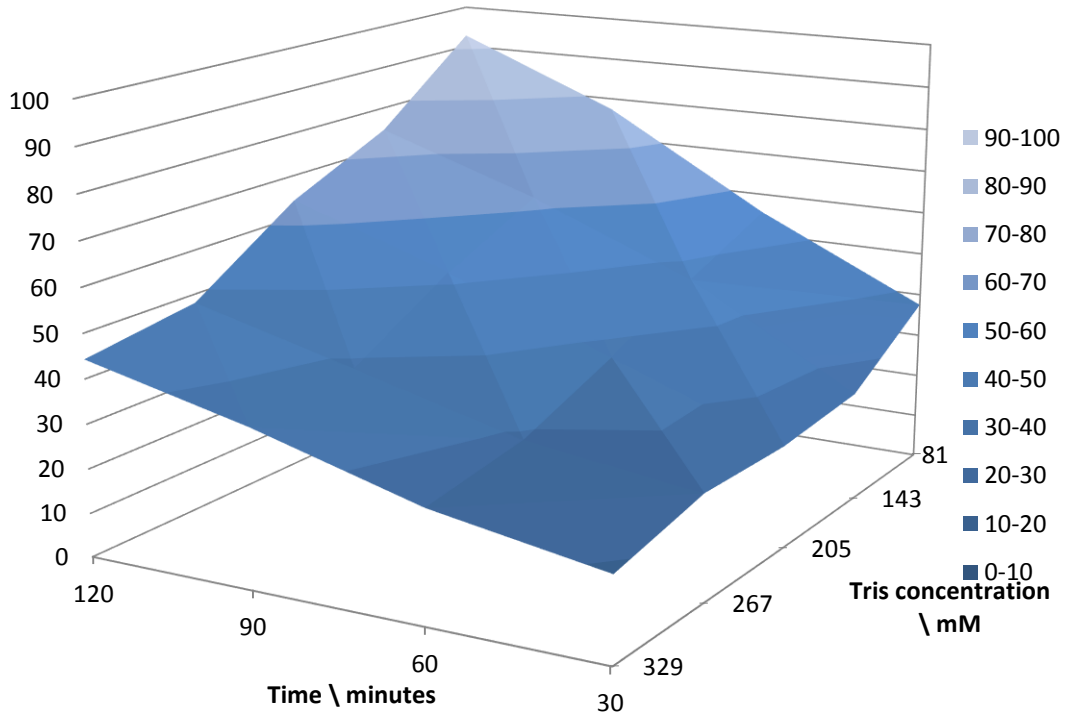


**Figure 48: Effect of Tris concentration on rate of ERY production.**

However, it was found that preparing the lysates in higher concentrations of Tris buffer could have a detrimental effect on the activity of TK (see Figure 49). The activity of two batches of TK lysate, prepared from the same harvest of cells from the same fermentation but lysed in 50 mM and 200 mM of Tris respectively. It was found that the TK lysed in 200 mM Tris was almost completely inactive, with a minimal amount of ERY being produced from 100 mM HPA and GA. By comparison, lysate prepared in 50 mM Tris had a normal level of activity compared to that previously shown. It was therefore decided that the concentration of Tris used to buffer the synthesis reactions should not be changed.

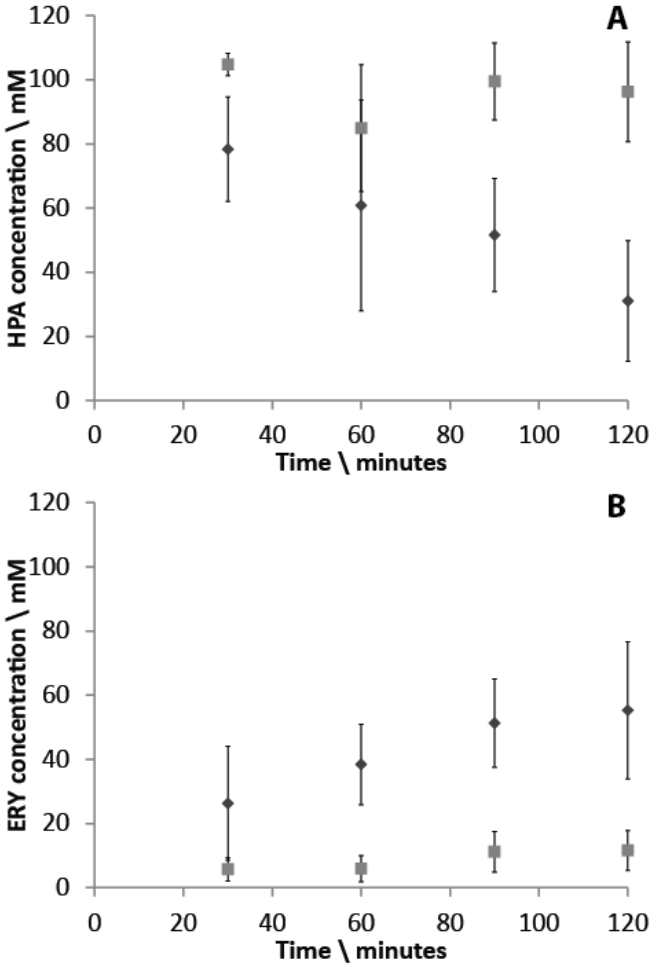


**Figure 49: Effect of Tris storage concentration reaction kinetics (n = 3).**
**(A) Rate of HPA consumption; (B) rate of ERY production. ♦ = 50 mM Tris, ■ = 200 mM Tris.**

## 5.4.2 Performance of the Multi-Input Reactor

The conversion of four different input concentrations of HPA was carried out in the MIR using the four different feeding schedules shown in Table 5. As a control, the same feeding

schedules were followed in fed-batch mode using microwell plates, diluting the reaction mixture with the equivalent dose of GA at the equivalent time point to that of the MIR. In each strategy the configuration or timing of GA feeding points was altered according to the estimated progress of the reaction, in order to avoid inhibitory effects on the enzyme whilst aiming for complete conversion to ERY (see Section 5.3). The flexibility of the reactor's input design was such that each of these feeding strategies could be tested with a minimal amount of effort in setting up, simply by changing the auxiliary connections and flow rates as required. Any ports which were not required in the synthesis reactions could be simply and reliably sealed using the PDMS plugs described in Section 5.2.1, which were held in place by standard M6 interconnects used in all devices presented in this thesis.

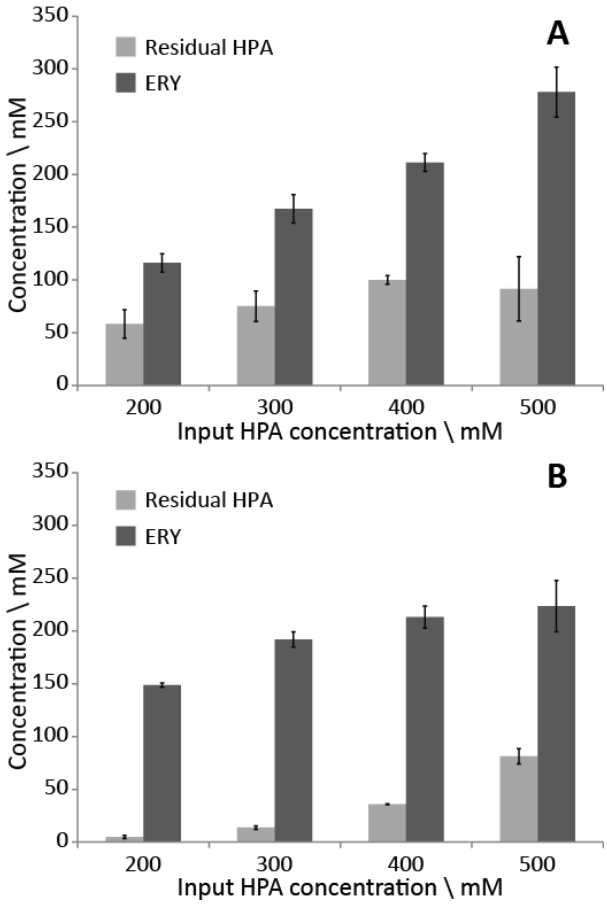


**Figure 50: End point concentrations from synthesis experiments performed in (A) the MIR and(B) in microwell plates (n = 3).**

Figure 50 shows the end-point concentrations of HPA and ERY from synthesis experiments performed under various input HPA concentrations in the MIR and microwell

plates. Compared with the microfluidic SHM reactor shown earlier, which had only a single substrate input microfluidic reactor (see Chapter 4), the use of multi-point feeding increased the yield of ERY from 50 mM to a maximum of 224 mM with the MIR. Compensating for the dilution caused by the nine GA inputs used in the feeding strategy, the maximum concentration of ERY generated is 313 mM.

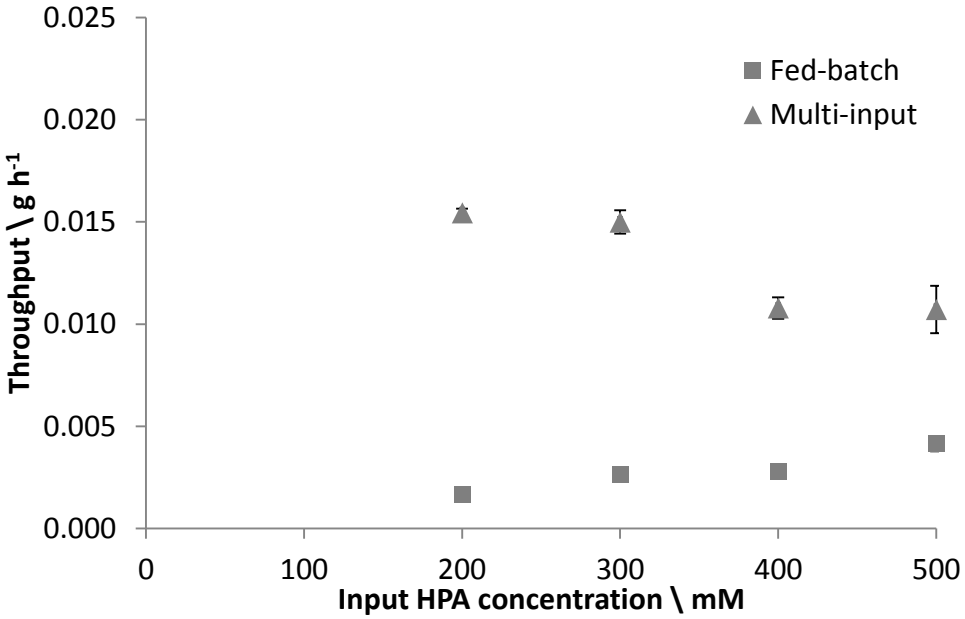


**Figure 51: Throughput of ERY from fed-batch microwell plate and continuous MIR synthesis experiments (n = 3).**

Figures 32, 33 and 34 show the throughput, conversion and volumetric productivity data respectively, from the MIR and equivalent fed-batch microwell plate reactions. Comparing the output from the two systems, a very large improvement in the throughput of ERY from the MIR was observed, regardless of the input HPA concentration used, with the highest observed increase being 8-fold at the lowest input concentration (Figure 51). There was also see an increase in throughput from 3.6 mg $h^{-1}$ to 15 mg $h^{-1}$ when compared with the SHM reactor discussed in Chapter 4. This clearly shows the improvements in throughput and space-time yield that are the foremost advantage of continuous flow reactors over batch or fed-batch reactors, which is in agreement with similar examples of such reactors for biocatalytic synthesis (Itabaiana et al., 2013). A continuous flow system is also of great interest for use in

multi-step synthesis processes, where a cascade of separate reactors can be created to perform a complex conversion. The MIR would be well-suited to this, having standard interconnect ports that would allow connection to other reactors or intermediate purification steps.

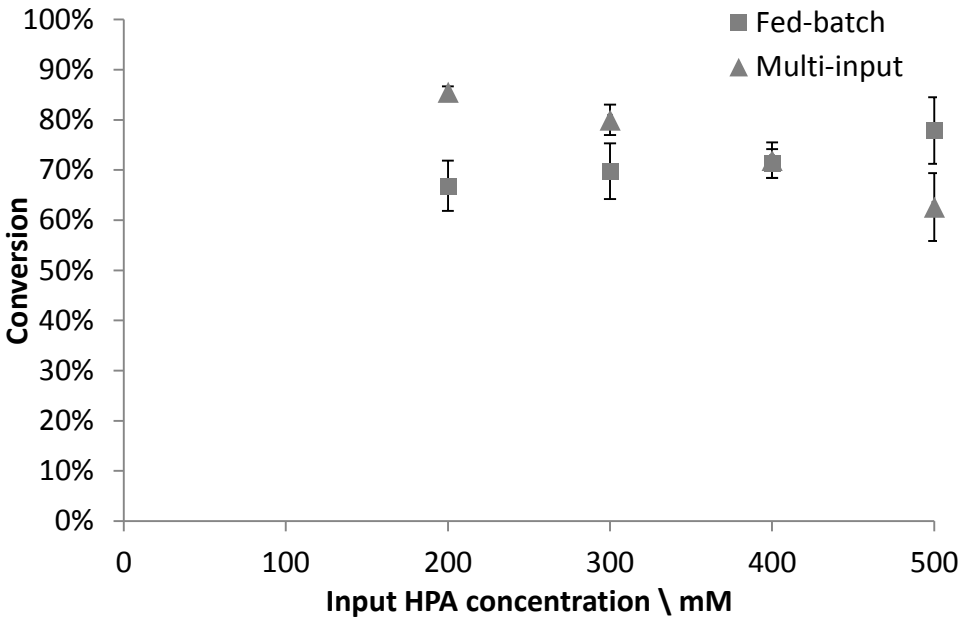


**Figure 52: Percentage conversion achieved in fed-batch microwell plate and continuous MIR synthesis experiments (n = 3).**

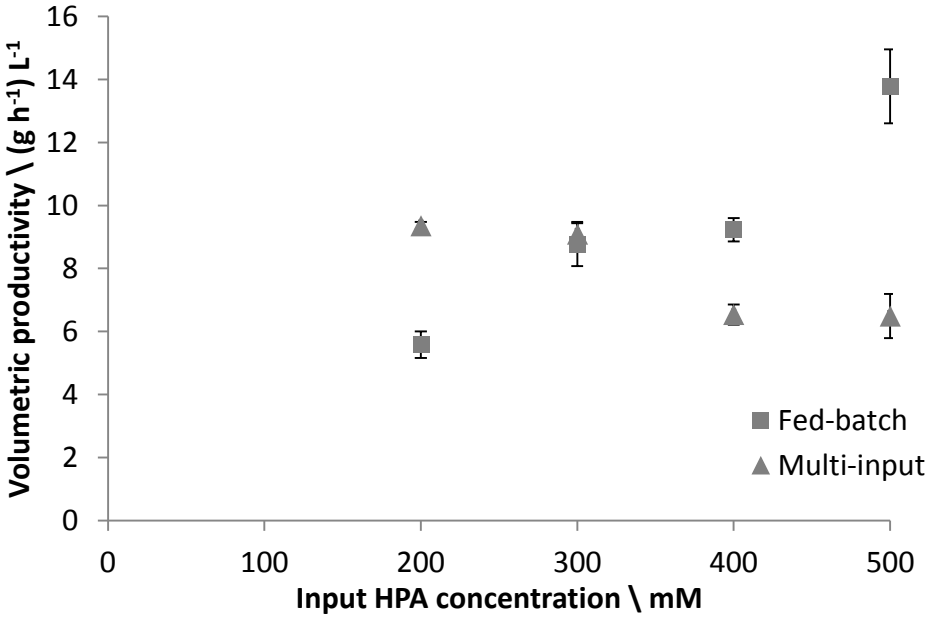


**Figure 53: Volumetric productivity from fed-batch microwell plate and continuous MIR synthesis experiments (n = 3).**

The volumetric productivity and conversion achieved in the MIR was higher than that of the fed-batch microwell plate reactions at lower input HPA concentrations, reaching a maximum of 9.4 (g $h^{-1}$) $L^{-1}$ and 86% respectively (Figure 52 and Figure 53). At higher HPA concentrations the conversion and productivity of the fed-batch microwell plate reactions surpassed that of the MIR. This may have been caused by decreasing pH as the reaction progressed, due to the evolution of $CO_2$ as a by-product, which was released to the headspace in the microwells but remained in solution in the MIR.

A reaction system designed for synthesis should aim to reach 100% conversion in order to minimise the downstream requirement for purification, or unintended side reactions when used as part of a multi-step process. Any change in pH could be mitigated in a manner analogous to that of a pH-stat reactor. This could be accomplished by using some of the auxiliary inputs on the MIR to feed a base solution, thereby counteracting the pH drop and allowing complete conversion of substrate to product. However, to investigate this further would require integration of online pH monitoring into the MIR; a technology that has thus far only been used in cellular microreactors (Schäpper et al., 2009).

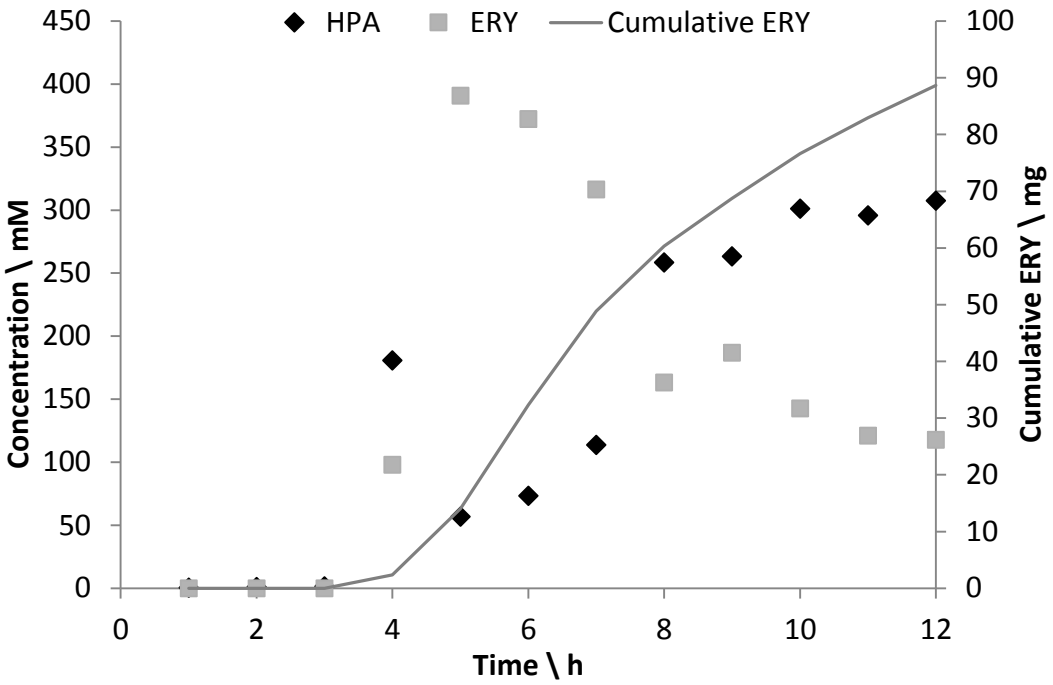


**Figure 54: Concentration of HPA and ERY at MIR output over 12 hours of operation with 500 mM input HPA setup.**

**HPA and ERY concentrations (left axis) were measured from samples taken hourly, the cumulative ERY output is an estimate calculated from the ERY concentration measured and total volume collected each hour.**

Figure 54 shows the output concentration profiles of HPA and ERY from a continuous synthesis experiment performed in the MIR 12 hours, using the feeding schedule developed for a 500 mM HPA input concentration. The reaction was sampled every hour with an automated sampling arm. The reaction equilibrated between hour 4 and 5 (as might be expected given that the residence time was 286 minutes), with a maximum output concentration of around 400 mM ERY. An estimated 90 mg of ERY was produced over the course of the experiment. The output concentration drops continuously between hours 5 and 12, suggesting decay in TK activity due to exposure to room temperature conditions. This may provide a further explanation of the decrease in conversion observed at higher input HPA concentrations (Figure 52). The reactions were each sampled at 2.5 residence times, at between 5 and 12 hours (depending on the input HPA concentration). The data in Figure 54 would suggest that the TK activity may have already decayed significantly by the time that the reactions with longer residence times, i.e. those for input concentrations of 400 and 500 mM HPA, had reached their respective equilibration time and were sampled.

A modification that could be made to overcome this problem is the addition of a cooling system to maintain the stability of the solubilised enzyme. The enzyme could be thermo-stated to the desired temperature shortly before it is introduced into the reactor. A mutant of the TK enzyme with greater temperature stability could also be used. If the initial concentration of ERY observed in figure 4 could be maintained, this would allow production at a rate of 19 mg $h^{-1}$, and thus would have led to a total of 171 mg over the 12 hours.

## 5.5 Summary of Findings

In this chapter, the design of a continuous flow multi-input reactor for biocatalytic synthesis has been shown, which is capable of mimicking fed-batch feeding strategies for use in overcoming substrate inhibition of biocatalysts. The reactor was designed to be fabricated rapidly with the use of laser ablation, such that entire devices can be assembled from scratch in a few hours. The speed with which the devices can be fabricated leaves open the possibility of modifying the design, for example to tailor it to specific feeding schedules or to scale up to achieve greater throughput.

The MIR was applied to the synthesis of ERY using TK, with feeding strategies being designed for the conversion of 200 – 500 mM HPA, based on kinetic data from literature. The reactor was able to achieve more than a four-fold increase in yield by comparison with the output from the SHM reactor discussed in Chapter 4, and a five-fold increase in throughput. The throughput from the MIR was also shown to be 2.5 – 8 times that of the equivalent fed-batch reactions, depending on the input concentration of HPA. Furthermore, a continuous flow synthesis experiment, operated using the maximum input HPA concentration, was able to produce a maximum of 400 mM of ERY immediately after equilibration, with the output concentration dropping to 120 mM over the next seven hours. The experiment produced a total of around 90 mg of ERY over the course of 12 hours.

The application of the MIR to biocatalytic synthesis using an inhibiting substrate represents a step towards process intensification at the microfluidic scale, having been used to

produce concentrations of a metabolite that are rarely achieved at such scales. However, approaching these concentrations has created new challenges, such as the increased evolution of $CO_2$ and concomitant pH drop which that could bring. Overcoming this problem would likely require monitoring of pH such that a basic solution could be fed to counteract the drop. It seems likely that other biocatalytic reactions would require similar monitoring. In addition, the long-term stability of the enzyme when it is exposed to room temperature appears to be a problem for sustained synthesis reactions. In this case a cooling system might be necessary to maintain the activity of the enzyme that has yet to be fed into the reactor, with a heating circuit to raise the temperature of the enzyme feed before it enters the reaction channel. Again, this would likely be required for applications involving other biocatalysts.

Beyond this, the consistency of design of the MIR with the other devices shown in this thesis means that it could be integrated into a wider network of purification or reaction steps in order to work up to more complex products.

# 6

# Conclusions and Future Work

## 6.1 Conclusions

### 6.1.1 Development of Microfluidic Tangential Flow Filter

After several iterations, a microfluidic filter was designed which could be clamp sealed and could therefore be used with two commercial membranes, avoiding problems with pore blocking encountered when membranes were glued, or problems with chemical compatibility that might be encountered in other bonding methods. The main body of the filter could be reused multiple times, and its fabrication in polycarbonate meant that it could sterilized by autoclaving for the purposes of cell handling, in particular mammalian cell recovery.

The burst pressure of the assembled filter was shown to be dependent upon the torsion applied to the assembly screws. A strong seal was achieved using a torsion of 10 cN-m on all assembly screws, giving a burst pressure of 100 psi. The filter was tested for the purification of a small molecular product in a biocatalytic synthesis process (Chapter 4) and the separation of mammalian cells from a suspension containing trypsin (Appendix C), using two different commercially available membranes.

### 6.1.2 Biocatalytic Synthesis Using Inline Microfluidic Filtration Device

The filter was used in combination with a staggered herringbone mixer reactor to synthesize ERY using a TK enzyme as the biocatalyst, with the filter being used to retain the enzyme after the reaction. The two devices were first used separately to determine the best conditions for conversion and filtration. Full conversion of 50 mM HPA and GA to ERY was achieved in 120 minutes using the SHM reactor. The kinetic data in the reactor was shown to be comparable to equivalent experiments performed in 96-well plates, with similar enantiomeric excess of ERY 90% and 87% in the well plate and SHM reactor respectively.

A commercially available 10 kDa molecular weight cut-off polysulphone membrane was tested in the microfluidic filter to retain the cell debris containing TK, which was capable of fully retaining the material. Capillaries with specified diameters were used in combination

with specific flow rates in order to control the pressure in the filter; a capillary diameter of 50µm and a flow rate of 10 µl $min^{-1}$ was found to give the best yield of ERY.

Having determined the best conditions for conversion and filtration, the two devices were connected together into a continuous system to synthesise and purify ERY. The system was operated for 10 hours, giving a peak of ERY output in the permeate immediately after equilibration of 100%. This decreased over the next 3-4 hours, but was shown to be restored by backflushing with tris buffer. No HPA was present throughout the experiment, indicating that the conversion to ERY in the reactor was complete. The cumulative yield of ERY was approximately 3.2 mg.

The successful addition of a downstream processing step to a biocatalytic synthesis reaction at the microfluidic scale opens up possibilities for the evaluation of whole bioprocesses at this scale. Furthermore, the ability to retain the product of a biocatalytic reaction performed with solubilised enzyme could allow the integration of several such reaction step into one continuous operation. Here the compartmentalisation of the reactions could prevent formation of side products and also allow each biocatalyst to be operated at its own ideal conditions.

### 6.1.3 Microfluidic Multi-Input Reactor for Biocatalytic Synthesis

A microfluidic multi-input reactor was designed for the purposes of mimicking fed-batch reactions in a continuous-flow system. The reactor consisted of a 3.3 meter channel with two main inlets and multiple additional inputs along its length, to allow additional substrate to be fed into the reaction mixture, analogous to the feeding of substrate at fixed time points in a fed-batch reactor. The reactor was designed to be fabricated by a laser with a relatively small operating window, with an overall footprint of 85 x 85 mm, and the complete fabrication of a new reactor could be completed in two hours excluding the modular interconnect blocks.

Reported kinetic data for transketolase was used to design feeding strategies for the conversion of different concentrations of HPA, estimating the overall residence time, the

points at which GA would need to be fed and the flow rates required. Using these feeding strategies, the highest concentration of ERY yielded by the reactor was 224 mM (4.5 times that of the SHM reactor used previously), or 313 mM accounting for the dilution by additional GA. An 8-fold increase in throughput over equivalent fed-batch reactions was also determined.

The yield of ERY from the MIR tended to decrease as the input HPA concentration used was increased, a trend which was not observed in the equivalent fed-batch reactions. This could be attributed to the build-up of $CO_2$ in the MIR, which appeared to remain in solution and could have reduced the pH below the operating range of the enzyme. Further improvement of the reactor would be required to overcome this problem (detailed in Section 6.2) though if the theoretically calculated conversion could be reached it would represent a significant step towards the level of throughput that is commonly associated with chemical microreactors. This could be used as a way of intensifying synthesis reactions with biocatalysts, with processes developed at the microfluidic scale being scaled up or out to pilot or even industrial scales, in much the same way as observed with chemical microreactors in recent years.

## 6.2 Future Work

Further experiments are envisioned which could focus on three main themes:

1. The scaled-down (and intensified) production of chiral metabolites.
2. Cascading of multiple reaction and purification steps to find novel routes to metabolites for process development.
3. Analysis and optimisation of the operational space of individual process steps at the microfluidic scale.

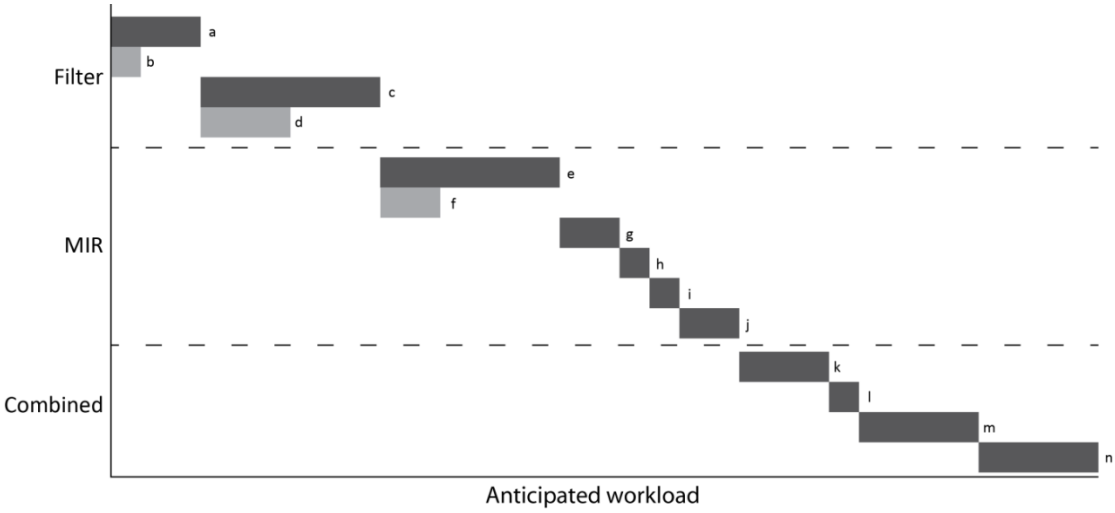


**Figure 55: Critical path analysis of additional activity towards enhancing the design of the microfluidic filter, multi-input reactor, and combining the two devices for multi-step synthesis. The two streams of work on the filter and MIR could alternatively be carried out in parallel, while the 'Combined' stream would require both devices. The length of the bars indicates the predicted workload involved in each aspect of the project. Lighter grey bars indicate activities with a lower priority.**

Initial work involving the filter could focus on further investigation of processing conditions for the removal of transketolase from a reaction mixture after synthesis, in order to maintain a higher yield than was achieved in previous experiments in Chapter 4 (bar a of the critical path analysis shown in Figure 55). In particular, this might include the testing of other membrane materials, pore sizes and a more detailed evaluation of the effects of TMP to define the critical pressure for the process. Given the volume of experiments required it is imagined that this will create a larger workload, relating to a longer bar on the critical path analysis. Addition of pressure transducers to the inlets and outlets of the device along with computer-controlled micrometering valves (b), as opposed to manual valves which were found to give

poor control of pressure, would help to achieve more precise pressure control for this purpose and give a greater quantity of data on the filtration process, and should therefore be done early on. This should be a relatively trivial step, although identifying valves capable of delivering pressure control at such low flow rates may be a challenge.

Key scaling parameters could be identified in experiments performed with the microfluidic device and compared with those of larger equivalent units used more routinely in process development, in order to better establish the value of the device as a tool for scale-down process development (c). This could allow the device to be used in scale-down bioprocess development for other processes; however I believe the primary worth of the device is as an intermediary purification step in a network of microfluidic reactors, so this would be less of a priority. A higher priority would be increasing the filtration area of the device itself, either by elongation or by widening the filtration channel, using flow splitters to ensure an even flow rate over the surface of the membrane (d). This should help to reduce effects of fouling on flux and make the device more useful for separations at the microfluidic scale.

The MIR could also be further developed, either after or in parallel to the experiments carried out with the tangential flow filter. The initial focus of work on the MIR should be to establish pH sensing within the reactor channel (e), in order to confirm whether the downward trend in conversion with higher input HPA concentrations is indeed caused by a drop in pH. Initial tests might require that off-the-shelf pH sensors are incorporated into the fluidic circuit through additional ports and tubing, with more sophisticated versions potentially using a pH sensing coating that can be interrogated by Fourier transform infrared spectroscopy. The addition of a method of chilling the reaction mixture before it enters the MIR would also be necessary to rule out the possible effects of enzyme inactivation at room temperature (f). The technical challenges involved in step (e), including the evaluation of methods for incorporating the necessary sensors and fibers, and the modification of the reactor to make detection possible, would create quite a large workload. Step (f) would be relatively trivial;

however both of these steps would be beneficial to intensifying the production of the chosen chiral metabolite.

With the pH sensing system in place, the substrate feeding strategies previously developed could be modified to neutralise any changes to the pH of the reaction mixture that would adversely affect the activity of the enzyme, for instance feeding in a slightly basic solution of GA. The synthesis experiments performed in Chapter 5 could then be repeated to see if there was better agreement between the continuous-flow and fed-batch reactors (g), a relatively time-consuming process but one that shouldn't present any technical challenges.

Assuming that the data from the continuous-flow and fed-batch reactions were more closely aligned, the feeding strategy with the best conversion could be improved further. This could be achieved by modifying the design of the reactor to feed the substrate more closely to the point that it was required, either by changing the point at which each input joined the main channel or making slight modifications to the channel width, to change the residence time between sections (h). The reactor might also be scaled up to increase the throughput achieved (i), moving the MIR from a scaled-down tool for process development and intensification to a bench-top reactor, a step which is in-keeping with current trends in the use of microreactor designs in the chemistry industry. The speed of the laser fabrication process would allow both of these steps to be completed relatively quickly. Again, this scaled-up and tailored design could be compared with a bench-top fed-batch reactor to demonstrate its value as a method for generating a continuous supply of a chiral product (j).

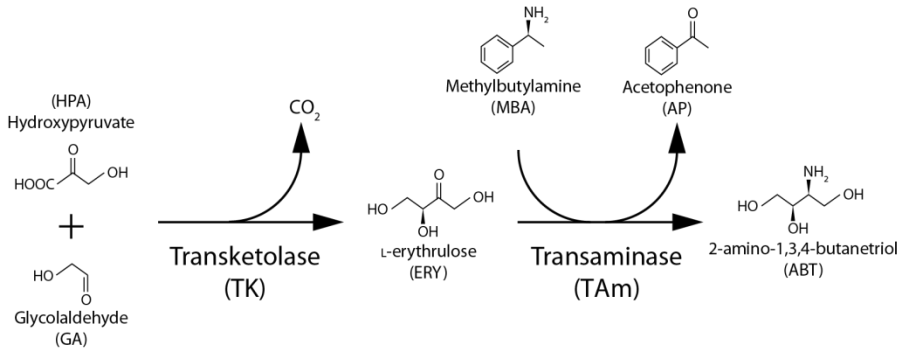


**Figure 56: The transketolase – transaminase pathway for the production of ABT.**

Having performed the work described above, the tangential flow filter and the MIR could be combined to perform a two-step synthesis process, using the transketolase – transaminase pathway to produce 2-amino-1,3,4-butanetriol (ABT; see Figure 56). This would serve as a useful proof-of-concept for pharmaceutical production, given that the molecules produced by the pathway can be used as precursors for protease inhibitors (Ingram et al., 2007). The same process that was used to create feeding strategies for the synthesis of ERY could be applied to transaminase using the available kinetic data, based on the conversion of the established output concentration of ERY and using methylbutylamine as the inhibiting substrate (Rios-Solis et al., 2013). These strategies could be tested in the MIR (k) and a new reactor could be fabricated which is tailored to the best optimised strategy (l). Using the data gathered in the earlier optimisation of the filtration conditions for TK, a set of conditions could be established for the separation of TK and TAm downstream from their respective reactors (m). Finally, the two reactions could be combined in a single network consisting of two MIRs and two tangential filters, producing a continuous stream of ABT (n).

This work would further validate the devices presented in this thesis for the purpose of evaluating biocatalytic process conditions and intensifying the production of the desired chiral products. Not only that, but it would represent a significant step towards the use of microreactor designs for multi-step industrial biocatalysis, something that has to date only been explored for chemical synthesis.

# 7 References

Alam, M. N. H. Z.; Pinelo, M.; Samanta, K.; Jonsson, G.; Meyer, A.; Gernaey, K. V. A Continuous Membrane Microbioreactor System for Development of Integrated Pectin Modification and Separation Processes. *Chem. Eng. J.* **2011**, *167*, 418–426.

Anderson, N. G. Practical Use of Continuous Processing in Developing and Scaling Up Laboratory Processes. *Org. Process Res. Dev.* **2001**, *5*, 613–621.

Ansari, M. A.; Kim, K.-Y. Shape Optimization of a Micromixer with Staggered Herringbone Groove. *Chem. Eng. Sci.* **2007**, *62*, 6687–6695.

Baboo, J. Automated High-Throughput Approaches for the Development and Investigation of Novel Oxidative Biocatalytic Processes, UCL (University College London), 2012.

Barbulovic-Nad, I.; Au, S. H.; Wheeler, A. R. A Microfluidic Platform for Complete Mammalian Cell Culture. *Lab Chip* **2010**, *10*, 1536–1542.

Barrett, L. M.; Skulan, A. J.; Singh, A. K.; Cummings, E. B.; Fiechtner, G. J. Dielectrophoretic Manipulation of Particles and Cells Using Insulating Ridges in Faceted Prism Microchannels. *Anal. Chem.* **2005**, *77*, 6798–6804.

Barthe, P.; Guermeur, C.; Lobet, O.; Moreno, M.; Woehl, P.; Roberge, D. M.; Bieler, N.; Zimmermann, B. Continuous Multi-Injection Reactor for Multipurpose Production - Part I. *Chem. Eng. Technol.* **2008**, *31*, 1146–1154.

Belfort, C.; Davies, R. H.; Zydney, A. L. The Behavior of Suspensions and Macromolecular Solutions in Crossflow Microfiltration. *J. Memb. Sci.* **1994**, *96*, 1–58.

Bernate, J. A.; Liu, C.; Lagae, L.; Konstantopoulos, K.; Drazer, G. Vector Separation of Particles and Cells Using an Array of Slanted Open Cavities. *Lab Chip* **2013**, *13*, 1086–1092.

Bolivar, J. M.; Wiesbauer, J.; Nidetzky, B. Biotransformations in Microstructured Reactors: More than Flowing with the Stream? *Trends Biotechnol.* **2011**, *29*, 333–342.

Bolton, G.; LaCasse, D.; Kuriyel, R. Combined Models of Membrane Fouling: Development and Application to Microfiltration and Ultrafiltration of Biological Fluids. *J. Memb. Sci.* **2006**, *277*, 75–84.

Bornscheuer, U. T.; Pohl, M. Improved Biocatalysts by Directed Evolution and Rational Protein Design. *Curr. Opin. Chem. Biol.* **2001**, *5*, 137–143.

Bornscheuer, U. T.; Buchholz, K. Highlights in Biocatalysis - Historical Landmarks and Current Trends. *Eng. Life Sci.* **2005**, *5*, 309–323.

Bornscheuer, U. T.; Huisman, G. W.; Kazlauskas, R. J.; Lutz, S.; Moore, J. C.; Robins, K. Engineering the Third Wave of Biocatalysis. *Nature* **2012**, *485*, 185–194.

Brody, J. P.; Yager, P.; Goldstein, R. E.; Austin, R. H. Biotechnology at Low Reynolds Numbers. *Biophysical Journal*, 1996, *71*, 3430–3441.

Carlson, R. H.; Gabel, C. V; Chan, S. S.; Austin, R. H.; Brody, J. P.; Winkelman, J. W. Self-Sorting of White Blood Cells in a Lattice. *Phys. Rev. Lett.* **1997**, *79*, 2149–.

Cázares, A.; Galman, J. L.; Crago, L. G.; Smith, M. E. B.; Strafford, J.; Ríos-Solís, L.; Lye, G. J.; Dalby, P. A.; Hailes, H. C. Non-Alpha-Hydroxylated Aldehydes with Evolved Transketolase Enzymes. *Org. Biomol. Chem.* **2010**, *8*, 1301–1309.

Cervera-Padrell, A. E.; Nielsen, J. P.; Jønch Pedersen, M.; Müller Christensen, K.; Mortensen, A. R.; Skovby, T.; Dam-Johansen, K.; Kiil, S.; Gernaey, K. V. Monitoring and Control of a Continuous Grignard Reaction for the Synthesis of an Active Pharmaceutical Ingredient Intermediate Using Inline NIR Spectroscopy. *Org. Process Res. Dev.* **2012**, *16*, 901–914.

Chambers, R. D.; Fox, M. A.; Holling, D.; Nakano, T.; Okazoe, T.; Sandford, G. Versatile Gas/Liquid Microreactors for Industry. *Chem. Eng. Technol.* **2005**, *28*, 344–352.

Chang-Yen, D. A.; Gale, B. K. An Integrated Optical Oxygen Sensor Fabricated Using Rapid-Prototyping Techniques. *Lab Chip* **2003**, *3*, 297–301.

Charmantray, F.; Hélaine, V.; Legeret, B.; Hecquet, L. Preparative Scale Enzymatic Synthesis of D-Sedoheptulose-7-Phosphate from B-Hydroxypyruvate and D-Ribose-5-Phosphate. *J. Mol. Catal. B Enzym.* **2009**, *57*, 6–9.

Chen, B. H.; Baganz, F.; Woodley, J. M. Modelling and Optimisation of a Transketolase-Mediated Carbon–carbon Bond Formation Reaction. *Chem. Eng. Sci.* **2007 a**, *62*, 3178–3184.

Chen, G. W.; Zhao, Y. C.; Yuan, Q. Development of Microreaction Technology from Lab to Industrial Applications. In *12th The International Conferences on Microreaction Technology*; 2011 a.

Chen, G. W.; Zhao, Y. C.; Yuan, Q. Development of Microreaction Technology from Lab to Industrial Applications. In *12th The International Conferences on Microreaction Technology*; 2011 b.

Chen, V.; Li, H.; Fane, A. . Non-Invasive Observation of Synthetic Membrane Processes – a Review of Methods. *J. Memb. Sci.* **2004**, *241*, 23–44.

Chen, X.; Cui, D.; Liu, C.; Li, H.; Chen, J. Continuous Flow Microfluidic Device for Cell Separation, Cell Lysis and DNA Purification. *Anal. Chim. Acta* **2007 b**, *584*, 237–243.

Chen, X.; Cui, D. F.; Liu, C. C.; Li, H. Microfluidic Chip for Blood Cell Separation and Collection Based on Crossflow Filtration. *Sensors Actuators B Chem.* **2008**, *130*, 216–221.

Choi, S.; Park, J.-K. Continuous Hydrophoretic Separation and Sizing of Microparticles Using Slanted Obstacles in a Microchannel. *Lab Chip* **2007**, *7*, 890–897.

Clouthier, C. M.; Pelletier, J. N. Expanding the Organic Toolbox: A Guide to Integrating Biocatalysis in Synthesis. *Chem. Soc. Rev.* **2012**, *41*, 1585–1605.

Crowley, T. A.; Pizziconi, V. Isolation of Plasma from Whole Blood Using Planar Microfilters for Lab-on-a-Chip Applications. *Lab Chip* **2005**, *5*, 922–929.

DeMello, A. J. Control and Detection of Chemical Reactions in Microfluidic Systems. *Nature* **2006**, *442*, 394–402.

Doh, I.; Cho, Y.-H. A Continuous Cell Separation Chip Using Hydrodynamic Dielectrophoresis (DEP) Process. *Sensors Actuators A Phys.* **2005**, *121*, 59–65.

Doran, P. M. *Bioprocess Engineering Principles*; Elsevier Academic Press: London, 2004.

Ducrée, J.; Haeberle, S.; Lutz, S.; Pausch, S.; Stetten, F. von; Zengerle, R. The Centrifugal Microfluidic Bio-Disk Platform. *J. Micromechanics Microengineering* **2007**, *17*, S103–S115.

Duffy, D. C.; McDonald, J. C.; Schueller, O. J. A.; Whitesides, G. M. Rapid Prototyping of Microfluidic Systems in Poly(dimethylsiloxane). *Analytical Chemistry*, 1998, *70*, 4974–4984.

Duke, T.; Austin, R. Microfabricated Sieve for the Continuous Sorting of Macromolecules. *Phys. Rev. Lett.* **1998**, *80*, 1552–1555.

Edwards, T. L.; Gale, B. K.; Frazier, A. B. A Microfabricated Thermal Field-Flow Fractionation System. *Anal. Chem.* **2002**, *74*, 1211–1216.

Fernandes, P. Miniaturization in Biocatalysis. *Int. J. Mol. Sci.* **2010**, *11*, 858–879.

Field, R. W.; Wu, D.; Howell, J. A.; Gupta, B. B. Critical Flux Concept for Microfiltration Fouling. *J. Memb. Sci.* **1995**, *100*, 259–272.

Floriano, P. N.; Christodoulides, N.; Romanovicz, D.; Bernard, B.; Simmons, G. W.; Cavell, M.; McDevitt, J. T. Membrane-Based on-Line Optical Analysis System for Rapid Detection of Bacteria and Spores. *Biosens. Bioelectron.* **2005**, *20*, 2079–2088.

Fonslow, B. R.; Barocas, V. H.; Bowser, M. T. Using Channel Depth to Isolate and Control Flow in a Micro Free-Flow Electrophoresis Device. *Anal. Chem.* **2006**, *78*, 5369–5374.

Fu, J.; Schoch, R. B.; Stevens, A. L.; Tannenbaum, S. R.; Han, J. A Patterned Anisotropic Nanofluidic Sieving Structure for Continuous-Flow Separation of DNA and Proteins. *Nat Nano* **2007**, *2*, 121–128.

Funfak, A.; Cao, J.; Wolfbeis, O. S.; Martin, K.; Köhler, J. M. Monitoring Cell Cultivation in Microfluidic Segments by Optical pH Sensing with a Micro Flow-through Fluorometer Using Dye-Doped Polymer Particles. *Microchim. Acta* **2008**, *164*, 279–286.

Funke, M.; Buchenauer, A.; Schnakenberg, U.; Mokwa, W.; Diederichs, S.; Mertens, A.; Müller, C.; Kensy, F.; Büchs, J. Microfluidic Biolector-Microfluidic Bioprocess Control in Microtiter Plates. *Biotechnol. Bioeng.* **2010**, *107*, 497–505.

Galambos, P.; Forster, F. K. Micro-Fluidic Diffusion Coefficient Measurement. In *Micro Total Analysis Systems '98*; Banff, Canada, 1998; pp. 189–192.

Gómez-Sjöberg, R.; Leyrat, A. A.; Pirone, D. M.; Chen, C. S.; Quake, S. R. Versatile, Fully Automated, Microfluidic Cell Culture System. *Anal. Chem.* **2007**, *79*, 8557–8563.

Gyamerah, M.; Willetts, A. J.; Laboratories, W. S. Kinetics of Overexpressed Transketolase from Escherichia. *Enzyme* **1997**, *0229*, 127–134.

Hadd, A. G.; Raymond, D. E.; Halliwell, J. W.; Jacobson, S. C.; Ramsey, J. M. Microchip Device for Performing Enzyme Assays. *Anal. Chem.* **1997**, *69*, 3407–3412.

Hadd, A. G.; Jacobson, S. C.; Ramsey, J. M. Microfluidic Assays of Acetylcholinesterase Inhibitors. *Anal. Chem.* **1999**, *71*, 5206–5212.

Han, K.; Frazier, A. B. Reliability Aspects of Packaging and Integration Technology for Microfluidic Systems. *IEEE Trans. Device Mater. Reliab.* **2005**, *5*, 452–457.

Han, K.-H.; Frazier, A. B. Paramagnetic Capture Mode Magnetophoretic Microseparator for High Efficiency Blood Cell Separations. *Lab Chip* **2006**, *6*, 265–273.

Harris, N. R.; Hill, M.; Beeby, S.; Shen, Y.; White, N. M.; Hawkes, J. J.; Coakley, W. T. A Silicon Microfluidic Ultrasonic Separator. *Sensors Actuators B Chem.* **2003**, *95*, 425–434.

Hibbert, E. G.; Senussi, T.; Costelloe, S. J.; Lei, W.; Smith, M. E. B.; Ward, J. M.; Hailes, H. C.; Dalby, P. A. Directed Evolution of Transketolase Activity on Non-Phosphorylated Substrates. *J. Biotechnol.* **2007**, *131*, 425–432.

Hibbert, E. G.; Senussi, T.; Smith, M. E. B.; Costelloe, S. J.; Ward, J. M.; Hailes, H. C.; Dalby, P. A. Directed Evolution of Transketolase Substrate Specificity towards an Aliphatic Aldehyde. *J. Biotechnol.* **2008**, *134*, 240–245.

Hu, X.; Bessette, P.; Qian, J.; Meinhart, C. D.; Daugherty, P. S.; Soh, H. T. Marker-Specific Sorting of Rare Cells Using Dielectrophoresis. *Proc.Natl.Acad.Sci.*, 2005, *102*, 15757–15761.

Huang, L. R.; Tegenfeldt, J. O.; Kraeft, J. J.; Sturm, J. C.; Austin, R. H.; Cox, E. C. A DNA Prism for High-Speed Continuous Fractionation of Large DNA Molecules. *Nat Biotech*, 2002, *20*, 1048–1051.

Huang, L. R.; Cox, E. C.; Austin, R. H.; Sturm, J. C. Continuous Particle Separation through Deterministic Lateral Displacement. *Science* **2004**, *304*, 987–990.

Hughes, M. P. Strategies for Dielectrophoretic Separation in Laboratory-on-a-Chip Systems. *Electrophoresis*, 2002, *23*, 2569–2582.

Huh, D.; Bahng, J. H.; Ling, Y.; Wei, H.-H.; Kripfgans, O. D.; Fowlkes, J. B.; Grotberg, J. B.; Takayama, S. Gravity-Driven Microfluidic Particle Sorting Device with Hydrodynamic Separation Amplification. *Anal. Chem.* **2007**, *79*, 1369–1376.

Iffland, A.; Tafelmeyer, P.; Saudan, C.; Johnsson, K. Directed Molecular Evolution of Cytochrome c Peroxidase †. *Biochemistry* **2000**, *39*, 10790–10798.

Inglis, D. W.; Herman, N. A Scalable Approach for High Throughput Branch Flow Filtration. *Lab Chip* **2013**, *13*, 1724–1731.

Ingram, C. U.; Bommer, M.; Smith, M. E. B.; Dalby, P. A.; Ward, J. M.; Hailes, H. C.; Lye, G. J. One-Pot Synthesis of Amino-Alcohols Using a de-Novo Transketolase and Beta-Alanine: Pyruvate Transaminase Pathway in Escherichia Coli. *Biotechnol. Bioeng.* **2007**, *96*, 559–569.

Ismagilov, R. F.; Ng, J. M. K.; Kenis, P. J. A.; Whitesides, G. M. Microfluidic Arrays of Fluid-Fluid Diffusional Contacts as Detection Elements and Combinatorial Tools. *Analytical Chemistry*, 2001, *73*, 5207–5213.

Itabaiana, I.; de Mariz e Miranda, L. S.; de Souza, R. O. M. A. Towards a Continuous Flow Environment for Lipase-Catalyzed Reactions. *J. Mol. Catal. B Enzym.* **2013**, *85*, 1–9.

Jaccard, N.; Macown, R. J.; Super, A.; Griffin, L. D.; Veraitch, F. S.; Szita, N. Automated and Online Characterization of Adherent Cell Culture Growth in a Microfabricated Bioreactor. *J. Lab. Autom.* **2014**, 2211068214529288–.

Jaggi, R. D.; Sandoz, R.; Effenhauser, C. S. Microfluidic Depletion of Red Blood Cells from Whole Blood in High-Aspect-Ratio Microchannels. *Microfluidics and Nanofluidics*, 2007, *3*, 47–53.

Jähnisch, K.; Hessel, V.; Löwe, H.; Baerns, M. Chemistry in Microstructured Reactors. *Angew. Chemie Int. Ed.* **2004**, *43*, 406–446.

De Jong, J.; Lammertink, R. G. H.; Wessling, M. Membranes and Microfluidics: A Review. *Lab Chip* **2006**, *6*, 1125–1139.

Kalyanpur, M. Downstream Processing in the Biotechnology Industry. *Mol. Biotechnol.* **2002**, *22*, 87–98.

Kim, S.; Kim, H. J.; Jeon, N. L. Biological Applications of Microfluidic Gradient Devices. *Integr. Biol. (Camb).* **2010**, *2*, 584–603.

Klank, H.; Kutter, J. P.; Geschke, O. CO(2)-Laser Micromachining and Back-End Processing for Rapid Production of PMMA-Based Microfluidic Systems. *Lab Chip* **2002**, *2*, 242–246.

Koch, K.; Vandenberg, R.; Nieuwland, P.; Wijtmans, R.; Wubbolts, M.; Schoemaker, H.; Rutjes, F.; Vanhest, J. Enzymatic Synthesis of Optically Pure Cyanohydrins in Microchannels Using a Crude Cell Lysate. *Chem. Eng. J.* **2008**, *135*, S89–S92.

Kockmann, N.; Gottsponer, M.; Roberge, D. M. Scale-up Concept of Single-Channel Microreactors from Process Development to Industrial Production. *Chem. Eng. J.* **2011**, *167*, 718–726.

Kohlheyer, D.; Besselink, G. A. J.; Schlautmann, S.; Schasfoort, R. B. M. Free-Flow Zone Electrophoresis and Isoelectric Focusing Using a Microfabricated Glass Device with Ion Permeable Membranes. *Lab Chip* **2006**, *6*, 374–380.

Kriváková, L.; Bocek, P. Continuous Free-Flow Electrophoresis. *Electrophoresis* **1998**, *19*, 1064–1074.

Kurita, R.; Hayashi, K.; Fan, X.; Yamamoto, K.; Kato, T.; Niwa, O. Microfluidic Device Integrated with Pre-Reactor and Dual Enzyme-Modified Microelectrodes for Monitoring in Vivo Glucose and Lactate. *Sensors Actuators B Chem.* **2002**, *87*, 296–303.

Kuswandi, B.; Nuriman; Huskens, J.; Verboom, W. Optical Sensing Systems for Microfluidic Devices: A Review. *Anal. Chim. Acta* **2007**, *601*, 141–155.

Ladisch, M. R.; Kohlmann, K. L. Recombinant Human Insulin. *Biotechnol. Prog.* **1992**, *8*, 469–478.

Ladisch, M. R.; Cooney, C. L.; Dean, R. C.; Humphrey, A. E.; Kirk, T. K.; McIntire, L. V; Michaels, A. S.; Myers-Keith, P.; Ryu, D. D. Y.; Swartz, J. R.; et al. Current Bioprocess

Technology, Products and Opportunities. In *Putting Biotechnology to Work: Bioprocess Engineering*; The National Academy of Sciences: Washington, D.C., 1992; pp. 50–76.

Lawrence, J.; O'Sullivan, B.; Lye, G. J.; Wohlgemuth, R.; Szita, N. Microfluidic Multi-Input Reactor for Biocatalytic Synthesis Using Transketolase. *J. Mol. Catal. B Enzym.* **2013**, *95*, 111–117.

Li, Y.; Dalton, C.; Crabtree, H. J.; Nilsson, G.; Kaler, K. V. I. S. Continuous Dielectrophoretic Cell Separation Microfluidic Device. *Lab on a Chip*, 2007, *7*, 239–248.

Liese, A.; Müller, M.; Pohl, M.; Tittmann, K.; Wohlgemuth, R. C2-Ketol Elongation by Transketolase-Catalyzed Asymmetric Synthesis. *J. Mol. Catal. B Enzym.* **2009**, *61*, 23–29.

Lye, G. J.; Ayazi-Shamlou, P.; Baganz, F.; Dalby, P. A.; Woodley, J. M. Accelerated Design of Bioconversion Processes Using Automated Microscale Processing Techniques. *Trends Biotechnol.* **2003**, *21*, 29–37.

MacDonald, M. P.; Spalding, G. C.; Dholakia, K. Microfluidic Sorting in an Optical Lattice. *Nature* **2003**, *426*, 421–424.

Machsun, A. L.; Gozan, M.; Nasikin, M.; Setyahadi, S.; Yoo, Y. J. Membrane Microreactor in Biocatalytic Transesterification of Triolein for Biodiesel Production. *Biotechnol. Bioprocess Eng.* **2011**, *15*, 911–916.

Macounová, K.; Cabrera, C. R.; Yager, P. Concentration and Separation of Proteins in Microfluidic Channels on the Basis of Transverse IEF. *Anal. Chem.* **2001**, *73*, 1627–1633.

Mahoney, M. J.; Chen, R. R.; Tan, J.; Saltzman, W. M. The Influence of Microchannels on Neurite Growth and Architecture. *Biomaterials* **2005**, *26*, 771–778.

Mair, D. A.; Geiger, E.; Pisano, A. P.; Fréchet, J. M. J.; Svec, F. Injection Molded Microfluidic Chips Featuring Integrated Interconnects. *Lab Chip* **2006**, *6*, 1346–1354.

Majd, H.; Wipff, P.-J.; Buscemi, L.; Bueno, M.; Vonwil, D.; Quinn, T. M.; Hinz, B. A Novel Method of Dynamic Culture Surface Expansion Improves Mesenchymal Stem Cell Proliferation and Phenotype. *Stem Cells* **2009**, *27*, 200–209.

Mak, X. Y.; Laurino, P.; Seeberger, P. H.; Bielstien, J. Asymmetric Reactions in Continuous Flow. *J Org Chem* **2009**, *5*.

Marques, M. P. C.; Fernandes, P. Microfluidic Devices: Useful Tools for Bioprocess Intensification. *Molecules* **2011**, *16*, 8368–8401.

Matosevic, S.; Micheletti, M.; Woodley, J.; Lye, G.; Baganz, F. Quantification of Kinetics for Enzyme-Catalysed Reactions: Implications for Diffusional Limitations at the 10-Ml Scale. *Biotechnol. Lett.* **2008**, *30*, 995–1000.

Matosevic, S.; Lye, G. J.; Baganz, F. Design and Characterization of a Prototype Enzyme Microreactor: Quantification of Immobilized Transketolase Kinetics. *Biotechnol. Prog.* **2010**, *26*, 118–126.

Meyer, H.-P.; Eichhorn, E.; Hanlon, S.; Lütz, S.; Schürmann, M.; Wohlgemuth, R.; Coppolecchia, R. The Use of Enzymes in Organic Synthesis and the Life Sciences:

Perspectives from the Swiss Industrial Biocatalysis Consortium (SIBC). *Catal. Sci. Technol.* **2013**, *3*, 29.

Micheletti, M.; Lye, G. J. Microscale Bioprocess Optimisation. *Curr. Opin. Biotechnol.* **2006**, *17*, 611–618.

Miyazaki, M.; Maeda, H. Microchannel Enzyme Reactors and Their Applications for Processing. *Trends Biotechnol.* **2006**, *24*, 463–470.

Miyazaki, M.; Honda, T.; Yamaguchi, H.; Briones, M. P. P.; Maeda, H. Enzymatic Processing in Microfluidic Reactors. *Biotechnol. Genet. Eng. Rev.* **2008**, *25*, 405–428.

Mores, W. D.; Davis, R. H. Direct Visual Observation of Yeast Deposition and Removal during Microfiltration. *J. Memb. Sci.* **2001**, *189*, 217–230.

Murphy, E. R.; Martinelli, J. R.; Zaborenko, N.; Buchwald, S. L.; Jensen, K. F. Accelerating Reactions with Microreactors at Elevated Temperatures and Pressures: Profiling Aminocarbonylation Reactions. *Angew. Chem. Int. Ed. Engl.* **2007**, *46*, 1734–1737.

Ng, J. M. K.; Gitlin, I.; Stroock, A. D.; Whitesides, G. M. Components for Integrated Poly(dimethylsiloxane) Microfluidic Systems. *Electrophoresis* **2002**, *23*, 3461–3473.

Ngene, I. S.; Lammertink, R. G. H.; Wessling, M.; van der Meer, W. A Microfluidic Membrane Chip for in Situ Fouling Characterization. *J. Memb. Sci.* **2010**, *346*, 202–207.

Nilsson, A.; Petersson, F.; Jönsson, H.; Laurell, T. Acoustic Control of Suspended Particles in Micro Fluidic Chips. *Lab Chip* **2004**, *4*, 131–135.

Nittis, V.; Fortt, R.; Legge, C. H.; de Mello, A. J. A High-Pressure Interconnect for Chemical Microsystem Applications. *Lab Chip* **2001**, *1*, 148–152.

O'Sullivan, B.; Al-Bahrani, H.; Lawrence, J.; Campos, M.; Cázares, A.; Baganz, F.; Wohlgemuth, R.; Hailes, H. C.; Szita, N. Modular Microfluidic Reactor and Inline Filtration System for the Biocatalytic Synthesis of Chiral Metabolites. *J. Mol. Catal. B Enzym.* **2012**, *77*, 1–8.

Ordidge, G. C.; Mannall, G.; Liddell, J.; Dalby, P. A.; Micheletti, M. A Generic Hierarchical Screening Method for the Analysis of Microscale Refolds Using an Automated Robotic Platform. *Biotechnol. Prog.* **2012**, *28*, 435–444.

Pamme, N. Continuous Flow Separations in Microfluidic Devices. *Lab Chip* **2007 a**, *7* , 1644–1659.

Pamme, N. Continuous Flow Separations in Microfluidic Devices. *Lab Chip* **2007 b**, *7*, 1644–1659.

Pamme, N.; Wilhelm, C. Continuous Sorting of Magnetic Cells via on-Chip Free-Flow Magnetophoresis. *Lab Chip* **2006**, *6*, 974–980.

Petersson, F.; Nilsson, A.; Holm, C.; Jonsson, H.; Laurell, T. Continuous Separation of Lipid Particles from Erythrocytes by Means of Laminar Flow and Acoustic Standing Wave Forces. *Lab Chip* **2005**, *5*, 20–22.

Pihl, J.; Sinclair, J.; Sahlin, E.; Karlsson, M.; Petterson, F.; Olofsson, J.; Orwar, O. Microfluidic Gradient-Generating Device for Pharmacological Profiling. *Anal. Chem.* **2005**, *77*, 3897–3903.

Placzek, M. R.; Chung, I.-M.; Macedo, H. M.; Ismail, S.; Mortera Blanco, T.; Lim, M.; Cha, J. M.; Fauzi, I.; Kang, Y.; Yeo, D. C. L.; et al. Stem Cell Bioprocessing: Fundamentals and Principles. *J. R. Soc. Interface* **2009**, *6*, 209–232.

Pohar, A.; Žnidaršič-Plazl, P.; Plazl, I. Integrated System of a Microbioreactor and a Miniaturized Continuous Separator for Enzyme Catalyzed Reactions. *Chem. Eng. J.* **2012**, *189*, 376–382.

Pollard, D. J.; Woodley, J. M. Biocatalysis for Pharmaceutical Intermediates: The Future Is Now. *Trends Biotechnol.* **2007**, *25*, 66–73.

Pollard, D.; Truppo, M.; Pollard, J.; Chen, C.; Moore, J. Effective Synthesis of (S)-3,5-Bistrifluoromethylphenyl Ethanol by Asymmetric Enzymatic Reduction. *Tetrahedron: Asymmetry* **2006**, *17*, 554–559.

Pollice, A.; Brookes, A.; Jefferson, B.; Judd, S. Sub-Critical Flux Fouling in Membrane Bioreactors — a Review of Recent Literature. *Desalination* **2005**, *174*, 221–230.

Puskeiler, R.; Kaufmann, K.; Weuster-Botz, D. Development, Parallelization, and Automation of a Gas-Inducing Milliliter-Scale Bioreactor for High-Throughput Bioprocess Design (HTBD). *Biotechnol. Bioeng.* **2005**, *89*, 512–523.

Raymond, D. E.; A., M.; Widmer, H. M. Continuous Sample Pretreatment Using a Free-Flow Electrophoresis Device Integrated onto a Silicon Chip. *Anal. Chem.* **1994**, *66*, 2858–2865.

Reichen, M. Multiplexed Microfabricated Cell Culture Device for Stem Cell Process Development, University College London, 2011, pp. 62–63.

Reichen, M.; Veraitch, F. S.; Szita, N. An Automated and Multiplexed Microfluidic Bioreactor Platform with Time-Lapse Imaging for Cultivation of Embryonic Stem Cells and Online Assessment of Morphology and Pluripotency Markers. In *Proceedings of the 14th International Conference on Miniaturized Systems for Chemistry and the Life Sciences*; 2010; pp. 848–850.

Van Reis, R.; Zydney, A. L. Bioprocess Membrane Technology. *J. Memb. Sci.* **2007**, *297*, 16–50.

Van Reis, R.; Leonard, L. C.; Hsu, C. C.; Builder, S. E. Industrial Scale Harvest of Proteins from Mammalian Cell Culture by Tangential Flow Filtration. *Biotechnol. Bioeng.* **1991**, *38*, 413–422.

Rhimi, M.; Aghajari, N.; Juy, M.; Chouayekh, H.; Maguin, E.; Haser, R.; Bejar, S. Rational Design of Bacillus Stearothermophilus US100 L-Arabinose Isomerase: Potential Applications for D-Tagatose Production. *Biochimie* **2009**, *91*, 650–653.

Rios-Solis, L.; Bayir, N.; Halim, M.; Du, C.; Ward, J. M.; Baganz, F.; Lye, G. J. Non-Linear Kinetic Modelling of Reversible Bioconversions: Application to the Transaminase Catalyzed Synthesis of Chiral Amino-Alcohols. *Biochem. Eng. J.* **2013**, *73*, 38–48.

Rivet, C.; Lee, H.; Hirsch, A.; Hamilton, S.; Lu, H. Microfluidics for Medical Diagnostics and Biosensors. *Chem. Eng. Sci.* **2011**, *66*, 1490–1507.

Roberge, D. M.; Bieler, N.; Mathier, M.; Eyholzer, M.; Zimmermann, B.; Barthe, P.; Guermeur, C.; Lobet, O.; Moreno, M.; Woehl, P. Development of an Industrial Multi-Injection Microreactor for Fast and Exothermic Reactions - Part II. *Chem. Eng. Technol.* **2008 a**, *31*, 1155–1161.

Roberge, D. M.; Zimmermann, B.; Rainone, F.; Gottsponer, M.; Eyholzer, M.; Kockmann, N. Microreactor Technology and Continuous Processes in the Fine Chemical and Pharmaceutical Industry: Is the Revolution Underway? *Org. Process Res. Dev.* **2008 b**, *12*, 905–910.

Sahoo, H. R.; Kralj, J. G.; Jensen, K. F. Multistep Continuous-Flow Microchemical Synthesis Involving Multiple Reactions and Separations. *Angew. Chemie* **2007**, *119*, 5806–5810.

Saibi, W.; Abdeljalil, S.; Masmoudi, K.; Gargouri, A. Biocatalysts: Beautiful Creatures. *Biochem. Biophys. Res. Commun.* **2012**, *426*, 289–293.

Schäpper, D.; Alam, M. N. H. Z.; Szita, N.; Eliasson Lantz, A.; Gernaey, K. V. Application of Microbioreactors in Fermentation Process Development: A Review. *Anal. Bioanal. Chem.* **2009**, *395*, 679–695.

Schoenmakers, P. J.; Vangelooven, J.; Desmet, G. Computer Aided Design Optimisation of Microfluidic Flow Distributors. *J. Chromatogr. A* **2010**, *1217*, 6724–6732.

Sethu, P.; Sin, A.; Toner, M. Microfluidic Diffusive Filter for Apheresis (leukapheresis). *Lab Chip* **2006**, *6*, 83–89.

Smith, M. E. B.; Hibbert, E. G.; Jones, A. B.; Dalby, P. A.; Hailes, H. C. Enhancing and Reversing the Stereoselectivity of Escherichia Coli Transketolase via Single-Point Mutations. *Adv. Synth. Catal.* **2008**, *350*, 2631–2638.

Smith, M. E. B.; Chen, B. H.; Hibbert, E. G.; Kaulmann, U.; Smithies, K.; Galman, J. L.; Baganz, F.; Dalby, P. A.; Hailes, H. C.; Lye, G. J.; et al. A Multidisciplinary Approach Toward the Rapid and Preparative-Scale Biocatalytic Synthesis of Chiral Amino Alcohols: A Concise Transketolase-/w-Transaminase-Mediated Synthesis of (2S,3S)-2-Aminopentane-1,3-Diol. *Org. Process Res. Dev.* **2009**, *14*, 99–107.

Squires, T. M.; Quake, S. R. Microfluidics: Fluid Physics at the Nanoliter Scale. *Rev.Mod.Phys.*, 2005, *77*, 977–.

Straathof, A. J. J. Quantitative Analysis of Industrial Biotransformation. In *Industrial Biotransformations*; Liese, A.; Seelbach, K.; Wandrey, C., Eds.; Wiley-VCH Verlag GmbH & Co. KGaA: Weinheim, FRG, 2006.

Stroock, A. D.; Dertinger, S. K. W.; Ajdari, A.; Mezic, I.; Stone, H. A.; Whitesides, G. M. Chaotic Mixer for Microchannels. *Science* **2002**, *295*, 647–651.

Tabeling, P. Introduction to Microfluidics, 2006, *First*, -.

Takagi, J.; Yamada, M.; Yasuda, M.; Seki, M. Continuous Particle Separation in a Microchannel Having Asymmetrically Arranged Multiple Branches. *Lab Chip* **2005**, *5*, 778–784.

Theberge, A. B.; Courtois, F.; Schaerli, Y.; Fischlechner, M.; Abell, C.; Hollfelder, F.; Huck, W. T. S. Microdroplets in Microfluidics: An Evolving Platform for Discoveries in Chemistry and Biology. *Angew. Chem. Int. Ed. Engl.* **2010**, *49*, 5846–5868.

Tišma, M.; Zelić, B.; Vasić-Rački, Đ.; Žnidaršič-Plazl, P.; Plazl, I. Modelling of Laccase-Catalyzed L-DOPA Oxidation in a Microreactor. *Chem. Eng. J.* **2009**, *149*, 383–388.

Torres, R. J. M. Characterisation of the Structural Stability of Transketolase under Biocatalytically Relevant Conditions, University College London, 2008.

Tudorache, M.; Mahalu, D.; Teodorescu, C.; Stan, R.; Bala, C.; Parvulescu, V. I. Biocatalytic Microreactor Incorporating HRP Anchored on Micro-/nano-Lithographic Patterns for Flow Oxidation of Phenols. *J. Mol. Catal. B Enzym.* **2011**, *69*, 133–139.

Umehara, S.; Wakamoto, Y.; Inoue, I.; Yasuda, K. On-Chip Single-Cell Microcultivation Assay for Monitoring Environmental Effects on Isolated Cells. *Biochem. Biophys. Res. Commun.* **2003**, *305*, 534–540.

VanDelinder, V.; Groisman, A. Separation of Plasma from Whole Human Blood in a Continuous Cross-Flow in a Molded Microfluidic Device. *Anal. Chem.* **2006**, *78*, 3765–3771.

VanDelinder, V.; Groisman, A. Perfusion in Microfluidic Cross-Flow: Separation of White Blood Cells from Whole Blood and Exchange of Medium in a Continuous Flow. *Analytical Chemistry*, 2007, *79*, 2023–2030.

Vangelooven, J.; De Malsche, W.; Op De Beeck, J.; Eghbali, H.; Gardeniers, H.; Desmet, G. Design and Evaluation of Flow Distributors for Microfabricated Pillar Array Columns. *Lab Chip* **2010**, *10*, 349–356.

Wang, J. On-Chip Enzymatic Assays. *Electrophoresis* **2002**, *23*, 713–718.

Wang, P. C.; Gao, J.; Lee, C. S. High-Resolution Chiral Separation Using Microfluidics-Based Membrane Chromatography. *Journal of Chromatography A*, 2002, *942*, 115–122.

Weuster-Botz, D.; Puskeiler, R.; Kusterer, A.; Kaufmann, K.; John, G. T.; Arnold, M. Methods and Milliliter Scale Devices for High-Throughput Bioprocess Design. *Bioprocess Biosyst. Eng.* **2005**, *28*, 109–119.

Whitesides, G. M. The Origins and the Future of Microfluidics. *Nature* **2006**, *442*, 368–373.

Wiles, C.; Watts, P. Continuous Flow Reactors, a Tool for the Modern Synthetic Chemist. *European J. Org. Chem.* **2008**, *2008*, 1655–1671.

Wohlgemuth, R. Tools and Ingredients for the Biocatalytic Synthesis of Metabolites. *Biotechnol. J.* **2009**, *4*, 1253–1265.

Wohlgemuth, R. Biocatalysis--Key to Sustainable Industrial Chemistry. *Curr. Opin. Biotechnol.* **2010**, *21*, 713–724.

Wojcieszyn, J. W.; Schlegel, R. A.; Wu, E. S.; Jacobson, K. A. Diffusion of Injected Macromolecules within the Cytoplasm of Living Cells. *Proc. Natl. Acad. Sci. U. S. A.* **1981**, *78*, 4407–4410.

Woodley, J. M. New Opportunities for Biocatalysis: Making Pharmaceutical Processes Greener. *Trends Biotechnol.* **2008**, *26*, 321–327.

Wu, M.-H.; Huang, S.-B.; Lee, G.-B. Microfluidic Cell Culture Systems for Drug Research. *Lab Chip* **2010**, *10*, 939–956.

Xia, N.; Hunt, T. P.; Mayers, B. T.; Alsberg, E.; Whitesides, G. M.; Westervelt, R. M.; Ingber, D. E. Combined Microfluidic-Micromagnetic Separation of Living Cells in Continuous Flow. *Biomed. Microdevices* **2006**, *8*, 299–308.

Xu, Y.; Zhang, C.-X.; Janasek, D.; Manz, A. Sub-Second Isoelectric Focusing in Free Flow Using a Microfluidic Device. *Lab Chip* **2003**, *3*, 224–227.

Yager, P.; Brody, J. P. Absorption-Enhanced Differential Extraction Device, 2004, -.

Yamada, M.; Seki, M. Hydrodynamic Filtration for on-Chip Particle Concentration and Classification Utilizing Microfluidics. *Lab on a Chip*, 2005, *5*, 1233–1239.

Yamada, M.; Nakashima, M.; Seki, M. Pinched Flow Fractionation: Continuous Size Separation of Particles Utilizing a Laminar Flow Profile in a Pinched Microchannel. *Analytical Chemistry*, 2004, *76*, 5465–5471.

Yang, T. H.; Kim, T. W.; Kang, H. O.; Lee, S.-H.; Lee, E. J.; Lim, S.-C.; Oh, S. O.; Song, A.-J.; Park, S. J.; Lee, S. Y. Biosynthesis of Polylactic Acid and Its Copolymers Using Evolved Propionate CoA Transferase and PHA Synthase. *Biotechnol. Bioeng.* **2010**, *105*, 150–160.

Yoshida, J.; Nagaki, A.; Yamada, D. Continuous Flow Synthesis. *Drug Discov. Today Technol.* **2013**, *10*, e53–e59.

You, L.; Arnold, F. H. Directed Evolution of Subtilisin E in Bacillus Subtilis to Enhance Total Activity in Aqueous Dimethylformamide. *"Protein Eng. Des. Sel.* **1996**, *9*, 77–83.

Zeman, L. J.; Zydney, A. L. *Microfiltration and Ultrafiltration: Principles and Applications*; First.; Marcel Dekker Inc.: New York, USA, 1996.

Zhang, C.-X.; Manz, A. High-Speed Free-Flow Electrophoresis on Chip. *Anal. Chem.* **2003**, *75*, 5759–5766.

Zhang, L.; Su, Y.; Zheng, Y.; Jiang, Z.; Shi, J.; Zhu, Y.; Jiang, Y. Sandwich-Structured Enzyme Membrane Reactor for Efficient Conversion of Maltose into Isomaltooligosaccharides. *Bioresour. Technol.* **2010**, *101*, 9144–9149.

Zhang, X.; Stefanick, S.; Villani, F. J. Application of Microreactor Technology in Process Development. *Org. Process Res. Dev.* **2004**, *8*, 455–460.

Zhao, L.; Ran, N. Recent Advances in Developing Chemoenzymatic Processes for Active Pharmaceutical Ingredients. *Org. Process Res. Dev.* **2007**, *11*, 259–267.

# Appendix A – Program Code

Presented in this appendix is the LabVIEW program for the recording of pressure data from a transducer burst pressure and back pressure monitoring experiments performed in the tangential flow filtration device. The use of a Hagen-Poiseuille model to determine condition sets for achieving particular TMP values in the filtration device is also shown.

Also presented is a comparison of the methods used to estimate TK activity, using the same kinetic data in an Excel spreadsheet and the MATLAB ODE solver.

## A.1 LabVIEW Virtual Instruments for Pressure Monitoring

LabVIEW Virtual Instruments (VIs) were used to monitor and record data from a pressure transducer connected to the tangential flow filter. The transducer was attached to a DAQ card with a 1 kHz maximum sample rate. For the recording of burst pressure, voltage measurements were made at the maximum sample rate of the card and written directly to an Excel spreadsheet, with a simple graphical output so that the user could monitor the change in pressure in real time (see Figure 57).

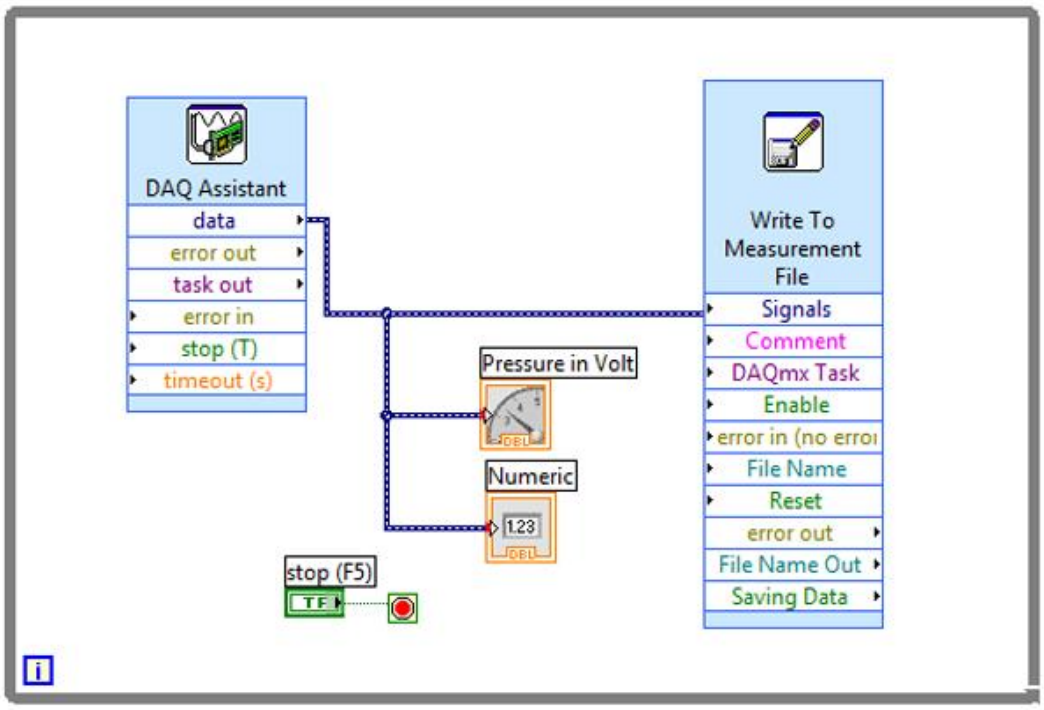


**Figure 57: A LabVIEW VI designed to acquire voltage data from the pressure transducer at the maximum sample rate of the DAQ, for burst pressure measurements.**

A separate VI was made for the recording of back pressure measurements from the filter, as the flow rate and therefore the pressure had to be allowed to stabilise over the period of several minutes to an hour. Using the maximum possible sampling rate was impractical in this case as it consumed too much memory and caused frequent crashes. Instead, the sampling rate was limited to 1 Hz with an infinite loop (see Figure 58). The data was written to an Excel file in the same way as before, and a live trace of recent measurements was also included for the purpose of troubleshooting slow leaks.

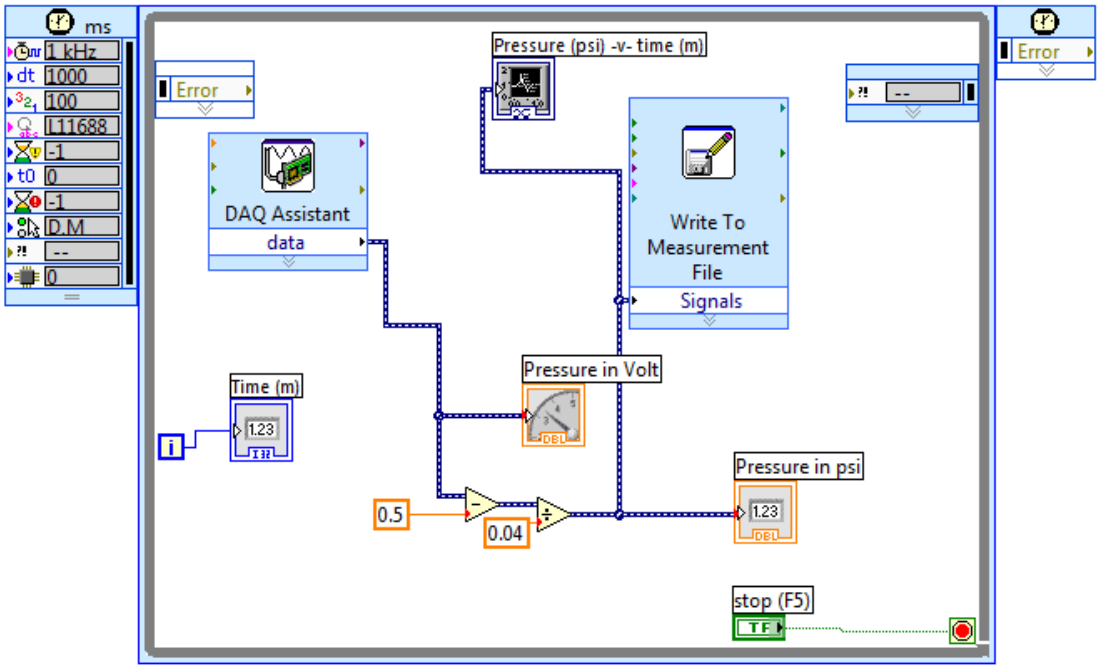


**Figure 58: A LabVIEW VI designed to acquire voltage data from the pressure transducer at 1 Hz, for back pressure measurements.**

## A.2 Comparison of an Excel Spreadsheet and MATLAB ODE Solver for TK Reaction Estimation

An Excel spreadsheet was used to make an iterative model of the progress of the TK reaction in the MIR, to estimate time points at which GA should be fed into the reaction mixture in order to sustain the reaction without causing substrate inhibition. As discussed in Section 5.3, the model was based on kinetic parameters determined by Willetts and Gyamerah and effectively assumed that the reaction was occurring in a single plug of fluid travelling down the length of the reactor (Gyamerah et al., 1997).

The spreadsheet calculations used are shown in Figure 59A, with the flow of information through the spreadsheet illustrated in Figure 59B. The model divided the reaction's progress into time intervals of defined length (10 sec to 5 min). The initial concentrations of HPA (a), GA (b) and ERY (d) were used with the equation determined by Willetts and Gyamerah (shown below) and the kinetic parameters (c) to determine the rate of reaction.

$$V = \frac{k_{cat}E_i[A][B]}{K_B[A]\left(1+\frac{[A]}{K_{iA}}\right)+K_A[B]\left(1+\frac{[B]}{K_{iB}}\right)+[A][B]+\left(\frac{K_A}{K_{iP}}\right)[B][Q]+\left(\frac{K_AK_{iB}}{K_{iP}}\right)[Q]} \quad (13)$$

The calculated rate (f) was used with the time interval (e) and the dilution factor (g) to determine the depletion and resulting concentrations of HPA, GA and ERY over the course of a single interval, assuming that the reaction rate was constant for that time. These updated concentrations were then used to recalculate the reaction rate for the next interval and the process was repeated.

At the beginning of each new interval, the concentration of GA from the previous interval (h) was compared to the reaction rate (i). If the concentration and reaction rate were such that the GA would fall below 5 mM, the model automatically assumed that another 1M GA input was required, causing the dilution factor of the reaction mixture to increase by 1/20$^{th}$ (j) and increasing the GA concentration for the next iteration accordingly (k). This information was also used to update the concentrations of HPA and ERY to reflect the dilution.

The accuracy of iterative model created in Excel was compared to that of a model created using the ODE solver function in MATLAB (The Mathworks, Inc., Natick, USA), using real data generated in the SHM T-piece reactor (see Figure 36, Section 4.2.3). Both models used the same kinetic parameters and starting conditions of 50 mM HPA and GA, with a $V_{max}$ of 5.3 mM $min^{-1}$. The MATLAB ODE solver program used is shown over the page. The models were programmed to determine the change in concentration of HPA and GA over a 120 minute reaction, and the output from each was compared to the real data already acquired (Figure 60).

There was quite a large discrepancy between the both models and the real data in the early stages of the reaction, with both models underestimating the rate of reaction over the first 30 minutes (Figure 60A). The Excel-based model appeared to fit the real data closer than the MATLAB model, catching up to the real concentration of ERY more quickly and being closer to the real data overall (Figure 60B). The divergence from the real data could well have occurred because the mutant of TK used differed from that used to determine the kinetic parameters used; however this was outside the scope of the project.

Since there was no improvement in the accuracy of the predicted data from the use of a MATLAB model, the Excel-based model was used, as it could more easily be adapted to simulate GA feeding. The data generated from the model was used to estimate where GA would need to be fed into the MIR in order to sustain the reaction without causing substrate inhibition.

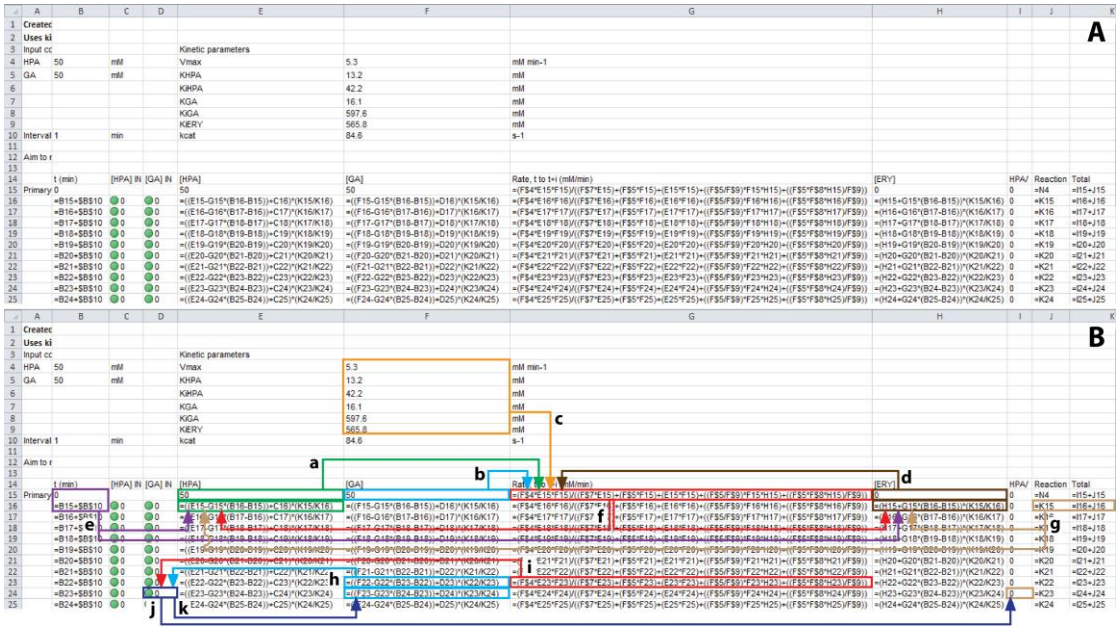


**Figure 59: The equations used in iterative Excel model of TK activity.**

**(A) Shows the equations and data used in their raw form; the overlaid boxes and arrows in (B) represent the flow of data from one data point/formula to the next.**

```
function [ dydt ] = tkmm( t, y, kcat, E, ka, kb, kia, kib, kiq )

%A refers to HPA, B to GA and Q to ERY

ERY = y(1);
HPA = y(2);
GA = y(3);

dydt     =     [     (kcat*E*HPA*GA)/(     (kb*HPA*(1+HPA/kia))     +
(ka*GA*(1+GA/kib))     +     (HPA*GA)     +     ((ka/kiq)*GA*ERY)     +
((ka*kib/kiq)*ERY) );
    -(kcat*E*HPA*GA)/(  (kb*HPA*(1+HPA/kia))  +  (ka*GA*(1+GA/kib))
+ (HPA*GA) + ((ka/kiq)*GA*ERY) + ((ka*kib/kiq)*ERY) );
    -(kcat*E*HPA*GA)/(  (kb*HPA*(1+HPA/kia))  +  (ka*GA*(1+GA/kib))
+ (HPA*GA) + ((ka/kiq)*GA*ERY) + ((ka*kib/kiq)*ERY) );
 ];
```

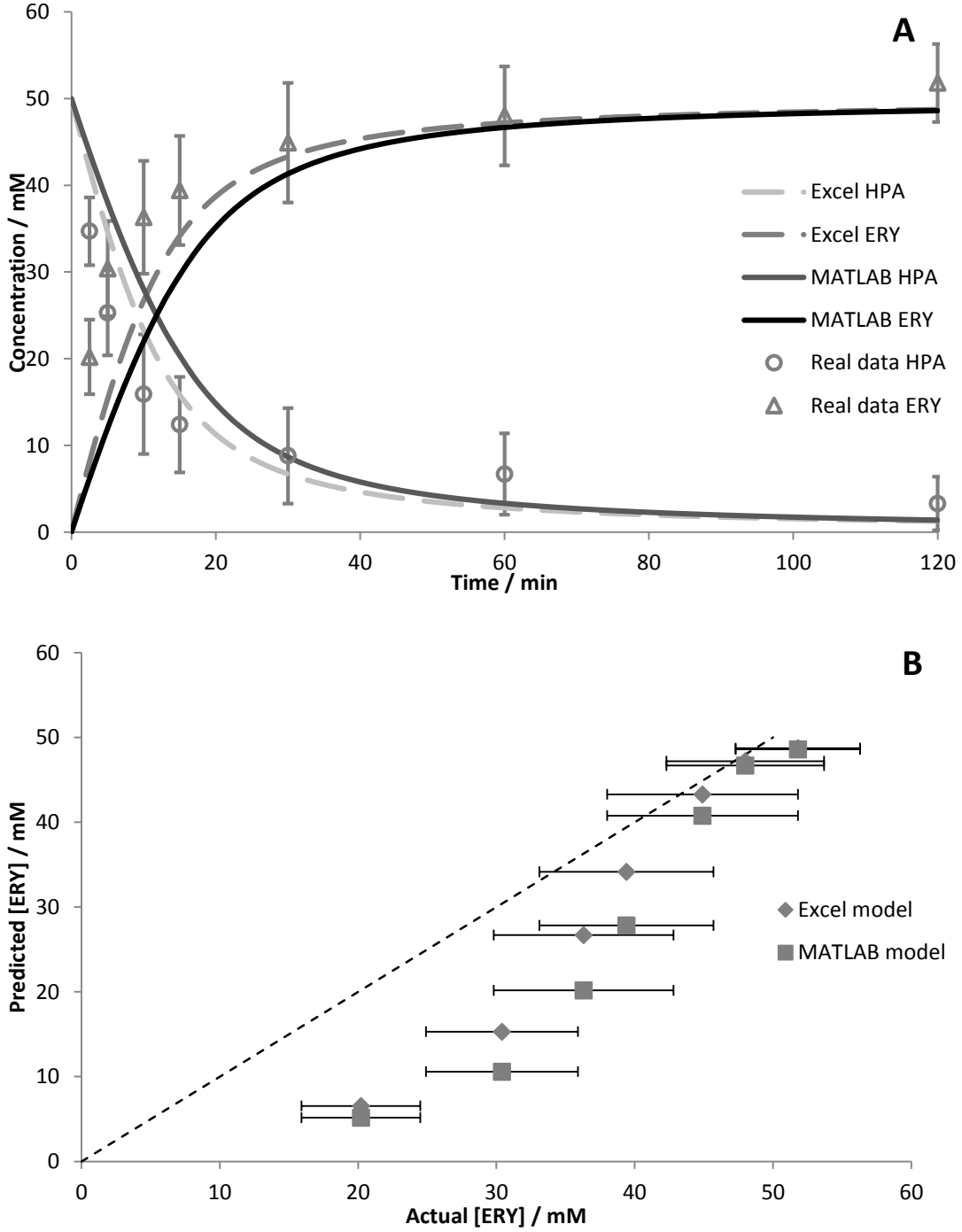


**Figure 60: Comparison of predicted reaction kinetics to real data generated in SHM reactor. (A) Reaction profile of real data compared to profiles predicted with MATLAB and Excel models (n = 6, error bars are standard deviation); (B) predicted versus actual concentration of ERY (n = 6, error bars are standard deviation).**

## A.3 Excel Spreadsheet for Prediction of TMP

Glass capillaries of determined diameter were used to constrict flow and apply pressure to the fluid in the microfluidic tangential flow filter. A range of capillary diameters were available; the Hagen-Poiseulle equation was used in a spreadsheet to estimate the transmembrane pressure (TMP) in the filter when the flow from the retentate and permeate outlets was constricted by different capillary diameters. A TMP value was then determined by finding the difference in pressure between the retentate and permeate sides (Figure 61). The pressure generated for a range of different capillary diameters (0.32, 0.5, 0.6 and 0.8 mm) was evaluated at different flow rates (0.01, 0.1, 1 and 5 mL $min^{-1}$). Different combinations of capillary diameter on the retentate and permeate were also evaluated.

Each TMP value for calculated the various condition sets was automatically tabulated in a separate sheet by a macro; the program code for this is shown over the page. The calculated TMP values are shown in Table 7.

| | A | B | C | D | E | F | G | H | I | J | K |
|---|---|---|---|---|---|---|---|---|---|---|---|
| 1 | | ρ (kg/m³) | 1000 | | | Ctrl+a to run flow ra | | | | | |
| 2 | Fluid properties | ρ (g/mm³) | =C1*1000/(1000^3) | | | Test space (copy fro | | | | | |
| 3 | | | | | | | Retentate | d | 0.8 | | |
| 4 | | μ (kg/ms) | 0.1 | | | | | l | 20 | | |
| 5 | | μ (g/mms) | =C4 | | | | Permeate | d | 0.8 | | |
| 6 | | | | | | | | l | 20 | | |
| 7 | | | | | | | | | | | |
| 8 | | | | | | | | | Q (retentate) | | |
| 9 | **Retentate** | | | | | Transmembrane P | | 0.01 | 0.1 | 1 | 5 |
| 10 | | Q (ml/min) | 5 | | | Q(permeate) | 0.01 | 0.0000113176848420 | 0.0041159236671820 | 0.146002555433607 | 2.99487603677853 |
| 11 | | Q (mm³/s) | =C10*1000/60 | | | | 0.1 | -0.0029728374981306 | 0.0011317684842090 | 0.143018400250634 | 2.99189188159556 |
| 12 | | | | | | | 1 | -0.0328143893278611 | -0.0287097833455211 | 0.113176848420903 | 2.96205032976583 |
| 13 | | | | | | | 5 | -0.1654435085711071 | -0.1613389025887671 | -0.0194522708223427 | 2.82942121052258 |
| 14 | **In** | | | | | | | | | | |
| 15 | Channel | d (mm) | 1 | | | | | | | | |
| 16 | | l (mm) | 2 | | | Macro 3 currently ru | | | | | |
| 17 | | P (Pa) | =((8*$C$2*C11^2)/(P | | | | | | | | |
| 18 | Total | P (Pa) | =C17+C23 | | | | | | | | |
| 19 | | | | | | | | | | | |
| 20 | **Out** | | | | | | | | | | |
| 21 | Capillary | d (mm) | =I3 | | | | | | | | |
| 22 | | l (mm) | =I4 | | | | | | | | |
| 23 | | P (Pa) | =((8*$C$2*C11^2)/(P | | | | | | | | |
| 24 | | | | | | | | | | | |
| 25 | | | | | | | | | | | |
| 26 | **Permeate** | | | | | | | | | | |
| 27 | | Q (ml/min) | 5 | | | | | | | | |
| 28 | | Q (mm³/s) | =C27*1000/60 | | | | | | | | |
| 29 | | | | | | | | | | | |
| 30 | Capillary | d (mm) | =I5 | | | | | | | | |
| 31 | | l (mm) | =I6 | | | | | | | | |
| 32 | | P (Pa) | =((8*$C$2*C28^2)/(P | | | | | | | | |
| 33 | | | | | | | | | | | |
| 34 | | | | | | | | | | | |
| 35 | **TMP** | | | | | | | | | | |
| 36 | | P (Pa) | =((C18+C23)/2)-C32 | | | | | | | | |
| 37 | | P (bar) | =C36*10^-5 | | | | | | | | |

**Figure 61: Equations used in TMP calculating spreadsheet.**

Condition sets were selected from Table 7 to match three TMP values as closely as possible for the cell filtration experiments. These values were 0.689, 1.379 and 2.068 bar (10, 20 and 30 psi). The condition sets used are shown in Table 8.

```
    Sub Macro_fr_&_d()
    ' fr_&_d_adjust Macro
    ' Uses flow rate adjust macro to sequence through permeate diameters (fixed length 20cm), changes retentate diameter and length, tabulates in Sheet 2

        Range("I4").Select
        ActiveCell.FormulaR1C1 = "10"
        Range("I5").Select
        ActiveCell.FormulaR1C1 = "0.32"
        Range("I3").Select
        ActiveCell.FormulaR1C1 = "0.32"
        Application.Run "'pressure drop expt space.xls'!flow_rate_adjust"
        Range("H10:K13").Select
        Application.CutCopyMode = False
        Selection.Copy
        Sheets("Sheet2").Select
        Range("d20").Select
        ActiveSheet.Paste
        Sheets("Sheet1").Select
        Range("I3").Select
        Application.CutCopyMode = False
        ActiveCell.FormulaR1C1 = "0.5"
        Range("I4").Select
        Application.Run "'pressure drop expt space.xls'!flow_rate_adjust"
        Range("H10:K13").Select
        Application.CutCopyMode = False
        Selection.Copy
        Sheets("Sheet2").Select
        Range("h20").Select
        ActiveSheet.Paste
        Sheets("Sheet1").Select
        Range("I3").Select
        Application.CutCopyMode = False
        ActiveCell.FormulaR1C1 = "0.6"
        Range("I4").Select
        Application.Run "'pressure drop expt space.xls'!flow_rate_adjust"
        Range("H10:K13").Select
        Application.CutCopyMode = False
        Selection.Copy
        Sheets("Sheet2").Select
        Range("l20").Select
        ActiveSheet.Paste
        Sheets("Sheet1").Select
        Range("I3").Select
        Application.CutCopyMode = False
        ActiveCell.FormulaR1C1 = "0.8"
        Range("I4").Select
        Application.Run "'pressure drop expt space.xls'!flow_rate_adjust"
        Range("H10:K13").Select
        Application.CutCopyMode = False
        Selection.Copy
        Sheets("Sheet2").Select
        Range("p20").Select
        ActiveSheet.Paste
        Sheets("Sheet1").Select

        Range("I4").Select
        ActiveCell.FormulaR1C1 = "20"
        Range("I3").Select
        ActiveCell.FormulaR1C1 = "0.32"
        Application.Run "'pressure drop expt space.xls'!flow_rate_adjust"
        Range("H10:K13").Select
        Application.CutCopyMode = False
        Selection.Copy
        Sheets("Sheet2").Select
        Range("T20").Select
        ActiveSheet.Paste
        Sheets("Sheet1").Select
        Range("I3").Select
        Application.CutCopyMode = False
        ActiveCell.FormulaR1C1 = "0.5"
        Range("I4").Select
        Application.Run "'pressure drop expt space.xls'!flow_rate_adjust"
        Range("H10:K13").Select
        Application.CutCopyMode = False
        Selection.Copy
        Sheets("Sheet2").Select
        Range("X20").Select
        ActiveSheet.Paste
        Sheets("Sheet1").Select
        Range("I3").Select
        Application.CutCopyMode = False
        ActiveCell.FormulaR1C1 = "0.6"
        Range("I4").Select
        Application.Run "'pressure drop expt space.xls'!flow_rate_adjust"
        Range("H10:K13").Select
        Application.CutCopyMode = False
        Selection.Copy
        Sheets("Sheet2").Select
        Range("AB20").Select
        ActiveSheet.Paste
        Sheets("Sheet1").Select
        Range("I3").Select
        Application.CutCopyMode = False
        ActiveCell.FormulaR1C1 = "0.8"
        Range("I4").Select
        Application.Run "'pressure drop expt space.xls'!flow_rate_adjust"
        Range("H10:K13").Select
        Application.CutCopyMode = False
        Selection.Copy
        Sheets("Sheet2").Select
        Range("AF20").Select
        ActiveSheet.Paste
        Sheets("Sheet1").Select

        'Repeat for next permeate d value
        Range("I4").Select
        ActiveCell.FormulaR1C1 = "10"
        Range("I5").Select
        ActiveCell.FormulaR1C1 = "0.5"
        Range("I3").Select
        ActiveCell.FormulaR1C1 = "0.32"
        Application.Run "'pressure drop expt space.xls'!flow_rate_adjust"
        Range("H10:K13").Select
        Application.CutCopyMode = False
        Selection.Copy
        Sheets("Sheet2").Select
        Range("d24").Select
        ActiveSheet.Paste
        Sheets("Sheet1").Select
        Range("I3").Select
        Application.CutCopyMode = False
```

```
        ActiveCell.FormulaR1C1 = "0.5"
        Range("I4").Select
        Application.Run "'pressure drop
expt space.xls'!flow_rate_adjust"
        Range("H10:K13").Select
        Application.CutCopyMode = False
        Selection.Copy
        Sheets("Sheet2").Select
        Range("h24").Select
        ActiveSheet.Paste
        Sheets("Sheet1").Select
        Range("I3").Select
        Application.CutCopyMode = False
        ActiveCell.FormulaR1C1 = "0.6"
        Range("I4").Select
        Application.Run "'pressure drop
expt space.xls'!flow_rate_adjust"
        Range("H10:K13").Select
        Application.CutCopyMode = False
        Selection.Copy
        Sheets("Sheet2").Select
        Range("l24").Select
        ActiveSheet.Paste
        Sheets("Sheet1").Select
        Range("I3").Select
        Application.CutCopyMode = False
        ActiveCell.FormulaR1C1 = "0.8"
        Range("I4").Select
        Application.Run "'pressure drop
expt space.xls'!flow_rate_adjust"
        Range("H10:K13").Select
        Application.CutCopyMode = False
        Selection.Copy
        Sheets("Sheet2").Select
        Range("p24").Select
        ActiveSheet.Paste
        Sheets("Sheet1").Select

        Range("I4").Select
        ActiveCell.FormulaR1C1 = "20"
        Range("I3").Select
        ActiveCell.FormulaR1C1 = "0.32"
        Application.Run "'pressure drop
expt space.xls'!flow_rate_adjust"
        Range("H10:K13").Select
        Application.CutCopyMode = False
        Selection.Copy
        Sheets("Sheet2").Select
        Range("T24").Select
        ActiveSheet.Paste
        Sheets("Sheet1").Select
        Range("I3").Select
        Application.CutCopyMode = False
        ActiveCell.FormulaR1C1 = "0.5"
        Range("I4").Select
        Application.Run "'pressure drop
expt space.xls'!flow_rate_adjust"
        Range("H10:K13").Select
        Application.CutCopyMode = False
        Selection.Copy
        Sheets("Sheet2").Select
        Range("X24").Select
        ActiveSheet.Paste
        Sheets("Sheet1").Select
        Range("I3").Select
        Application.CutCopyMode = False
        ActiveCell.FormulaR1C1 = "0.6"
        Range("I4").Select
        Application.Run "'pressure drop
expt space.xls'!flow_rate_adjust"
        Range("H10:K13").Select
        Application.CutCopyMode = False
        Selection.Copy
        Sheets("Sheet2").Select
        Range("AB24").Select
        ActiveSheet.Paste
        Sheets("Sheet1").Select
        Range("I3").Select
        Application.CutCopyMode = False
        ActiveCell.FormulaR1C1 = "0.8"
        Range("I4").Select
        Application.Run "'pressure drop
expt space.xls'!flow_rate_adjust"
        Range("H10:K13").Select
        Application.CutCopyMode = False
        Selection.Copy
        Sheets("Sheet2").Select
        Range("AF24").Select
        ActiveSheet.Paste
        Sheets("Sheet1").Select

        'Repeat for next permeate d
value
        Range("I4").Select
        ActiveCell.FormulaR1C1 = "10"
        Range("I5").Select
        ActiveCell.FormulaR1C1 = "0.6"
        Range("I3").Select
        ActiveCell.FormulaR1C1 = "0.32"
        Application.Run "'pressure drop
expt space.xls'!flow_rate_adjust"
        Range("H10:K13").Select
        Application.CutCopyMode = False
        Selection.Copy
        Sheets("Sheet2").Select
        Range("d28").Select
        ActiveSheet.Paste
        Sheets("Sheet1").Select
        Range("I3").Select
        Application.CutCopyMode = False
        ActiveCell.FormulaR1C1 = "0.5"
        Range("I4").Select
        Application.Run "'pressure drop
expt space.xls'!flow_rate_adjust"
        Range("H10:K13").Select
        Application.CutCopyMode = False
        Selection.Copy
        Sheets("Sheet2").Select
        Range("h28").Select
        ActiveSheet.Paste
        Sheets("Sheet1").Select
        Range("I3").Select
        Application.CutCopyMode = False
        ActiveCell.FormulaR1C1 = "0.6"
        Range("I4").Select
        Application.Run "'pressure drop
expt space.xls'!flow_rate_adjust"
        Range("H10:K13").Select
        Application.CutCopyMode = False
        Selection.Copy
        Sheets("Sheet2").Select
        Range("l28").Select
        ActiveSheet.Paste
        Sheets("Sheet1").Select
        Range("I3").Select
        Application.CutCopyMode = False
```

```
        ActiveCell.FormulaR1C1 = "0.8"
        Range("I4").Select
        Application.Run "'pressure drop
expt space.xls'!flow_rate_adjust"
        Range("H10:K13").Select
        Application.CutCopyMode = False
        Selection.Copy
        Sheets("Sheet2").Select
        Range("p28").Select
        ActiveSheet.Paste
        Sheets("Sheet1").Select

        Range("I4").Select
        ActiveCell.FormulaR1C1 = "20"
        Range("I3").Select
        ActiveCell.FormulaR1C1 = "0.32"
        Application.Run "'pressure drop
expt space.xls'!flow_rate_adjust"
        Range("H10:K13").Select
        Application.CutCopyMode = False
        Selection.Copy
        Sheets("Sheet2").Select
        Range("T28").Select
        ActiveSheet.Paste
        Sheets("Sheet1").Select
        Range("I3").Select
        Application.CutCopyMode = False
        ActiveCell.FormulaR1C1 = "0.5"
        Range("I4").Select
        Application.Run "'pressure drop
expt space.xls'!flow_rate_adjust"
        Range("H10:K13").Select
        Application.CutCopyMode = False
        Selection.Copy
        Sheets("Sheet2").Select
        Range("X28").Select
        ActiveSheet.Paste
        Sheets("Sheet1").Select
        Range("I3").Select
        Application.CutCopyMode = False
        ActiveCell.FormulaR1C1 = "0.6"
        Range("I4").Select
        Application.Run "'pressure drop
expt space.xls'!flow_rate_adjust"
        Range("H10:K13").Select
        Application.CutCopyMode = False
        Selection.Copy
        Sheets("Sheet2").Select
        Range("AB28").Select
        ActiveSheet.Paste
        Sheets("Sheet1").Select
        Range("I3").Select
        Application.CutCopyMode = False
        ActiveCell.FormulaR1C1 = "0.8"
        Range("I4").Select
        Application.Run "'pressure drop
expt space.xls'!flow_rate_adjust"
        Range("H10:K13").Select
        Application.CutCopyMode = False
        Selection.Copy
        Sheets("Sheet2").Select
        Range("AF28").Select
        ActiveSheet.Paste
        Sheets("Sheet1").Select

        'Repeat  for  next  permeate  d
value
        Range("I4").Select
        ActiveCell.FormulaR1C1 = "10"
        Range("I5").Select
        ActiveCell.FormulaR1C1 = "0.8"
        Range("I3").Select
        ActiveCell.FormulaR1C1 = "0.32"
        Application.Run "'pressure drop
expt space.xls'!flow_rate_adjust"
        Range("H10:K13").Select
        Application.CutCopyMode = False
        Selection.Copy
        Sheets("Sheet2").Select
        Range("d32").Select
        ActiveSheet.Paste
        Sheets("Sheet1").Select
        Range("I3").Select
        Application.CutCopyMode = False
        ActiveCell.FormulaR1C1 = "0.5"
        Range("I4").Select
        Application.Run "'pressure drop
expt space.xls'!flow_rate_adjust"
        Range("H10:K13").Select
        Application.CutCopyMode = False
        Selection.Copy
        Sheets("Sheet2").Select
        Range("h32").Select
        ActiveSheet.Paste
        Sheets("Sheet1").Select
        Range("I3").Select
        Application.CutCopyMode = False
        ActiveCell.FormulaR1C1 = "0.6"
        Range("I4").Select
        Application.Run "'pressure drop
expt space.xls'!flow_rate_adjust"
        Range("H10:K13").Select
        Application.CutCopyMode = False
        Selection.Copy
        Sheets("Sheet2").Select
        Range("l32").Select
        ActiveSheet.Paste
        Sheets("Sheet1").Select
        Range("I3").Select
        Application.CutCopyMode = False
        ActiveCell.FormulaR1C1 = "0.8"
        Range("I4").Select
        Application.Run "'pressure drop
expt space.xls'!flow_rate_adjust"
        Range("H10:K13").Select
        Application.CutCopyMode = False
        Selection.Copy
        Sheets("Sheet2").Select
        Range("p32").Select
        ActiveSheet.Paste
        Sheets("Sheet1").Select

        Range("I4").Select
        ActiveCell.FormulaR1C1 = "20"
        Range("I3").Select
        ActiveCell.FormulaR1C1 = "0.32"
        Application.Run "'pressure drop
expt space.xls'!flow_rate_adjust"
        Range("H10:K13").Select
        Application.CutCopyMode = False
        Selection.Copy
        Sheets("Sheet2").Select
        Range("T32").Select
        ActiveSheet.Paste
        Sheets("Sheet1").Select
        Range("I3").Select
```

```
        Application.CutCopyMode = False
        ActiveCell.FormulaR1C1 = "0.5"
        Range("I4").Select
        Application.Run "'pressure drop
expt space.xls'!flow_rate_adjust"
        Range("H10:K13").Select
        Application.CutCopyMode = False
        Selection.Copy
        Sheets("Sheet2").Select
        Range("X32").Select
        ActiveSheet.Paste
        Sheets("Sheet1").Select
        Range("I3").Select
        Application.CutCopyMode = False
        ActiveCell.FormulaR1C1 = "0.6"
        Range("I4").Select
        Application.Run "'pressure drop
expt space.xls'!flow_rate_adjust"
        Range("H10:K13").Select
        Application.CutCopyMode = False
        Selection.Copy
        Sheets("Sheet2").Select
        Range("AB32").Select
        ActiveSheet.Paste
        Sheets("Sheet1").Select
        Range("I3").Select
        Application.CutCopyMode = False
        ActiveCell.FormulaR1C1 = "0.8"
        Range("I4").Select
        Application.Run "'pressure drop
expt space.xls'!flow_rate_adjust"
        Range("H10:K13").Select
        Application.CutCopyMode = False
        Selection.Copy
        Sheets("Sheet2").Select
        Range("AF32").Select
        ActiveSheet.Paste
        Sheets("Sheet1").Select
    End Sub
```

| l (mm) | | | 100 | | | | | | | | | | | | | | | |
|---|---|---|---|---|---|---|---|---|---|---|---|---|---|---|---|---|---|---|
| | d (mm) | | 0.32 | | | | 0.5 | | | | 0.6 | | | | 0.8 | | | |
| | | Q (ml min$^{-1}$) | 0.01 | 0.1 | 1 | 5 | 0.01 | 0.1 | 1 | 5 | 0.01 | 0.1 | 1 | 5 | 0.01 | 0.1 | 1 | 5 |
| 100 | 0.32 | 0.01 | 0.00 | 0.06 | 0.75 | 6.06 | -0.01 | 0.01 | 0.22 | 3.37 | -0.01 | 0.00 | 0.16 | 3.08 | -0.01 | 0.00 | 0.12 | 2.91 |
| | | 0.1 | -0.06 | 0.00 | 0.70 | 6.00 | -0.06 | -0.05 | 0.16 | 3.31 | -0.06 | -0.06 | 0.10 | 3.03 | -0.06 | -0.06 | 0.06 | 2.85 |
| | | 1 | -0.64 | -0.58 | 0.11 | 5.42 | -0.65 | -0.64 | -0.43 | 2.73 | -0.65 | -0.64 | -0.48 | 2.44 | -0.65 | -0.64 | -0.52 | 2.26 |
| | | 5 | -3.23 | -3.17 | -2.48 | 2.83 | -3.24 | -3.23 | -3.02 | 0.13 | -3.24 | -3.23 | -3.07 | -0.15 | -3.24 | -3.24 | -3.11 | -0.33 |
| | 0.5 | 0.01 | 0.01 | 0.06 | 0.76 | 6.07 | 0.00 | 0.01 | 0.22 | 3.37 | 0.00 | 0.01 | 0.16 | 3.09 | 0.00 | 0.00 | 0.13 | 2.91 |
| | | 0.1 | 0.00 | 0.06 | 0.75 | 6.06 | -0.01 | 0.00 | 0.21 | 3.36 | -0.01 | 0.00 | 0.15 | 3.08 | -0.01 | -0.01 | 0.12 | 2.90 |
| | | 1 | -0.10 | -0.04 | 0.65 | 5.96 | -0.11 | -0.10 | 0.11 | 3.26 | -0.11 | -0.10 | 0.06 | 2.98 | -0.11 | -0.11 | 0.02 | 2.80 |
| | | 5 | -0.54 | -0.48 | 0.22 | 5.52 | -0.54 | -0.53 | -0.32 | 2.83 | -0.54 | -0.54 | -0.38 | 2.55 | -0.54 | -0.54 | -0.41 | 2.37 |
| | 0.6 | 0.01 | 0.01 | 0.07 | 0.76 | 6.07 | 0.00 | 0.01 | 0.22 | 3.37 | 0.00 | 0.01 | 0.17 | 3.09 | 0.00 | 0.00 | 0.13 | 2.91 |
| | | 0.1 | 0.00 | 0.06 | 0.76 | 6.06 | 0.00 | 0.01 | 0.22 | 3.37 | 0.00 | 0.00 | 0.16 | 3.09 | -0.01 | 0.00 | 0.12 | 2.91 |
| | | 1 | -0.05 | 0.01 | 0.71 | 6.02 | -0.05 | -0.04 | 0.17 | 3.32 | -0.05 | -0.05 | 0.11 | 3.04 | -0.05 | -0.05 | 0.08 | 2.86 |
| | | 5 | -0.26 | -0.20 | 0.50 | 5.81 | -0.26 | -0.25 | -0.04 | 3.11 | -0.26 | -0.26 | -0.10 | 2.83 | -0.26 | -0.26 | -0.13 | 2.65 |
| | 0.8 | 0.01 | 0.01 | 0.07 | 0.76 | 6.07 | 0.00 | 0.01 | 0.22 | 3.37 | 0.00 | 0.01 | 0.17 | 3.09 | 0.00 | 0.00 | 0.13 | 2.91 |
| | | 0.1 | 0.00 | 0.06 | 0.76 | 6.07 | 0.00 | 0.01 | 0.22 | 3.37 | 0.00 | 0.00 | 0.16 | 3.09 | 0.00 | 0.00 | 0.13 | 2.91 |
| | | 1 | -0.01 | 0.05 | 0.74 | 6.05 | -0.02 | 0.00 | 0.21 | 3.36 | -0.02 | -0.01 | 0.15 | 3.07 | -0.02 | -0.01 | 0.11 | 2.90 |
| | | 5 | -0.08 | -0.02 | 0.68 | 5.98 | -0.08 | -0.07 | 0.14 | 3.29 | -0.08 | -0.08 | 0.08 | 3.01 | -0.08 | -0.08 | 0.05 | 2.83 |
| 200 | 0.32 | 0.01 | -0.01 | 0.05 | 0.75 | 6.05 | -0.01 | 0.00 | 0.21 | 3.36 | -0.01 | -0.01 | 0.15 | 3.08 | -0.01 | -0.01 | 0.12 | 2.90 |
| | | 0.1 | -0.12 | -0.06 | 0.63 | 5.94 | -0.13 | -0.12 | 0.09 | 3.24 | -0.13 | -0.12 | 0.04 | 2.96 | -0.13 | -0.13 | 0.00 | 2.78 |
| | | 1 | -1.29 | -1.23 | -0.53 | 4.77 | -1.29 | -1.28 | -1.07 | 2.08 | -1.29 | -1.29 | -1.13 | 1.80 | -1.30 | -1.29 | -1.17 | 1.62 |
| | | 5 | -6.47 | -6.41 | -5.72 | -0.41 | -6.47 | -6.46 | -6.25 | -3.10 | -6.48 | -6.47 | -6.31 | -3.38 | -6.48 | -6.47 | -6.35 | -3.56 |
| | 0.5 | 0.01 | 0.00 | 0.06 | 0.76 | 6.07 | 0.00 | 0.01 | 0.22 | 3.37 | 0.00 | 0.00 | 0.16 | 3.09 | 0.00 | 0.00 | 0.13 | 2.91 |
| | | 0.1 | -0.02 | 0.04 | 0.74 | 6.05 | -0.02 | -0.01 | 0.20 | 3.35 | -0.02 | -0.02 | 0.14 | 3.07 | -0.02 | -0.02 | 0.11 | 2.89 |
| | | 1 | -0.21 | -0.15 | 0.54 | 5.85 | -0.22 | -0.21 | 0.00 | 3.16 | -0.22 | -0.21 | -0.05 | 2.87 | -0.22 | -0.21 | -0.09 | 2.70 |
| | | 5 | -1.08 | -1.02 | -0.33 | 4.98 | -1.09 | -1.07 | -0.86 | 2.29 | -1.09 | -1.08 | -0.92 | 2.00 | -1.09 | -1.08 | -0.96 | 1.83 |
| | 0.6 | 0.01 | 0.01 | 0.06 | 0.76 | 6.07 | 0.00 | 0.01 | 0.22 | 3.37 | 0.00 | 0.01 | 0.16 | 3.09 | 0.00 | 0.00 | 0.13 | 2.91 |
| | | 0.1 | 0.00 | 0.06 | 0.75 | 6.06 | -0.01 | 0.00 | 0.21 | 3.36 | -0.01 | 0.00 | 0.16 | 3.08 | -0.01 | -0.01 | 0.12 | 2.90 |
| | | 1 | -0.10 | -0.04 | 0.66 | 5.96 | -0.10 | -0.09 | 0.12 | 3.27 | -0.10 | -0.10 | 0.06 | 2.99 | -0.10 | -0.10 | 0.02 | 2.81 |
| | | 5 | -0.52 | -0.46 | 0.24 | 5.54 | -0.52 | -0.51 | -0.30 | 2.85 | -0.52 | -0.52 | -0.36 | 2.57 | -0.52 | -0.52 | -0.39 | 2.39 |
| | 0.8 | 0.01 | 0.01 | 0.07 | 0.76 | 6.07 | 0.00 | 0.01 | 0.22 | 3.37 | 0.00 | 0.01 | 0.17 | 3.09 | 0.00 | 0.00 | 0.13 | 2.91 |
| | | 0.1 | 0.00 | 0.06 | 0.76 | 6.06 | 0.00 | 0.01 | 0.22 | 3.37 | 0.00 | 0.00 | 0.16 | 3.09 | 0.00 | 0.00 | 0.13 | 2.91 |
| | | 1 | -0.03 | 0.03 | 0.73 | 6.03 | -0.03 | -0.02 | 0.19 | 3.34 | -0.03 | -0.03 | 0.13 | 3.06 | -0.03 | -0.03 | 0.10 | 2.88 |
| | | 5 | -0.16 | -0.10 | 0.59 | 5.90 | -0.16 | -0.15 | 0.06 | 3.21 | -0.17 | -0.16 | 0.00 | 2.93 | -0.17 | -0.16 | -0.04 | 2.75 |

| l (mm) | | | 200 | | | | | | | | | | | | | | | |
|---|---|---|---|---|---|---|---|---|---|---|---|---|---|---|---|---|---|---|
| | d (mm) | | 0.32 | | | | 0.5 | | | | 0.6 | | | | 0.8 | | | |
| | | Q (ml min$^{-1}$) | 0.01 | 0.1 | 1 | 5 | 0.01 | 0.1 | 1 | 5 | 0.01 | 0.1 | 1 | 5 | 0.01 | 0.1 | 1 | 5 |
| 100 | 0.32 | 0.01 | 0.01 | 0.12 | 1.40 | 9.30 | 0.00 | 0.02 | 0.32 | 3.91 | -0.01 | 0.01 | 0.21 | 3.35 | -0.01 | 0.00 | 0.14 | 2.99 |
| | | 0.1 | -0.05 | 0.07 | 1.34 | 9.24 | -0.06 | -0.04 | 0.27 | 3.85 | -0.06 | -0.05 | 0.15 | 3.29 | -0.06 | -0.06 | 0.08 | 2.93 |
| | | 1 | -0.63 | -0.52 | 0.76 | 8.66 | -0.65 | -0.62 | -0.32 | 3.27 | -0.65 | -0.64 | -0.43 | 2.71 | -0.65 | -0.64 | -0.50 | 2.35 |
| | | 5 | -3.23 | -3.11 | -1.83 | 6.07 | -3.24 | -3.22 | -2.91 | 0.68 | -3.24 | -3.23 | -3.02 | 0.12 | -3.24 | -3.23 | -3.09 | -0.24 |
| | 0.5 | 0.01 | 0.01 | 0.13 | 1.41 | 9.30 | 0.00 | 0.02 | 0.33 | 3.91 | 0.00 | 0.01 | 0.22 | 3.35 | 0.00 | 0.00 | 0.15 | 2.99 |
| | | 0.1 | 0.00 | 0.12 | 1.40 | 9.29 | -0.01 | 0.01 | 0.32 | 3.91 | -0.01 | 0.00 | 0.21 | 3.34 | -0.01 | -0.01 | 0.14 | 2.98 |
| | | 1 | -0.10 | 0.02 | 1.30 | 9.20 | -0.11 | -0.09 | 0.22 | 3.81 | -0.11 | -0.10 | 0.11 | 3.24 | -0.11 | -0.10 | 0.04 | 2.89 |
| | | 5 | -0.53 | -0.41 | 0.87 | 8.76 | -0.54 | -0.52 | -0.21 | 3.37 | -0.54 | -0.53 | -0.33 | 2.81 | -0.54 | -0.54 | -0.40 | 2.45 |
| | 0.6 | 0.01 | 0.01 | 0.13 | 1.41 | 9.30 | 0.00 | 0.02 | 0.33 | 3.92 | 0.00 | 0.01 | 0.22 | 3.35 | 0.00 | 0.00 | 0.15 | 2.99 |
| | | 0.1 | 0.01 | 0.13 | 1.40 | 9.30 | 0.00 | 0.02 | 0.33 | 3.91 | 0.00 | 0.01 | 0.21 | 3.35 | 0.00 | 0.00 | 0.14 | 2.99 |
| | | 1 | -0.04 | 0.08 | 1.36 | 9.25 | -0.05 | -0.03 | 0.28 | 3.86 | -0.05 | -0.04 | 0.17 | 3.30 | -0.05 | -0.05 | 0.09 | 2.94 |
| | | 5 | -0.25 | -0.13 | 1.15 | 9.04 | -0.26 | -0.24 | 0.07 | 3.65 | -0.26 | -0.25 | -0.04 | 3.09 | -0.26 | -0.26 | -0.12 | 2.73 |
| | 0.8 | 0.01 | 0.01 | 0.13 | 1.41 | 9.31 | 0.00 | 0.02 | 0.33 | 3.92 | 0.00 | 0.01 | 0.22 | 3.35 | 0.00 | 0.00 | 0.15 | 3.00 |
| | | 0.1 | 0.01 | 0.13 | 1.41 | 9.30 | 0.00 | 0.02 | 0.33 | 3.91 | 0.00 | 0.01 | 0.22 | 3.35 | 0.00 | 0.00 | 0.14 | 2.99 |
| | | 1 | 0.00 | 0.11 | 1.39 | 9.29 | -0.01 | 0.01 | 0.31 | 3.90 | -0.02 | 0.00 | 0.20 | 3.34 | -0.02 | -0.01 | 0.13 | 2.98 |
| | | 5 | -0.07 | 0.05 | 1.33 | 9.22 | -0.08 | -0.06 | 0.25 | 3.83 | -0.08 | -0.07 | 0.14 | 3.27 | -0.08 | -0.08 | 0.06 | 2.91 |
| 200 | 0.32 | 0.01 | 0.00 | 0.12 | 1.40 | 9.29 | -0.01 | 0.01 | 0.32 | 3.90 | -0.01 | 0.00 | 0.21 | 3.34 | -0.01 | -0.01 | 0.13 | 2.98 |
| | | 0.1 | -0.12 | 0.00 | 1.28 | 9.18 | -0.13 | -0.11 | 0.20 | 3.79 | -0.13 | -0.12 | 0.09 | 3.22 | -0.13 | -0.13 | 0.02 | 2.87 |
| | | 1 | -1.28 | -1.16 | 0.11 | 8.01 | -1.29 | -1.27 | -0.96 | 2.62 | -1.29 | -1.28 | -1.08 | 2.06 | -1.29 | -1.29 | -1.15 | 1.70 |
| | | 5 | -6.46 | -6.35 | -5.07 | 2.83 | -6.47 | -6.45 | -6.15 | -2.56 | -6.47 | -6.46 | -6.26 | -3.12 | -6.48 | -6.47 | -6.33 | -3.48 |
| | 0.5 | 0.01 | 0.01 | 0.13 | 1.41 | 9.30 | 0.00 | 0.02 | 0.33 | 3.91 | 0.00 | 0.01 | 0.22 | 3.35 | 0.00 | 0.00 | 0.14 | 2.99 |
| | | 0.1 | -0.01 | 0.11 | 1.39 | 9.28 | -0.02 | 0.00 | 0.31 | 3.89 | -0.02 | -0.01 | 0.20 | 3.33 | -0.02 | -0.02 | 0.12 | 2.97 |
| | | 1 | -0.20 | -0.09 | 1.19 | 9.09 | -0.22 | -0.19 | 0.11 | 3.70 | -0.22 | -0.21 | 0.00 | 3.14 | -0.22 | -0.21 | -0.07 | 2.78 |
| | | 5 | -1.07 | -0.96 | 0.32 | 8.22 | -1.08 | -1.06 | -0.76 | 2.83 | -1.09 | -1.07 | -0.87 | 2.27 | -1.09 | -1.08 | -0.94 | 1.91 |
| | 0.6 | 0.01 | 0.01 | 0.13 | 1.41 | 9.30 | 0.00 | 0.02 | 0.33 | 3.91 | 0.00 | 0.01 | 0.22 | 3.35 | 0.00 | 0.00 | 0.15 | 2.99 |
| | | 0.1 | 0.00 | 0.12 | 1.40 | 9.29 | -0.01 | 0.01 | 0.32 | 3.91 | -0.01 | 0.00 | 0.21 | 3.34 | -0.01 | -0.01 | 0.14 | 2.98 |
| | | 1 | -0.09 | 0.03 | 1.30 | 9.20 | -0.10 | -0.08 | 0.23 | 3.81 | -0.10 | -0.09 | 0.11 | 3.25 | -0.10 | -0.10 | 0.04 | 2.89 |
| | | 5 | -0.51 | -0.39 | 0.88 | 8.78 | -0.52 | -0.50 | -0.19 | 3.39 | -0.52 | -0.51 | -0.31 | 2.83 | -0.52 | -0.52 | -0.38 | 2.47 |
| | 0.8 | 0.01 | 0.01 | 0.13 | 1.41 | 9.31 | 0.00 | 0.02 | 0.33 | 3.92 | 0.00 | 0.01 | 0.22 | 3.35 | 0.00 | 0.00 | 0.15 | 2.99 |
| | | 0.1 | 0.01 | 0.13 | 1.41 | 9.30 | 0.00 | 0.02 | 0.33 | 3.91 | 0.00 | 0.01 | 0.21 | 3.35 | 0.00 | 0.00 | 0.14 | 2.99 |
| | | 1 | -0.02 | 0.10 | 1.38 | 9.27 | -0.03 | -0.01 | 0.30 | 3.88 | -0.03 | -0.02 | 0.18 | 3.32 | -0.03 | -0.03 | 0.11 | 2.96 |
| | | 5 | -0.15 | -0.04 | 1.24 | 9.14 | -0.16 | -0.14 | 0.16 | 3.75 | -0.16 | -0.15 | 0.05 | 3.19 | -0.17 | -0.16 | -0.02 | 2.83 |

**Table 7: Transmembrane pressure values calculated using the Hagen-Poiseuille spreadsheet.**

**Parameters along the top of the table correspond to the conditions on the retentate side, parameters along the left side of the table correspond to conditions on the permeate side. l is capillary length, d is capillary diameter and Q is flow rate.**

| TMP (bar/psi) | l (capillary length, mm) | | d (capillary diameter, mm) | | Q (flow rate, mm $min^{-1}$) | |
|---|---|---|---|---|---|---|
| | **Retentate** | **Permeate** | **Retentate** | **Permeate** | **Retentate** | **Permeate** |
| **0.696/10** | 100 | 100 | 0.32 | 0.32 | 0.1 | 1.0 |
| **1.344/20** | 200 | 100 | 0.32 | 0.32 | 0.1 | 1.0 |
| **2.078/30** | 100 | 200 | 0.5 | 0.32 | 1.0 | 5.0 |

**Table 8: Condition sets used to achieve specific TMP in cell filtration experiments.**

# Appendix B – Mechanical Drawings

This appendix contains the mechanical drawings for the individual PC or PMMA parts that made up the microfluidic tangential flow filtration device and multi-input reactor used in this thesis, as well as PMMA moulds used for the casting of PDMS parts. Unless otherwise indicated, all dimensions are shown in mm.

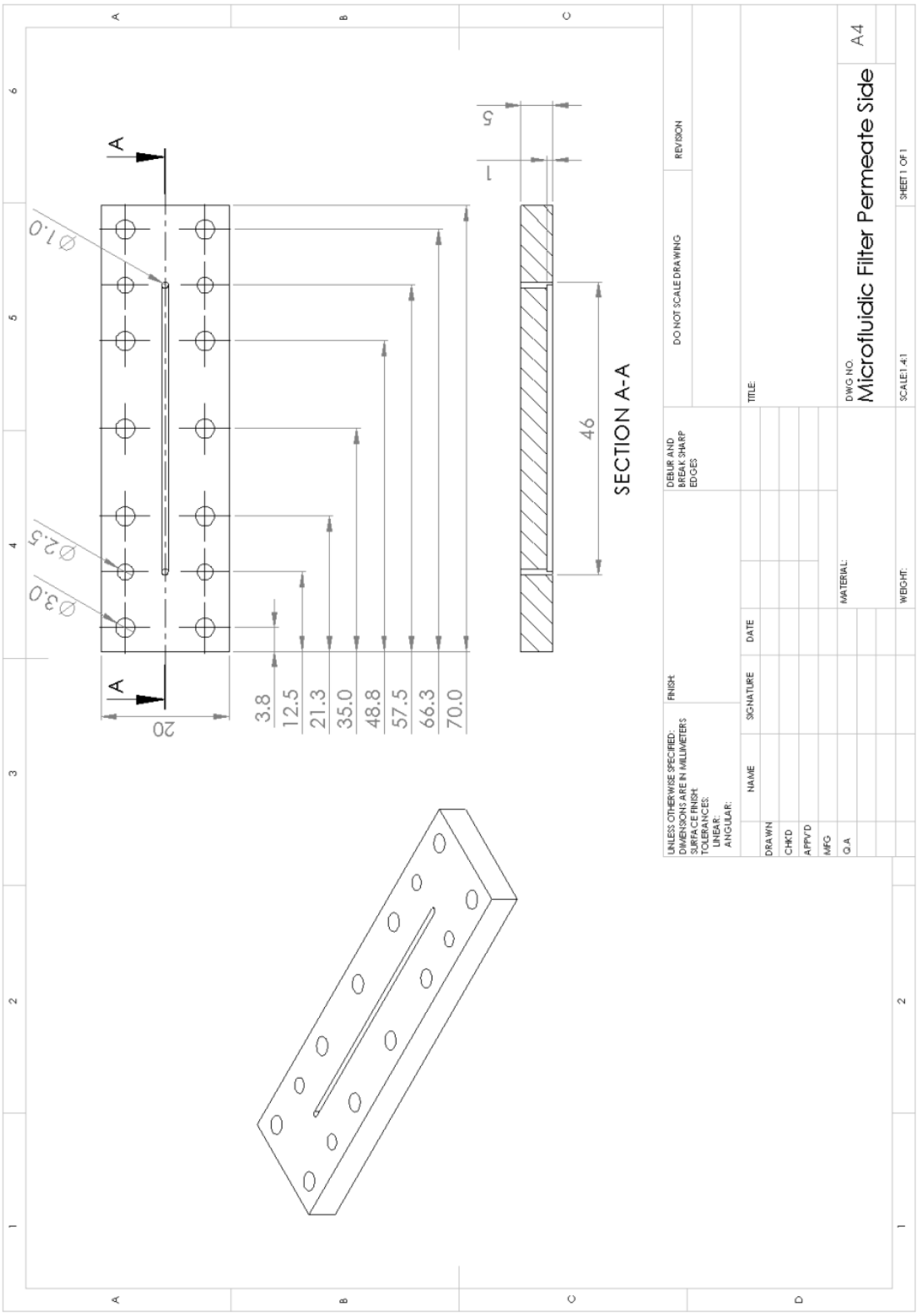
SECTION A-A
Microfluidic Filter Permeate Side
A4
DO NOT SCALE DRAWING
REVISION
DEBUR AND BREAK SHARP EDGES
FINISH
UNLESS OTHERWISE SPECIFIED:
DIMENSIONS ARE IN MILLIMETERS
SURFACE FINISH:
TOLERANCES:
LINEAR:
ANGULAR:
NAME
SIGNATURE
DATE
DRAWN
CHK'D
APPV'D
MFG
Q.A
MATERIAL:
TITLE:
DWG NO.
SCALE 1:4.1
WEIGHT:
SHEET 1 OF 1
Ø1.0
Ø2.5
Ø3.0
20
3.8
12.5
21.3
35.0
48.8
57.5
66.3
70.0
46
5
1

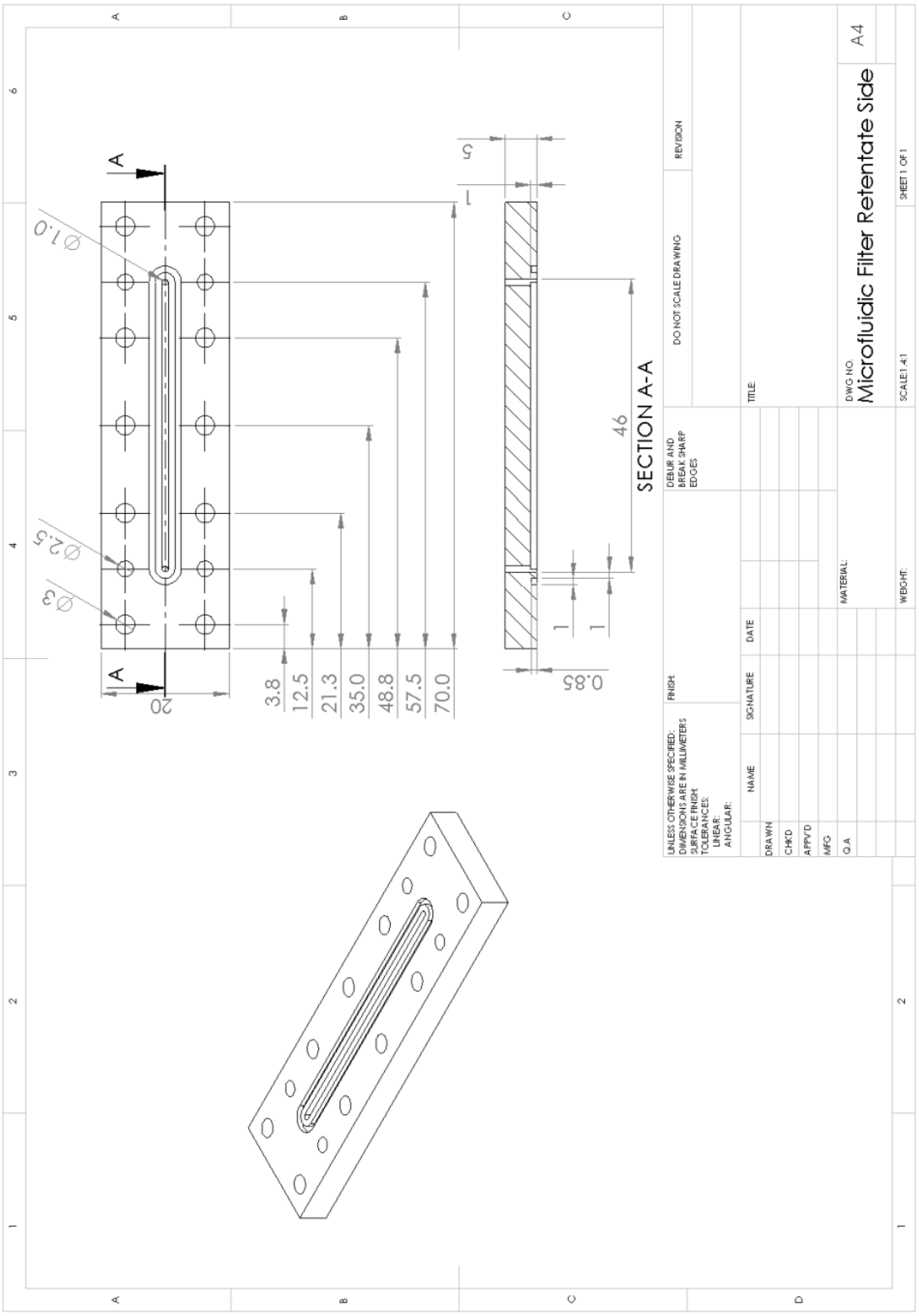
SECTION A-A
Microfluidic Filter Retentate Side
A4
DO NOT SCALE DRAWING
REVISION
DEBUR AND BREAK SHARP EDGES
FINISH
UNLESS OTHERWISE SPECIFIED:
DIMENSIONS ARE IN MILLIMETERS
SURFACE FINISH:
TOLERANCES:
LINEAR:
ANGULAR:
NAME
SIGNATURE
DATE
DRAWN
CHK'D
APPV'D
MFG
Q.A
MATERIAL:
TITLE:
DWG NO.
SCALE 1:4.1
WEIGHT:
SHEET 1 OF 1
3.8
12.5
21.3
35.0
48.8
57.5
70.0
46
20
5
1
0.85

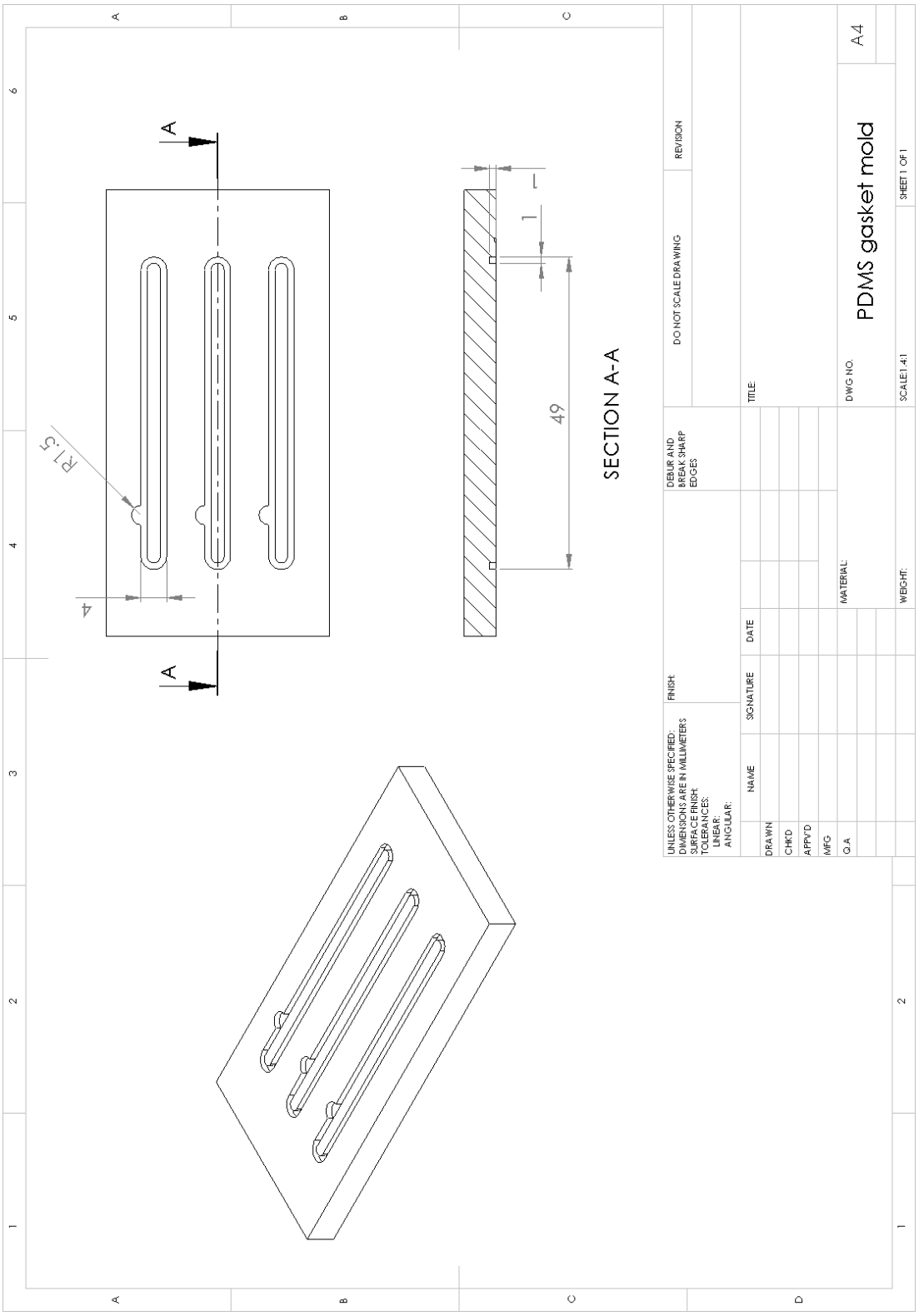
A
B
C
D
1
2
3
4
5
6
A
A
R1.5
4
SECTION A-A
1
49
DO NOT SCALE DRAWING
REVISION
DEBUR AND BREAK SHARP EDGES
FINISH:
UNLESS OTHERWISE SPECIFIED:
DIMENSIONS ARE IN MILLIMETERS
SURFACE FINISH:
TOLERANCES:
LINEAR:
ANGULAR:
NAME
SIGNATURE
DATE
DRAWN
CHK'D
APPV'D
MFG
Q.A
MATERIAL:
TITLE:
DWG NO.
PDMS gasket mold
A4
WEIGHT:
SCALE 1:4:1
SHEET 1 OF 1

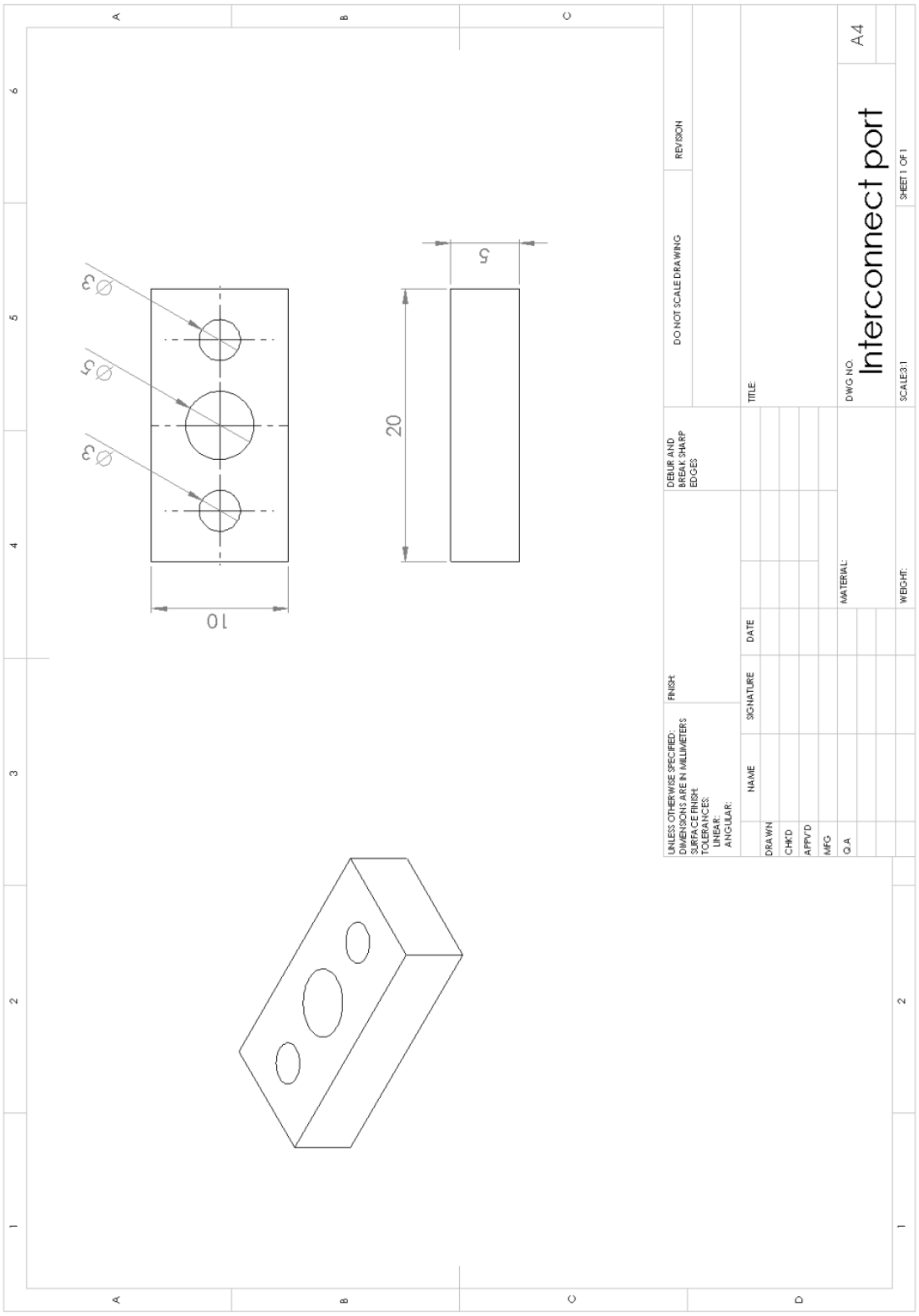
Interconnect port
A4
DWG NO.
SCALE:3:1
SHEET 1 OF 1
REVISION
DO NOT SCALE DRAWING
DEBUR AND BREAK SHARP EDGES
FINISH
UNLESS OTHERWISE SPECIFIED:
DIMENSIONS ARE IN MILLIMETERS
SURFACE FINISH:
TOLERANCES:
LINEAR:
ANGULAR:
NAME
SIGNATURE
DATE
DRAWN
CHK'D
APPV'D
MFG
Q.A
MATERIAL:
WEIGHT:
TITLE:
3Ø
5Ø
3Ø
10
20
5

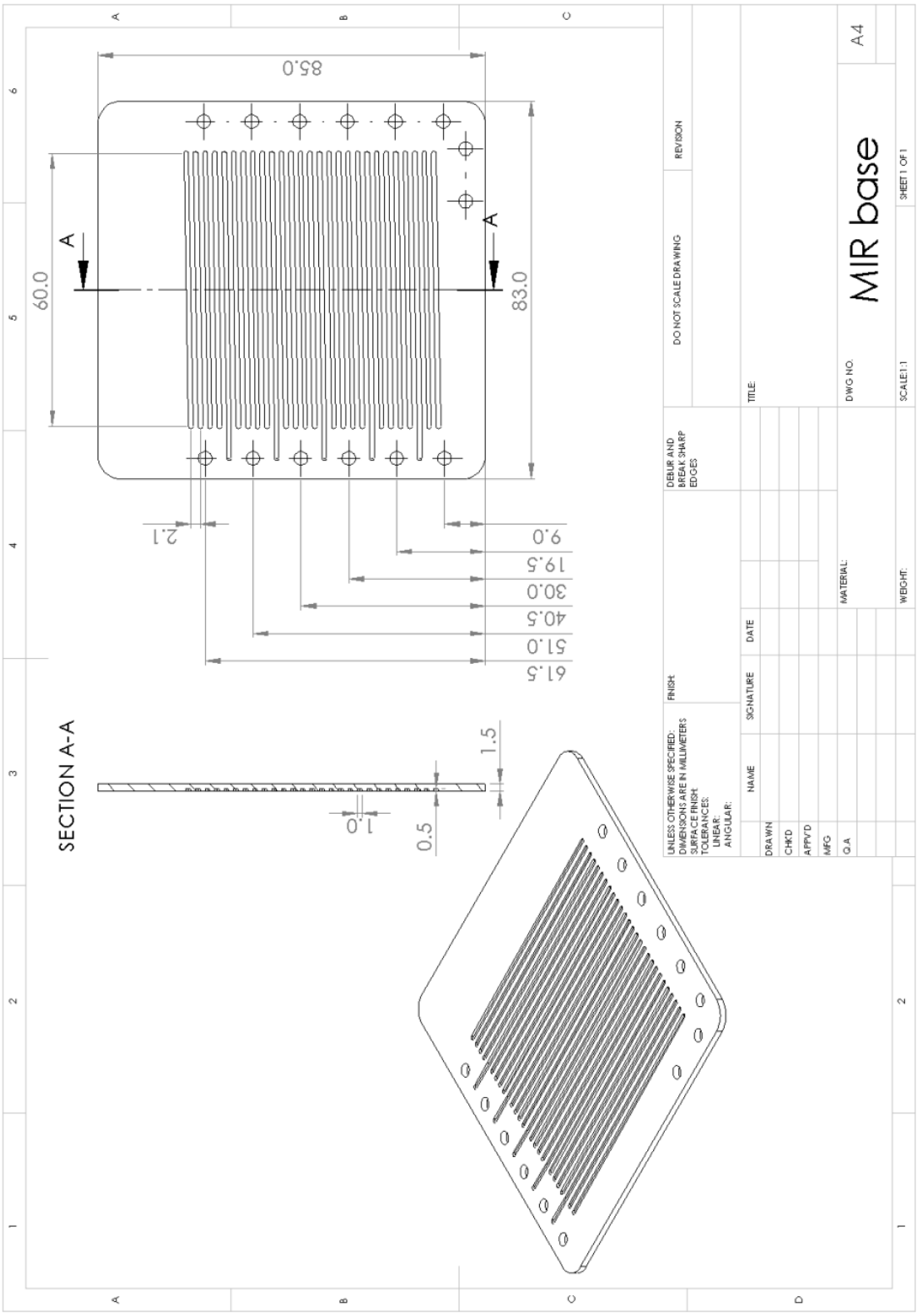
85.0
60.0
83.0
A
A
2.1
9.0
19.5
30.0
40.5
51.0
61.5
SECTION A-A
1.5
1.0
0.5
MIR base
A4
DO NOT SCALE DRAWING
REVISION
DEBUR AND BREAK SHARP EDGES
FINISH
UNLESS OTHERWISE SPECIFIED:
DIMENSIONS ARE IN MILLIMETERS
SURFACE FINISH:
TOLERANCES:
LINEAR:
ANGULAR:
NAME
SIGNATURE
DATE
DRAWN
CHK'D
APPV'D
MFG
Q.A
MATERIAL:
TITLE:
DWG NO.
WEIGHT:
SCALE:1:1
SHEET 1 OF 1

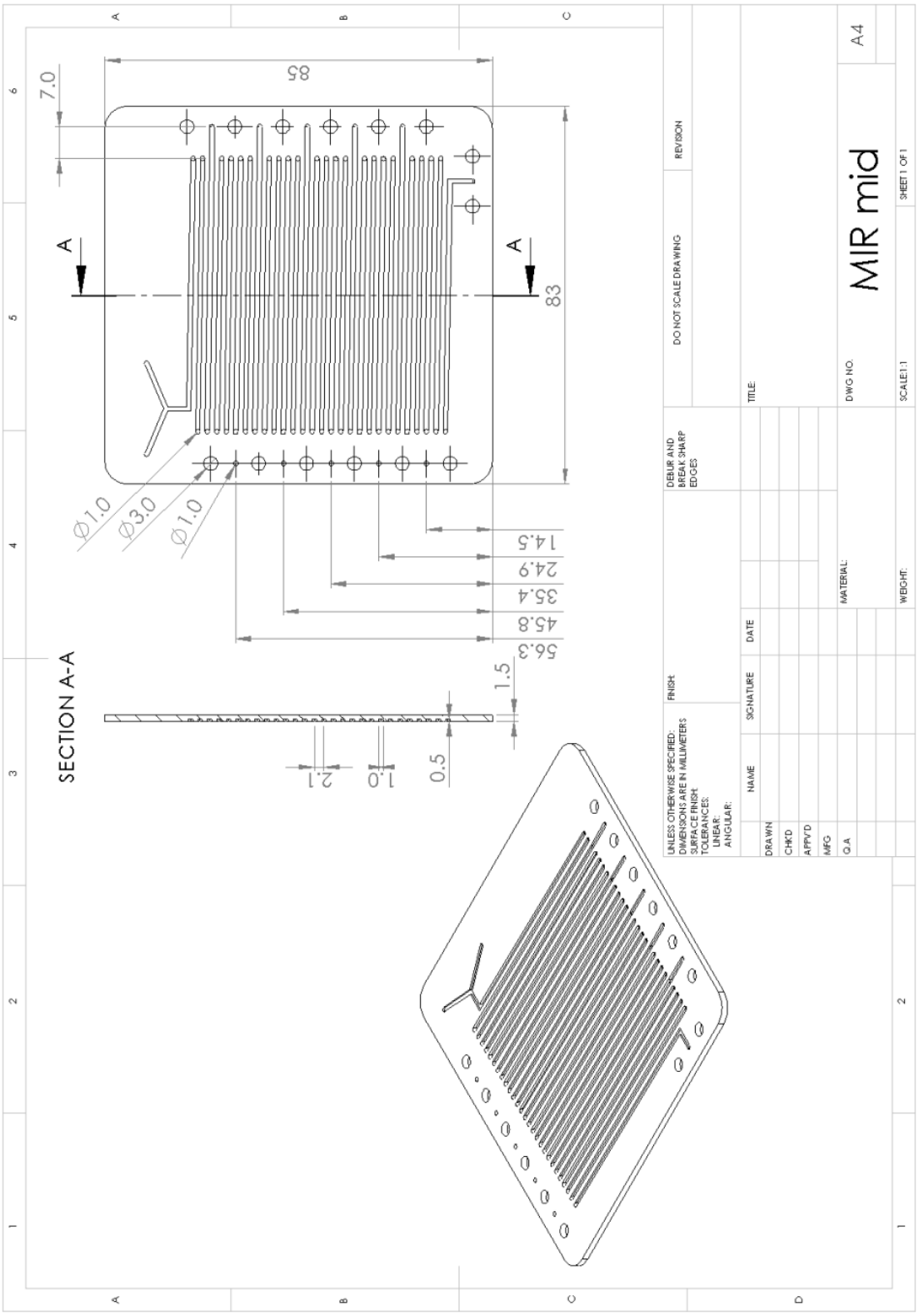
85
7.0
83
A
A
Ø1.0
Ø3.0
Ø1.0
14.5
24.9
35.4
45.8
56.3
SECTION A-A
1.5
0.5
1.0
2.1
MIR mid
A4
SCALE 1:1
SHEET 1 OF 1
DO NOT SCALE DRAWING
REVISION
DEBUR AND BREAK SHARP EDGES
UNLESS OTHERWISE SPECIFIED:
DIMENSIONS ARE IN MILLIMETERS
SURFACE FINISH:
TOLERANCES:
LINEAR:
ANGULAR:
FINISH
NAME
SIGNATURE
DATE
DRAWN
CHK'D
APPV'D
MFG
Q.A
MATERIAL:
WEIGHT:
TITLE:
DWG NO.

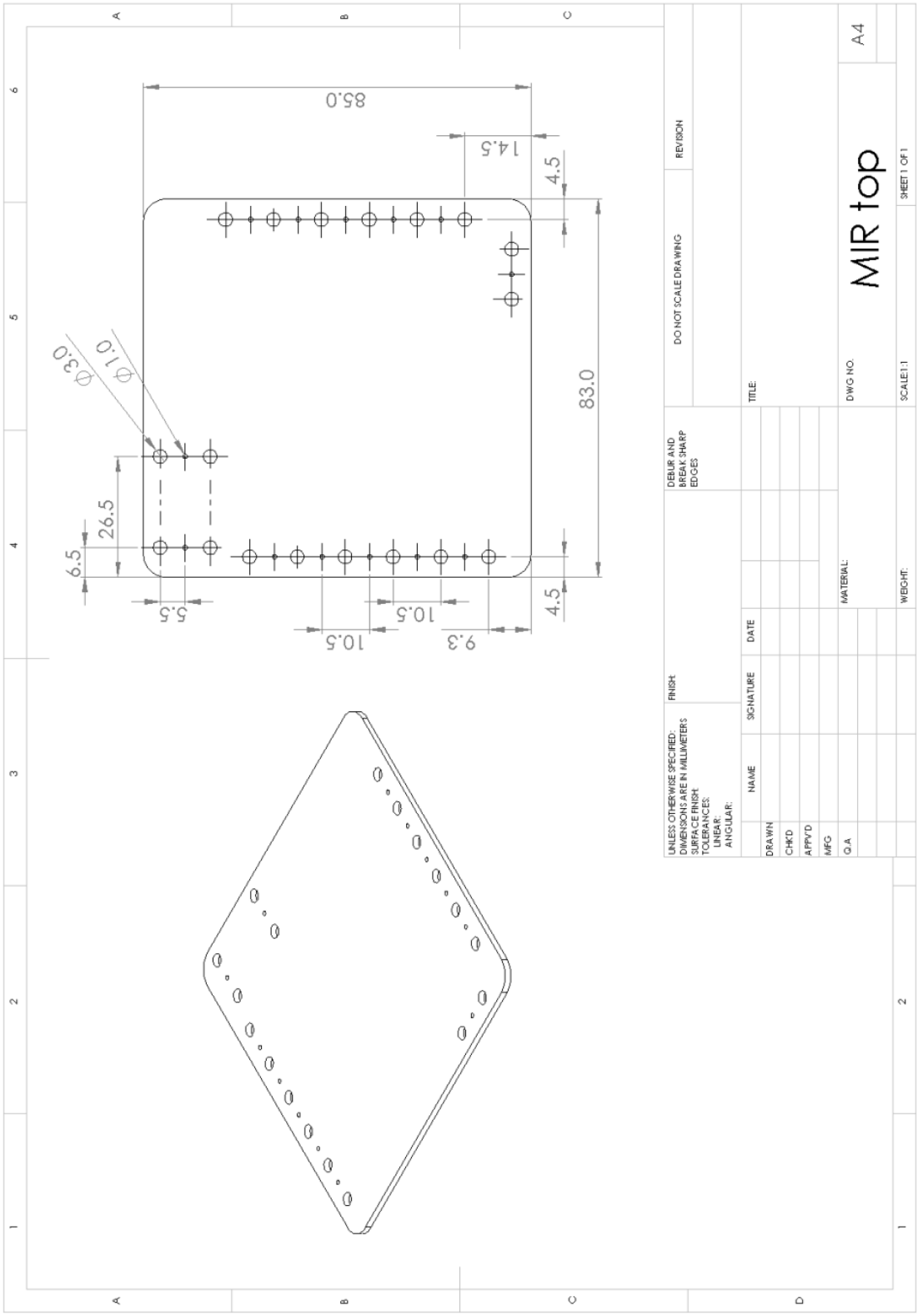
85.0
14.5
4.5
83.0
4.5
26.5
6.5
5.5
10.5
10.5
9.3
Ø3.0
Ø1.0
MIR top
A4
DO NOT SCALE DRAWING
REVISION
DEBUR AND BREAK SHARP EDGES
FINISH
UNLESS OTHERWISE SPECIFIED:
DIMENSIONS ARE IN MILLIMETERS
SURFACE FINISH
TOLERANCES:
LINEAR
ANGULAR
NAME
SIGNATURE
DATE
DRAWN
CHK'D
APPV'D
MFG
Q.A
MATERIAL:
TITLE
DWG NO.
WEIGHT:
SCALE:1:1
SHEET 1 OF 1

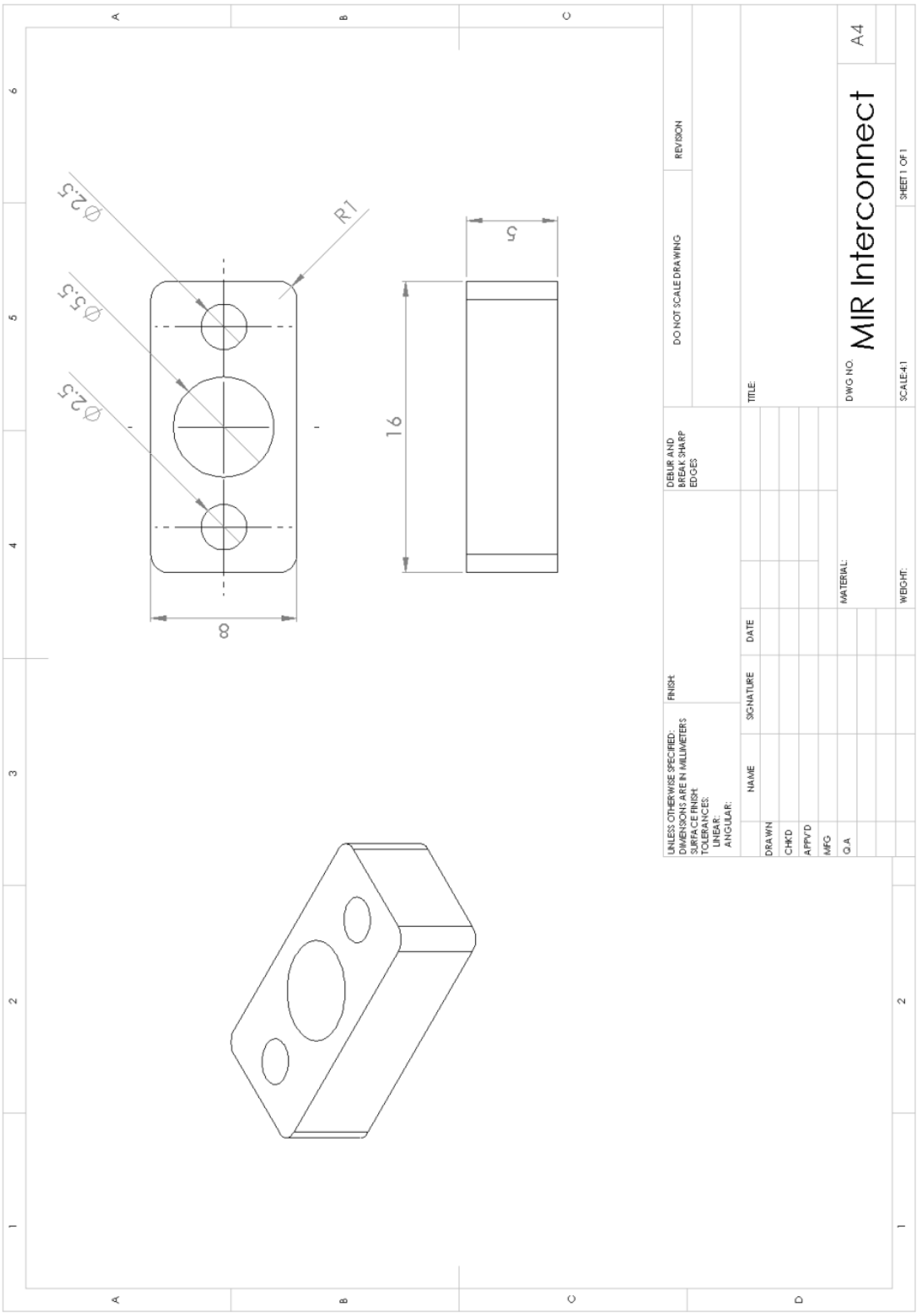
Ø2.5
Ø5.5
Ø2.5
R1
8
16
5
MIR Interconnect
A4
DO NOT SCALE DRAWING
REVISION
DEBUR AND BREAK SHARP EDGES
UNLESS OTHERWISE SPECIFIED:
DIMENSIONS ARE IN MILLIMETERS
SURFACE FINISH:
TOLERANCES:
LINEAR:
ANGULAR:
FINISH
NAME
SIGNATURE
DATE
DRAWN
CHK'D
APPV'D
MFG
Q.A
MATERIAL:
TITLE:
DWG NO.
SCALE:4:1
WEIGHT:
SHEET 1 OF 1

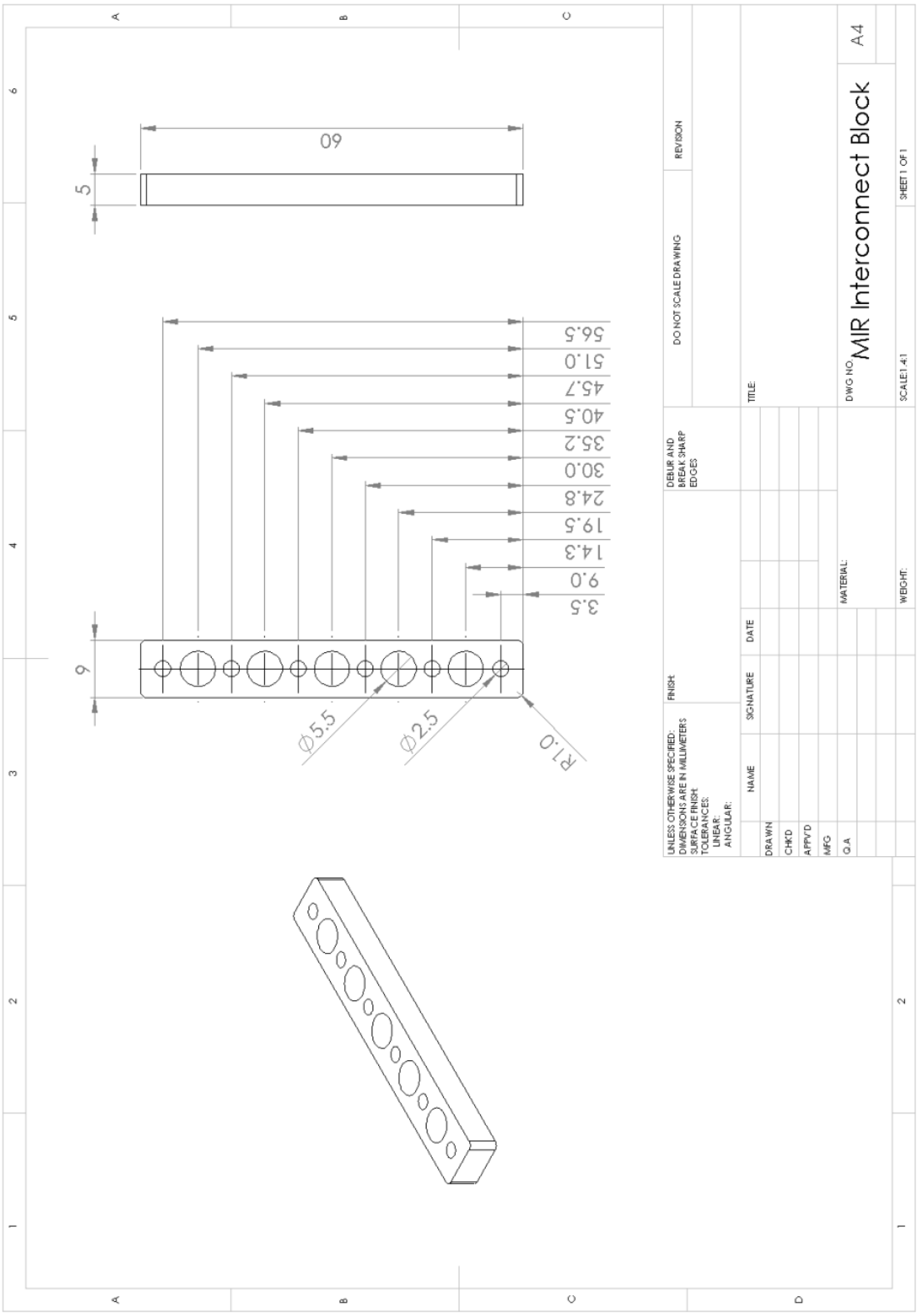
60
5
56.5
51.0
45.7
40.5
35.2
30.0
24.8
19.5
14.3
9.0
3.5
9
Ø5.5
Ø2.5
R1.0
DO NOT SCALE DRAWING
REVISION
DEBUR AND BREAK SHARP EDGES
FINISH
UNLESS OTHERWISE SPECIFIED:
DIMENSIONS ARE IN MILLIMETERS
SURFACE FINISH:
TOLERANCES:
LINEAR:
ANGULAR:
NAME
SIGNATURE
DATE
DRAWN
CHK'D
APPV'D
MFG
Q.A
TITLE:
MATERIAL:
DWG NO
MIR Interconnect Block
A4
WEIGHT:
SCALE 1:4.1
SHEET 1 OF 1

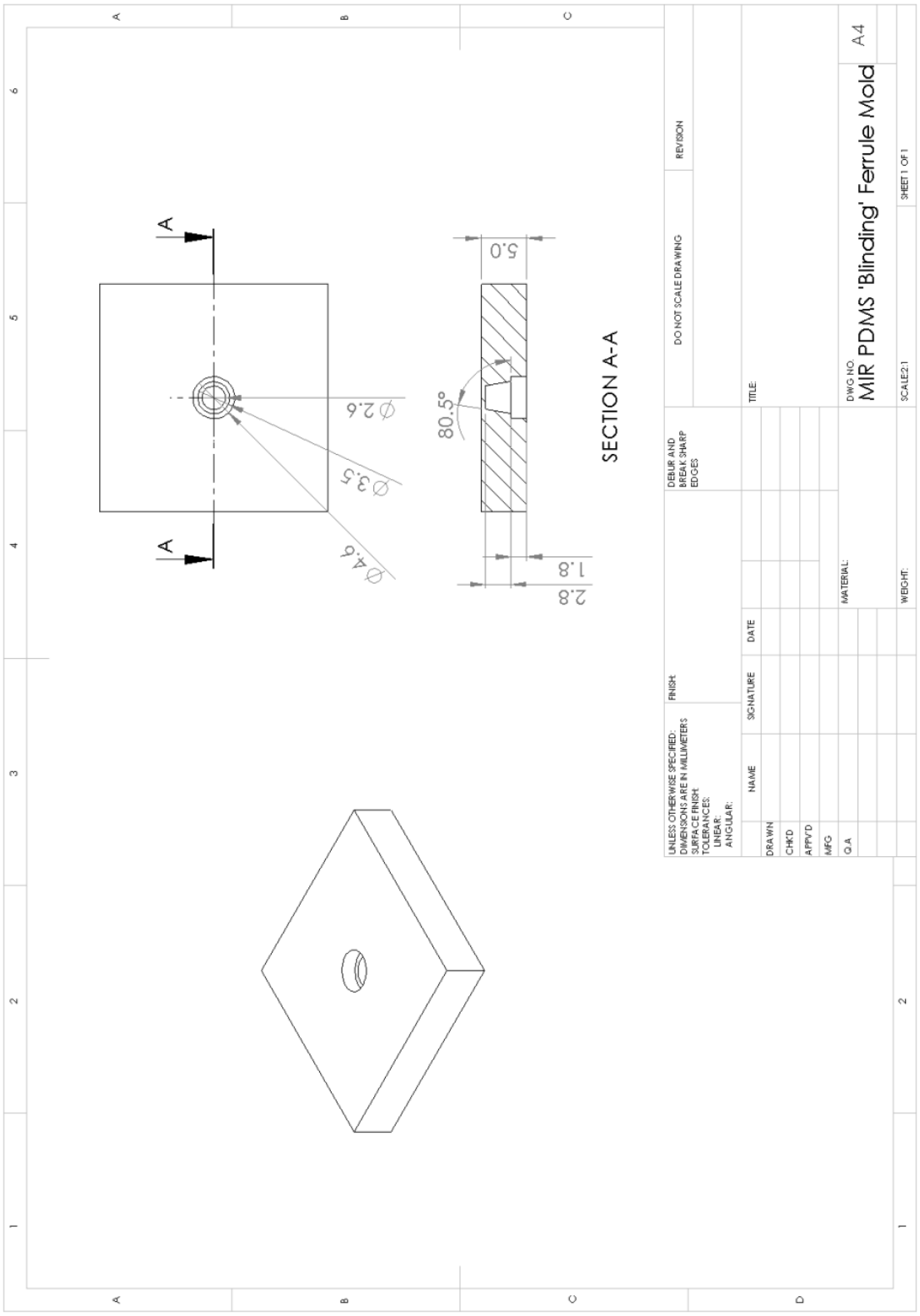
A
A
Ø2.6
Ø3.5
Ø4.6
5.0
80.5°
2.8
1.8
SECTION A-A
DO NOT SCALE DRAWING
REVISION
DEBUR AND BREAK SHARP EDGES
TITLE:
UNLESS OTHERWISE SPECIFIED:
DIMENSIONS ARE IN MILLIMETERS
SURFACE FINISH:
TOLERANCES:
LINEAR:
ANGULAR:
FINISH
NAME
SIGNATURE
DATE
DRAWN
CHK'D
APPV'D
MFG
Q.A
MATERIAL:
DWG NO.
MIR PDMS 'Blinding' Ferrule Mold
A4
WEIGHT:
SCALE:2:1
SHEET 1 OF 1

# Appendix C – Publications

Selected results from Chapters 3 and 4 have been published as a journal article in '*Modular Microfluidic Reactor and Inline Filtration System for the Biocatalytic Synthesis of Chiral Metabolites*' (J. Mol. Cat. B, 2012, 77: 1-8). The results of Chapter 5 were also published as a journal article in '*Microfluidic Multi-Input Reactor for Biocatalytic Synthesis Using Transketolase*' (J Mol. Cat. B, 2013, 95: 111-117). Reproductions of these publications have been removed the electronic version of this thesis for copyright reasons, but are available in the printed version.